WT-1161

Copy No. 175 A

Operation TEAPOT

NEVADA TEST SITE

February – May 1955

Projects 34.1 and 34.3

EFFECTS OF AN ATOMIC EXPLOSION ON GROUP AND FAMILY TYPE SHELTERS

Issuance Date: January 21, 1957

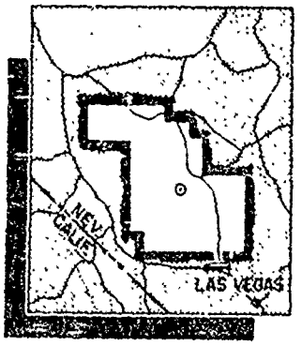

CIVIL EFFECTS TEST GROUP

If this report is no longer needed, return it to
AEC Technical Information Service Extension
P. O. Box 401
Oak Ridge, Tennessee

WT-1161

This document consists of 192 pages
No. 175 of 280 copies, Series A

Report to the Test Director

EFFECTS OF AN ATOMIC EXPLOSION ON GROUP AND FAMILY TYPE SHELTERS

By

L. J. Vortman, Director, Program 34

Technical Associates

Harold Birnbaum and Edward Laing, Ammann & Whitney

Frank G. Ort and Ralph V. Schumacher, Army Chemical Center

Craig C. Hudson, Sandia Corporation

Approved by: ROBERT L. CORSBIE
Director, Civil Effects Test Group

Sandia Corporation
Albuquerque, New Mexico

Federal Civil Defense Administration
Battle Creek, Michigan

December 1955

Statement A
Approved for public release;
Distribution unlimited

ACKNOWLEDGMENTS

The author wishes to express sincere appreciation to the following individuals for their cooperation in behalf of these projects:

R. L. Corsbie, Atomic Energy Commission, Director, Civil Effects Test Group
Dr. E. F. Cox, Sandia Corporation
L. J. Deal, Atomic Energy Commission
Phyllis Flanders, Sandia Corporation
J. C. Greene, Federal Civil Defense Administration
Dr. P. S. Harris, Los Alamos Scientific Laboratory
R. S. Millican, Sandia Corporation
R. W. Newman, Los Alamos Scientific Laboratory
Dr. G. W. Rollosson, Sandia Corporation
H. H Sander, Sandia Corporation
B. C. Taylor, Federal Civil Defense Administration
Dr. C. S. White, Lovelace Foundation

ABSTRACT

This joint Federal Civil Defense Administration–Atomic Energy Commission project was conducted to evaluate several shelter designs.

Two underground shelters (50-man capacity), one open and one closed, were exposed to Apple I shot, and two were exposed to Apple II shot (at 1050 ft). Three basement exit shelters were exposed to Apple I shot at 1350 ft; four were exposed to Apple II shot, two at 1270 ft and two at 1470 ft. Groups of three aboveground utility type shelters, one of masonry blocks, one of precast reinforced concrete, and one of poured-in-place reinforced concrete, were placed at 2250, 2750, and 3750 ft from Apple II shot. Reinforced-concrete bathroom shelters were placed in rambler type houses (Project 31.1) at 2700 and 10,500 ft from Apple II shot. Three types of basement shelters were constructed in two frame houses (Project 31.1) at 5500 and 7800 ft, and two types of basement shelters were constructed in two brick houses (Project 31.1) at 4700 and 10,500 ft from the same burst.

Instrumentation consisted of Wiancko pressure gauges, q-tubes, temperature- and noise-metering devices, gamma-radiation film dosimeters, and neutron detectors. No measurements of structural behavior were made. Mannequins were placed in some shelters on Apple II shot for demonstration purposes.

On neither shot was structural damage sustained by the large underground personnel shelters. Occupants of the closed shelter would not have been disturbed by blast, debris, or radiation. Damage to the basement exit shelters was inversely proportional to their distance from Ground Zero (GZ) and was directly proportional to the amount of opening in the entrance. The closed shelter at the greatest distance received the least damage but was not satisfactory as a personnel shelter at the lowest pressure tested. Utility shelters provided unsatisfactory protection from radiation. All indoor family type shelters were satisfactory as tested and would have provided adequate protection for occupants.

CONTENTS

CONTENTS (Continued)

CONTENTS (Continued)

ILLUSTRATIONS

ILLUSTRATIONS (Continued)

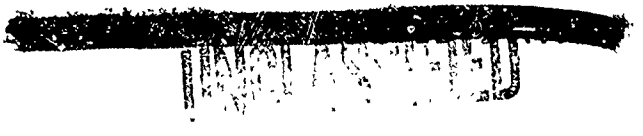

ILLUSTRATIONS (Continued)

ILLUSTRATIONS (Continued)

TABLES

TABLES (Continued)

CHAPTER 1

INTRODUCTION

1.1 OBJECTIVE

The primary purpose of Projects 34.1 and 34.3 was to evaluate shelter designs proposed by the Federal Civil Defense Administration (FCDA) for protection against nuclear and thermal radiation and blast effects. The effectiveness of two types of protective ventilation for buried shelters was evaluated by the Army Chemical Center. Advantage was taken of the instrumentation provided for Program 33 to obtain a better understanding of blast loading inside an underground shelter.

1.2 BACKGROUND

Lehigh University Institute of Research designed for FCDA several types of home shelters of which four types [(1) covered-trench, (2) metal-arch, (3) wood-arch, and (4) basement lean-to] were field tested during Operation Buster-Jangle.[1] Weaknesses in the more successful of these shelters were strengthened, and these modified versions, together with designs of new shelter types, were tested during Operation Upshot-Knothole.[2] A basement lean-to shelter similar to that tested during Operation Buster-Jangle and a newly designed basement corner-room shelter were located in the basements of two frame test houses on Operation Upshot-Knothole. The houses were exposed to approximately 5 and 1.7 psi, but no instrumentation was provided to determine the relation of outside overpressure to that to which occupants of the shelter would have been subjected. The manner in which failure of these two frame houses occurred was such that maximum debris did not load the shelters. It was desired also to test these shelters under the greater debris load of a brick house. Thus, for Operation Teapot, basement lean-to (Figs. 1.1 and 1.2) and basement corner-room shelters (Figs. 1.3 and 1.4) were placed in all the brick and frame houses with basements. The designs were essentially the same as those tested on Operation Upshot-Knothole except that the width of the basement lean-to shelter had been reduced from 8 to 6 ft. A shelter consisting of a narrow room of reinforced concrete was constructed in the basement next to the stair well of the frame houses of Operation Teapot (Figs. 1.5 and 1.6).

Since many houses in the United States do not have basements, another new type of indoor home shelter was designed by FCDA. This consisted of modifying the bathroom of a conventional one-story frame residence built on a flat slab. Bathroom walls and ceiling were made of 8-in. reinforced concrete, the thickness of the floor slab was increased from 4 to 12 in., and the window and door were covered with blast doors made of two thicknesses of 1-in. plywood which were glued and screwed together (Figs. 1.7 and 1.8).

A basement exit shelter which connects to the house through the basement wall was also tested during Operation Upshot-Knothole. The shelter was exposed to about 23 psi and was

located with the entrance end toward Ground Zero (GZ) with the entrance oriented 90° from GZ. It was desired to evaluate this shelter at a higher pressure level, with a blast-resistant door, and at its most vulnerable orientation with the entrance facing GZ. Other than the addition of the door, the only significant change in the Upshot-Knothole design was an increased thickness of reinforced concrete in the wall of the entrance (Figs. 1.9 through 1.11). For Operation Teapot three shelters were tested on Apple I shot: one with the four-section door closed, one with the two center sections of the door removed, and one without a door. Shelters on Apple II were tested in pairs, one with the door closed and one without a door, each at two different pressure levels. The varying door openings were a requirement of Program 33 but gave information on the overpressures to which occupants would be subjected under the conditions tested.

An aboveground utility type shelter was designed by Ammann & Whitney from a concept furnished by FCDA, which could be used as a tool shed when not needed as a shelter (Figs. 1.12 through 1.14). Inside floor dimensions were 6 by 6 ft, and the interior was 7 ft high. Walls were 6 in. thick, except the wall with the door which was 8 in. thick. An outside blast door of 3- by 8-in. lumber was provided. Three variations of this shelter were designed and constructed — masonry block, precast reinforced concrete, and poured-in-place reinforced concrete. One of each of the three types was tested at three different pressure levels.

The FCDA was aware of the need for providing shelters for industrial and civic use and furnished requirements to Ammann & Whitney, who designed an underground personnel shelter to accommodate 50 persons (Figs. 1.15 through 1.17, Apple I shot; Fig. 1.18, Apple II shot). Two were built for Apple I shot and two for Apple II shot. One of each pair was modified by a reinforced-concrete partition dividing the shelter into two chambers, each 12 by 12 by 8 ft (Figs. 1.19 through 1.21). These were tested with doors and escape hatches open but partially obstructed (hatches had air inlet — 19-in. diameter for Apple I; 36-in. diameter for Apple II) to meter air into the chambers at a rate satisfactory to the requirements of the biomedical program (Program 33). The room into which the escape hatch entered is referred to as the "slow-fill" room and the other as the "fast-fill" room. Three shelters were oriented with the entrance toward GZ, and the fourth (Station 34.3 a-2) was rotated 90° counterclockwise (Fig. 1.23).

Table 1.1 lists the shelters tested on Operation Teapot. Five outdoor underground personnel types were tested on Apple I shot (15-kt burst atop a 500-ft tower, Mar. 29, 1955), Fig. 1.22. Six outdoor underground, nine outdoor aboveground, and twelve indoor shelters were tested on Apple II shot (30-kt burst atop a 500-ft tower, May 5, 1955), Fig. 1.23.

1.3 INSTRUMENTATION

Gauges allotted to each shelter are listed in Table 1.1; gauge locations within the shelters are shown in Figs. 1.1, 1.4, 1.8, 1.9, 1.12, 1.17, 1.18, and 1.19. The locations of ground baffle gauges provided by Project 39.2 (reference 3) for measuring "free field" presssures are shown in Figs. 1.22 and 1.23. Instrumentation for noise was made for the benefit of Project 33.2 and is covered in the Project 33.2 report.[4] Temperature gauges in the open group shelters were designed to measure transient temperatures (see Chap. 3 for gauge details).

REFERENCES

1. A. P. Flynn, FCDA Family Shelter Evaluation, Operation Buster Report, WT-359, March 1952.
2. J. B. Byrnes, Effects of an Atomic Explosion on Underground and Basement Type Home Shelters, Operation Upshot-Knothole Report, WT-801, March – June 1953.
3. G. W. Rollosson, Static and Dynamic Overpressure Measurements, Operation Teapot Report, ITR-1192 (to be superseded by WT-1192).
4. F. G. Hirsch et al., The Effects of Noise on Biological Systems, Operation Teapot Report, WT-1180, December 1955.

Table 1.1—SUMMARY OF SHELTERS TESTED

Project No.	Structure	Station No.	Shot	Distance, ft	Desired overpressure, psi	Actual overpressure, psi	Instrumentation
34.1a	Basement lean-to shelters						
	Brick house	31.1 a-1	Apple II	4,700	5	4.85–5.1	1 pressure
	Brick house	31.1 a-2	Apple II	10,500	1.7		
	Frame house	31.1 b-1	Apple II	5,500	4		
	Frame house	31.1 b-2	Apple II	7,800	2.5		
34.1a	Basement corner-room shelter						
	Brick house	31.1 a-1	Apple II	4,700	5		
	Brick house	31.1 a-2	Apple II	10,500	1.7		
	Frame house	31.1 b-1	Apple II	5,500	4	3.75	1 pressure
	Frame house	31.1 b-2	Apple II	7,800	2.5		
34.1a	Basement reinforced concrete						
	Frame house	31.1 b-1	Apple II	5,500	4		
	Frame house	31.1 b-2	Apple II	7,800	2.5		
34.1a	Reinforced-concrete bathroom shelter						
	Rambler house	31.1 c-1	Apple II	4,700	5	4.85–5.1	1 pressure
	Rambler house	31.1 c-2	Apple II	10,500	1.7		
34.1b	Masonry utility type shelters	34.1 g	Apple II	2,250	13	11.7	
		34.1 j	Apple II	2,750	10	11.6	
		34.1 m	Apple II	3,750	7	7.8	
34.1b	Reinforced-concrete utility type shelters (poured-in-place)	34.1 f	Apple II	2,250	13	11.7	1 pressure
		34.1 i	Apple II	2,750	10	11.6	1 pressure
		34.1 l	Apple II	3,750	7	7.8	1 pressure
34.1b	Reinforced-concrete utility type shelters (precast)	34.1 e	Apple II	2,250	13	11.7	
		34.1 h	Apple II	2,750	10	11.6	
		34.1 k	Apple II	3,750	7	7.8	
34.1b	Basement exit shelters						
	Closed	34.1 b-1	Apple I	1,350	45	17.3	2 pressure
	Partly open	34.1 b-2	Apple I	1,350	45	17.3	2 pressure
	Open	34.1 b-3	Apple I	1,350	45	17.3	2 pressure
	Closed	34.1 c-1	Apple II	1,270	55	44.4	1 pressure
	Open	34.1 c-2	Apple II	1,270	55	44.4	1 pressure
	Closed	34.1 d-1	Apple II	1,470	35		1 pressure
	Open	34.1 d-2	Apple II	1,470	35		1 pressure
34.3	Group shelters						
	Structural	34.3 a-1	Apple I	1,050	100	47	3 pressure, 1 noise
	Biomedical	34.3 b-1	Apple I	1,050	100	47	12 pressure, 1 noise, 2 temperature, 1 dynamic pressure
	Structural	34.3 a-2	Apple II	1,050	100	91.9	3 pressure, 1 noise, 1 acceleration
	Biomedical	34.3 b-2	Apple II	1,050	100	91.9	12 pressure, 1 noise, 2 temperature, 1 dynamic pressure
34.3	Blast line		Apple I	1,050	100	47	1 pressure
			Apple I	1,350	45	17.3	1 pressure
			Apple II	1,050	100	91.9	1 pressure
				1,270	55	44.4	1 pressure
				1,470	35		1 pressure
				2,250	13	11.7	1 pressure
				2,750	10	11.6	1 pressure
				3,750	7	7.8	1 pressure
				4,700	5	4.85–5.1	3 pressure
				10,500	1.7	1.7–2.1	3 pressure
				15,000	1	1.26	1 pressure

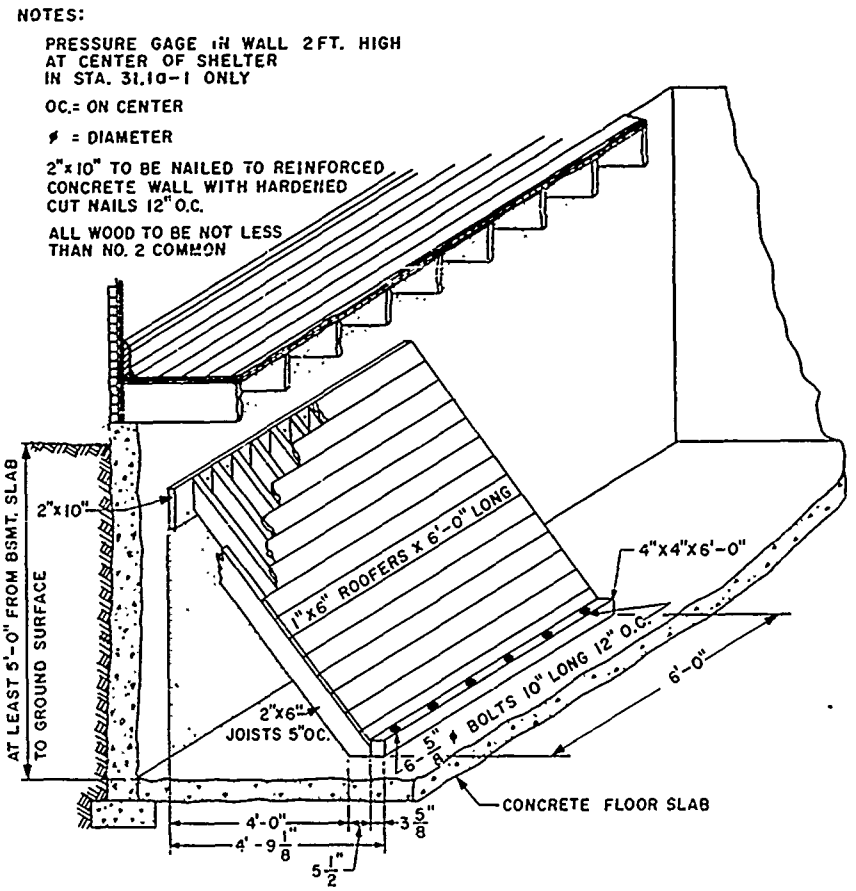

Fig. 1.1—Sketch of basement lean-to shelter.

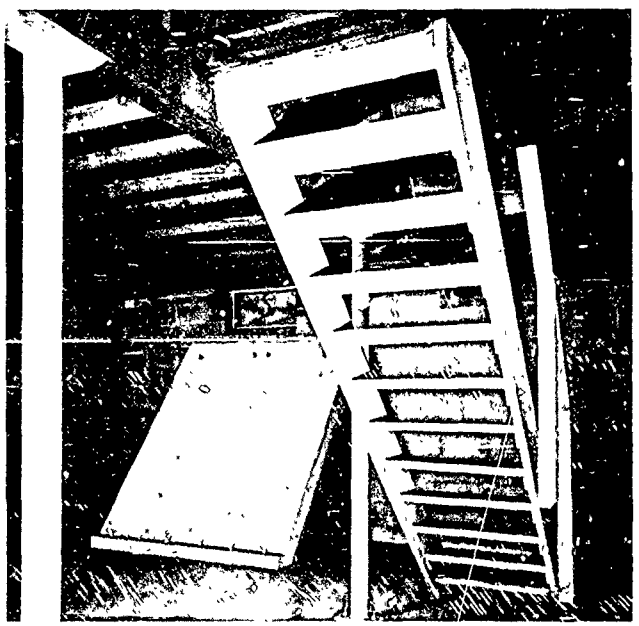

Fig. 1.2—Basement lean-to shelter.

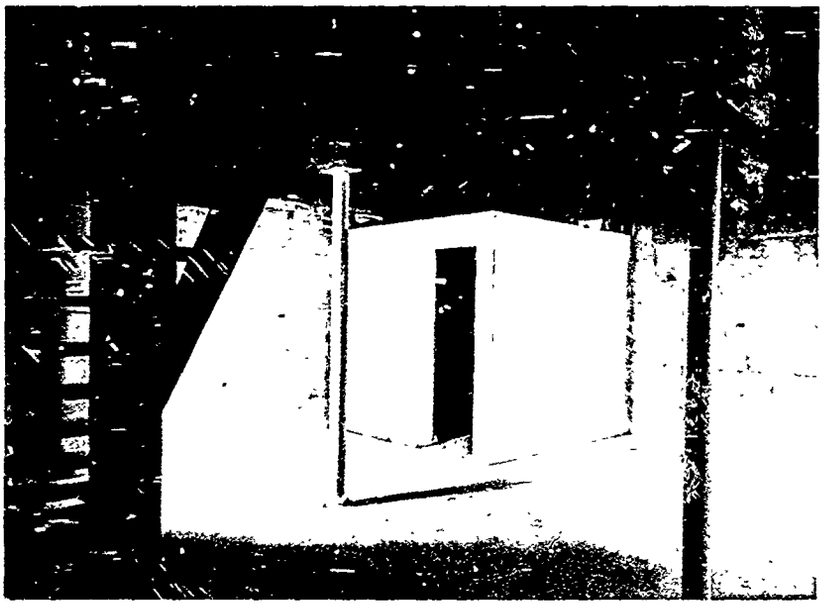

Fig. 1.3—Basement corner-room shelter.

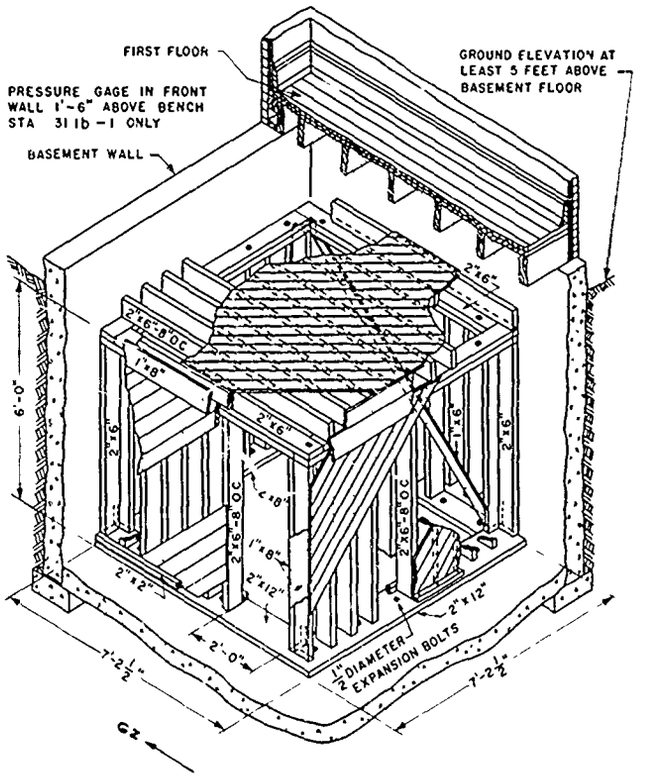

Fig. 1.4—Sketch of basement corner-room shelter.

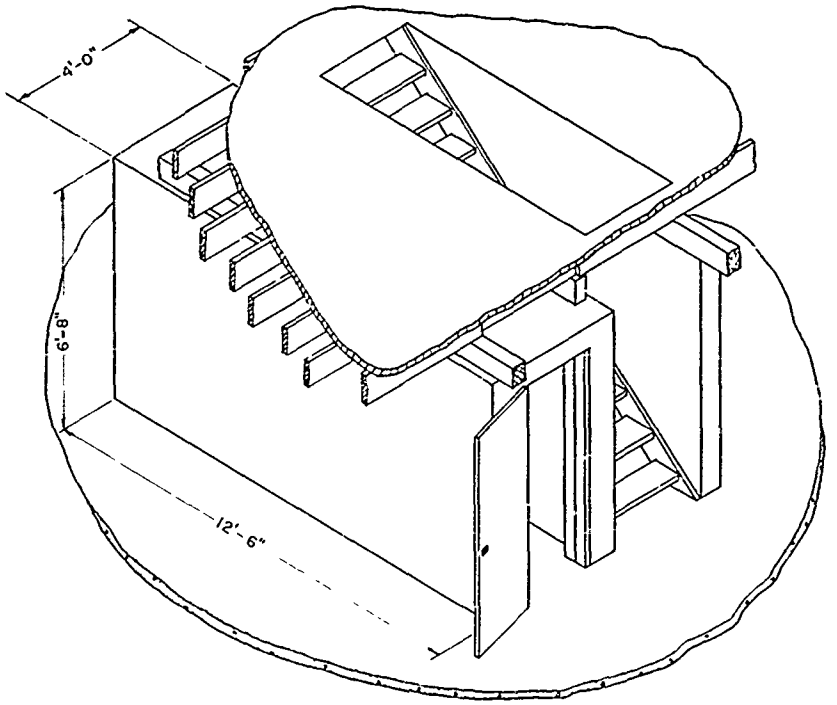

Fig. 1.5—Sketch of basement concrete room shelter.

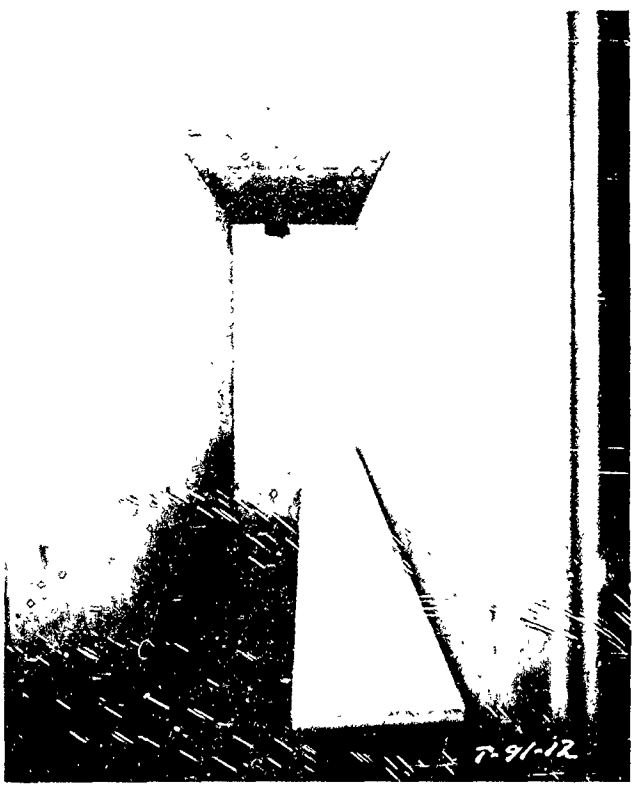

Fig. 1.6—Interior of basement concrete room shelter.

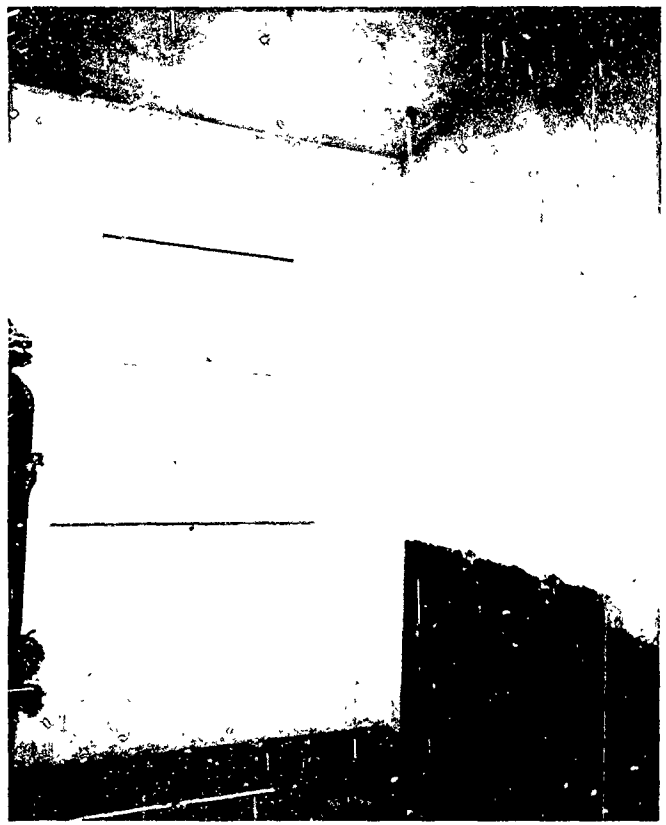

Fig. 1.7—Interior of bathroom shelter.

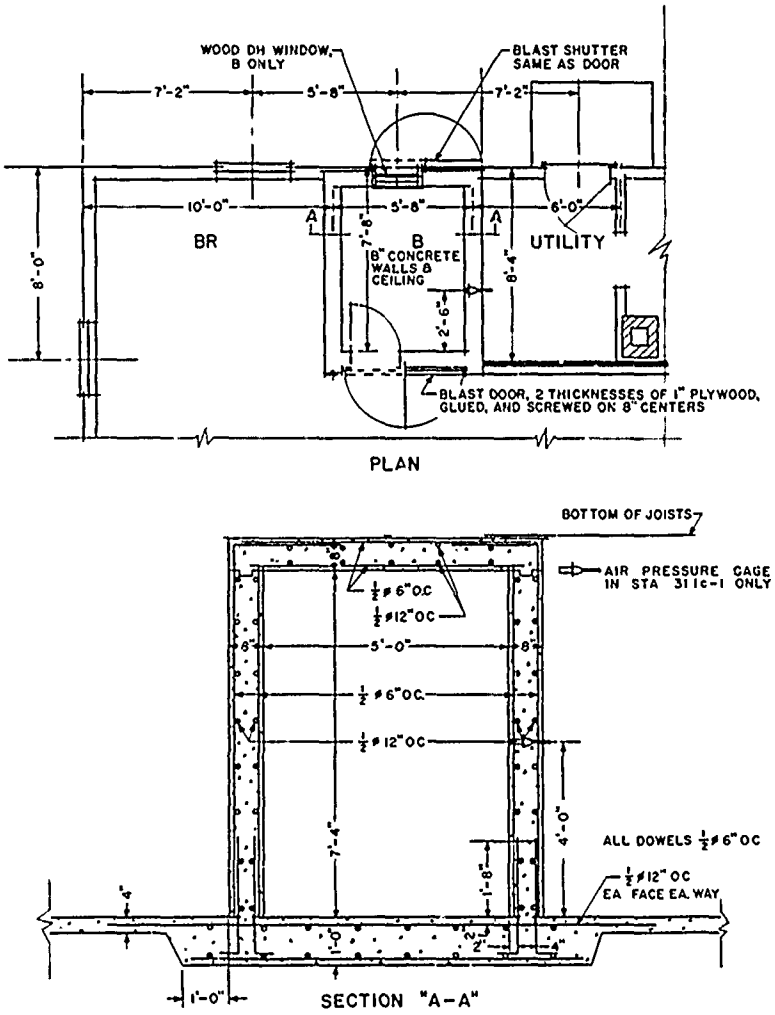

Fig. 1.8—Plan and section of concrete bathroom shelter.

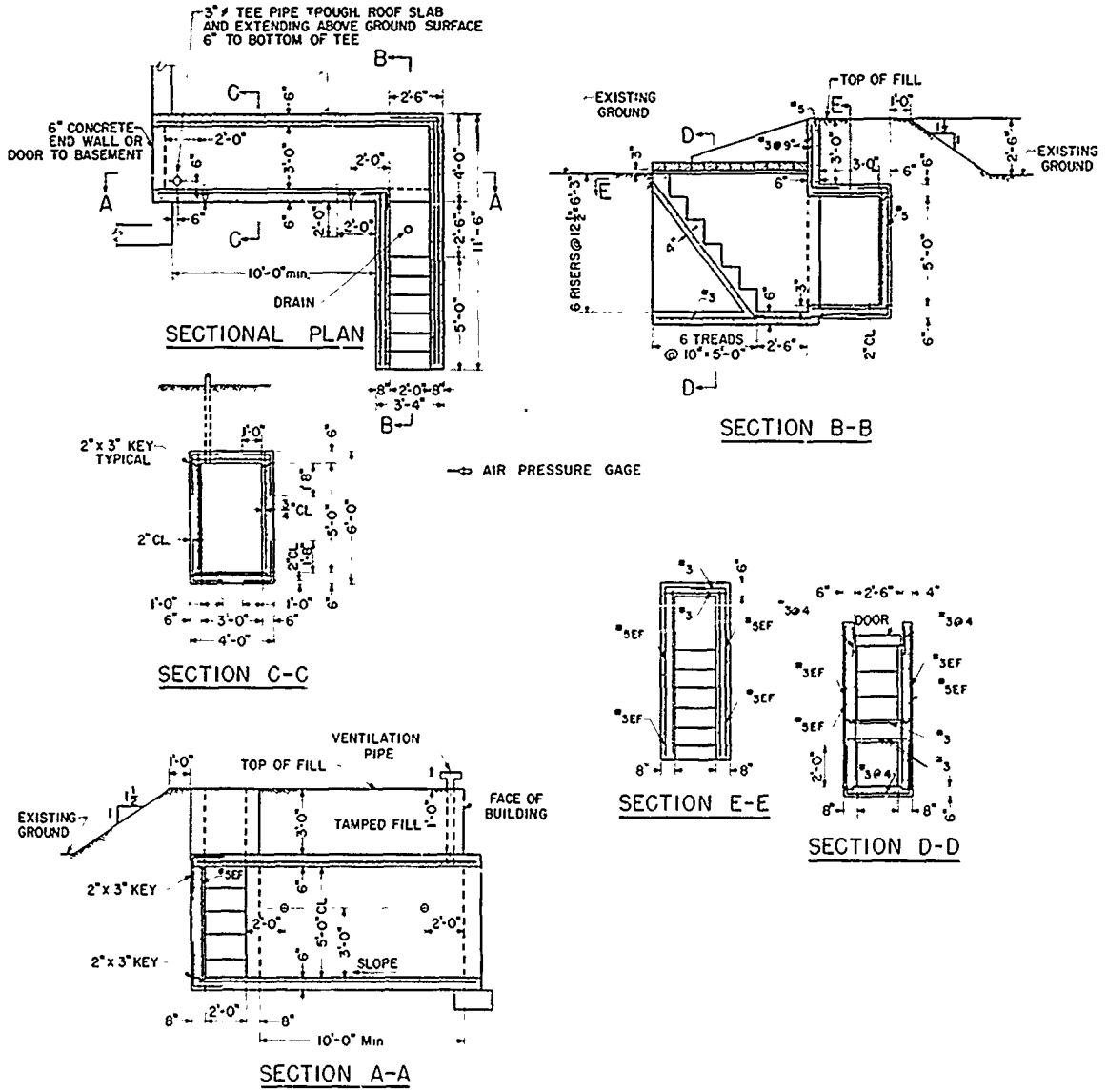

Fig. 1.9 — Details of basement exit shelter; Stations 4-34.1 b, 1-34.1 c, and 1-34.1 d.

Fig. 1.10—Exterior of basement exit shelter; Stations 4-34.1 b, 1-34.1 c, and 1-34.1 d.

Fig. 1.11—Interior of basement exit shelter; Stations 4-34.1 b, 1-34.1 c, and 1-34.1 d.

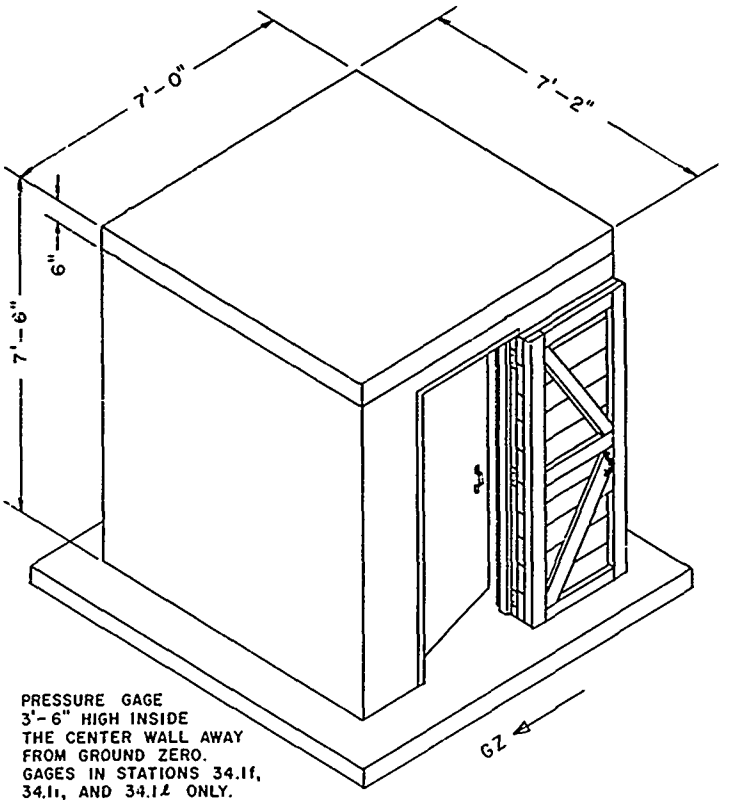

Fig. 1.12—Sketch of utility type shelter; Stations 1-34.1 e to m.

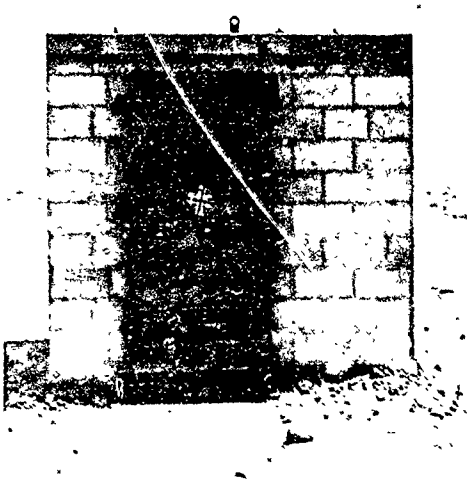

Fig. 1.13—Exterior of masonry utility type shelter; Stations 1-34.1 g, j, and m.

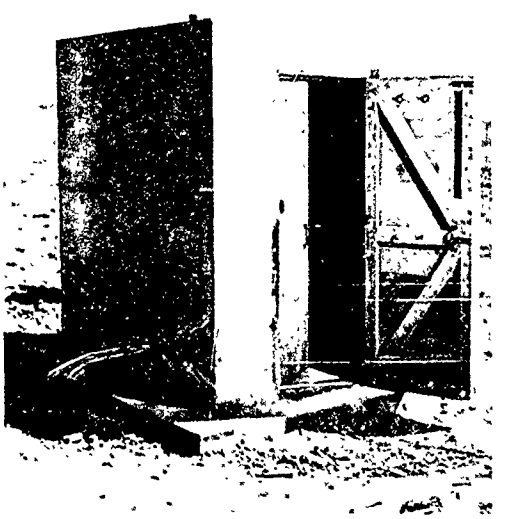

Fig. 1.14—Exterior of reinforced-concrete utility type shelter; Stations 1-34.1 f, i, and l

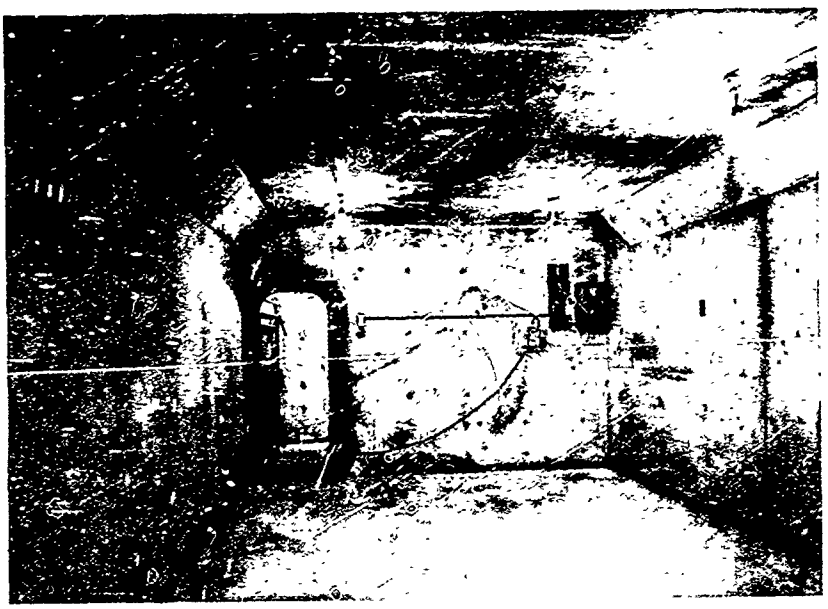

Fig. 1.15—Interior of underground personnel shelter (unfinished); Station 4-34.3 a-1.

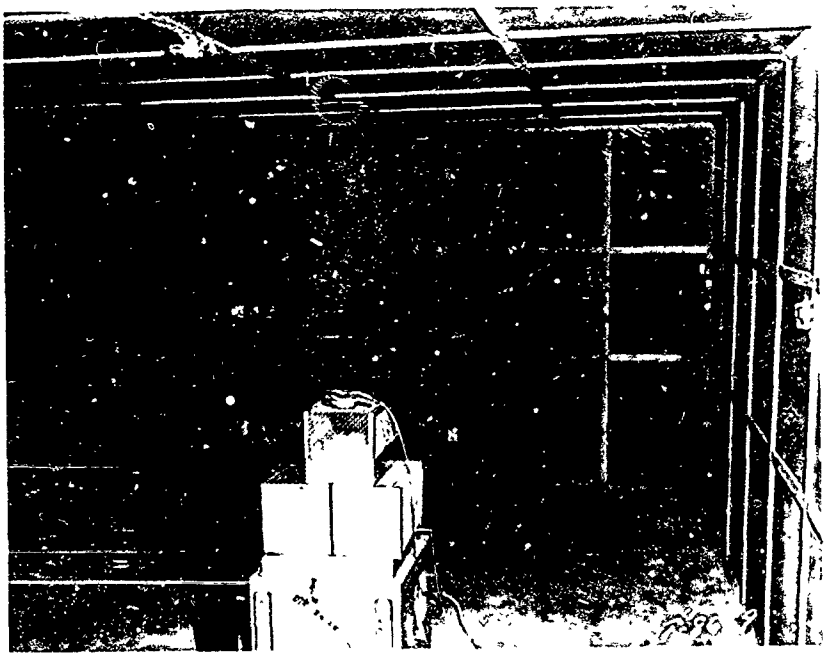

Fig. 1.16—Interior of underground personnel shelter (finished); Station 4-34.3 a-1.

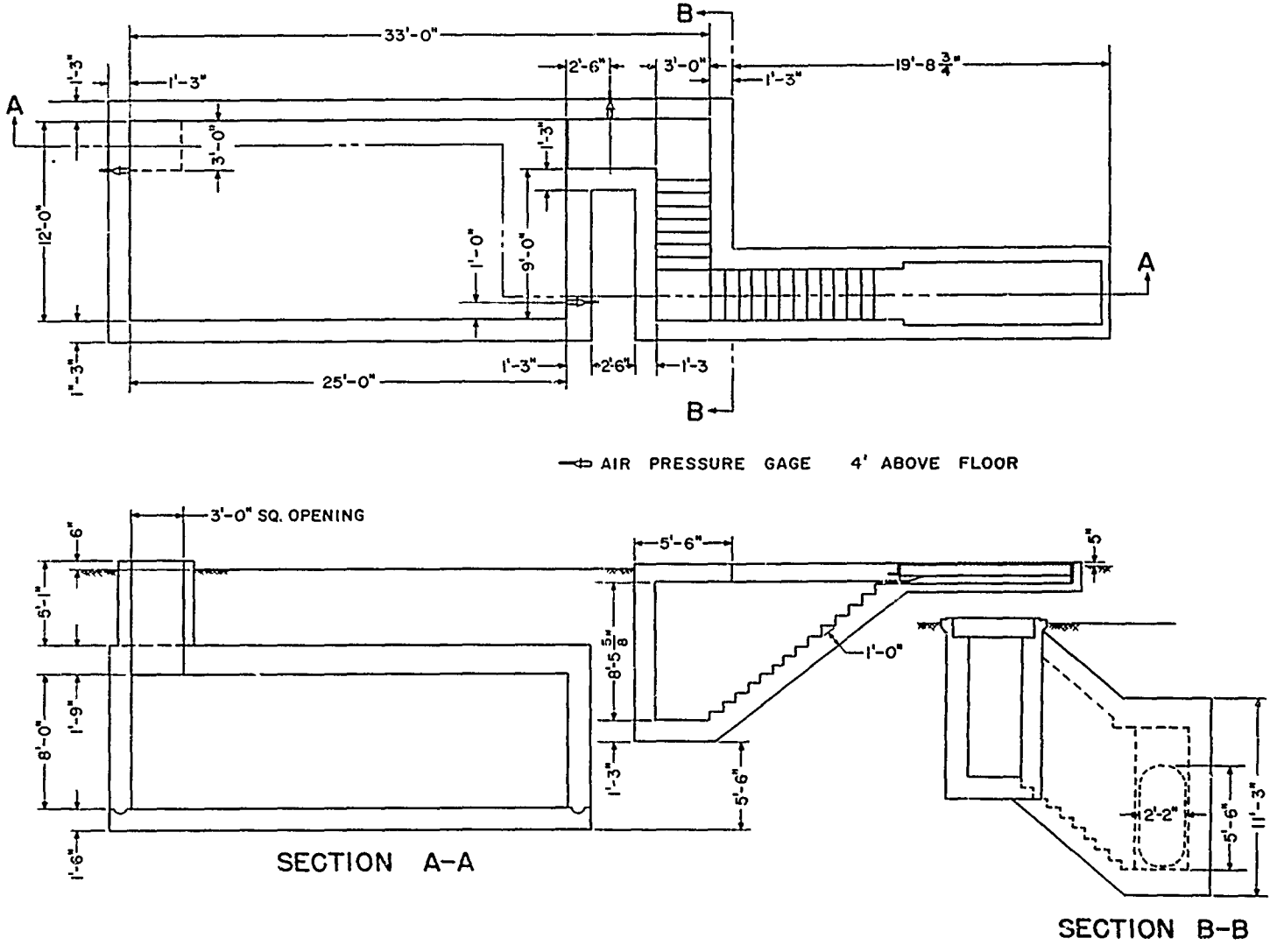

Fig. 1.17—Plan and section of underground personnel shelter (structural), Apple I shot; Station 4-34.3 a-1.

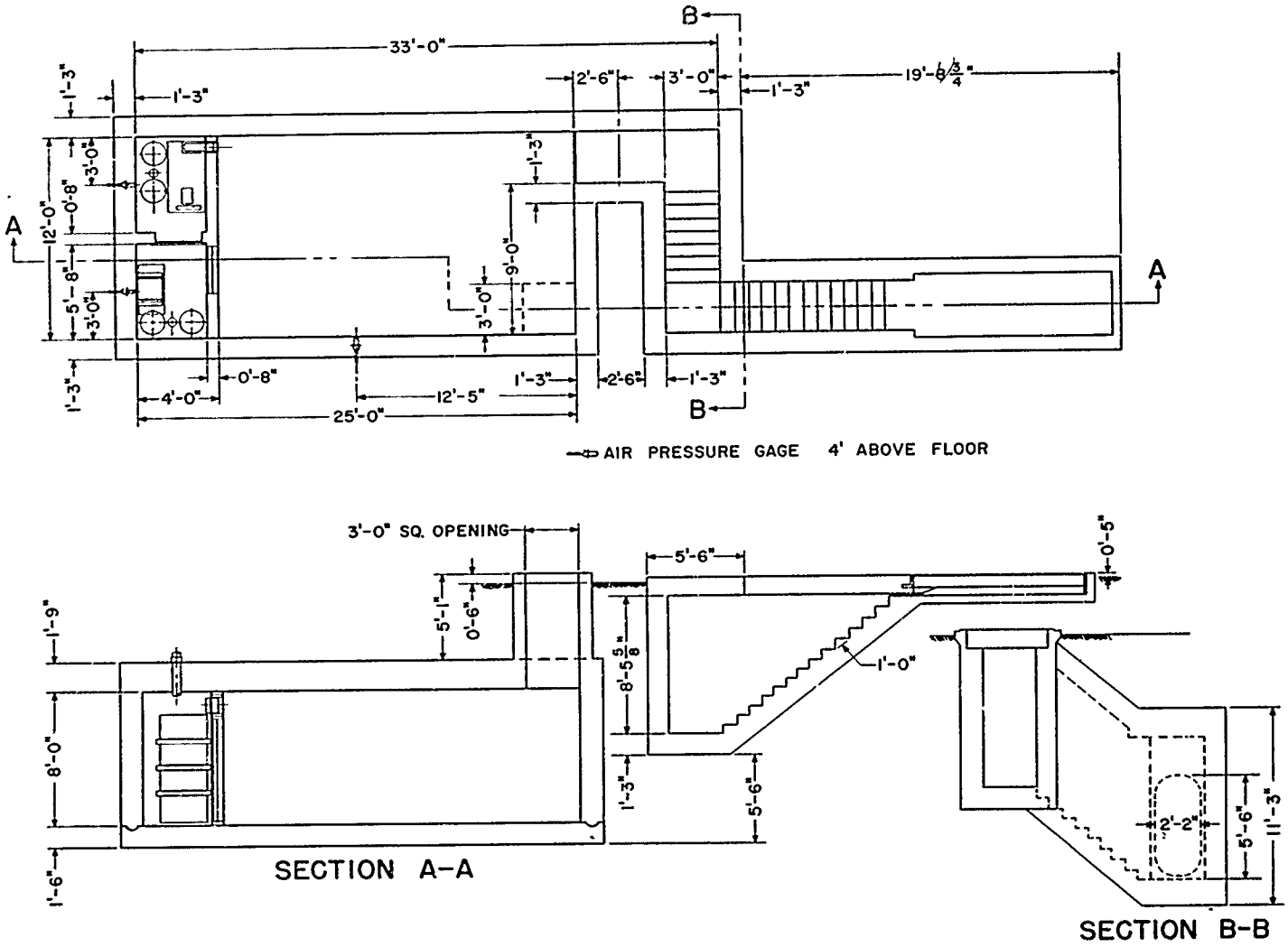

Fig. 1.18—Plan and section of underground personnel shelter (structural), Apple II shot, Station 1-34.3 a-2.

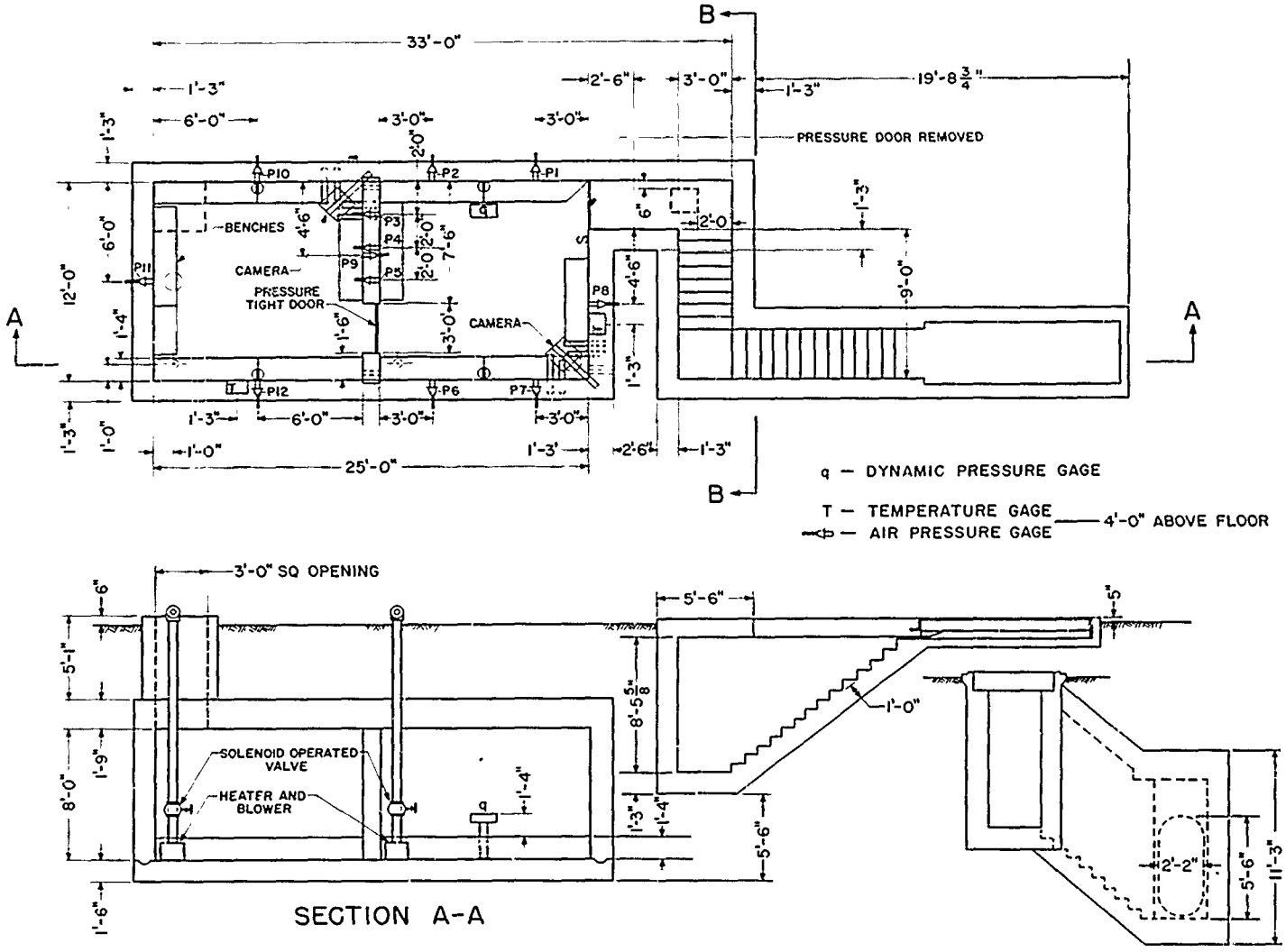

Fig. 1.19—Plan and section of underground personnel shelter (biomedical), Apple I and Apple II shots; Stations 4-34.3 b-1 and 1-34.3 b-2.

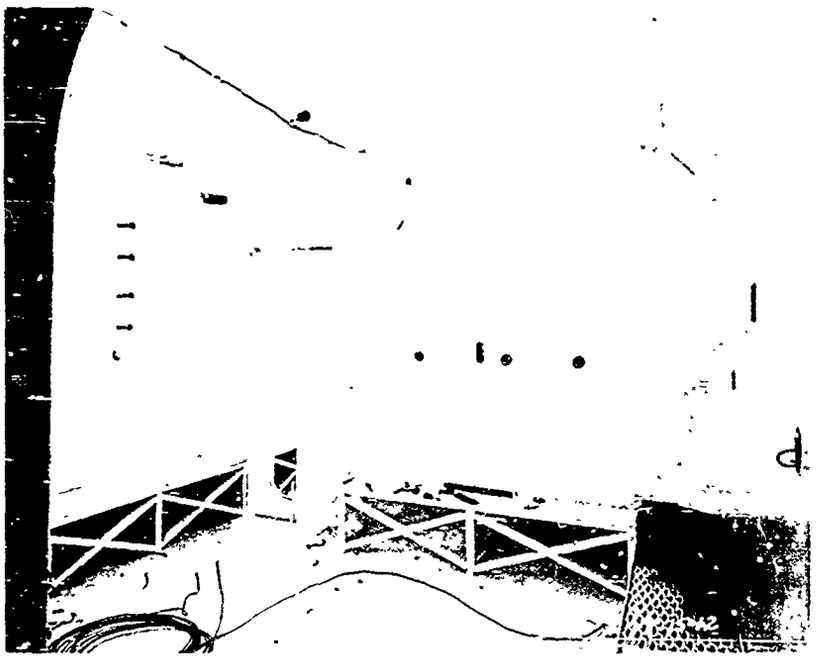

Fig. 1.20—Fast-fill room of partitioned underground personnel shelter; Station 4-34.3 b-1.

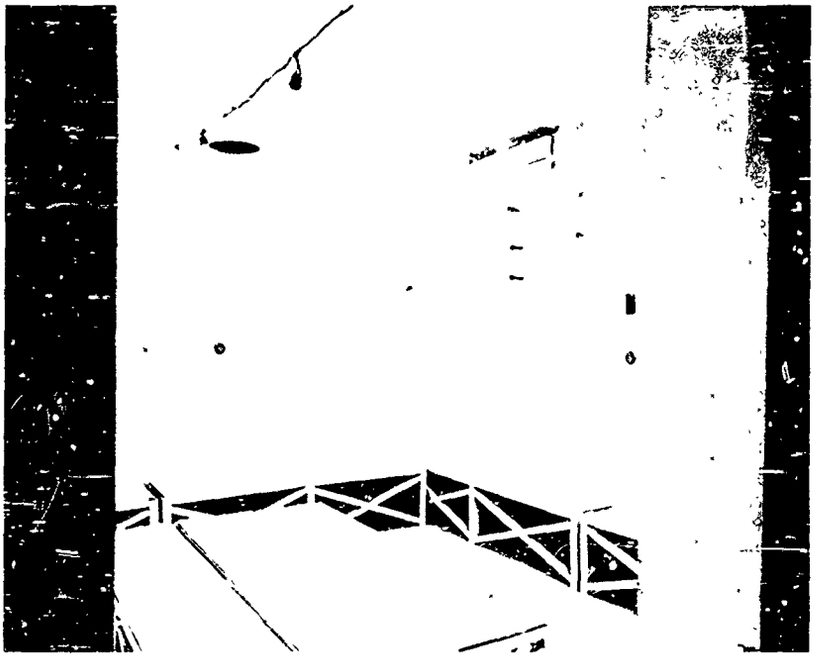

Fig. 1.21—Slow-fill room of partitioned underground personnel shelter· Station 4-34.3 b-1.

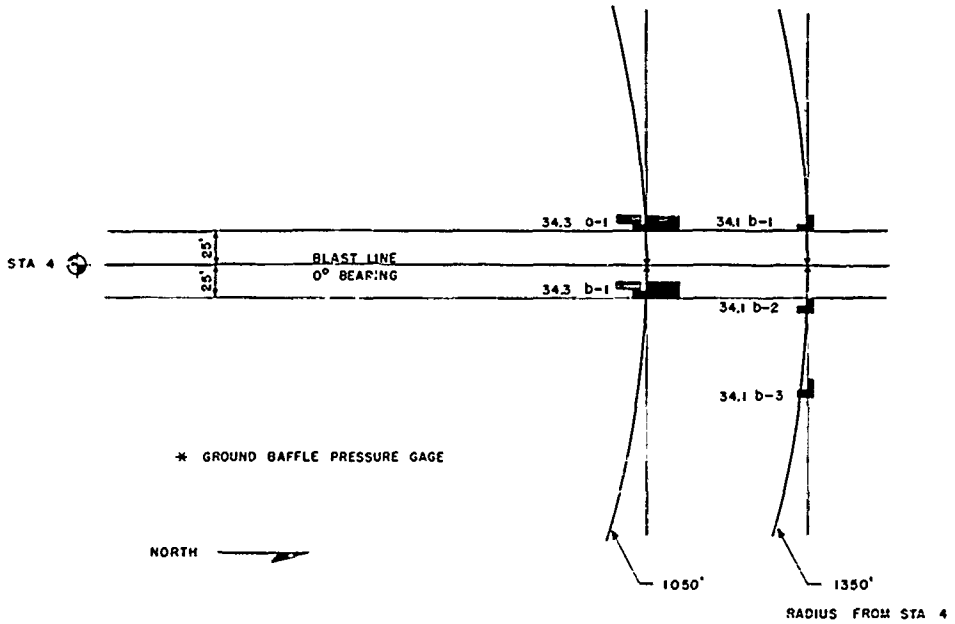

Fig. 1.22—Location of test structures for Apple I shot.

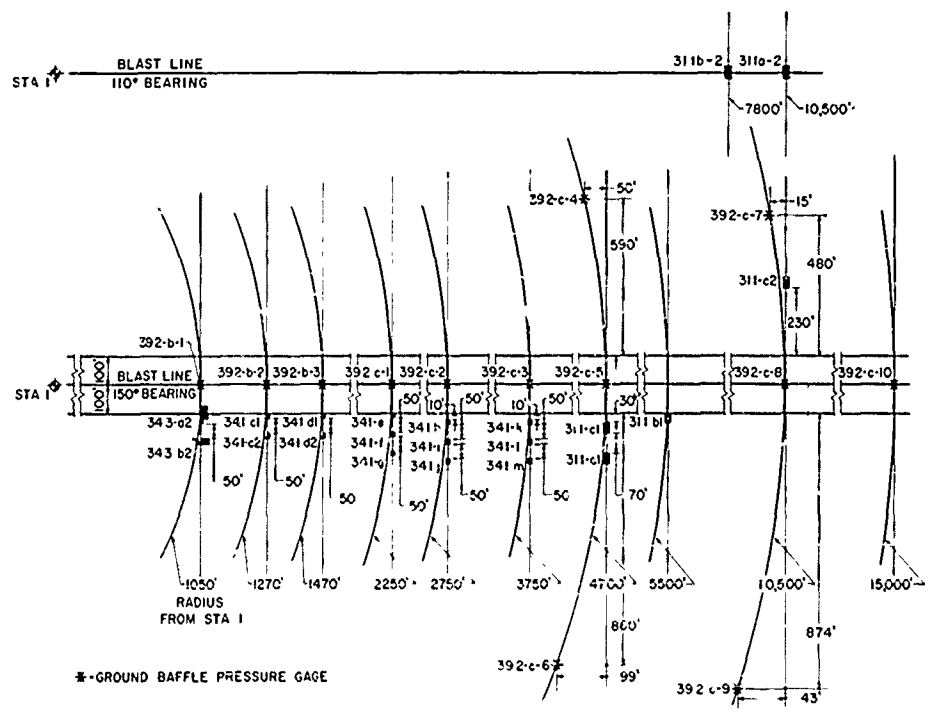

Fig. 1.23—Location of test structures for Apple II shot.

CHAPTER 2

NUCLEAR RADIATION PENETRATION

2.1 RADIATION DETECTORS

Gamma radiation was measured with film dosimeters developed by the National Bureau of Standards.[1] Each dosimeter contained five film types of overlapping ranges. Where radiation intensity was expected to be high, low-range film was replaced with very high range film.

Gold, sulfur, germanium,[2] and chemical neutron[3] threshold detectors were used. Gold detectors give an index of the number of neutrons per square centimeter in that portion of the energy spectrum up to 4 ev. Sulfur detectors range above 3 Mev. Germanium detectors cover the range above 1000 ev, with readings based on the permanent change in electrical conductivity of germanium caused by a neutron flux. Single-phase chemical dosimeters have a greater sensitivity to fast neutrons (0.5 to 8.0 Mev) than do two-phase types. Hence, if both types of chemical dosimeters are irradiated by a mixture of fast neutrons and gammas, either radiation can be estimated with reasonable accuracy.[3]

For locations and readings of dosimeters placed in the shelters, see Figs. 2.10 through 2.18 and Tables 2.2 through 2.17. Neutron measurements were not made in utility or indoor family type shelters.

2.2 INCIDENT RADIATION

2.2.1 Gamma Radiation

Project 39.6 measured incident gamma radiation,[4] and values of the dosimeters give plots of incident gamma radiation vs distance for Apple I and Apple II shots (Fig. 2.1). Incident gamma radiation on Apple I was measured along a 90 and a 290° line; the shelters were located on a 150° line. Because the direction of fall-out was 325°, the radiation measured along the 90° line is probably more nearly that on the shelter line and hence was used in Fig. 2.1.

2.2.2 Neutron Radiation

Program 32 measured incident neutron radiation. On Apple I shot sulfur and gold detectors were placed at only two locations. Averages of those buried 4 in. at each location were used to determine plots of incident radiation, Fig. 2.2.

On Apple II shot detectors were placed at six distances out to 5500 ft. Detectors at the two closer stations were buried 4 in., and the last two were at or near ground surface. The solid line for sulfur detectors in Fig. 2.3 was chosen as the most accurate representation of the fast-neutron radiation. This presupposes that the differences between the solid and dashed lines are due to attenuation through 4 in. of soil and that the difference in the third station is due to reduction of fast neutrons by the masonry shelter.

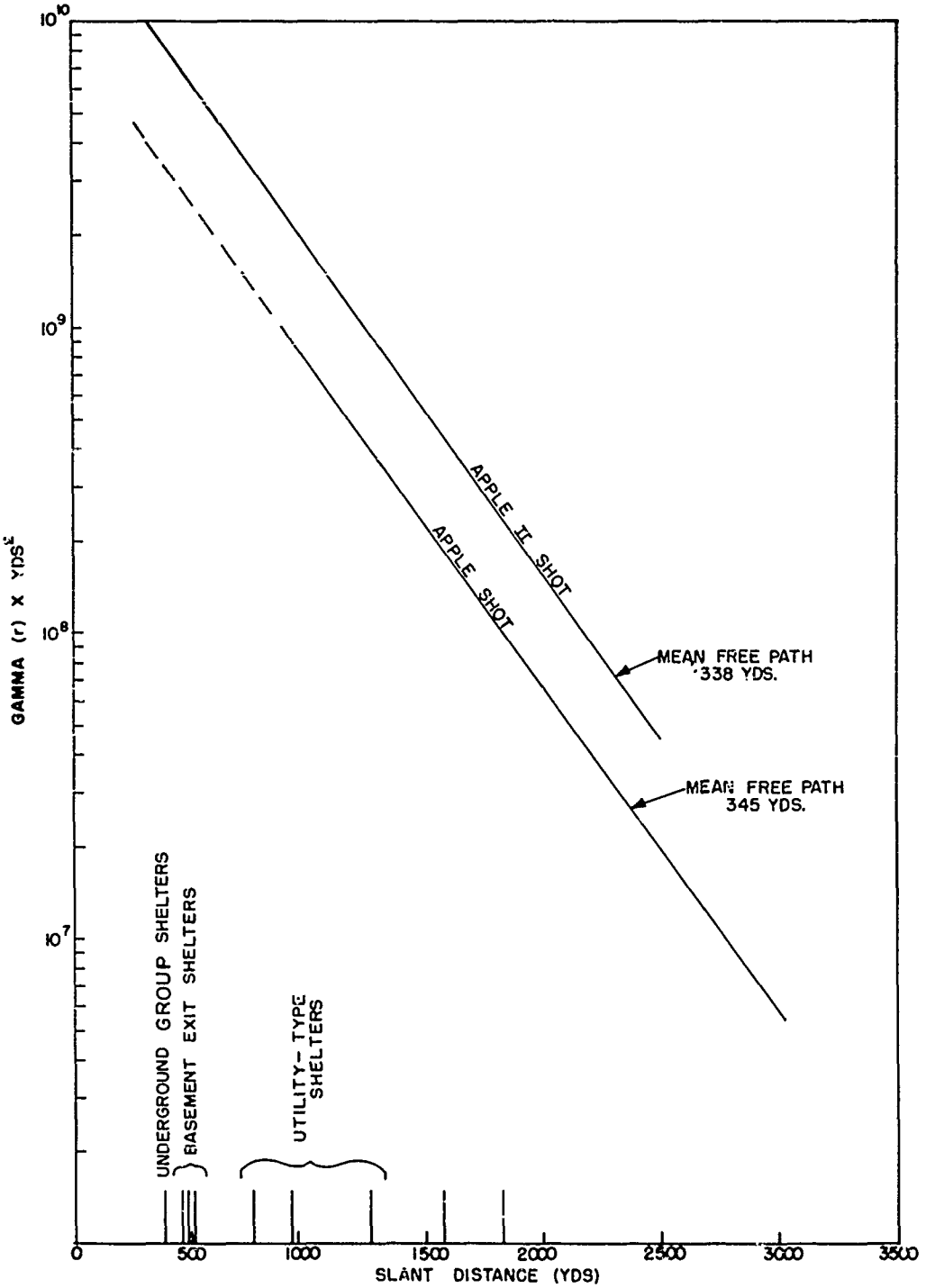

Fig. 2.1 — Incident gamma radiation vs distance.

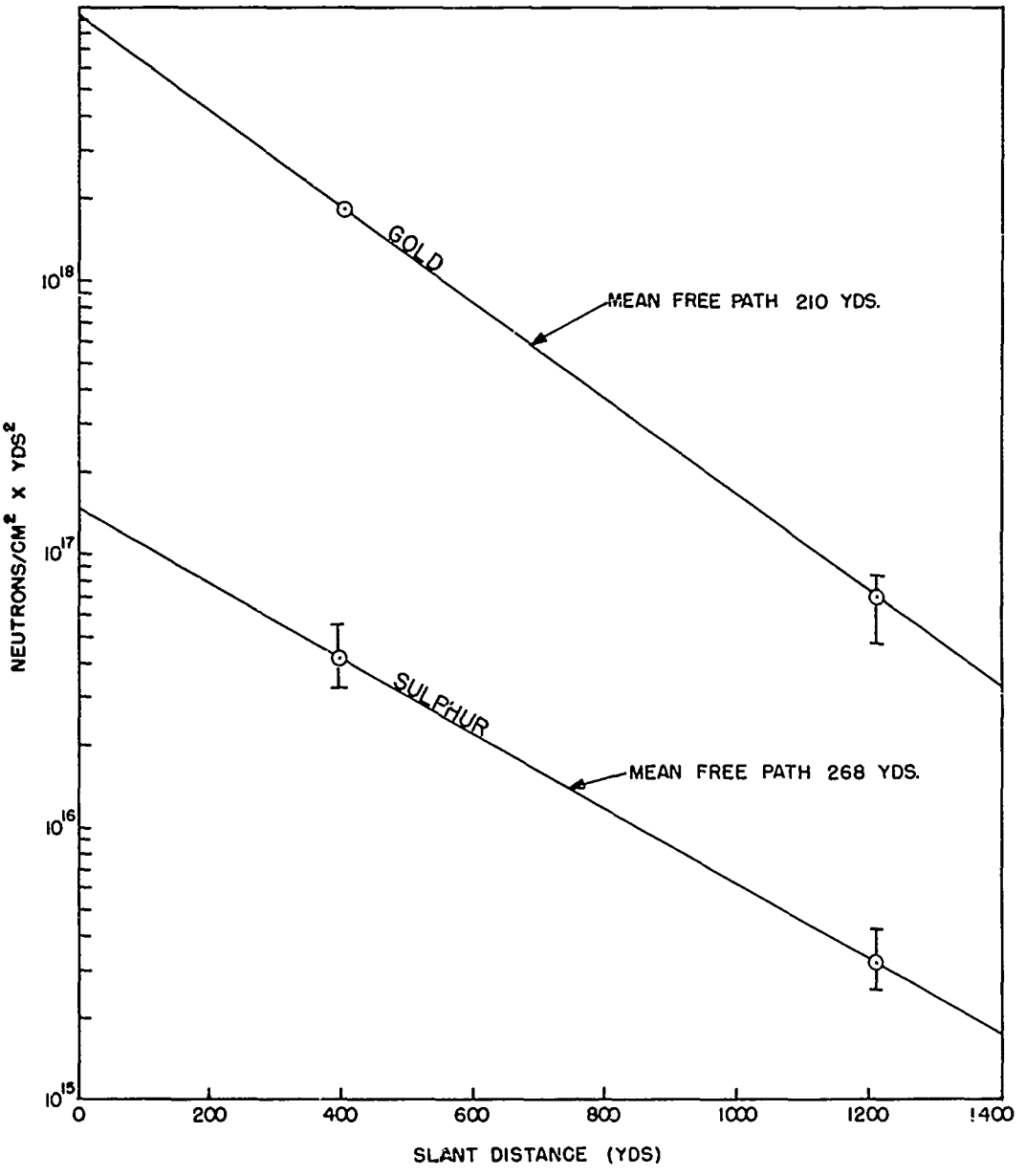

Fig. 2.2—Incident neutron radiation, Apple I shot.

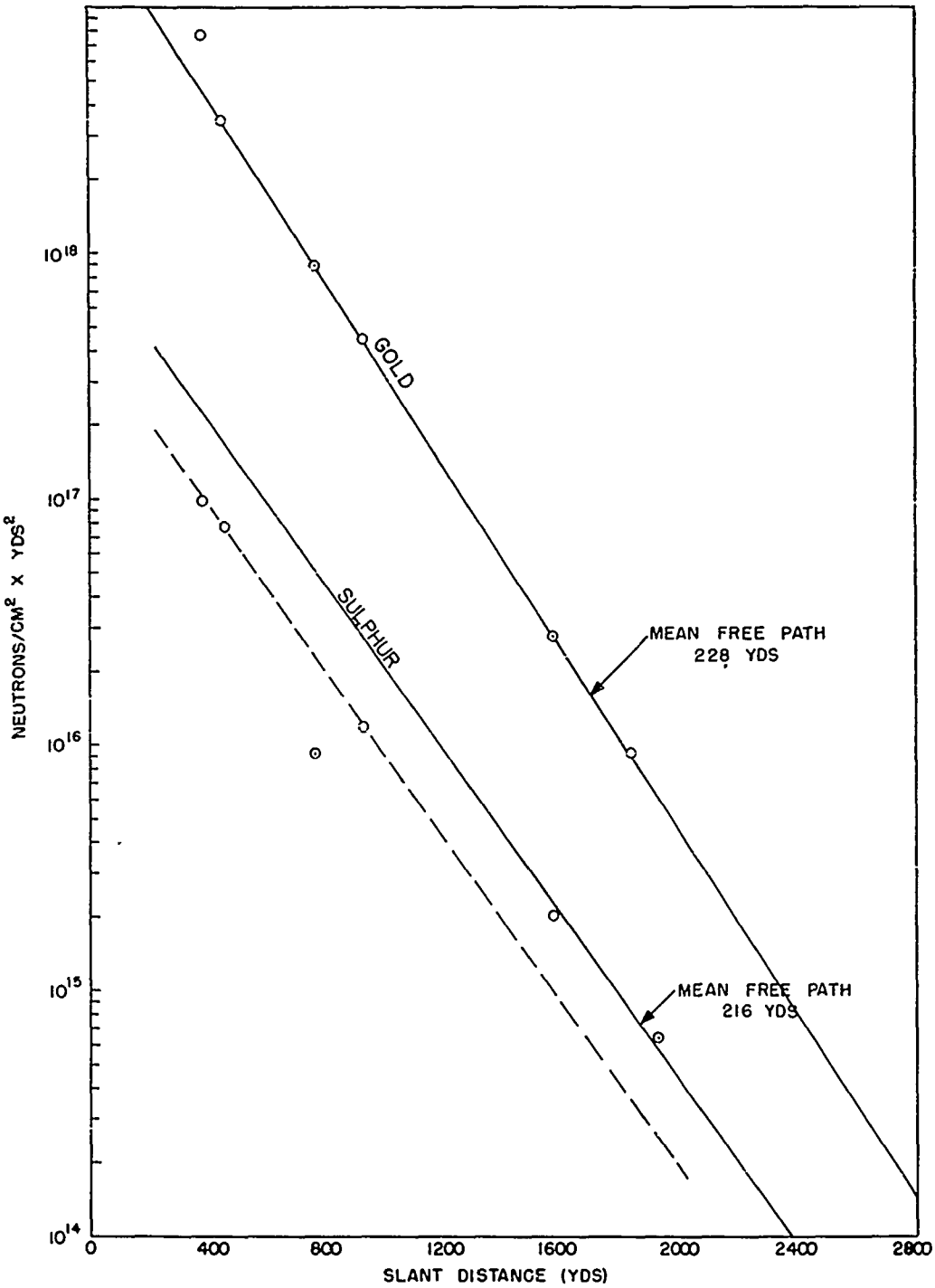

Fig. 2.3—Incident neutron radiation, Apple II shot.

It is interesting to note that for thermal neutrons the flux inside the masonry shelter is consistent with measurements outside the shelters at other distances. It may be that any slow neutrons that were filtered out in passing through the concrete were replaced by an equal number degraded from those starting through at higher energies or that some of those which penetrated the shelter bounced around so that they had more than one chance to be captured by the detector.

2.3 UNDERGROUND PERSONNEL SHELTER (STRUCTURAL)

2.3.1 Shot Apple I (Station 4-34.3 a-1)

Gamma film dosimeters were recovered at H + 5 hr, and therefore the readings show total gamma dosage for 5 hr plus the radiation the dosimeters recorded while being removed from the area. Since the minimum reading is 0.6 r, no more could have been received during recovery, and the amount was probably much less. Attenuation of radiation intensity from 8500 r at the first riser to 5 r at the outside of the steel door indicates the high degree of effectiveness of the entrance configuration (Fig. 2.4). Total readings inside the shelter were all 1 r or less, except on the inside surface of the door. There seems to be no significant increase in intensity directly under the escape hatch. The reading of 4.1 to 4.4 r at the inside face of the Navy type door indicates that there is a small portion of the shelter floor area directly adjacent to the entrance where the radiation intensity is relatively high compared with the remainder of the shelter (Fig. 2.4).

A reading (1.72×10^8 neutrons/cm^2) was obtained only from the sulfur detector in this shelter.

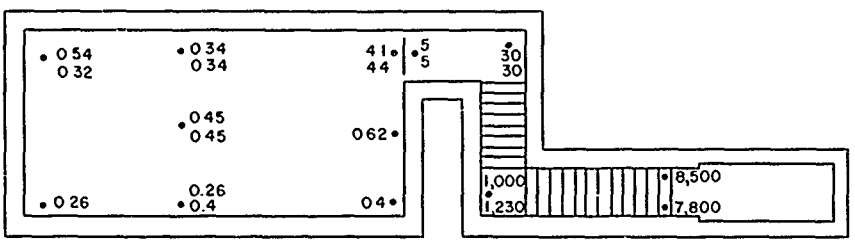

Fig. 2.4 — Gamma radiation (in roentgens) in underground personnel shelter (structural), Apple I shot; Station 4-34.3 a-1, 1050 ft.

2.3.2 Shot Apple II (Station 1-34.3 a-2)

Gamma radiation inside the closed shelter (Fig. 2.5) was nearly five times that inside the corresponding Apple I shelter, whereas the incident radiation was only about 2.5 times that on Apple I shot. Although gamma-radiation levels inside the shelter were low, it would be interesting to know whether there is a true increase in interior radiation with the increase in incident or whether the dosimeters were merely reading a contribution from thermal neutrons inside the shelter. It is reported that the film dosimeter records 4×10^9 thermal neutrons as 1 r (of Co^{60} gamma rays).[5] Thermal-neutron flux inside these shelters was below this value (4×10^8 was the highest), but, since gamma-radiation levels were always below 2 r, it is possible that this small flux could have made a fractional contribution which could account for the increase.

Three pairs of neutron detectors were placed in this shelter. The sulfur readings were 2×10^6 neutrons/cm^2 at the west (entrance) end of the main room, 2.94×10^7 at the center, and 4.01×10^8 at the east end. Gold readings were 7.75×10^8, 8.85×10^8, and 2.33×10^8 at the same locations.[a]

[a] The gold detector at one position was lost.

Readings of sulfur detectors are particularly interesting since a layer of boron-containing colemanite was spread on the ground surface above the west half of the main room but not over the east half. Detectors placed 4 in. under the colemanite did not show any noticeable reduction in the fast-neutron flux, but they showed a reduction in the thermal-neutron flux to about one-half that where there was no colemanite. The reduction of fast neutrons inside the shelter in relation to the placement of colemanite is probably only coincidental.

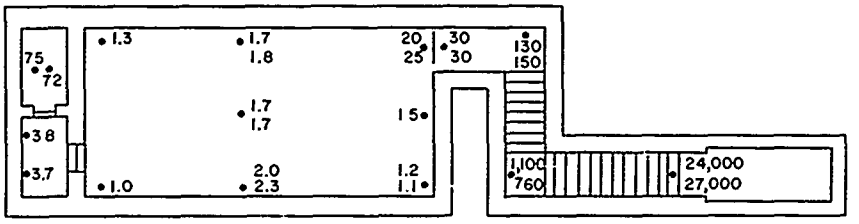

Fig. 2.5—Gamma radiation (in roentgens) in underground personnel shelter (structural), Apple II shot; Station 1-34.3 a-2, 1050 ft.

2.4 UNDERGROUND PERSONNEL SHELTER (BIOMEDICAL)

2.4.1 Shot Apple I (Station 4-34.3 b-1)

Film dosimeters were recovered at approximately H+5 hr, and the readings (Fig. 2.6) represent the same total dose as described for Station 4-34.3 a-1. Incident gamma radiation was about 23,000 r (Fig. 2.1); yet the readings of dosimeters in clear line-of-sight locations are considerably less, probably because of the inability of the film packet to record high levels of radiation and because of the shielding from side scattering of the incident radiation. The average of three readings at the landing of this shelter was more than three times the average of the readings at the same location on the closed shelter (4-34.3 a-1). This is a measure of the effectiveness of the reinforced-concrete sliding door covering the closed shelter. Values of 5850 r at a point 1 ft from the roof and 3470 r at a point 1 ft from the floor in the same wall are consistent with the amount of line-of-sight shielding supplied by the stair-well roof and the

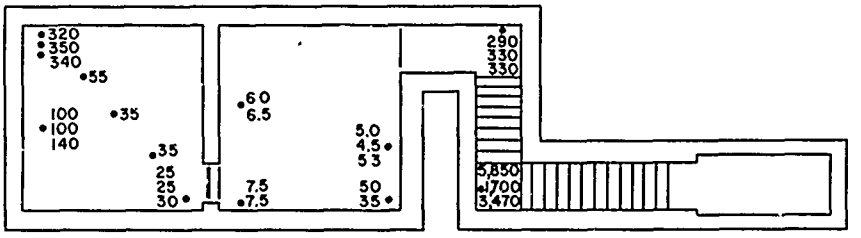

Fig. 2.6—Gamma radiation (in roentgens) in underground personnel shelter (biomedical), Apple I shot; Station 4-34.3 b-1, 1050 ft.

stairs and earth, respectively. The value at the point between (1700 r) should be higher (closer to 17,000) than either of the other two since incident radiation is estimated at 23,000 r; hence an error in transcription of the value has been assumed. In the structural shelter the reading at the foot of the stairs is significantly reduced from those at the first landing. Readings in the fast-fill chamber indicate a radiation level of 5 to 10 r. The camera mounted directly under a ventilation pipe in the fast-fill side received total gamma radiation of about 50 r, which can be attributed to the radiation scatter from the ventilation pipe.

Gamma-radiation intensity in the slow-fill side varied from about 340 r directly under the escape-hatch opening to 25 r at the diagonally opposite corner. The radiation gradient in this chamber plus the generally higher level of radiation when compared with the fast-fill chamber can be attributed to the amount of radiation scatter from the escape-hatch opening.

A reading (7.18×10^8 neutrons/cm^2) was obtained from the only sulfur neutron detector in this shelter. It should be noted that the fast-neutron flux was about four times greater than in the closed shelter on the same shot.

2.4.2 Shot Apple II (Station 1-34.3 b-2)

Gamma radiation inside (Fig. 2.7) varied from 30 to 70 r in the fast-fill chamber and from 190 to 1000 r in the slow-fill side. Estimated incident radiation (Fig. 2.1) is 57,000 r; thus the 50,000 r measured in the stair well is nearly the full incident dose.

Both fast- and slow-neutron fluxes were greater immediately below the open escape hatch of the slow-fill chamber than at the foot of the entrance stairs, and the slow-neutron flux was greater by a larger factor than the fast-neutron flux.

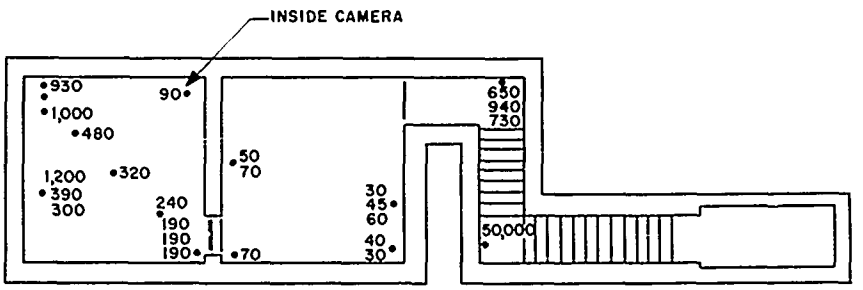

Fig. 2.7 — Gamma radiation (in roentgens) in underground personnel shelter (biomedical), Apple II shot; Station 1-34.3 b-2, 1050 ft.

2.5 BASEMENT EXIT SHELTERS

2.5.1 Shot Apple I (Stations 4-34.1 b-1, b-2, b-3)

Gamma radiation was attenuated toward the closed end of the shelter (Fig. 2.8). It is shown in Fig. 2.8 that the doors, by keeping the contaminated dirt out of the shelter, were relatively effective in reducing radiation intensity. The average radiation reading at the first riser for the completely open shelter was 7125 r; for the partially open shelter, 6725 r; and for the completely closed shelter, about 5525 r. Ratios of these intensities are consistent with those which existed all along the shelter interiors and can be attributed to the amount of earth that was blown into the open and partially open shelters. Incident radiation is estimated (Fig. 2.1) to be 12,000 r. No successful neutron measurements were made.

2.5.2 Shot Apple II (Stations 1-34.1 c-1, c-2, d-1, d-2)

In general, gamma-radiation patterns were similar to those on Apple I, with somewhat higher internal radiation (Fig. 2.9). Incident radiation is estimated (Fig. 2.1) to be 35,000 r for shelters at 1270 ft and 23,500 r for those at 1470 ft. Even though the doors failed on the closed shelters, they remained in place long enough to keep out some of the contaminated materials so that the general radiation level in the closed shelters was one-half or one-third that in the open shelters.

Neutron detectors show a lower neutron flux inside the closed shelters than inside the open shelters.

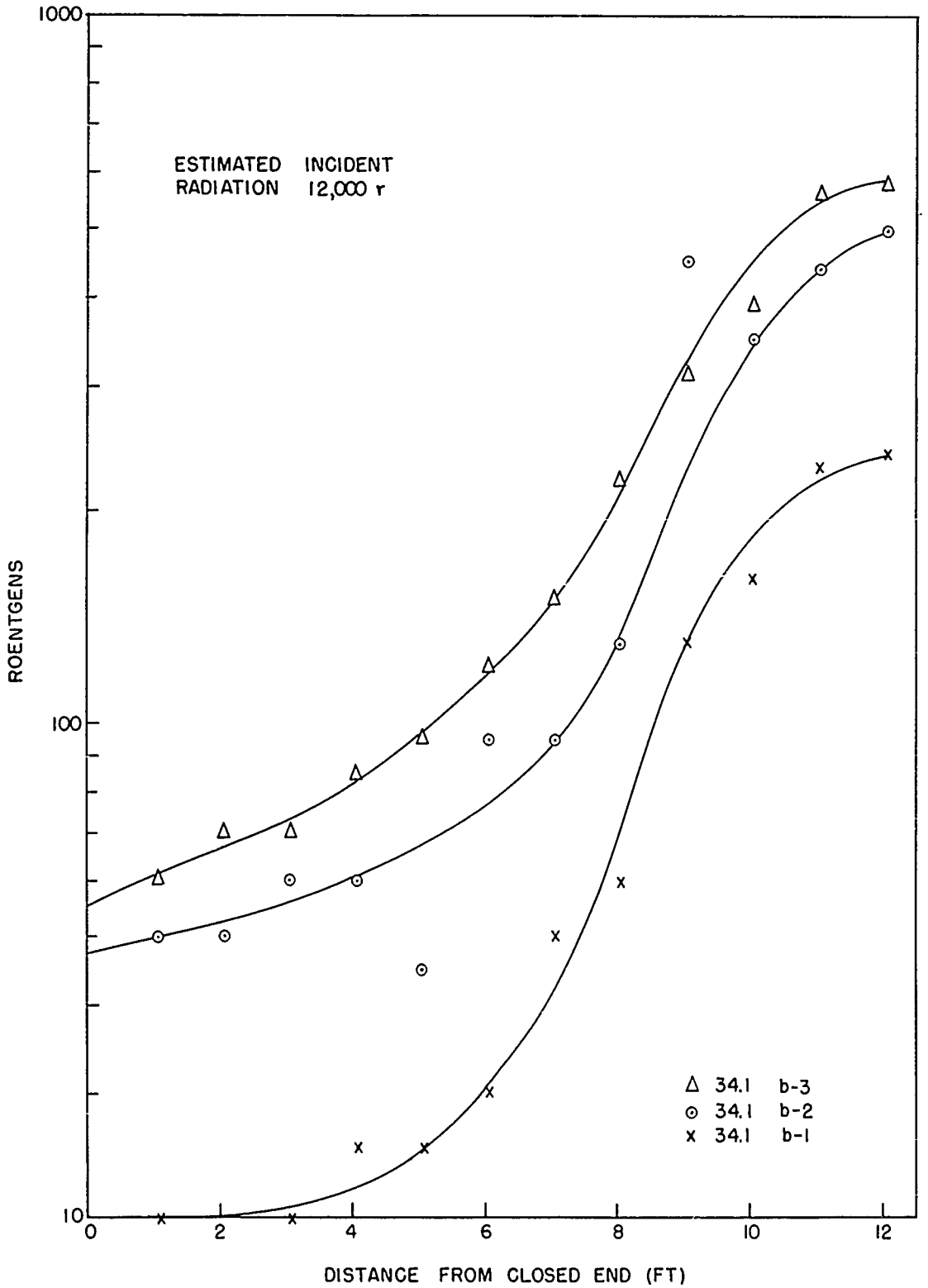

Fig. 2.8—Gamma radiation in basement exit shelters, Apple I shot; Stations 4-34.1 b-1, b-2, and b-3, 1350 ft.

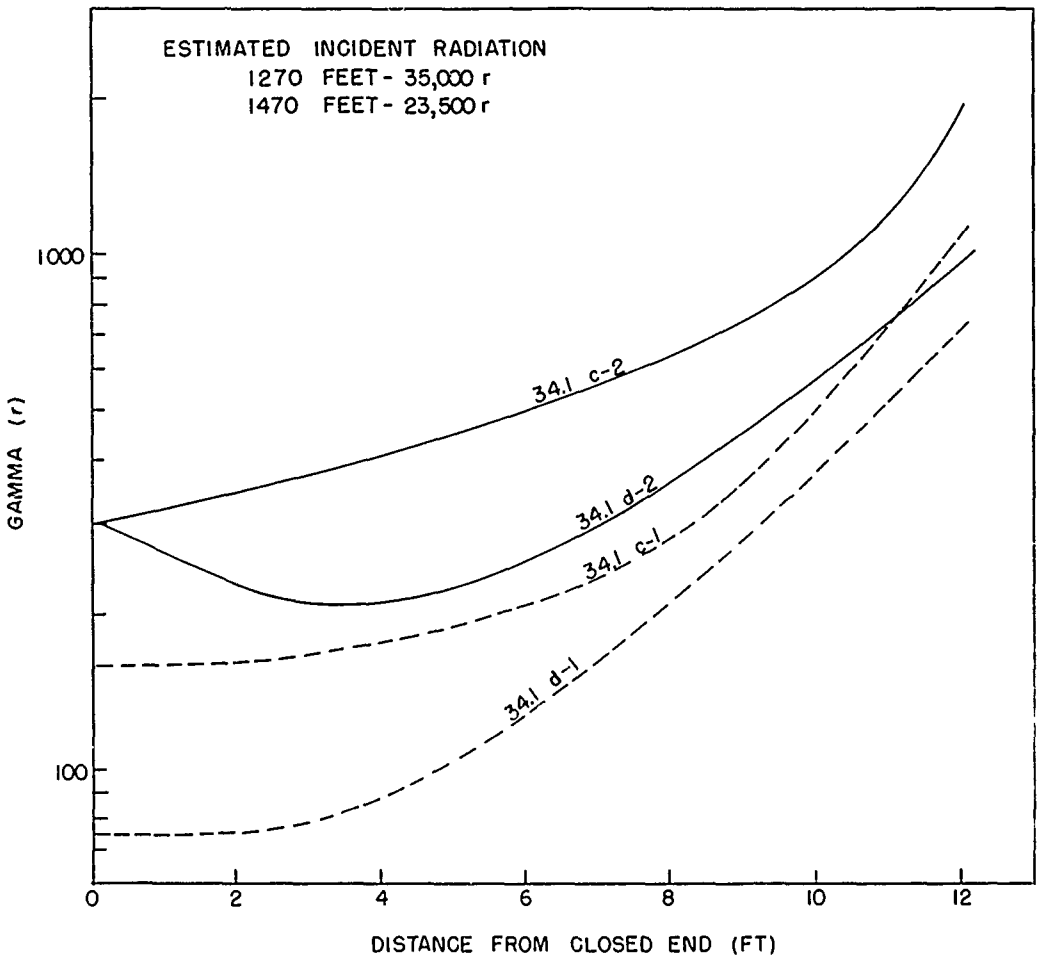

Fig. 2.9—Gamma radiation in basement exit shelters, Apple II shot; Stations 1-34.1 c-1 and c-2, 1270 ft; Stations 1-34.1 d-1 and d-2, 1470 ft.

2.6 UTILITY TYPE SHELTERS

2.6.1 Shot Apple II (Stations 1-34.1 c to m)

Shelters located at 2250, 2750, and 3750 ft were subjected to an estimated (Fig. 2.1) incident gamma radiation of 5750, 2600, and 630 r, respectively. For each, the average radiation (average of all film packets) inside each shelter showed gamma radiation to be one-half to one-third that outside.

Program 32 placed neutron detectors only in the masonry block shelter, which was destroyed. As pointed out earlier, thermal neutrons measured by the gold detector were the same as would have been expected outside, whereas fast neutrons were only one-fifth of those to be expected outside (Fig. 2.3).

2.7 INDOOR FAMILY TYPE SHELTERS

2.7.1 Shot Apple II

The averages of gamma-radiation measurements inside the shelters and incident radiation estimated from Fig. 2.1 are shown in Table 2.1.

Table 2.1—AVERAGE GAMMA RADIATION INSIDE FAMILY TYPE SHELTERS

Ground distance, ft	Estimated incident radiation, r	Basement lean-to, r	Basement corner room, r	Basement concrete room, r	Reinforced-concrete bathroom, r
4,700	180	6.7	26.00		51.00
5,500	70	2.48	21.00	1.77	
7,800	11	0.67	1.22	0.20	
10,500	0.3	0.10	0.13		0.24

REFERENCES

1. M. Ehrlich, Delayed Gamma-ray Measurements: Film Dosimeter Measurements, Operation Greenhouse Report, WT-81, May 1952.
2. B. Cassen et al., Measurement and Permanent Recording of Fast Neutrons by Effects on Semiconductors, Operation Teapot Report, WT-1170.
3. G. V. Taplin et al., Measurement of Initial and Residual Radiations by Chemical Methods, Operation Teapot Report, ITR-1171 (to be superseded by WT-1171).
4. L. J. Deal, Gamma and Neutron Radiation Measurements, Operation Teapot Report, ITR-1174 (to be superseded by WT-1174).
5. P. S. Harris, Physical Measurement of Neutron and Gamma Radiation Dose from High Neutron Yield Weapons and Correlation of Dose with Biological Effect, Operation Teapot Report, ITR-1167 (to be superseded by WT-1167).

Table 2.2 — UNDERGROUND PERSONNEL SHELTER (STRUCTURAL)
Apple I shot, Station 4-34.3 a-1 (1050 ft)

Film dosimeters

Pt.	Location	Dosimeter No.[a]	Reading, r
1	Center of top riser, west	41415-H	7800
1	Center of top riser, east	41414-H	8500
2	4 ft above floor slab, 1 ft from wall	41413-H	1000
2	4 ft above floor slab, 2 ft from wall	41412-H	1230
3	4 ft above floor slab, 1 ft from wall	41153	30
3	4 ft above floor slab, 2 ft from wall	41152	30
4	Mid-point of door, outside	41151	5
4	Mid-point of door, outside	41150	5
5	Mid-point of door, inside	41149	4.1
5	Mid-point of door, inside	41148	4.4
6	4 ft above floor slab	41147	0.4
7	4 ft above floor slab	41146	0.4
7	4 ft above floor slab	41145	0.26
8	4 ft above floor slab	41144	0.26
9	Mid-point of undersurface of escape hatch	41143	0.54
9	Floor slab directly under escape-hatch mid-point	41142	0.32
10	4 ft above floor slab	41141	0.34
10	4 ft above floor slab	41140	0.34
11	Roof slab	41139	0.45
11	Floor slab	41138	0.45
12	Against effluent side of commercial type dust-stop filter	41137	0.62

Neutron detectors

Pt.	Location	Type	No.	Reading
3	On floor	Gold	524	Lost
		Sulfur	390	1.72×10^8

[a] High-range dosimeters are indicated by an "H" following the dosimeter number.

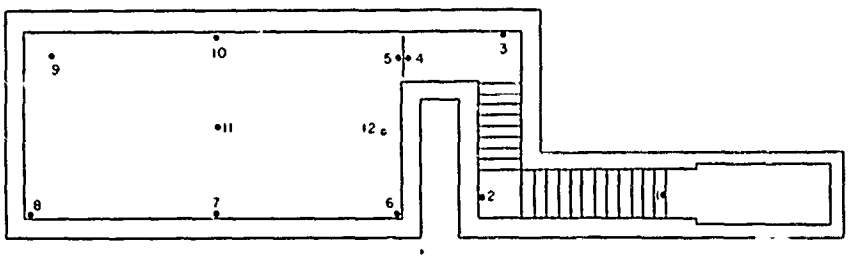

Fig. 2.10 — Film dosimeter and neutron detector locations in underground personnel shelter (structural), Apple I shot; Station 4-34 [illegible] -1, 1050 ft.

Table 2.3 — UNDERGROUND PERSONNEL SHELTER (STRUCTURAL)
Apple II shot, Station 1-34.3 a-2 (1050 ft)

Film dosimeters

Pt.	Location	Dosimeter No.[a]	Reading, r
1	Center of top riser	45821-H	24,000
1	Center of top riser	45822-H	27,000
2	1 ft above floor slab	45823-H	1,100
2	4 ft above floor slab	45824-H	760
3	1 ft above floor slab	45825-H	130
3	4 ft above floor slab	45826-H	150
4	Mid-point of door, outside	42473	30
4	Mid-point of door, outside	42474	30
5	Mid-point of door, inside	42471	20
5	Mid-point of door, inside	42472	25
6	4 ft above floor slab	42475	1.3
7	4 ft above floor slab	42476	2.0
7	4 ft above floor slab	42477	2.3
8	4 ft above floor slab	42478	1.0
9	4 ft above floor slab	42479	1.2
9	On floor slab directly under escape-hatch mid-point	42480	1.1
10	4 ft above floor slab	42481	1.8
10	4 ft above floor slab	42482	1.7
11	At roof slab	42483	1.7
11	On floor slab	42484	1.7
12	Mid-point of wall	42485	1.5
13	5 ft above floor slab, 2 ft in from side wall	42486	3.7
14	5 ft above floor slab, 2 ft in from partition	42487	3.8
15	On top of filter	42488	7.5
16	On top of filter	42489	7.2

Neutron detectors

Pt.	Location	Type	No.	Reading
17	At floor slab	Sulfur	157	4.01×10^8
17	At floor slab	Gold	557–558	Lost
10	At floor slab	Chemical (single phase)	12	
10	At floor slab	Chemical (double phase)	23	
10	At floor slab	Sulfur	150	2.94×10^7
10	At floor slab	Gold	623–624	2.33×10^8
11	At floor slab	Chemical (single phase)	13	
11	At floor slab	Chemical (double phase)	25	
18	At floor slab	Sulfur	154	$< 2 \times 10^6$
18	At floor slab	Gold	549–550	7.75×10^8
18	At floor slab	Chemical (single phase)	10	
18	At floor slab	Chemical (double phase)	22	

[a]High-range dosimeters are indicated by an "H" following the dosimeter number.

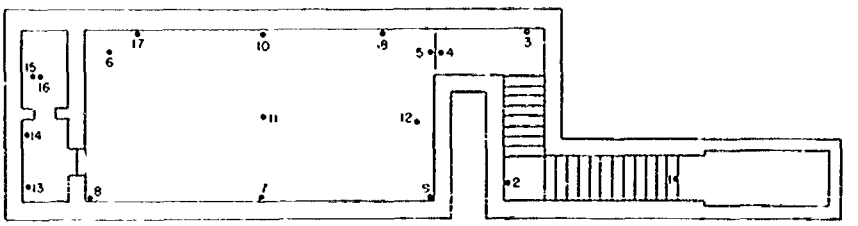

Fig. 2.11 — Film dosimeter and neutron detector locations in underground personnel shelter (structural), Apple II shot; Station 1-34.3 a-2, 1050 ft.

Table 2.4 — UNDERGROUND PERSONNEL SHELTER (BIOMEDICAL)
Apple I shot, Station 4-34.3 b-1 (1050 ft)

Film dosimeters

Pt.	Location	Dosimeter No.[a]	Reading, r
1	Intersection of roof and wall	41411-H	5850
1	4 ft above floor	41410-H	1700
1	Intersection of wall and floor	41409-H	3470
2	Intersection of roof and wall	41408-H	290
2	4 ft above floor	41407-H	330
2	Intersection of wall and floor	41406-H	330
3	Under bench	41096	5
3	Under bench	41095	4.5
3	Under bench	41094	5.3
4	On camera mount	41093	50
4	On camera mount	41092	35
5	Under seat	41136	6
5	Under seat	41135	6.5
6	On vent pipe	41134	7.5
6	On vent pipe	41133	7.5
7	At roof	41132	55
8	At roof	41131	35
9	At roof	41130	35
10	At floor 6 in. from side wall	41129	320
11	At floor 1 ft 6 in. from side wall	41128	350
12	At floor 2 ft 6 in. from side wall	41127	340
13	Under bench	41126	100
13	Under bench	41125	100
13	Under bench	41124	140
14	At intersection of roof and wall	41123	25
14	3 ft 6 in. above floor	41122	30
14	1 ft above floor	41121	25

Neutron detectors

Pt.	Location	Type	No.	Reading
2	On floor	Gold	521	Lost
		Sulfur	389	7.18×10^8

[a]High-range dosimeters are indicated by an "H" following the dosimeter number.

Table 2.5 — UNDERGROUND PERSONNEL SHELTER (BIOMEDICAL)
Apple II shot, Station 1-34.3 b-2 (1050 ft)

Film dosimeters

Pt.	Location	Dosimeter No.[a]	Reading, r
1	Intersection of roof and wall	45827-H	Lost
1	4 ft above floor	45828-H	Lost
1	Intersection of wall and floor	45829-H	50,000
2	Intersection of roof and wall	45830-H	650
2	4 ft above floor	42490	940
2	Intersection of wall and floor	42831	730
3	Under bench	42832	30
3	Under bench	42833	45
3	Under bench	42834	60
4	On camera mount, inside	42835	40
4	On camera mount, outside	42836	30
5	Under seat	42837	50
5	Under seat	42838	70
6	On vent pipe	42839	70
6	On vent pipe	42840	Lost
7	At roof	42891	480
8	At roof	42892	320
9	At roof	42893	240
10	At floor 6 in. from side wall	42894	930
11	At floor 1 ft 6 in. from side wall	42895	Lost
12	At floor 2 ft 6 in. from side wall	42896	1,000
13	Under bench	42897	1,200
13	Under bench	42898	390
13	Under bench	42899	300
14	Intersection of roof and wall	42900	190
14	3 ft 6 in. above floor	42901	190
14	1 ft 0 in. above floor	42902	190
15	Camera mount, inside	43900	90
15	Camera mount, outside	43927	Lost

Neutron detectors

Pt.	Location	Type	No.	Reading
1	Upper part of entry, south wall	Germanium	290	b
1	Upper part of entry, south wall	Germanium	291	b
1	Upper part of entry, south wall	Germanium	292	b
1	Upper part of entry, south wall	Germanium	293	b
1	Upper part of entry, south wall	Germanium	294	b
2	Lower part of entry, west wall	Germanium	285	b
2	Lower part of entry, west wall	Germanium	286	b

Table 2.5 — (Continued)

Pt.	Location	Type	No.	Reading
2	Lower part of entry, west wall	Germanium	287	b
2	Lower part of entry, west wall	Germanium	288	b
2	Intersection of wall and floor	Sulfur	152	1.62×10^{9}
2	Intersection of wall and floor	Gold	551–552	1.03×10^{11}
3	Intersection of wall and roof	Chemical (single phase)	14	
3	Intersection of wall and roof	Chemical (double phase)	20	
3	Under bench	Chemical (single phase)	15	
3	Under bench	Chemical (double phase)	24	
11	Below escape hatch on floor	Chemical (single phase)	11	
11	Below escape hatch on floor	Chemical (double phase)	21	
11	Below escape hatch on floor	Sulfur	181	5.03×10^{9}
11	Below escape hatch on floor	Gold	621–622	8.56×10^{11}
11	Below escape hatch on floor	Germanium	283	b
11	Below escape hatch on floor	Germanium	284	b

[a] High-range dosimeters are indicated by an "H" following the dosimeter number.
[b] Results inconclusive (see Report WT-1170, reference 2).

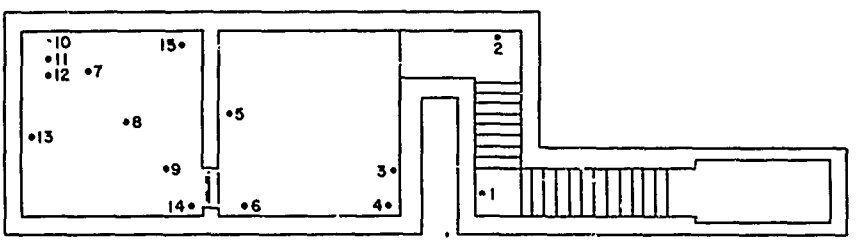

Fig. 2.12 — Film dosimeter and neutron detector locations in underground personnel shelter (biomedical). Apple I and Apple II shots; Stations 4-34.3 b-1 and 1-34.3 b-2, 1050 ft.

Table 2.6—BASEMENT EXIT SHELTER (CLOSED)
Apple I shot, Station 4-34.1 b-1 (1350 ft)

Film dosimeters

Pt.	Location	Dosimeter No.[a]	Reading, r
1	Center of top riser, west	41557-H	5,300
1	Center of top riser, east	41556-H	5,750
2	Undersurface of wooden door between doors 2 and 3, west	41555-H	17,900
2	Undersurface of wooden door between doors 2 and 3, east	41554-H	27,500
3	Undersurface of wooden door at mid-point of door 3, west	41553-H	15,000
3	Undersurface of wooden door at mid-point of door 3, east	41552-H	26,500
4	Intersection of roof and wall 1 ft 1 in. from far end	41120	20
5	Intersection of roof and wall 2 ft 1 in. from far end	41119	20
6	Intersection of roof and wall 3 ft 1 in. from far end	41118	20
7	Intersection of roof and wall 4 ft 1 in. from far end	41117	25
8	Intersection of roof and wall 5 ft 1 in. from far end	41116	25
9	Intersection of roof and wall 6 ft 1 in. from far end	41115	30
10	Intersection of roof and wall 7 ft 1 in. from far end	41114	50
11	Intersection of roof and wall 8 ft 1 in. from far end	41113	60
12	Intersection of roof and wall 9 ft 1 in. from far end	41551-H	130
13	Intersection of roof and wall 10 ft 1 in. from far end	41550-H	160
14	Intersection of roof and wall 11 ft 1 in. from far end	41543-H	230
15	Intersection of roof and wall 12 ft 1 in. from far end	41548-H	240

Neutron detectors

Pt.	Location	Type	No.	Reading
15	Foot of stairs, far wall	Gold	1039–1040	Lost
		Sulfur	388	Lost

[a]High-range dosimeters are indicated by an "H" following the dosimeter number.

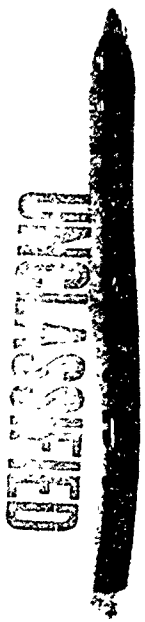

Table 2.7 — BASEMENT EXIT SHELTER (PARTIALLY CLOSED)
Apple 1 shot, Station 4-34.1 b-2 (1350 ft)

Film dosimeters

Pt.	Location	Dosimeter No.[a]	Reading, r
1	Center of top riser, west	41547-H	6900
1	Center of top riser, east	41546-H	6550
4	Intersection of roof and wall 1 ft 1 in. from far end	41112	50
5	Intersection of roof and wall 2 ft 1 in. from far end	41111	50
6	Intersection of roof and wall 3 ft 1 in. from far end	41110	60
7	Intersection of roof and wall 4 ft 1 in. from far end	41109	60
8	Intersection of roof and wall 5 ft 1 in. from far end	41108	45
9	Intersection of roof and wall 6 ft 1 in. from far end	41107	95
10	Intersection of roof and wall 7 ft 1 in. from far end	41106	95
11	Intersection of roof and wall 8 ft 1 in. from far end	41105	130
12	Intersection of roof and wall 9 ft 1 in. from far end	41545-H	450
13	Intersection of roof and wall 10 ft 1 in. from far end	41544-H	350
14	Intersection of roof and wall 11 ft 1 in. from far end	41543-H	440
15	Intersection of roof and wall 12 ft 1 in. from far end	41542-H	500

Neutron detectors

Pt.	Location	Type	No.	Reading
15	Foot of stairs, far wall	Gold	523	Lost
		Sulfur	387	Lost

[a]High-range dosimeters are indicated by an "H" following the dosimeter number.

Table 2.8 — BASEMENT EXIT SHELTER (OPEN)
Apple 1 shot, Station 4-34.1 b-3 (1350 ft)

Film dosimeters

Pt.	Location	Dosimeter No.[a]	Reading, r
1	Center of top riser, west	41541-H	7750
1	Center of top riser, east	41420-H	6500
4	Intersection of roof and wall 1 ft 1 in. from far end	41104	60
5	Intersection of roof and wall 2 ft 1 in. from far end	41103	70
6	Intersection of roof and wall 3 ft 1 in. from far end	41102	70
7	Intersection of roof and wall 4 ft 1 in. from far end	41101	85
8	Intersection of roof and wall 5 ft 1 in. from far end	41100	95
9	Intersection of roof and wall 6 ft 1 in. from far end	41099	120
10	Intersection of roof and wall 7 ft 1 in. from far end	41098	150
11	Intersection of roof and wall 8 ft 1 in. from far end	41097	220
12	Intersection of roof and wall 9 ft 1 in. from far end	41419-H	310
13	Intersection of roof and wall 10 ft 1 in. from far end	41418-H	390
14	Intersection of roof and wall 11 ft 1 in. from far end	41417-H	560
15	Intersection of roof and wall 12 ft 1 in. from far end	41416-H	580

Neutron detectors

Pt.	Location	Type	No.	Reading
15	Foot of stairs, far wall	Gold	522	Lost
		Sulfur	391	Lost

[a]High-range dosimeters are indicated by an "H" following the dosimeter number.

Table 2.9—BASEMENT EXIT SHELTER (CLOSED)
Apple II shot, Station 1-34.1 c-1 (1270 ft)

Film dosimeters

Pt.	Location	Dosimeter No.[a]	Reading, r
1	Center of top riser	46131-H	52,000
1	Center of top riser	46132-H	55,000
2	Undersurface of wooden door between doors 2 and 3	45831-H	70,000
2	Undersurface of wooden door between doors 2 and 3	45832-H	56,000
3	Undersurface of wooden door, mid-point of door 3	45833-H	Lost
3	Undersurface of wooden door, mid-point of door 3	45834-H	Lost
4	Intersection of roof and wall 1 ft 1 in. from far end	42903	160
5	Intersection of roof and wall 2 ft 1 in. from far end	42904	160
6	Intersection of roof and wall 3 ft 1 in. from far end	42905	170
7	Intersection of roof and wall 4 ft 1 in. from far end	42906	190
8	Intersection of roof and wall 5 ft 1 in. from far end	42907	220
9	Intersection of roof and wall 6 ft 1 in. from far end	42908	210
10	Intersection of roof and wall 7 ft 1 in. from far end	42909	230
11	Intersection of roof and wall 8 ft 1 in. from far end	42910	290
12	Intersection of roof and wall 9 ft 1 in. from far end	45835-H	370
13	Intersection of roof and wall 10 ft 1 in. from far end	45836-H	650
14	Intersection of roof and wall 11 ft 1 in. from far end	45837-H	640
15	Intersection of roof and wall 12 ft 1 in. from far end	45838-H	1,330

Neutron detectors

Pt.	Location	Type	No.	Reading
15	At floor slab	Sulfur	156	3.76×10^{10}
15	At floor slab	Gold	559–560	2.00×10^{12}

Apple II shot, Station 1-34.1 d-1 (1470 ft)

Film dosimeters

Pt.	Location	Dosimeter No.[a]	Reading, r
1	Center of top riser	45839-H	24,000
1	Center of top riser	45840-H	32,000
2	Undersurface of wooden door between doors 2 and 3	45841-H	Lost
2	Undersurface of wooden door between doors 2 and 3	45842-H	Lost
3	Undersurface of wooden door at mid-point of door 2	45843-H	Lost

Table 2.9— (Continued)

Pt.	Location	Dosimeter No.[a]	Reading, r
3	Undersurface of wooden door at mid-point of door 2	45844-H	150,000[b]
4	Intersection of roof and wall 1 ft 1 in. from far end	42911	75
5	Intersection of roof and wall 2 ft 1 in. from far end	42912	75
6	Intersection of roof and wall 3 ft 1 in. from far end	42913	75
7	Intersection of roof and wall 4 ft 1 in. from far end	42914	90
8	Intersection of roof and wall 5 ft 1 in. from far end	42915	100
9	Intersection of roof and wall 6 ft 1 in. from far end	42916	130
10	Intersection of roof and wall 7 ft 1 in. from far end	42917	170
11	Intersection of roof and wall 8 ft 1 in. from far end	42918	200
12	Intersection of roof and wall 9 ft 1 in. from far end	45845-H	290
13	Intersection of roof and wall 10 ft 1 in. from far end	45846-H	380
14	Intersection of roof and wall 11 ft 1 in. from far end	45847-H	600
15	Intersection of roof and wall 12 ft 1 in. from far end	45848-H	560

Neutron detectors

Pt.	Location	Type	No.	Reading
15	At floor slab	Sulfur	155	1.92×10^{10}
15	At floor slab	Gold	547–548	1.18×10^{12}

[a]High-range dosimeters are indicated by an "H" following the dosimeter number.
[b]Extrapolated and reading doubtful.

Table 2.10—BASEMENT EXIT SHELTER (OPEN)
Apple II shot, Station 1-34.1 c-2 (1270 ft)

Film dosimeters

Pt.	Location	Dosimeter No.[a]	Reading, r
1	Center of top riser	45849-H	56,000
1	Center of top riser	45850-H	
4	Intersection of roof and wall 1 ft 1 in. from far end	42919	310
5	Intersection of roof and wall 2 ft 1 in. from far end	42920	370
6	Intersection of roof and wall 3 ft 1 in. from far end	42921	370
7	Intersection of roof and wall 4 ft 1 in. from far end	42922	460
8	Intersection of roof and wall 5 ft 1 in. from far end	42923	500
9	Intersection of roof and wall 6 ft 1 in. from far end	42924	430
10	Intersection of roof and wall 7 ft 1 in. from far end	42925	Lost
11	Intersection of roof and wall 8 ft 1 in. from far end	42926	720
12	Intersection of roof and wall 9 ft 1 in. from far end	45851-H	730
13	Intersection of roof and wall 10 ft 1 in. from far end	45852-H	950
14	Intersection of roof and wall 11 ft 1 in. from far end	45853-H	1,150
15	Intersection of roof and wall 12 ft 1 in. from far end	45854-H	Lost

Neutron detectors

Pt.	Location	Type	No.	Reading
15	At floor slab	Sulfur	158	5.43×10^{10}
15	At floor slab	Gold	555–556	Lost

Apple II shot, Station 1-34.1 d-2 (1470 ft)

Film dosimeters

Pt.	Location	Dosimeter No.[a]	Reading, r
1	Center of top riser	45855-H	35,000
1	Center of top riser	45856-H	32,000
4	Intersection of roof and wall 1 ft 1 in. from far end	42928	270
5	Intersection of roof and wall 2 ft 1 in. from far end	42929	250
6	Intersection of roof and wall 3 ft 1 in. from far end	42930	190
7	Intersection of roof and wall 4 ft 1 in. from far end	42931	220
8	Intersection of roof and wall 5 ft 1 in. from far end	42932	220
9	Intersection of roof and wall 6 ft 1 in. from far end	42933	290

Table 2.10 — (Continued)

Pt.	Location	Dosimeter No.[a]	Reading, r
10	Intersection of roof and wall 7 ft 1 in. from far end	42934	270
11	Intersection of roof and wall 8 ft 1 in. from far end	42935	460
12	Intersection of roof and wall 9 ft 1 in. from far end	45857-H	2,100
13	Intersection of roof and wall 10 ft 1 in. from far end	45858-H	2,500
14	Intersection of roof and wall 11 ft 1 in. from far end	45859-H	730
15	Intersection of roof and wall 12 ft 1 in. from far end	45860-H	980

Neutron detectors

Pt.	Location	Type	No.	Reading
15	At floor slab	Sulfur	151	5.72×10^{10}
15	At floor slab	Gold	553–554	2.02×10^{12}

[a]High-level dosimeters are indicated by an "H" following the dosimeter number.

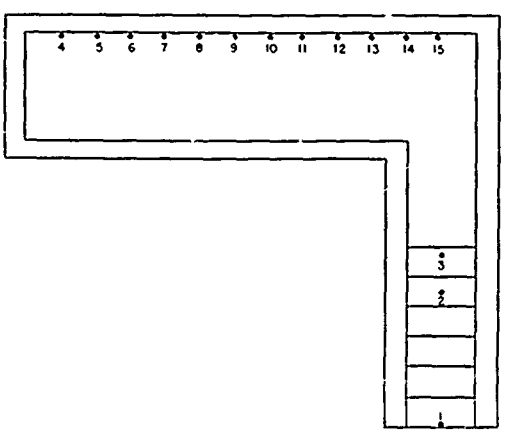

Fig. 2.13 — Film dosimeter and neutron detector locations in basement exit shelters, Apple I and Apple II shots; Stations 4-34.1 b-1, b-2, and b-3, Apple I shot, 1350 ft; 1-34.1 c-1 and c-2, Apple II shot, 1270 ft; 1-34.1 d-1 and d-2, Apple II shot, 1470 ft.

Table 2.11 — UTILITY SHELTER (FILM DOSIMETERS)
Apple II shot, 2250 ft

Pt.	Location	Dosimeter No.	Reading, r
	Station 1-34.1 e, reinforced-concrete precast		
1	Mid-point of blast door (exterior)	42936	Lost
2	Mid-point of blast door (interior)	42937	Lost
3	Mid-point of wall	42938	Lost
4	Mid-point of wall	42939	Lost
5	Mid-point of wall	42940	3300
6	Mid-point of roof, 1 ft 6 in. down	42941	Lost
6	Mid-point of roof, 3 ft 0 in. down	42942	Lost
6	Mid-point of roof, 4 ft 6 in. down	42943	2450
6	Mid-point of roof, 6 ft 0 in. down	42944	2200
	Station 1-34.1 f, reinforced-concrete poured-in-place		
1	Mid-point of blast door (exterior)	42945	5000
2	Mid-point of blast door (interior)	42946	2300
3	Mid-point of wall	42947	2450
4	Mid-point of wall	42948	1850
5	Mid-point of wall	42949	1900
6	Mid-point of roof, 1 ft 6 in. down	42950	2650
6	Mid-point of roof, 3 ft 0 in. down	42951	2650
6	Mid-point of roof, 4 ft 6 in. down	42952	2650
6	Mid-point of roof, 6 ft 0 in. down	42953	2650
	Station 1-34.1 g, masonry block		
1	Mid-point of blast door (exterior)	42954	Lost
2	Mid-point of blast door (interior)	42955	Lost
3	Mid-point of wall	42956	8000
4	Mid-point of wall	42957	Lost
5	Mid-point of wall	42958	6500
6	Mid-point of roof, 1 ft 6 in. down	42959	Lost
6	Mid-point of roof, 3 ft 0 in. down	42960	Lost
6	Mid-point of roof, 4 ft 6 in. down	42961	Lost
6	Mid-point of roof, 6 ft 0 in. down	42962	Lost

Table 2.12 — UTILITY SHELTER (FILM DOSIMETERS)
Apple II shot, 2750 ft

Pt.	Location	Dosimeter No.	Reading, r
	Station 1-34.1 h, reinforced-concrete precast		
1	Mid-point of blast door (exterior)	42974	1800
2	Mid-point of blast door (interior)	42975	1000
3	Mid-point of wall	42976	1650
4	Mid-point of wall	42977	890
5	Mid-point of wall	42978	1100
6	Mid-point of roof, 1 ft 6 in. down	42979	1250
6	Mid-point of roof, 3 ft 0 in. down	42980	1250
6	Mid-point of roof, 4 ft 6 in. down	42981	1250
6	Mid-point of roof, 6 ft 0 in. down	42982	1200
	Station 1-34.1 i, reinforced-concrete poured-in-place		
1	Mid-point of blast door (exterior)	42965	2200
2	Mid-point of blast door (interior)	42966	1050
3	Mid-point of wall	42967	1250
4	Mid-point of wall	42968	830
5	Mid-point of wall	42969	1080
6	Mid-point of roof, 1 ft 6 in. down	42970	1150
6	Mid-point of roof, 3 ft 0 in. down	42971	1120
6	Mid-point of roof, 4 ft 6 in. down	42972	1120
6	Mid-point of roof, 6 ft 0 in. down	42973	1000
	Station 1-34.1 j, masonry block		
1	Mid-point of blast door (exterior)	42651	1800
2	Mid-point of blast door (interior)	42652	Lost
3	Mid-point of wall	42653	1450
4	Mid-point of wall	42654	1000
5	Mid-point of wall	42655	1350
6	Mid-point of roof, 1 ft 6 in. down	42656	1350
6	Mid-point of roof, 3 ft 0 in. down	42657	1430
6	Mid-point of roof, 4 ft 6 in. down	42963	850
6	Mid-point of roof, 6 ft 0 in. down	42964	820

Table 2.13 — UTILITY SHELTER (FILM DOSIMETERS)
Apple II shot, 3750 ft

Pt.	Location	Dosimeter No.	Reading, r
	Station 1-34.1 k, reinforced-concrete precast		
1	Mid-point of blast door (exterior)	42983	420
2	Mid-point of blast door (interior)	42984	270
3	Mid-point of wall	42985	310
4	Mid-point of wall	42986	200
5	Mid-point of wall	42987	260
6	Mid-point of roof, 1 ft 6 in. down	42988	280
6	Mid-point of roof, 3 ft 0 in. down	42989	300
6	Mid-point of roof, 4 ft 6 in. down	42990	300
6	Mid-point of roof, 6 ft 0 in. down	42991	300
	Station 1-34.1 l, reinforced-concrete poured-in-place		
1	Mid-point of blast door (exterior)	42992	430
2	Mid-point of blast door (interior)	42993	220
3	Mid-point of wall	42994	320
4	Mid-point of wall	42995	200
5	Mid-point of wall	42996	280
6	Mid-point of roof, 1 ft 6 in. down	42997	280
6	Mid-point of roof, 3 ft 0 in. down	42998	320
6	Mid-point of roof, 4 ft 6 in. down	42999	290
6	Mid-point of roof, 6 ft 0 in. down	43000	290
	Station 1-34.1 m, masonry block		
1	Mid-point of blast door (exterior)	43001	490
2	Mid-point of blast door (interior)	43002	290
3	Mid-point of wall	43003	240
4	Mid-point of wall	43004	210
5	Mid-point of wall	43005	210
6	Mid-point of roof, 1 ft 6 in. down	43006	210
6	Mid-point of roof, 3 ft 0 in. down	43007	220
6	Mid-point of roof, 4 ft 6 in. down	43008	220
6	Mid-point of roof, 6 ft 0 in. down	43009	210

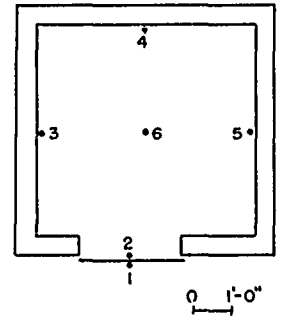

Fig. 2.14 — Film dosimeter locations in utility type shelters; Stations 1-34.1 e to m.

Table 2.14 — REINFORCED-CONCRETE BATHROOM SHELTER (FILM DOSIMETERS)

Pt.	Location	Dosimeter No.	Reading, r
	Apple II shot, Station 1-31.1 c-1 (4700 ft)		
1	Mid-height of door (exterior)	43976	Lost
2	Mid-height of door (interior)	43977	170
3	Intersection of roof and wall, 1 ft 0 in. from front wall	43978	30
4	Intersection of roof and wall, 3 ft 6 in. from front wall	43979	30
5	Intersection of roof and wall, 6 ft 0 in. from front wall	43980	25
6	Mid-point of shutter (interior)	43981	35
7	Mid-point of floor	43982	50
7	Mid-point of roof	43983	13.6
	Apple II shot, Station 1-31.1 c-2 (10,500 ft)		
1	Mid-height of door (exterior)	43984	0.5
2	Mid-height of door (interior)	43985	Lost
3	Intersection of roof and wall, 1 ft 0 in. from front wall	43986	0.21
4	Intersection of roof and wall, 3 ft 6 in. from front wall	43987	0.21
5	Intersection of roof and wall, 6 ft 0 in. from front wall	43988	0.17
6	Mid-point of shutter (interior)	43989	0.20
7	Mid-point of floor	43990	Lost
7	Mid-point of roof	43991	0.14

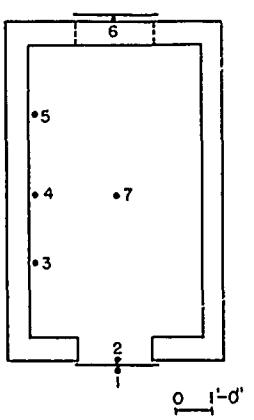

Fig. 2.15 — Film dosimeter locations in reinforced-concrete bathroom shelter in rambler houses; Stations 1-31.1 c-1 and c-2.

Table 2.15—BASEMENT REINFORCED-CONCRETE SHELTER (FILM DOSIMETERS)

Pt.	Location	Dosimeter No.	Reading, r
	Apple II shot, Station 1-31.1 b-1 (5500 ft)		
1	Mid-height of end wall along center line	43943	1.0
2	Intersection of roof and wall, 1 ft 0 in. from rear wall	43944	0.95
3	Intersection of roof and wall, 2 ft 0 in. from rear wall	43945	0.95
4	Intersection of roof and wall, 3 ft 0 in. from rear wall	43946	0.95
5	Intersection of roof and wall, 4 ft 0 in. from rear wall	43947	0.95
6	Intersection of roof and wall, 5 ft 0 in. from rear wall	43948	1.1
7	Intersection of roof and wall, 6 ft 0 in. from rear wall	43949	1.1
8	Intersection of roof and wall, 7 ft 0 in. from rear wall	43950	1.5
9	Intersection of roof and wall, 8 ft 0 in. from rear wall	43951	1.5
10	Intersection of roof and wall, 9 ft 0 in. from rear wall	43952	1.6
11	Intersection of roof and wall, 10 ft 0 in. from rear wall	43953	2.0
12	Mid-height of door (interior)	43955	7.6
13	Mid-height of door (exterior)	43956	12.0
	Apple II shot, Station 1-31.1 b-2 (7800 ft)		
1	Mid-height of end wall along center line	43899	0.18
2	Intersection of roof and wall, 1 ft 0 in. from rear wall	43901	0.1
3	Intersection of roof and wall, 2 ft 0 in. from rear wall	43902	0.1
4	Intersection of roof and wall, 3 ft 0 in. from rear wall	43903	0.18
5	Intersection of roof and wall, 4 ft 0 in. from rear wall	43904	0.23
6	Intersection of roof and wall, 5 ft 0 in. from rear wall	43905	0.27
7	Intersection of roof and wall, 6 ft 0 in. from rear wall	43906	0.18
8	Intersection of roof and wall, 7 ft 0 in. from rear wall	43907	0.15
9	Intersection of roof and wall, 8 ft 0 in. from rear wall	43908	0.15
10	Intersection of roof and wall, 9 ft 0 in. from rear wall	43909	0.20
11	Intersection of roof and wall, 10 ft 0 in. from rear wall	43910	0.27
12	Mid-height of door (interior)	43941	0.27
13	Mid-height of door (exterior)	43942	0.27

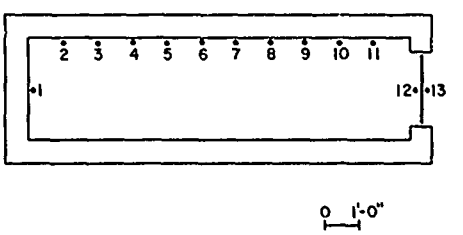

Fig. 2.16—Film dosimeter locations in basement reinforced-concrete room shelter in two-story frame houses; Stations 1-31.1 b-1 and b-2.

Table 2.16—BASEMENT CORNER-ROOM SHELTER (FILM DOSIMETERS)

Pt.	Location	Dosimeter No.	Reading, r
	Apple II shot, Station 1-31.1 a-1 (4700 ft)		
1	Intersection of roof and wall, 1 ft 6 in. from center line of wall	43997	12
2	Intersection of roof and wall, 6 in. from center line of wall	43998	12
3	Intersection of roof and wall, 6 in. from center line of wall	43999	12
4	Intersection of roof and wall, 1 ft 6 in. from center line of wall	44000	15
5	Intersection of roof and wall, 1 ft 6 in. from center line of wall	44061	25
6	Intersection of roof and wall, 6 in. from center line of wall	44062	30
7	Intersection of roof and wall, 6 in. from center line of wall	44063	30
8	Intersection of roof and wall, 1 ft 6 in. from center line of wall	44064	30
9	Intersection of roof and wall, 1 ft 6 in. from center line of wall	44065	40
10	Intersection of roof and wall, 6 in. from center line of wall	44066	40
11	Intersection of roof and wall, 6 in. from center line of wall	44067	45
12	Intersection of roof and wall, 1 ft 6 in. from center line of wall	44068	50
13	Mid-point of underside of roof	44069	40
14	Mid-point of floor along wall	44070	13
	Apple II shot, Station 1-31.1 a-2 (10,500 ft)		
1	Intersection of roof and wall, 1 ft 6 in. from center line of wall	44076	0.1
2	Intersection of roof and wall, 6 in. from center line of wall	44077	0.1
3	Intersection of roof and wall, 6 in. from center line of wall	44078	0.15
4	Intersection of roof and wall, 1 ft 6 in. from center line of wall	44079	0.1
5	Intersection of roof and wall, 1 ft 6 in. from center line of wall	44080	0 15
6	Intersection of roof and wall, 6 in. from center line of wall	44081	0.15
7	Intersection of roof and wall, 6 in. from center line of wall	44082	0.1
8	Intersection of roof and wall, 1 ft 6 in. from center line of wall	44083	0.15
9	Intersection of roof and wall, 1 ft 6 in. from center line of wall	44084	0.1
10	Intersection of roof and wall, 6 in. from center line of wall	44085	0.15
11	Intersection of roof and wall, 6 in. from center line of wall	44086	0.1
12	Intersection of roof and wall, 1 ft 6 in. from center line of wall	44087	0.18
13	Mid-point of underside of roof	44088	0.18
14	Mid-point of floor along wall	44089	0.15
	Apple II shot, Station 1-31.1 b-1 (5500 ft)		
1	Intersection of roof and wall, 1 ft 6 in. from center line of wall	43962	8.3
2	Intersection of roof and wall, 6 in. from center line of wall	43963	6.3
3	Intersection of roof and wall, 6 in. from center line of wall	43964	3.3
4	Intersection of roof and wall, 1 ft 6 in. from center line of wall	43965	3.3
5	Intersection of roof and wall, 1 ft 6 in. from center line of wall	43966	5.6
6	Intersection of roof and wall, 6 in. from center line of wall	43967	6.2
7	Intersection of roof and wall, 6 in. from center line of wall	43968	20.0

Table 2.16 — (Continued)

Pt.	Location	Dosimeter No.	Reading, r
	Apple II shot, Station 1-31.1 b-1 (5500 ft) (Continued)		
8	Intersection of roof and wall, 1 ft 6 in. from center line of wall	43969	14.0
9	Intersection of roof and wall, 1 ft 6 in. from center line of wall	43970	18.0
10	Intersection of roof and wall, 6 in. from center line of wall	43971	18.0
11	Intersection of roof and wall, 6 in. from center line of wall	43972	25.0
12	Intersection of roof and wall, 1 ft 6 in. from center line of wall	43973	25.0
13	Mid-point of underside of roof	43974	9.8
14	Mid-point of floor along wall	43975	4.4
	Apple II shot, Station 1-31.1 b-2 (7800 ft)		
1	Intersection of roof and wall, 1 ft 6 in. from center line of wall	43885	0.8
2	Intersection of roof and wall, 6 in. from center line of wall	43886	0.6
3	Intersection of roof and wall, 6 in. from center line of wall	43887	0.6
4	Intersection of roof and wall, 1 ft 6 in. from center line of wall	43888	0.7
5	Intersection of roof and wall, 1 ft 6 in. from center line of wall	43889	0.24
6	Intersection of roof and wall, 6 in. from center line of wall	43890	1.2
7	Intersection of roof and wall, 6 in. from center line of wall	43891	1.3
8	Intersection of roof and wall, 1 ft 6 in. from center line of wall	43892	1.6
9	Intersection of roof and wall, 1 ft 6 in. from center line of wall	43893	1.6
10	Intersection of roof and wall, 6 in. from center line of wall	43894	2.0
11	Intersection of roof and wall, 6 in. from center line of wall	43895	2.2
12	Intersection of roof and wall, 1 ft 6 in. from center line of wall	43896	2.5
13	Mid-point of underside of roof	43897	1.6
14	Mid-point of floor along wall	43898	0.2

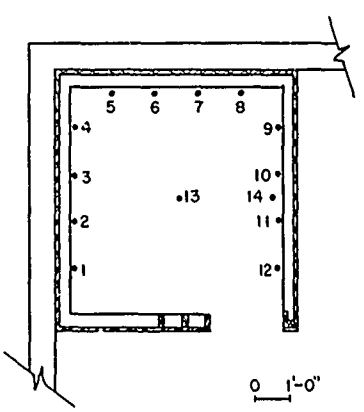

Fig. 2.17 — Film dosimeter locations in basement corner-room shelters in two-story houses; Stations 1-31.1 a-1, a-2, b-1, and b-2.

Table 2.17—BASEMENT LEAN-TO SHELTER (FILM DOSIMETERS)

Pt.	Location	Dosimeter No.	Reading, r
	Apple II shot, Station 1-31.1 a-1 (4700 ft)		
1	Mid-height of wall	43992	6.5
2	Underside of lean-to, 1 ft 6 in. from center line, mid-height of wall	43993	6.7
3	Underside of lean-to, 6 in. from center line, mid-height of wall	43994	6.7
4	Underside of lean-to, 6 in. from center line, mid-height of wall	43995	6.7
5	Underside of lean-to, 1 ft 6 in. from center line, mid-height of wall	43996	6.7
	Apple II shot, Station 1-31.1 a-2 (10,500 ft)		
1	Mid-height of wall	44071	< 0.1
2	Underside of lean-to, 1 ft 6 in. from center line, mid-height of wall	44072	< 0.1
3	Underside of lean-to, 6 in. from center line, mid-height of wall	44073	< 0.1
4	Underside of lean-to, 6 in. from center line, mid-height of wall	44074	< 0.1
5	Underside of lean-to, 1 ft 6 in. from center line, mid-height of wall	44075	< 0.1
	Apple II shot, Station 1-31.1 b-1 (5500 ft)		
1	Mid-height of wall	43957	2.2
2	Underside of lean-to, 1 ft 6 in. from center line, mid-height of wall	43958	3.2
3	Underside of lean-to, 6 in. from center line, mid-height of wall	43959	2.4
4	Underside of lean-to, 6 in. from center line, mid-height of wall	43960	2.4
5	Underside of lean-to, 1 ft 6 in. from center line, mid-height of wall	43961	2.2
	Apple II shot, Station 1-31.1 b-2 (7800 ft)		
1	Mid-height of wall	43010	0.18
2	Underside of lean-to, 1 ft 6 in. from center line, mid-height of wall	43881	0.22
3	Underside of lean-to, 6 in. from center line, mid-height of wall	43882	0.22
4	Underside of lean-to, 6 in. from center line, mid-height of wall	43883	0.22
5	Underside of lean-to, 1 ft 6 in. from center line, mid-height of wall	43884	2.5

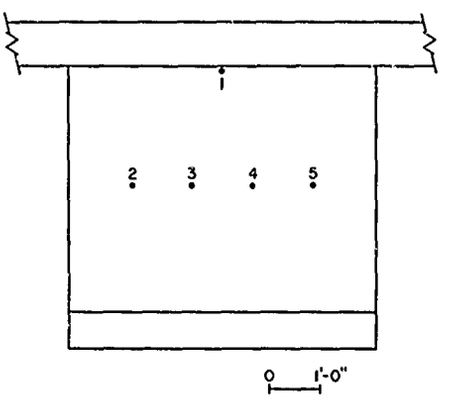

Fig. 2.18—Film dosimeter locations in basement lean-to shelters in two-story houses; Stations 1-31.1 a-1, a-2, b-1, b-2.

CHAPTER 3

THERMAL CONVECTION

3.1 PREDICTED TEMPERATURES

On Shots 1 and 8 of Operation Upshot-Knothole, temperature measurements were made in an underground shelter.[1] On Shot 1 only the measurement 14 ft from the entrance was successful, and this was considerably higher than that predicted from the peak reflected pressure by the Rankine-Hugoniot relation. On Shot 8 measured temperatures and those calculated from peak reflected pressures agreed near the rear of the shelter. The most logical explanation for the higher temperatures near the entrance was that air preheated by thermal radiation near the ground surface was being forced into the shelter during the positive phase and evacuated during the negative phase. This explanation is satisfactory for the Upshot-Knothole shelter since it was a tube about 7 ft in diameter and 48 ft long, with the door symmetrically located in one end wall. The ratio of chamber cross-section area to door area was only 2.65. The hot air entering the door at one end had relatively little chance to mix with ambient air before being discharged through the door. Further evidence that there was little mixing is the fact that the temperature during the negative phase fell below ambient in each of four successful measurements.

The door of the 12- by 12- by 8-ft Teapot shelter was not symmetrically located, and the ratio of chamber cross section to door area was over 8.0. Thus some mixing was to be expected, but the amount of mixing and, hence, whether the temperature would go below or return to ambient during the full pressure transient could not be anticipated. Teapot shelters were located in the 100-psi region, and one would hope to extrapolate Upshot-Knothole data from 8 and 20 psi to 100 psi by assuming no differences due to configuration. Because of the small size of the doorway with respect to shelter volume, it seemed reasonable that peak measured overpressures inside the shelter would be no greater than the expected incident overpressure.[a] This was later verified in results of shock-tube tests. Fourteen feet from the entrance of the Upshot-Knothole shelter on Shot 8, the measured temperature rise was less than twice that calculated for a peak measured overpressure of 8 psi. At the same point on Shot 1, the measured temperature rise was about $3\frac{3}{4}$ times that calculated for peak measured overpressure of 20 psi. If one assumes an extrapolated relation between measured and calculated temperatures for 100-psi reflected pressure, a measured temperature of between 3600 and 4500°C would be predicted.

Temperatures in the air measured inside the shelter are undoubtedly related to the preheated air outside the shelter. Inferred temperatures ahead of the shock front on Upshot-Knothole Shot 1 (reference 2) were scaled to 30 kt and are plotted as the long-dash line in Fig. 3.1.

[a] Here and throughout this report the phrase "incident overpressure" refers to that overpressure incident upon a structure whether it is in the region of Mach or regular reflection.

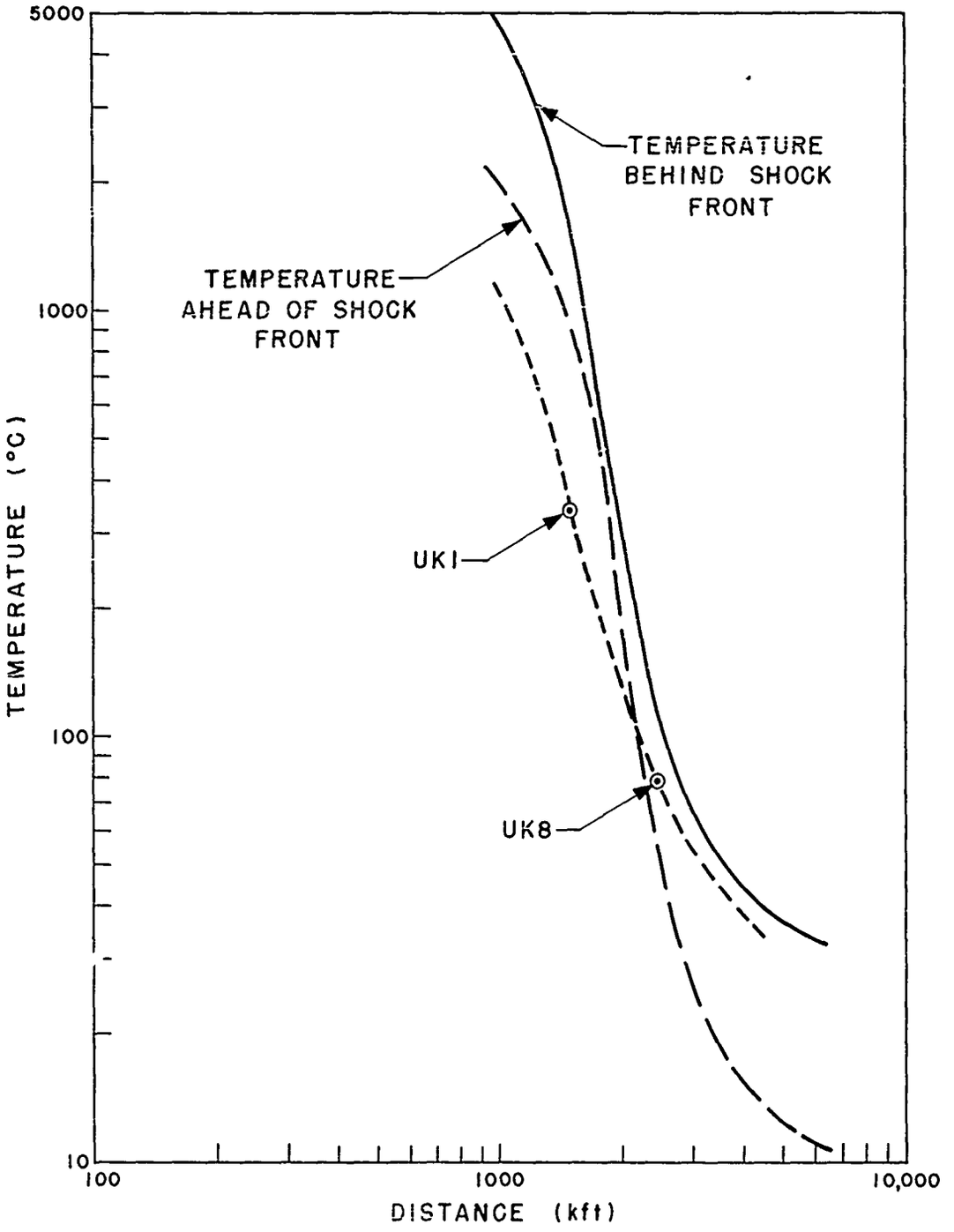

Fig. 3.1 — Temperature vs distance.

These are temperatures in the air immediately aboveground before shock arrival. With these temperatures as ambient, temperatures behind the shock front were calculated (solid line in Fig. 3.1). Note in Fig. 3.1 that at 1050 ft temperatures ahead of, and behind, the shock front outside the shelter bracket the earlier predicted 3600 and 4500°C. Hence the predictions are much too high. It would be logical to expect temperatures inside the shelter to be lower than outside temperatures but to have some relation to them. If one assumes that the Upshot-Knothole and Teapot shelters are similar in so far as the amount of preheated air is concerned, then the gradation from the outside to a point inside the entrance would be comparable. Thus, if Upshot-Knothole Shots 1 and 6 peak temperatures measured 14 ft inside the entrance were scaled to Apple II shot, they fall considerably below outside temperatures. If one assumes that there is an inside temperature vs distance curve which is a replica of that of temperature behind the shock outside, then the intercept with 1050 ft should be an approximation of the temperature expected for Apple II. Therefore, by shifting the solid curve in Fig. 3.1 so that it passes through the Upshot-Knothole data (short-dash line), a temperature of 1000°C was predicted at 1050 ft.

3.2 INSTRUMENTATION

Since predicted transient peak temperatures for Teapot had rise times faster than existing thermocouples would measure, a velocity-of-sound gauge, with known dependence of the velocity of sound on temperature, was used.[3] This gauge, still in an experimental stage and subject to failure, was used in pairs, one serving as backup for the other. This was fortunate since of eight gauges mounted in four positions one gauge in each position yielded a record which appeared satisfactory. It is probable that dust had an early effect on this gauge; even on those which gave apparently satisfactory records, the measurement was eventually affected by dust clogging the gauge orifice. None of the records was valid throughout the positive phase. There was an arrival time uncertainty which might have been as great as 40 msec, except for gauge 1B6 where the uncertainty was less than 1 msec.

Electronic instrumentation was not available for temperature measurements in other than the underground personnel shelters in Program 34. However, passive detecting devices such as were used in Upshot-Knothole shelters[4] were considered. They were not used because the predicted temperatures for Teapot were too low to register on the devices and because of the difficulty of interpreting them.

3.3 RESULTS

Records obtained on Apple I and Apple II shots are reproduced in Figs. 3.2 through 3.6. Errors involved in reducing the records are no greater than ±7 per cent of the temperature in degrees Kelvin. It is uncertain whether the "hash" [for example, gauge 2A2 (Fig. 3.6) between 240 and 310 msec] is a high-frequency temperature transient or a spurious reading caused by turbulence or dust. Such high-frequency transients would not have been noted before because thermocouples used on earlier tests are not capable of responding to small transient pulses in air. These transients, if they are real, are of such short duration that their contribution to burning of occupants is offset by equal downward transients, and the average is probably the only significant temperature. Peak temperatures in the shelters are shown in Table 3.1.

Gauge 1B6 (Fig. 3.5) has an early peak (250°C) at 230 msec, nearly 40 msec after arrival of the shock wave.

3.3.1 Underground Personnel Shelter (Biomedical)

(a) Shot Apple I (Station 4-34.3 b-1). The fast-fill room record appears valid (Fig. 3.2). Temperature arrival agrees with overpressure arrival, and the peak temperature occurs much later than the peak overpressure unless the temperature step at 343 msec is a shift due to dust. There is little confidence placed in either record from the slow-fill room.

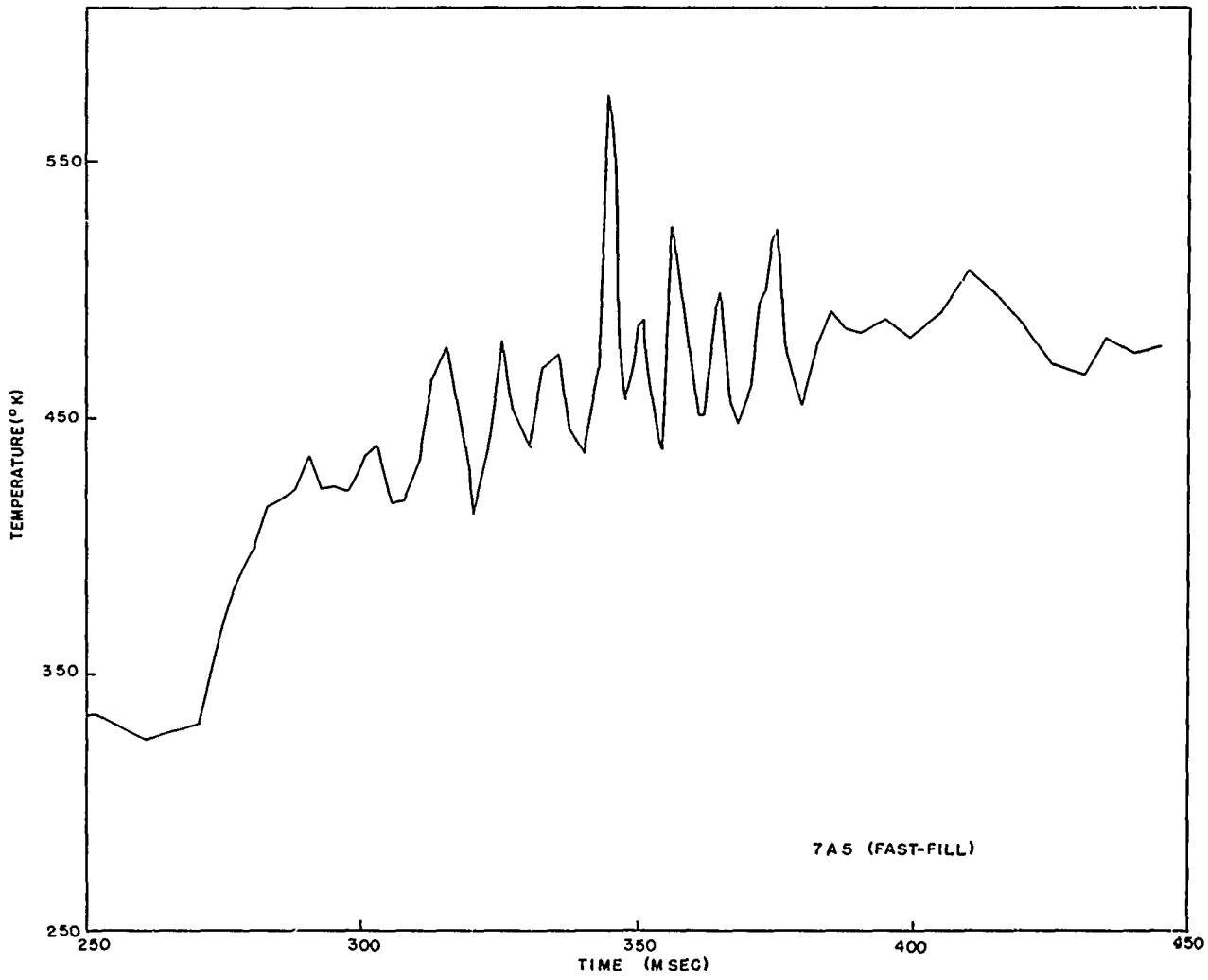

Fig. 3.2—Temperature in fast-fill room, underground personnel shelter, Apple I shot; Station 4-34.3 b-1.

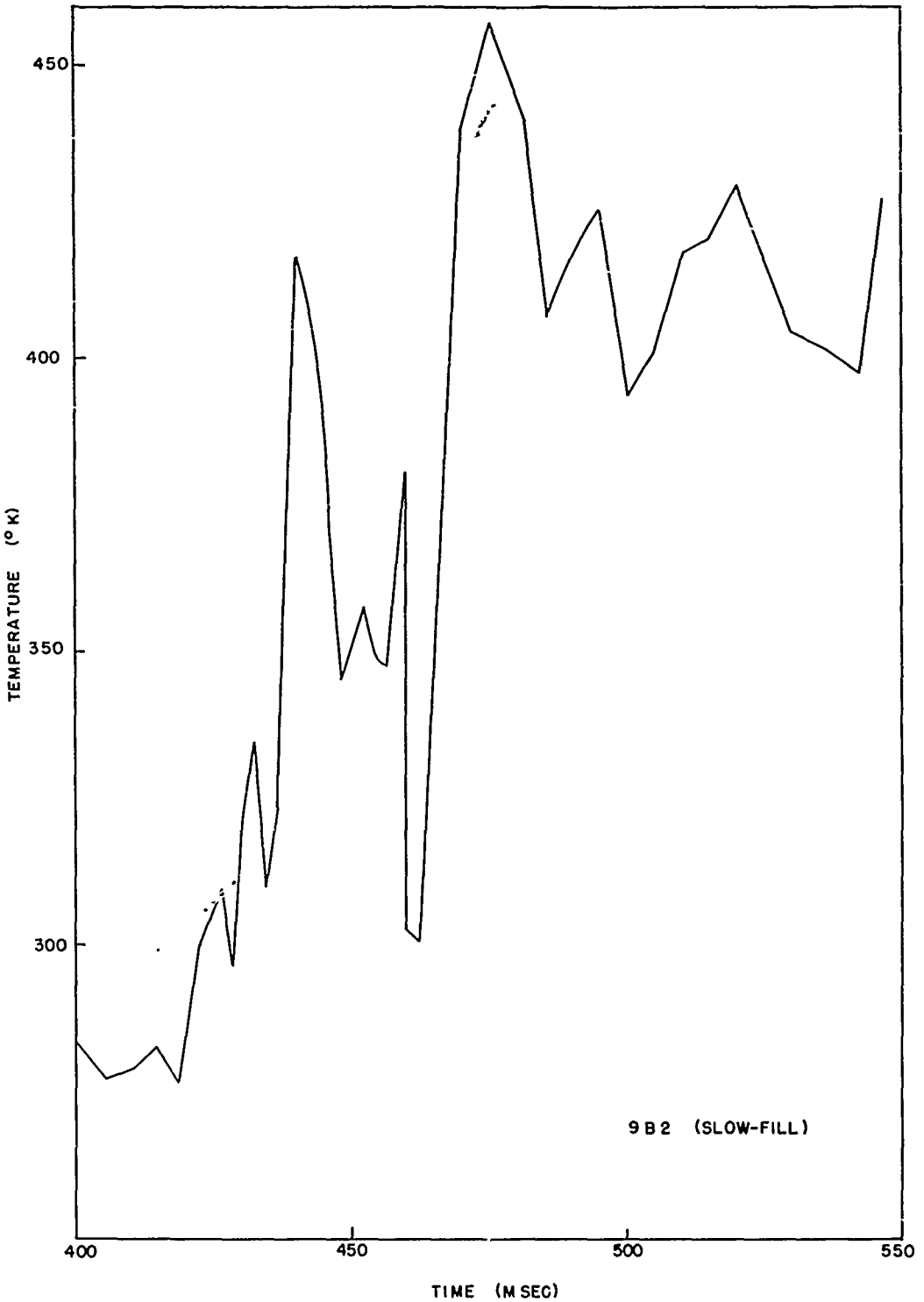

Fig. 3.3—Temperature in slow-fill room, underground personnel shelter, Apple I shot; Station 4-34.3 b-1.

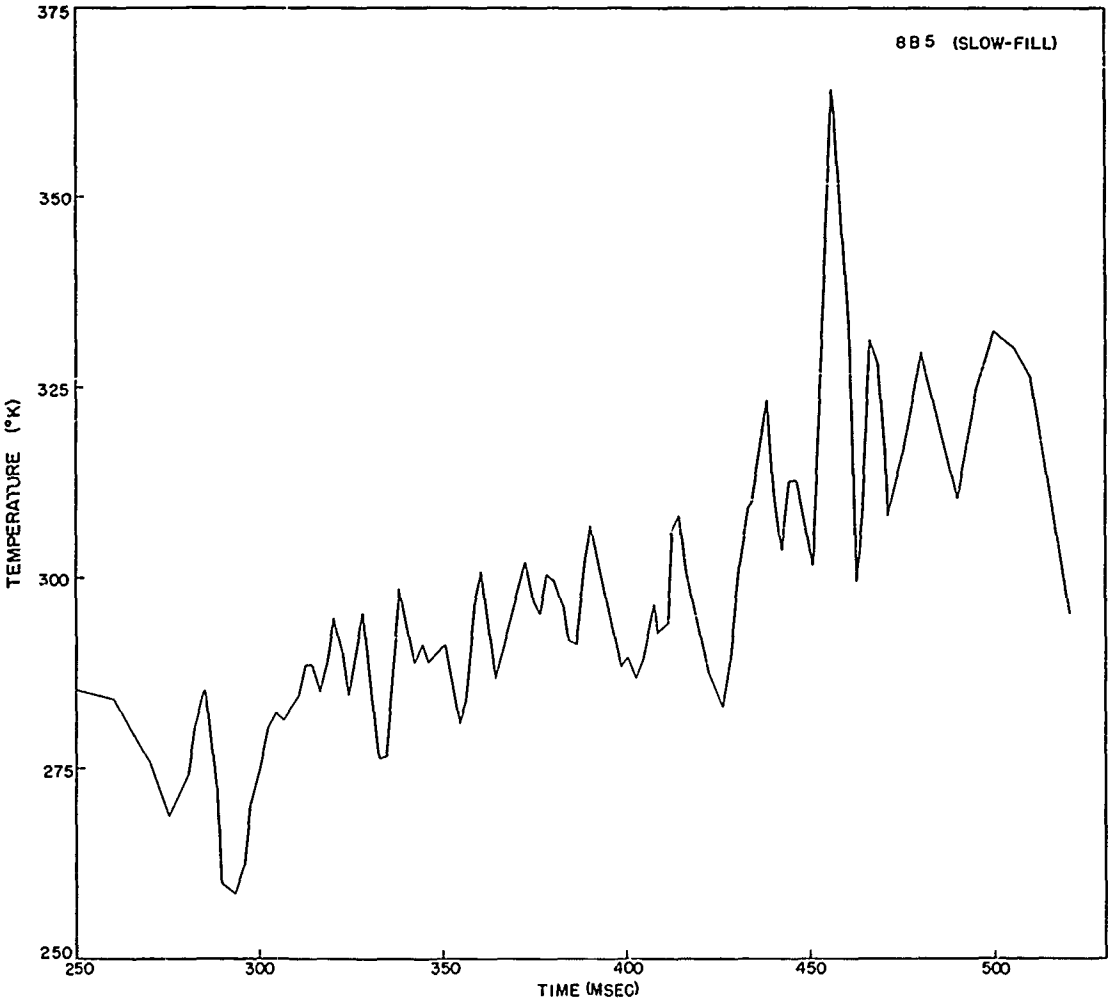

Fig. 3.4—Temperature in slow-fill room, underground personnel shelter, Apple I shot.

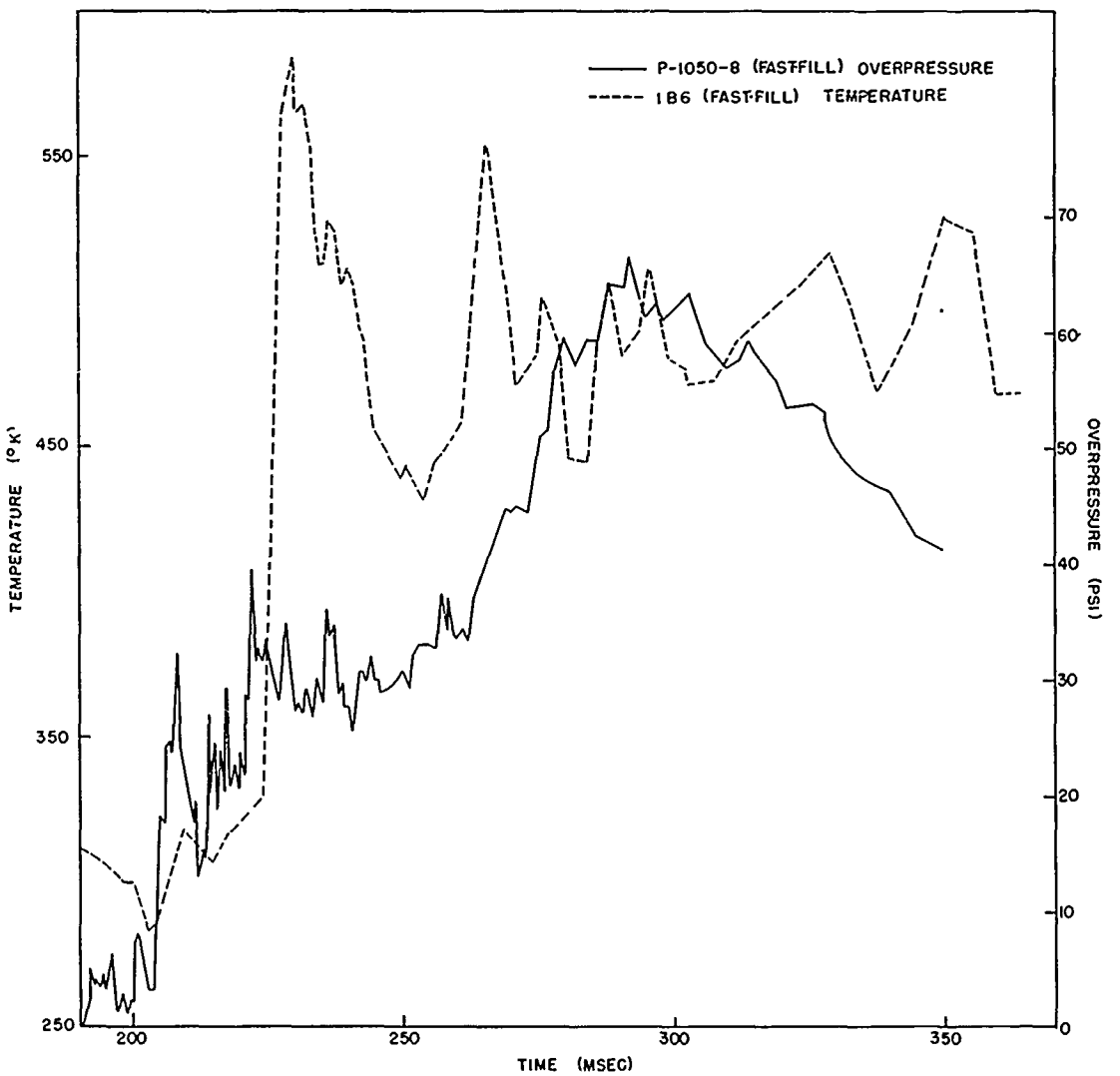

Fig. 3.5 — Temperature and overpressure in fast-fill room, underground personnel shelter, Apple II shot; Station 1-34.3 b-2.

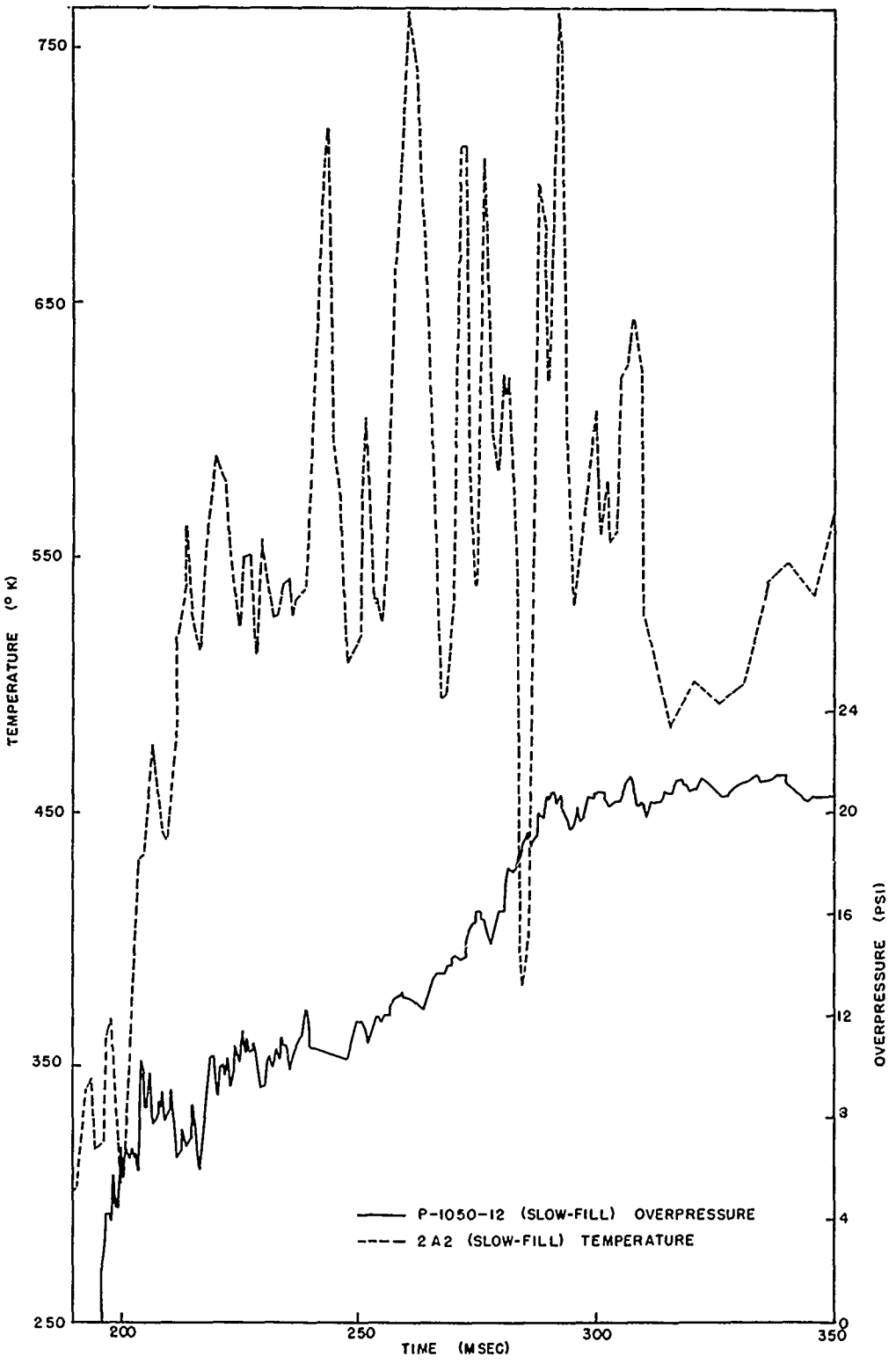

Fig. 3.6—Temperature and overpressure in slow-fill room, underground personnel shelter, Apple II shot; Station 1-34.3 b-2.

(b) Shot Apple II (Station 1-34.3 b-2). These are the two most valid records obtained (1B6, 2A2), Figs. 3.5 and 3.6. Arrival of the temperature pulse agrees with the arrival of the pressure pulse in the slow-fill room. In the fast-fill room, however, arrival of the pressure pulse precedes temperature pulse arrival by about 20 msec. If one concedes that the majority of the temperature increase is due to an influx of heated air from the outside, then the delay might be expected in the fast-fill room because of the longer passage the heated air has to traverse before arriving in the room. Passage into the slow-fill side is short, and outside air enters rapidly behind the shock front.

Table 3.1—PEAK TEMPERATURES

Station	Gauge	Peak, °C	Calculated temp.,[a] °C	Time of peak	Measured temp. vs cal. temp.
		Apple I			
4-34.3 b-1					
Fast-fill	7A5	195–225	150	410	1.3–1.5
Slow-fill	9B2	225–255[b]		520	
	8B5	145–155	30	510	4.8–5.2
		Apple II			
1-34.3 b-2					
Fast-fill	1B6	215–225	270	290	0.8–0.83
(Early peak)		300–320		230	1.1–1.2
Slow-fill	2A2	340–360	95	280	3.6–3.8

[a] By Rankine-Hugoniot.
[b] Doubtful.

REFERENCES

1. E. W. Ruhl, AEC Shelter Instrumentation, Operation Upshot-Knothole Report, WT-790, August 1953.
2. J. D. Shreve, Jr., Air Shock Pressure-Time Vs Distance for a Tower Shot, Operation Upshot-Knothole Report, WT-712, September 1954.
3. G. W. Rollosson, Static and Dynamic Overpressure Measurements, Operation Teapot Report, ITR-1192 (to be superseded by WT-1192).
4. J. B. Byrnes, Effects of an Atomic Explosion on Underground and Basement Type Home Shelters, Operation Upshot-Knothole Report, WT-801, March–June 1953.

CHAPTER 4

BLAST EFFECTS

Structures were located (Figs. 1.22 and 1.23) so as to receive a desired overpressure, estimates of which were based on IBM Problem M and the results of Upshot-Knothole Shots 1 and 10. Each of these estimates is shown in Fig. 4.1 scaled to Apple II yield. Superimposed on these estimates are Apple II measured peak overpressures. Below 8 psi measured overpressures agree with predictions. Above, they lie between the predictions, generally toward Upshot-Knothole values. Note that the precursor on Apple II terminated at a significantly higher pressure than that on Upshot-Knothole Shot 1. Although incident overpressure on Apple I shot was much less than had been expected, if measured peak overpressures were scaled to Apple II shot yield, they would appear as shown in Fig. 4.1.

A summary of gauge measurements from Apple I and Apple II shots is presented in Tables 4.1 and 4.2, and gauge records are reproduced in Figs. 4.2 through 4.10.

4.1 UNDERGROUND PERSONNEL SHELTER (STRUCTURAL)

4.1.1 Shot Apple I (Station 4-34.3 a-1)

Peak overpressure at this shelter (1050 ft) was only 47.2 psi (P-1050-16), where 100 psi had been predicted. This pressure wave (Fig. 4.4) was a classic precursor, rising almost instantly to 20 psi, dropping slightly during the first 55 msec, then rising steadily to 47.2 psi at 74 msec after arrival. After the peak, overpressure decayed in the usual fashion with a positive-phase duration of 349 msec.

Three gauges were placed in the closed shelter. One (P-1050-13, Fig. 4.4) was placed in the vestibule at the foot of the stairs between the sliding concrete door and the metal pressure-tight door to determine if there were any leakage in the outside door. This gauge rose to a peak of 4 psi at 317 msec, then settled at 1 psi until cable failure at 381 msec. Inside the main room, gauge P-1050-14 was placed behind the diffusion-board panel near the ventilation intake to check the efficiency of the antiblast closure valves. The gauge cable broke at 106 msec after shock arrival outside, but to that time no overpressure was recorded. Gauge P-1050-15 was located near the escape hatch but not behind the diffusion-board panel. The cable to this gauge broke 73 msec after shock arrival outside, and to that time no overpressure was recorded. The absence of overpressure at these two stations indicates that the antiblast closures operated satisfactorily.

4.1.2 Shot Apple II (Station 1-34.3 a-2)

Peak incident overpressure was 91.9 psi, nearly the anticipated 100 psi (Fig. 4.7). The wave had a precursor form but was not the classic precursor wave form observed on Apple I.

(Text continues on page 81)

Table 4.1—SUMMARY OF GAUGE MEASUREMENTS, SHOT APPLE I

Gauge	Location	Calibration pressure, psi	Time of arrival, msec	Peak overpressure, psi	Time of arrival to peak, msec	Positive-phase duration, msec	Peak negative pressure, psi	Time of arrival to peak negative, msec	Time of failure, msec
P-1050-1	4-34.3 b-1	75	270.4	26.6	85.0	371.3	−2.5	388.0	
P-1050-2	fast-fill	99	275.3	15.5[a]	21.7				295.7
P-1050-3	side	99	277.0	35.0	45.3	324.1	−6.4	1460.4	
P-1050-4		99	277.5	36.3	74.0	626.3	−2.4	896.8	
P-1050-5		99	277.5	34.1[a]	73.5				353.0
P-1050-6		75	279.3	36.9	68.1	328.2	−4.7	468.3	
P-1050-7		75	276.7	34.2[a]	66.2				342.9
P-1050-8		75	272.8	34.4	73.4	591.9	−2.4	684.6	
Q-1050-1		6	272.9	12.25	16.20				
P-1050-9	4-34.3 b-1	27	277.6	6.7	206.3	637.3	−2.7	1050.8	
P-1050-10	slow-fill	27	274.0	2.05	61.0				Read to 350.0
P-1050-11	side	27	273.3	5.14	120.0				765.0
P-1050-12		27	278.3	4.14	67.7				343.0
P-1050-13	4-34.3 a-1	20	273.4	4.00	43.3				381.0
P-1050-14		10		0					359.8
P-1050-15		10		0					326.9
P-1050-16	Ground baffle	99	253.8	47.2	74.0	572.2	−6.0	2004.2	
P-1350-1[b]	4-34.1 b-1	45	380.4	11.5	153.5				No crossover
P-1350-2		45	375.8	13.5	57.0	735.8	−1.4	1225.7	
P-1350-3[b]	4-34.1 b-2	90	371.1	38.6	36.6	443.6	−2.9	838.6	
P-1350-4		90	376.6	47.0	21.5				415.2
P-1350-5[b]	4-34.1 b-3	111	365.2	38.6	35.5				402.7
P-1350-6		111	373.4	43.1	5.5				402.3
P-1350-7	Ground baffle	45	369.7	17.3	76.8	430.8	−3.0	628.0	

[a] A higher peak may have been recorded had not the gauge failed.
[b] Gauge located near shelter entrance.

Table 4.2—SUMMARY OF GAUGE MEASUREMENTS, SHOT APPLE II

Gauge	Location	Calibration pressure, psi	Time of arrival, msec	Peak overpressure, psi	Time of arrival to peak, msec	Positive-phase duration, msec	Peak negative pressure, psi	Time of arrival to peak negative, msec	Time of failure, msec
P-1050-1	1-34 3 b-2	75	188.9	63.9	108.8	562.0	−3.9	1647.2	
P-1050-2	fast-fill	90	189.1	64.9	107.4	518.5	−6.0	1835.3	
P-1050-3	side	90	194.9	73.2	90.1	572.3	−4.6	617.1	
P-1050-4		90	194.9	67.2	102.5	565.6	−2.2	1172.1	
P-1050-5		90	195.2	65.5	91.9	555.1	−5.2	1064.4	
P-1050-6		75	196.1	63.6	95.6	546.3	−3.0	882.3	
P-1050-7		75	194.4	68.0	96.1	569.0	−2.9	1340.9	
P-1050-8		75	191.0	66.5	101.2	556.1	−3.2	1178.0	
Q-1050-1		6	191.3	12.70	2.2				
P-1050-9	1-34.3 b-2	27	194.1	22.3	130.8	565.3	−3.3	1465.3	
P-1050-10	slow-fill	27	191.2	21.5	139.3	568.1	−2.8	1451.0	
P-1050-11	side	27	190.4	22.8	121.2	567.8	−3.3	1518.0	
P-1050-12		27	195.9	21.4	111.8	569.8	−2.7	1492.6	
P-1050-13	1-34 3 a-2	9		0					280.0
P-1050-14		9							0
P-1050-15		9	240.9	0.17	355.2	583.8	−1.69	1947.8	
A-1050		24 g	177.1	3.67 g	76.6		−3.87 *	104.6	
P-1050-16	Ground baffle	99	182.0	91.9	63.6	550.9	−3.0	1081.3	
P-1270-1	1-34.1 c-2	1 .	236.2	85.8	4.0	569.5	−3.3	1131.0	
P-1270-2	1-34.1 c-1	54	236.3	71.6	110.9	567.1	−2.9	1571.3	
P-1270-3	Ground baffle	54	237.7	44.4	103.4	558.2	−2.7	1334.7	
P-1470-1	1-34.1 d-1	36	295.2	18.5	56.9	685.1	−1.9	1286.5	
P-1470-2	Ground baffle	36	302.0						302.0
P-1470-3	1-34 1 d-2	99		Experimental channel					
P-2250-1	1-34.1 f	24		Shelter failed					
P-2250-2	Ground baffle	12	700.6	11.7	65.8	746.5	−1.9	1848.6	
P-2750-1	1-34.1 i	21	1033.4	4.3	265.3	860.8	−1.4	1958.0	
P-2750-2	Ground baffle	9	1031.5	11.6	28.2	786.0	−1.8	1756.3	
P-3750-1	1-34.1 l	15	1723.4	2.6	276.4	739.8	−1.5	2057.9	
P-3750-2	Ground baffle	6	1716.6	7.8	9.8	959.2	−1.2	2289.0	
P-4700-1	1-31.1 c-1	6	2449.2	1.3	419.8	1346.4	−0.77	2338.3	
P-4700-2	1-31.1 a-2	6	2424.9	4.6	90.0	1051.1	−0.73	2361.9	
P-4700-3	Center g. baffle	6	2418.3	5.1	13.5	1120.0	−0.64	2488.5	
P-4700-4	West g. baffle	6	2417.5	4.0	25.4	1208.7	−0.42	2390.1	
P-4700-5	East g. baffle	6	2422.2	5.1	15.3	1160.7	−0.79	2385.5	
P-5500	1-31.1 b-1	6	3006.5	3.7	131.6	1232.0	−0.67	2501.9	
P-10500-1	Center g. baffle	1.62	7137.9	1.7	0.89	1805.3	−0.24	2851.4	
P-10500-2	West g. baffle	1.62	7137.6	2.1	2.2	1880.4	−0.18	3148.1	
P-10500-3	East g. baffle	1.62	7140.6	1.9	1.3	1497.1	−0.38	2973.6	
P-15000	Ground baffle	0.81	10988.7	1.3	3.6	1946.8	−0.20	3303.7	

*Acceleration measurement.

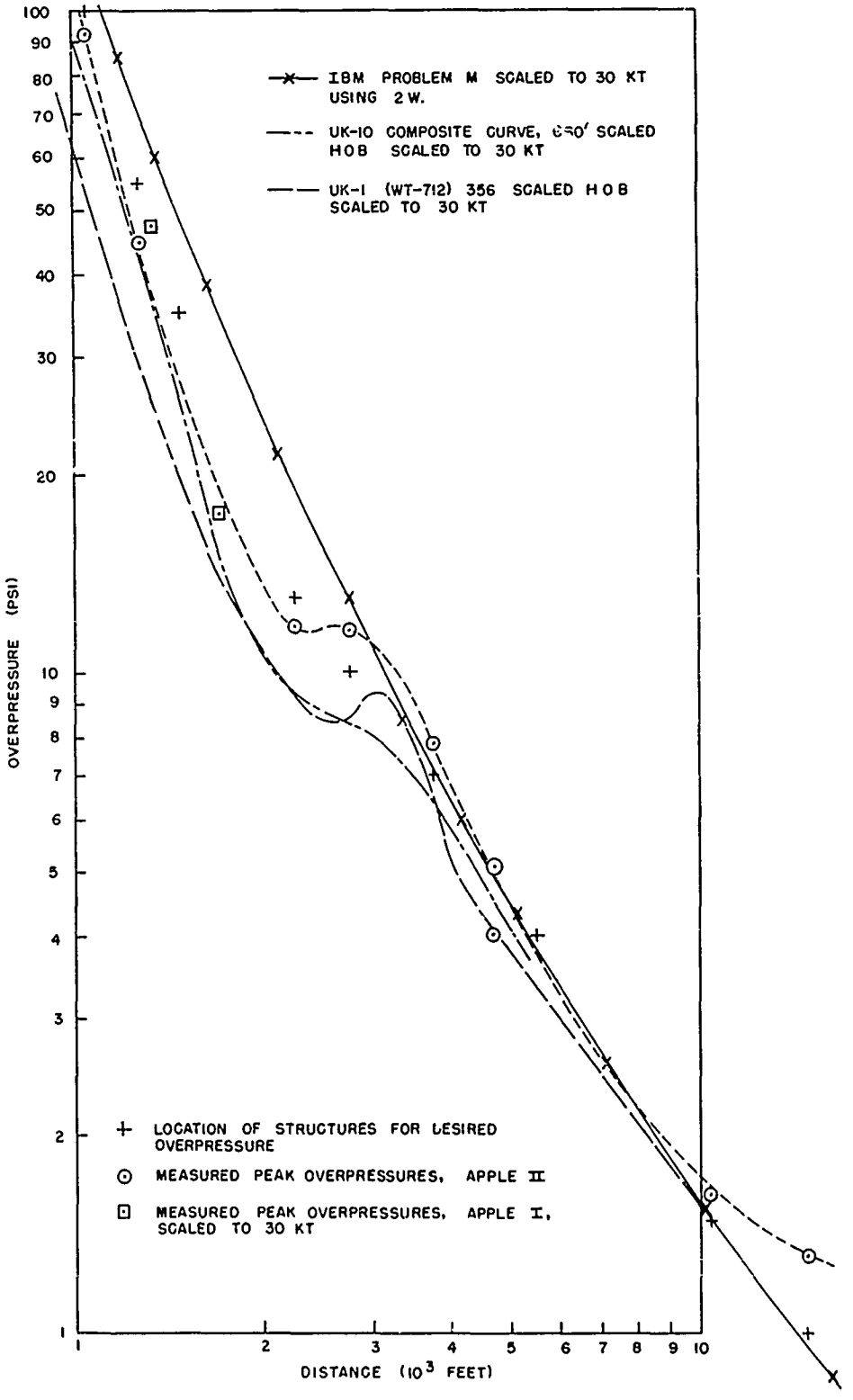

Fig. 4.1—Comparison of measured with predicted peak overpressures vs distance.

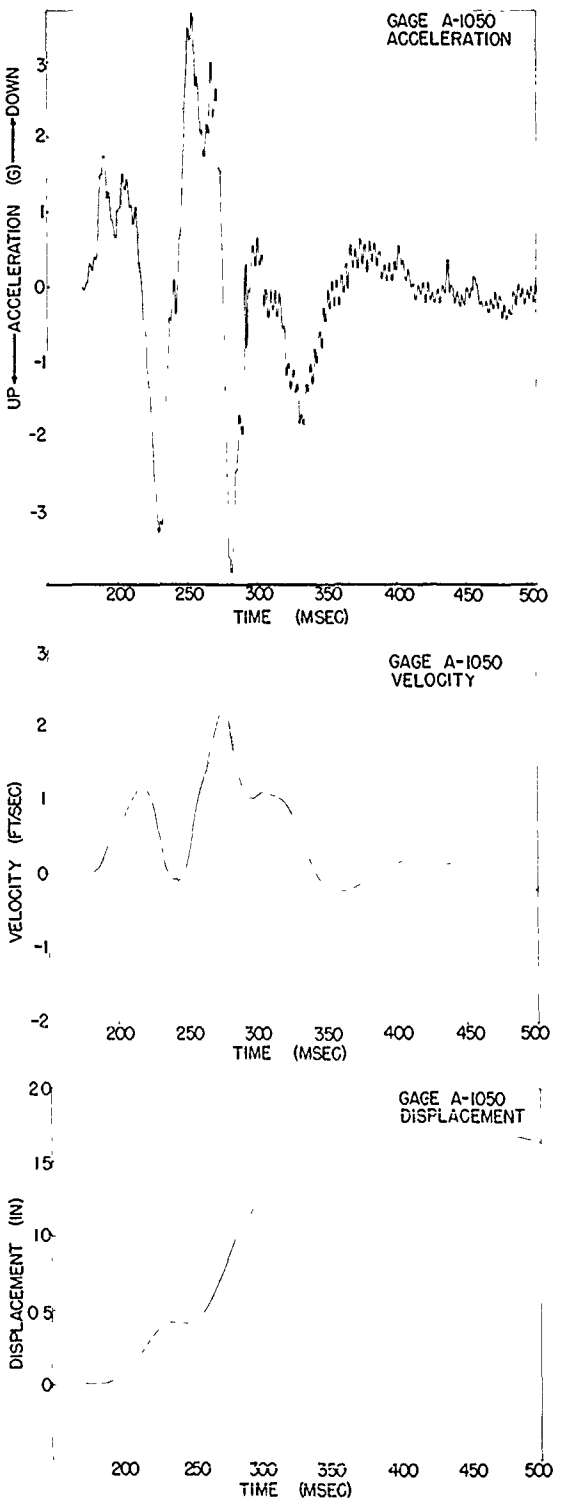

Fig. 4.2—Acceleration, velocity, and displacement records, underground personnel shelter, Apple II shot; Station 1-34.3 b-2.

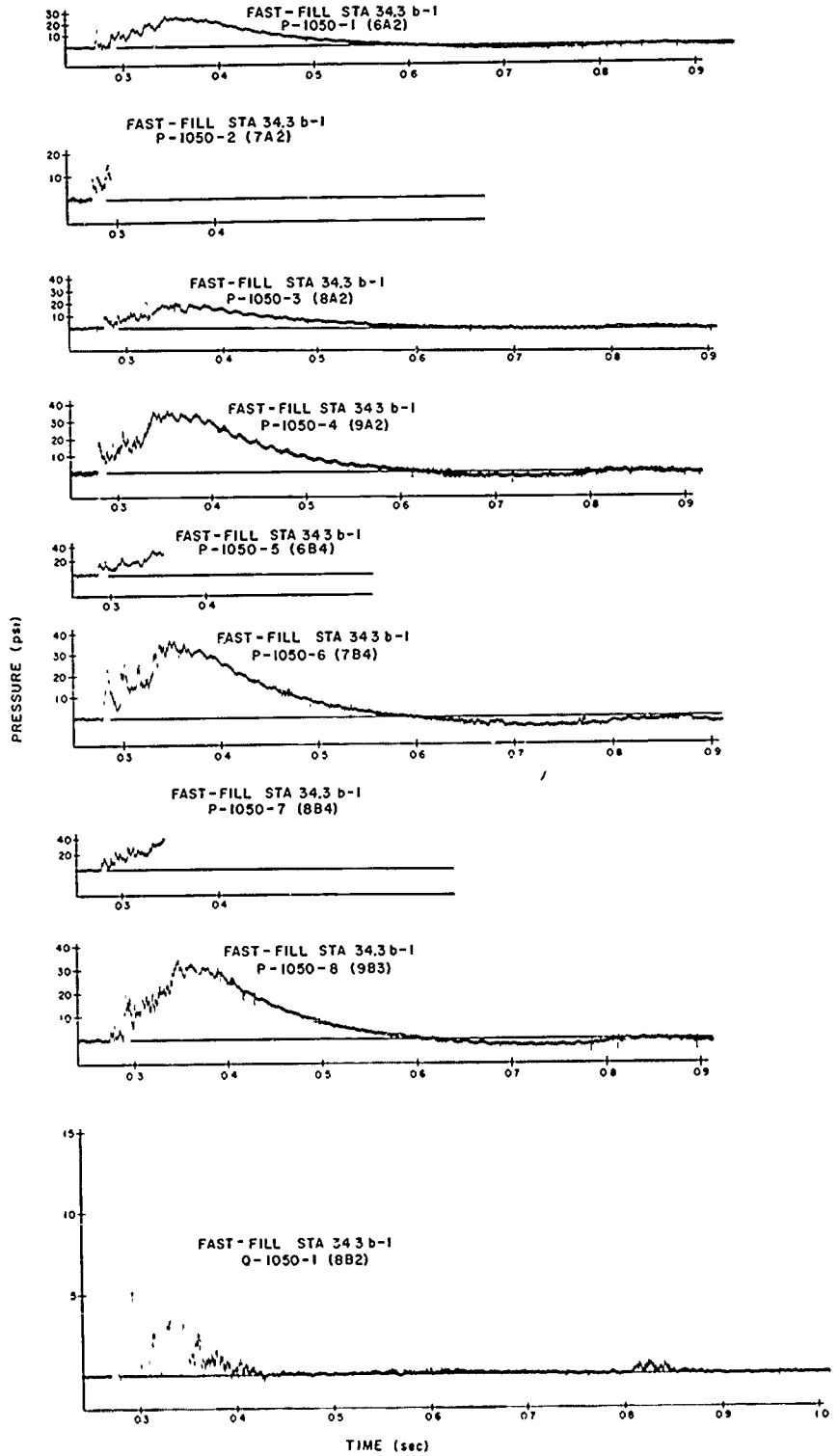

Fig. 4.3—Pressure vs time records, Apple I shot.

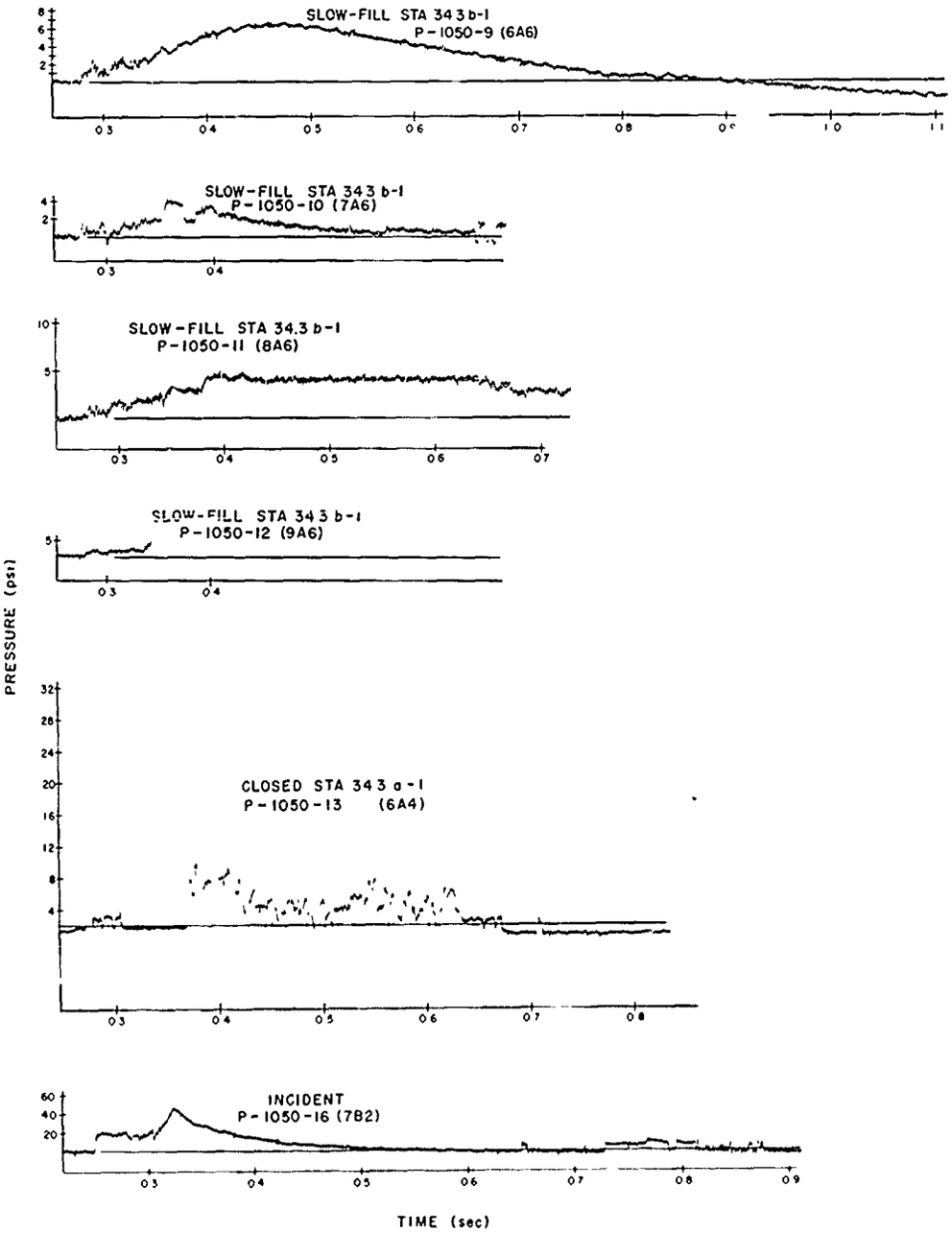

Fig. 4.4—Pressure vs time records, Apple I shot.

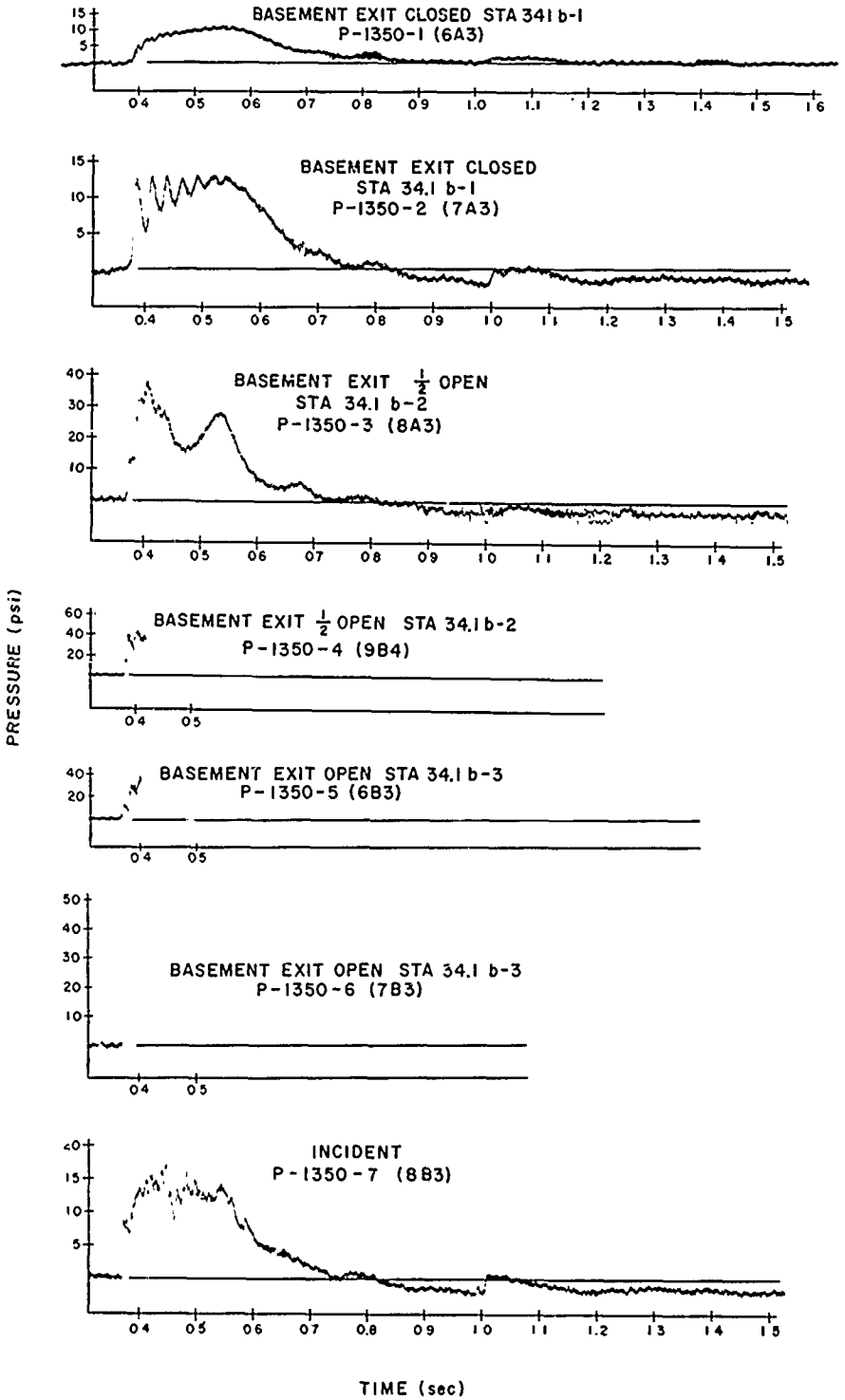

Fig. 4.5—Pressure vs time records, Apple I shot.

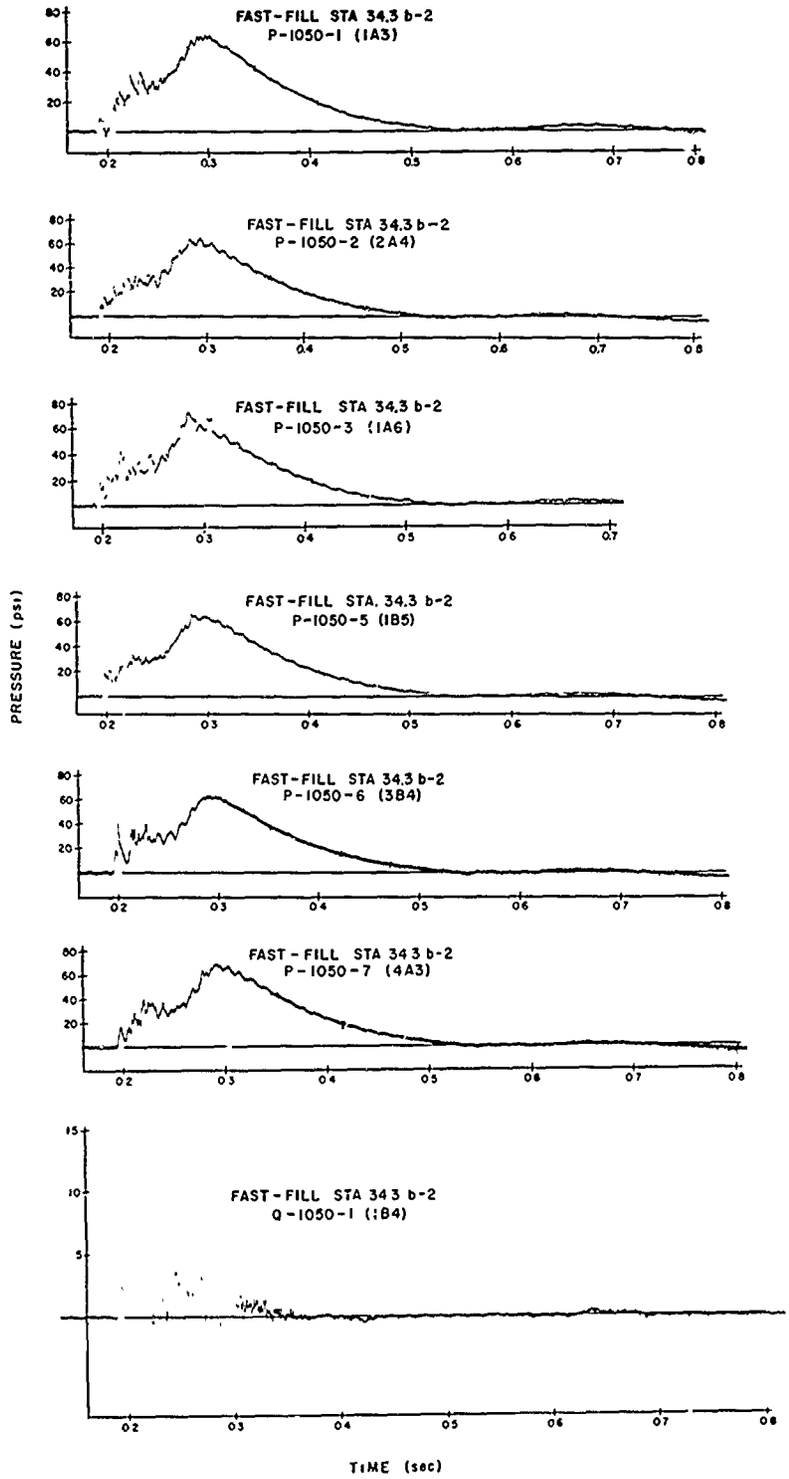

Fig. 4.6--Pressure vs time records, Apple II shot.

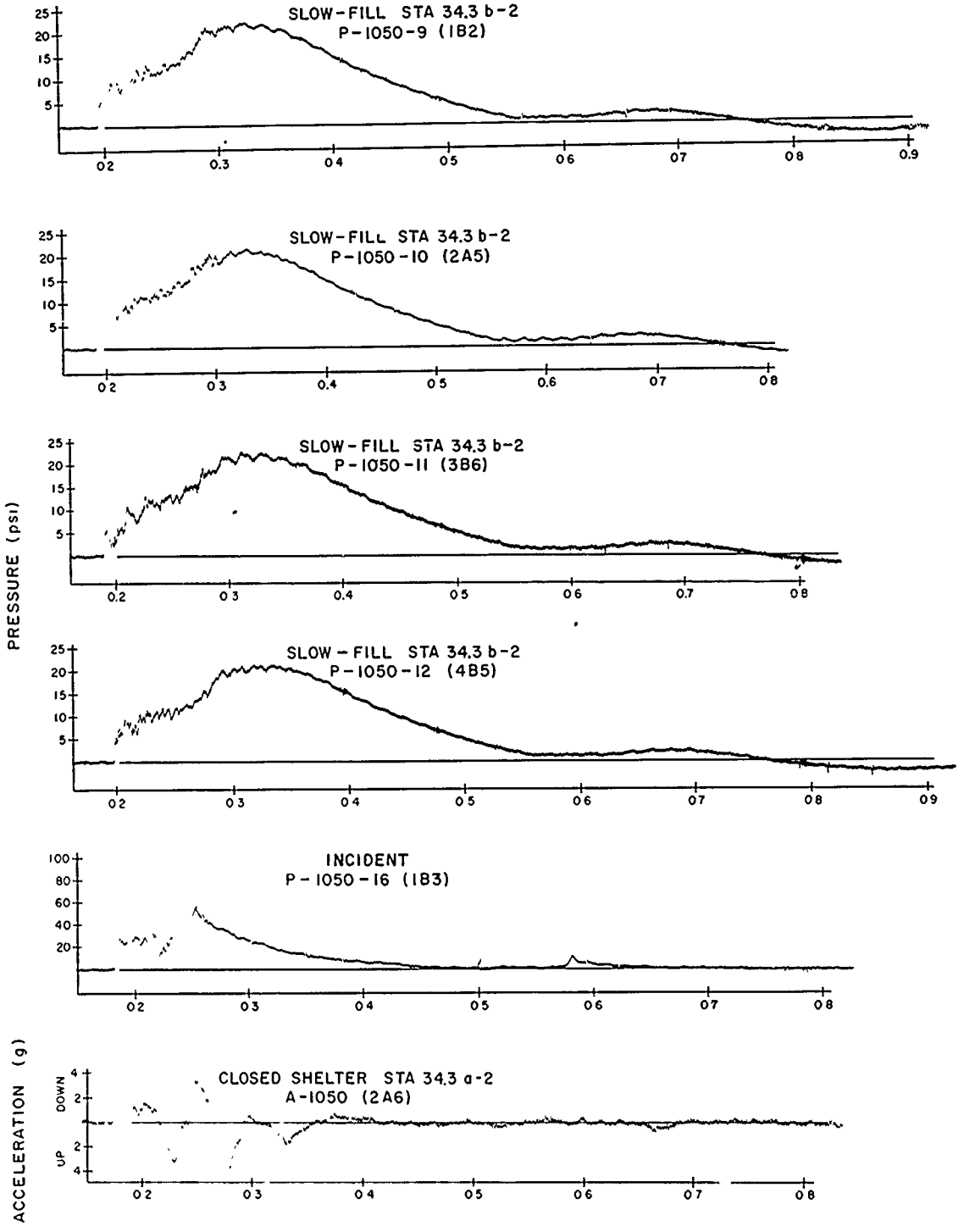

Fig. 4.7—Pressure vs time records, Apple II shot.

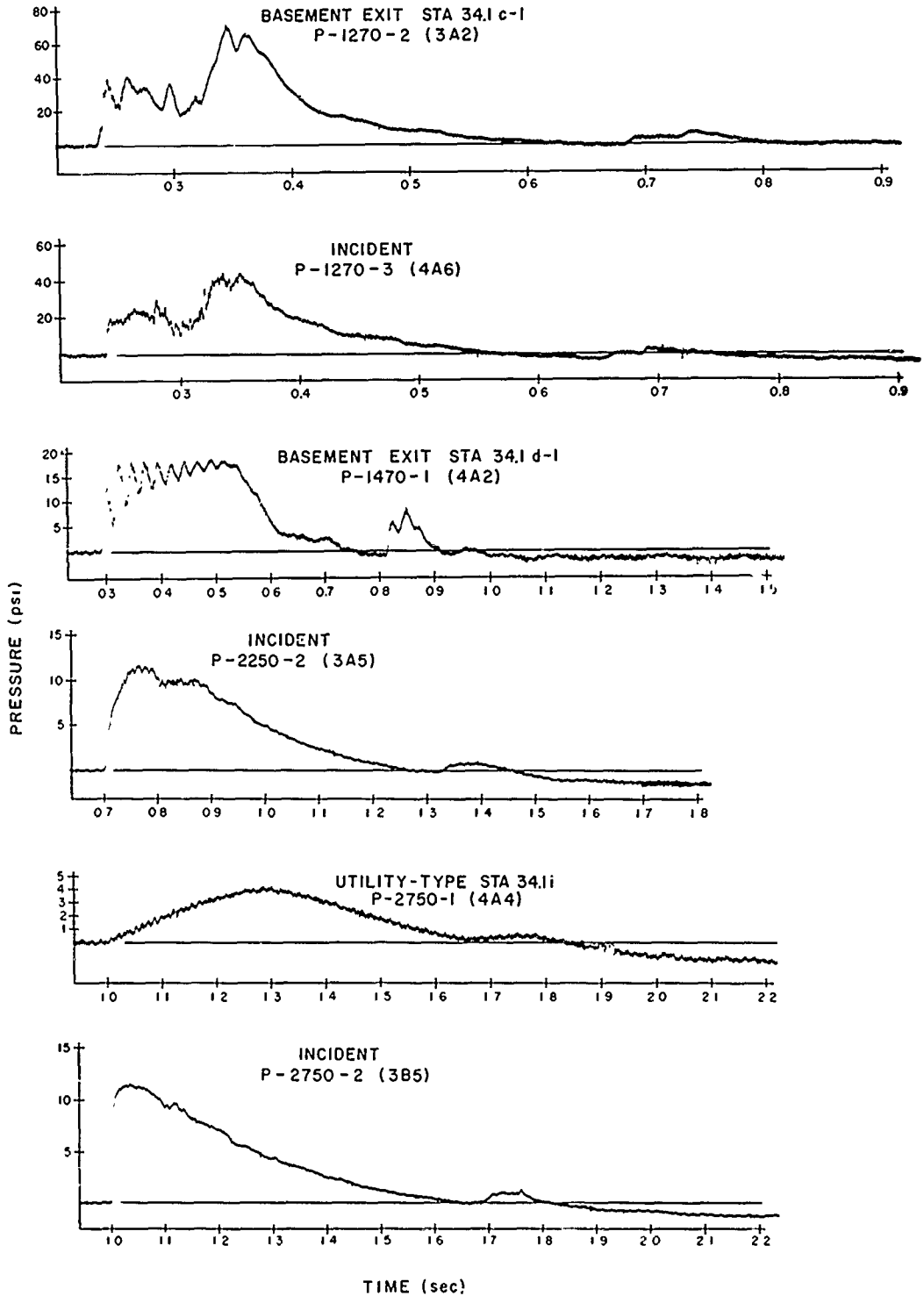

Fig. 4.8—Pressure vs time records, Apple II shot.

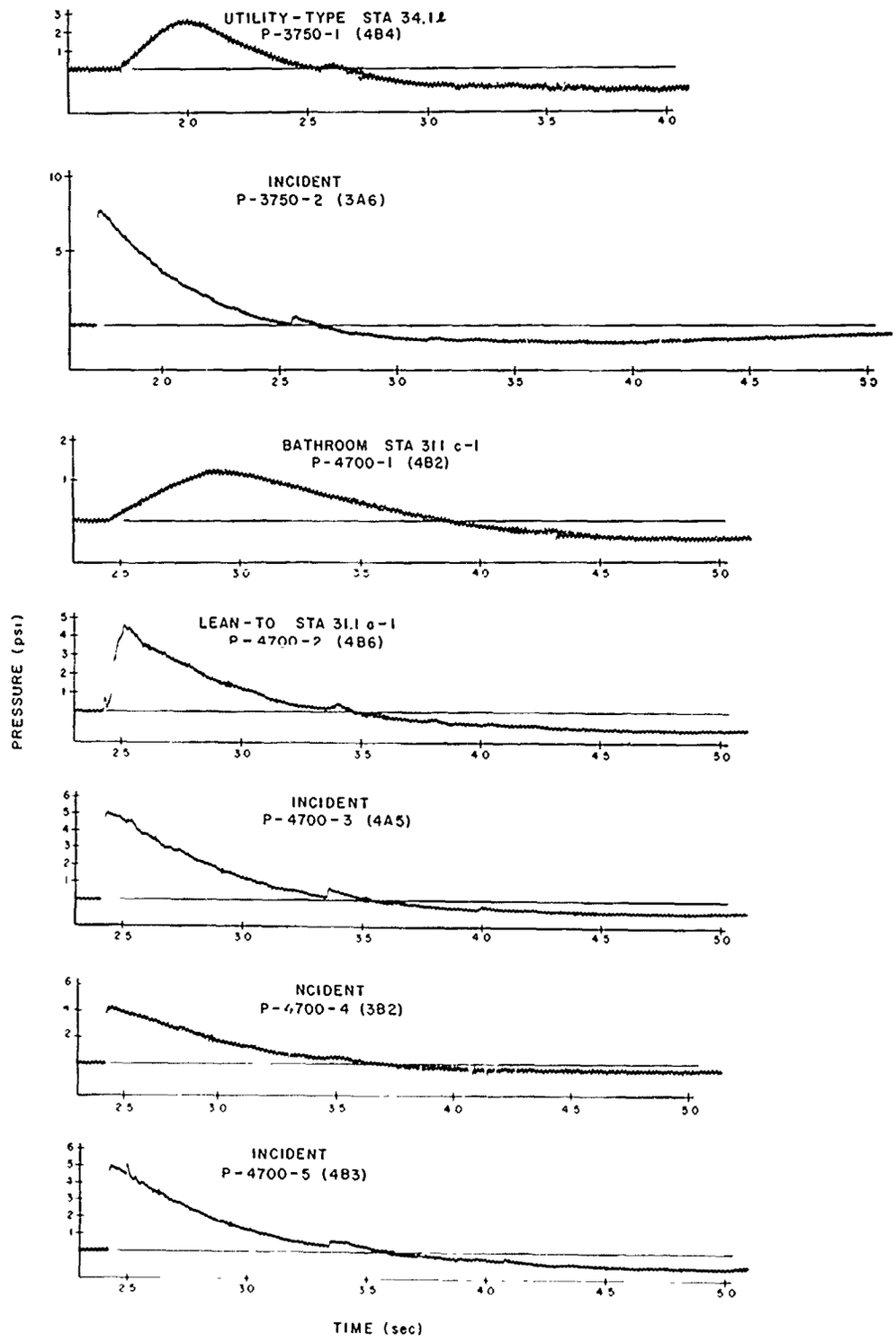

Fig. 4.9—Pressure vs time records, Apple II shot.

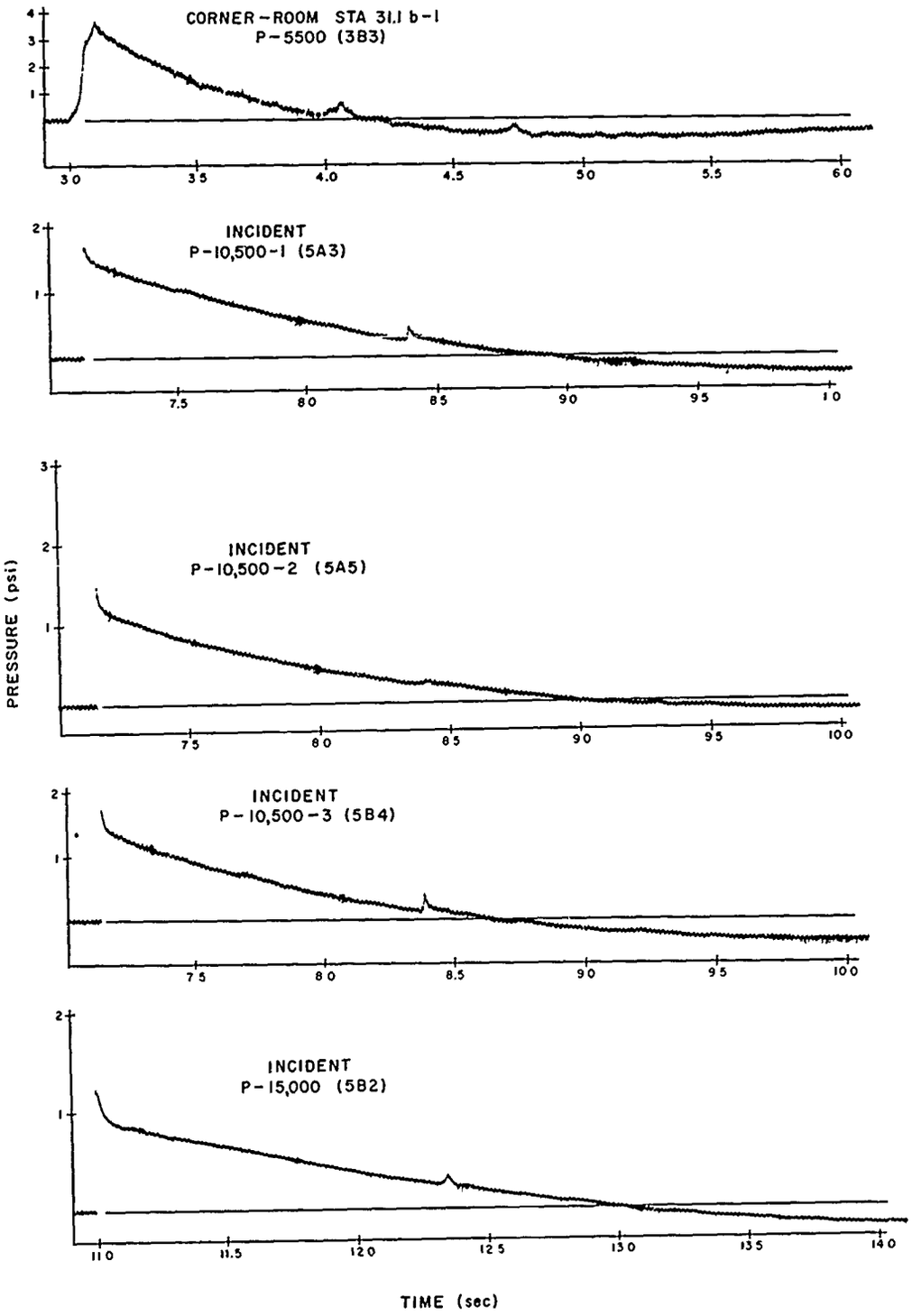

Fig. 4.10—Pressure vs time records, Apple II shot.

Three gauges were placed in the shelter: P-1050-13 in the large room, P-1050-14 in the exhaust room for the ventilating equipment, and P-1050-15 in the intake room. No overpressure had developed in the large room 96 msec after shock arrival when the gauge failed or the cable broke. The gauge in the exhaust room failed at zero time. The gauge in the intake room registered a positive overpressure of less than 0.2 psi, indicating that the antiblast closures worked properly.[a] However, since these antiblast closures are one-way devices, they permitted evacuation of air from the room and a negative pressure of 1.69 psi.

Based on free-soil accelerations on earlier tests,[1] a maximum vertical acceleration of 25 g had been expected, but the measured vertical acceleration had a maximum positive (downward) acceleration of only 3.7 g (Figs. 4.2 and 4.3). This gives a maximum positive velocity of 2.2 ft/sec and a maximum downward displacement of nearly 1.7 in. occurring at 470 msec (Fig. 4.2). Since all the displacement was downward, these accelerations should cause no harmful effect on occupants of the shelter.

4.2 UNDERGROUND PERSONNEL SHELTER (BIOMEDICAL)

For Project 33.1 requirements,[2] the entrance to the fast-fill room was left open, and the escape hatch in the slow-fill side was covered with a steel plate with a 19-in.-diameter hole in the center to meter air slowly into the shelter. For Apple II this air inlet was enlarged to 36 in. in diameter.

4.2.1 Shot Apple I (Station 4-34.3 b-1)

In the fast-fill side eight gauges (P-1050-1 through P-1050-8, Fig. 4.3) were located as shown in Fig. 1.19 to give pressures at particular points for Project 33.1, and a q-tube was placed 6 ft from the door to measure dynamic pressure. In the slow-fill side one pressure gauge (P-1050-9 to P-1050-12, Fig. 4.4) was located near the center of each wall (Fig. 1.19).

Measured dynamic pressure rose rapidly in the fast-fill room to nearly 7 psi at shock arrival, becoming negative some 10 msec later as the front was reflected off the back wall and the flow reversed. Flow became positive again during the approximately 15 msec it took the room to fill while the front was being rereflected off the front wall, with the peak dynamic pressure rising to over 12 psi. Thereafter, flow remained positive until 430 msec, indicating that the room continued to fill to that time.

For gauges on the wall to the left of the entrance of the fast-fill side, passage of the initial front and its reflection off the back wall can be noted. Thereafter, reverberations between one wall and another and between the floor and ceiling are superimposed, and it is difficult to attribute any one signal to a particular reflection.

In the slow-fill side the configuration is such that with the pressure entering over one corner there should be similarities between gauges P-1050-10 and P-1050-11 and between P-1050-9 and P-1050-12. The cable to P-1050-12 broke at 65 msec, and P-1050-10 was valid only to 76 msec; but to those times some similarities are apparent. Because the pressure wave enters the slow-fill side from above, one might expect the reverberations between the floor and the ceiling to be stronger than those between opposite walls. There is nothing in the records to substantiate this, however.

4.2.2 Shot Apple II (Station 1-34.3 b-2)

Gauge locations were identical to those for Apple I shot (Fig. 1.19). (No records are presented for gauges P-1050-4 and P-1050-8 because they were recorded on a Midwest recorder which gives a multitrace record from which a single trace cannot be photographically reproduced.

Measured overpressure inside both fast- and slow-fill rooms differed little from those of Apple I except for higher overpressure (Fig. 4.6). On many of the records it is possible to identify similar characteristics of the blast wave as it was reflected back and forth inside the

[a] No records are reproduced for these three gauges since there was no significant pressure change.

room. Despite the higher incident overpressure on this shot, the peak dynamic pressure (12.7 psi) was about the same as for Apple I shot. There were significant differences, however, in the shapes of the dynamic pressure waves. The Apple II shot record between 195 and 225 msec disagrees with the Apple I record and is inconsistent with the overpressure records from near the q-gauge. For this reason 30 msec of the Apple II is discounted.

Dynamic pressure as measured should be a function of the overpressure differential inside and outside the shelter. The overpressure differential indicates when the shelter is filling and emptying. When it is emptying, the dynamic pressure should be negative. The dynamic pressure as recorded in this station is in poor agreement with the overpressure differential.

4.3 BASEMENT EXIT SHELTERS

4.3.1 Shot Apple I (Stations 4-34.1 b-1, b-2, b-3)

Station 4-34.1 b-1 was closed, Station 4-34.1 b-2 was partially closed, and Station 4-34.1 b-3 was open. These were instrumented with two pressure gauges for Project 33.1: one inside 2 ft from the end wall on the wall nearest GZ and one inside 2 ft from the entrance on the same wall (Fig. 1.9).

The first (closest to GZ) of four doors of the closed shelter blew off, but the restricted entrance reduced the overpressure inside to about 75 per cent of the incident. The door must have blown off rapidly because there is no discontinuity of the pressure record to indicate the time at which it blew off.

It is interesting to note on the record of P-1350-2 (Fig. 4.5), located near the far end of the shelter, the reverberation of the blast back and forth in the shelter. Reverberation is absent from the record of P-1350-1 (Fig. 4.5), located near the door of the shelter, because the oscillation is probably damped out by the rush of air entering the opening. The small increase which occurs on P-1350-2 at 366.5 msec (which is ahead of shock arrival at P-1350-1, near the entrance) may be a signal from the ventilation pipe near the far end of the shelter.

For the open and partially closed shelters, differences resulting from the two opening configurations appear to be small. The cables to gauges P-1350-4, 5, and 6 probably broke after the peak overpressure inside the shelters had been recorded. In both shelters peak overpressures measured were more than twice the peak incident overpressure.

4.3.2 Shot Apple II (Stations 1-34.1 c-1, c-2, d-1, d-2)

Stations 1-34.1 c-1 and c-2, located at 1270 ft, were exposed to a precursor type shock wave (P-1270-3, Fig. 4.8) with a peak overpressure of 44.4 psi. Pressure in the closed shelter (c-1) rose rapidly enough to indicate that the doors failed almost instantly. Some reverberation can be seen on the record; little reverberation, however, appeared on the open shelter (c-2) record (not shown), perhaps because of the excessive damage done to the open end. Peak overpressure measured inside both shelters was nearly twice the peak incident overpressure. The record from the open shelter retains more of the character of the incident wave than does that from the shelter at 1470 ft.

Although the record of incident overpressure upon Stations d-1 and d-2 at 1470 ft is not valid, the peak can be inferred from measurements at other stations to be about 29 psi. The pressure record for the open shelter (d-1, Fig. 4.8) shows clearly the reverberation running the length of the shelter. No measurement was made in the open shelter (d-2).

4.4 UTILITY TYPE SHELTERS

4.4.1 Shot Apple II (Stations 1-34.1 f, i, l)

These shelters received incident overpressures of 11.7, 11.6, and 7.8, respectively (P-2250-2, P-2750-2, and P-3750-2, Figs. 4.8 and 4.9). At the first shelter there was a precursor to the extent that the incident overpressure wave had a relatively slow rise. At the second

shelter the incident wave had "shocked-up" but was still slightly rounded at the top. At the third shelter the form was similar to the second, rounded only a little at the top. The pressure in two of the three shelters built up slowly. The first shelter rolled over, breaking the cable to the pressure gauge before any pressure was recorded.

Maximum overpressures inside the two surviving sets of aboveground utility shelters rose to peaks of 4.3 and 2.6 psi, respectively, and decayed slowly. Thus they were reduced to about 35 per cent of the incident.

4.5 INDOOR FAMILY TYPE SHELTERS

4.5.1 Shot Apple II (Station 1-31.1 c-1)

The rambler house at 4700 ft was subjected to an incident overpressure of 5.1 psi (Fig. 4.9). The pressure inside the bathroom shelter (P-4700-1, Fig. 4.9) rose slowly to 1.3, or to less than one-third the peak incident overpressure, then decayed slowly. For incident overpressure records taken at 10,500 ft, where the last bathroom shelter was located, see Fig. 4.10.

4.5.2 Shot Apple II (Stations 1-31.1 a-1 and b-1)

The two-story brick house at 4700 ft was subjected to an incident overpressure of 5.1 psi. The overpressure inside the basement lean-to shelter (P-4700-2, Fig. 4.9) rose slightly as the shock came in the nearest window, increasing to 4.6 psi (only slightly below the incident) as the pressure built up within the basement.

At 5500 ft the two-story house in which the basement corner-room shelter was located was subjected to an incident overpressure of about 4 psi. The record (P-5500, Fig. 4.10) reflects the general rise to 3.7 psi within the basement. The shape of the pressure record inside was different from that outside. The fast rise of the incident wave was altered to a form with a slow rise that reached a maximum when the basement filled about 100 msec after shock arrival.

REFERENCES

1. V. Salmon and S. R. Hornig, Earth Acceleration Vs Time and Distance, Operation Tumbler-Snapper Report, WT-517, December 1952.
2. C. S. White et al., Effects of Overpressures on Biological Systems, Operation Teapot Report, ITR-1179 (to be superseded by WT-1179).

CHAPTER 5

STRUCTURAL DAMAGE

5.1 UNDERGROUND PERSONNEL SHELTERS (STRUCTURAL AND BIOMEDICAL)

5.1.1 Shot Apple I (Stations 4-34.3 a-1 and b-1), 1050 Ft

Neither shelter suffered any visible damage. Appreciable dirt and missiles littered the stair wells, and there was a separation between the grout under the steel plates that served as supports for a concrete sliding door and the walls of the stair well of the structural shelter (Fig. 5.1).

The concrete sliding door was used only on the structural shelter (4-34.3 a-1) and showed no evidence of damage. The bars that served to lock the door against an upward motion caused by negative pressures showed no distortion (Fig. 5.2). The rubber mat between the door and the stair well blew onto the steps. The Navy type door and escape hatch in the structural shelter were undamaged.

In the biomedical shelter (4-34.3 b-1), however, differential pressure between the fast- and slow-fill rooms was enough to distort the steel angle attaching the door frame to the 1-ft concrete partition wall (Figs. 5.3 and 5.4). Horizontal stiffeners prevented any significant horizontal distortion of the door, but considerable vertical distortion resulted from displacement of the door frame (Fig. 5.5).

Blast force distorted the vents, leaving them bent away from GZ at an angle of 30° (Fig. 5.6).

5.1.2 Shot Apple II (Stations 1-34.3 a-2 and b-2), 1050 Ft

Again, neither shelter suffered structural damage at a peak incident pressure of 92 psi, but dirt and missiles littered the stair wells. The blast tore off the vent tees at the junction of the tee and the vertical pipe.

(a) Station 1-34.3 a-2. The Army Chemical Corps ventilation equipment suffered no discernible damage. The failure of one of the rebound bolts from shearing of the thread indicates that these bolts were loaded to the limit of their capacity at the test pressure. An increase in bolt diameter, and therefore thread capacity, would supply a reserve strength to the rebound connection.

Two wheels of the sliding door were destroyed by missiles, and the rubber door bumper blew into the stair well (Fig. 5.7). Destruction of the wheels can be prevented by widening the door slab to provide a protective lip for the wheels. Despite the loss of the wheels, the door could have been jacked open from the inside. The retaining wall around the concrete door was damaged (Fig. 5.8).

(b) Station 1-34.3 b-2. Because of the larger opening (36 in. instead of 19 in.) in the slow-fill side escape hatch, the peak unbalanced pressure between the rooms in the biomedical

shelter was proportionately less than in the Apple I shelter, and the reinforced door frames in the partition wall sustained no plastic deformation from this unbalanced pressure.

5.2 BASEMENT EXIT SHELTERS

5.2.1 Shot Apple I (Stations 4-34.1 b-1, b-2, b-3)

The closed, partially closed, and open shelters suffered moderate, serious, and severe damage, respectively, caused by an excess of interior over exterior pressure on the walls. Retaining walls failed, exposing reinforcing steel in some places (Figs. 5.9, 5.10, and 5.11). Shelter walls cracked from tension in the closed and partially closed shelters, and in the open shelter the walls either separated from the roof and floor or were badly cracked (Figs. 5.12, 5.13, and 5.14). Ordinarily, pressure is transmitted through the soil to the outside of the wall, restraining it against the effect of interior pressure. In this case, however, the earth was uncompacted, did not give passive restraint, and transmitted little or no restraining pressure to the exterior of the wall. Because the layer of loose soil was thick, no air pressure was transmitted down through the voids.

Doors on the closed and partially closed shelters failed, indicating that a stronger rebound device is required. The device used to lock door No. 2 did not fail, and this design may be adequate. It consisted of an angle with a slit in its vertical leg and with its horizontal leg bolted to the outside of the door. A steel plate was anchored to the side retaining wall, and a steel loop was welded to the plate. When the door was in the closed position, the loop fitted into the slit in the angle leg. A steel bar was inserted into the loop to prevent upward motion of the door.

Shelters were littered with dirt and missiles.

5.2.2 Shot Apple II (Stations 1-34.1 c-1, c-2, d-1, d-2)

Closed shelters at 1270 ft sustained severe structural damage; all doors blew off in the positive phase, and rebound locks and retaining walls failed (Fig. 5.15) under a pressure of 45 psi. Interior walls were cracked and had outward deformations caused by an unbalance of interior over exterior pressure. This unbalance could be eliminated by a revised door design.

Closed shelters at 1470 ft suffered little interior damage, but all doors and retaining walls failed, apparently during the negative phase (Fig. 5.16).

Damage to open shelters at 1270 and 1470 ft reflected their respective distances from GZ. At 1270 ft the roof and side walls failed—the former from upward distortion, the latter from outward distortion. Retaining and entranceway side walls failed (Fig. 5.17). At 1470 ft retaining walls failed (Fig. 5.18), and interior walls cracked (Fig. 5.19) but not as severely as those at 1270 ft.

On each, some earth cover was blown away, and vent pipes were either blown away or bent.

5.3 UTILITY TYPE SHELTERS

5.3.1 Shot Apple II (Stations 1-34.1 e, f, g), 2250 Ft

The masonry shelter disintegrated (Fig. 5.20); the poured-in-place reinforced-concrete shelter remained intact but was swept 50 ft from its original position to lie on its side (Fig. 5.21); and the precast reinforced-concrete shelter failed (Fig. 5.22). On the latter, roof failure occurred in the slab and not in the high-strength bolts used to tie the roof to the walls. Door fastenings failed on the poured-in-place structure, and on the precast shelter the doors blew away.

5.3.2 Shot Apple II (Stations 1-34.1 h, i, j), 2750 Ft

These three shelters remained in place under slightly more than 10 psi, the design pres-

(Text continues on page 97)

Fig. 5.1—Separation of steel plate, Apple I shot; Station 4-34.3 a-1.

Fig. 5.2—Lock bars for shelter door, Apple I shot; Station 4-34.3 a-1.

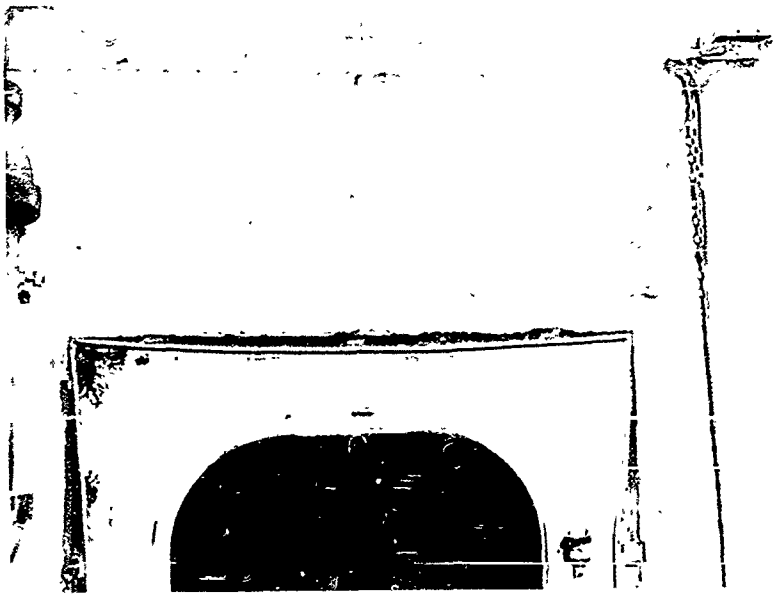

Fig. 5.3—Damage to blast door frame, Apple I shot; Station 4-34.3 b-1.

Fig. 5.4—Damage to blast door frame, Apple I shot; Station 4-34.3 b-1.

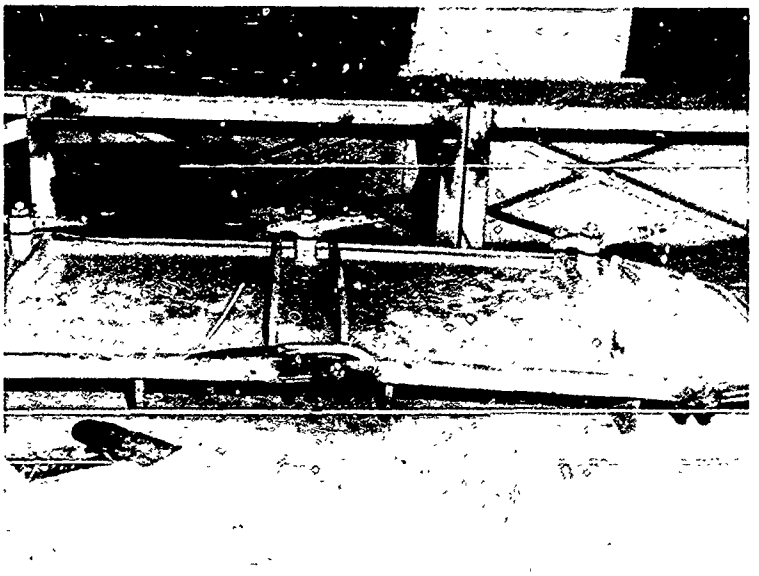

Fig. 5.5—Damage to blast door, Apple I shot; Station 4-34.3 b-1.

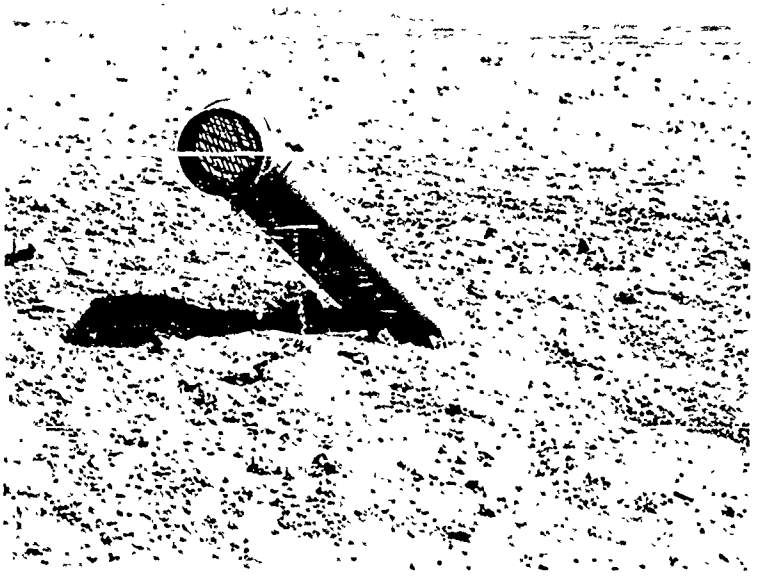

Fig. 5.6—Permanent distortion of vent pipe, Apple I shot, Station 4-34.3 a-1.

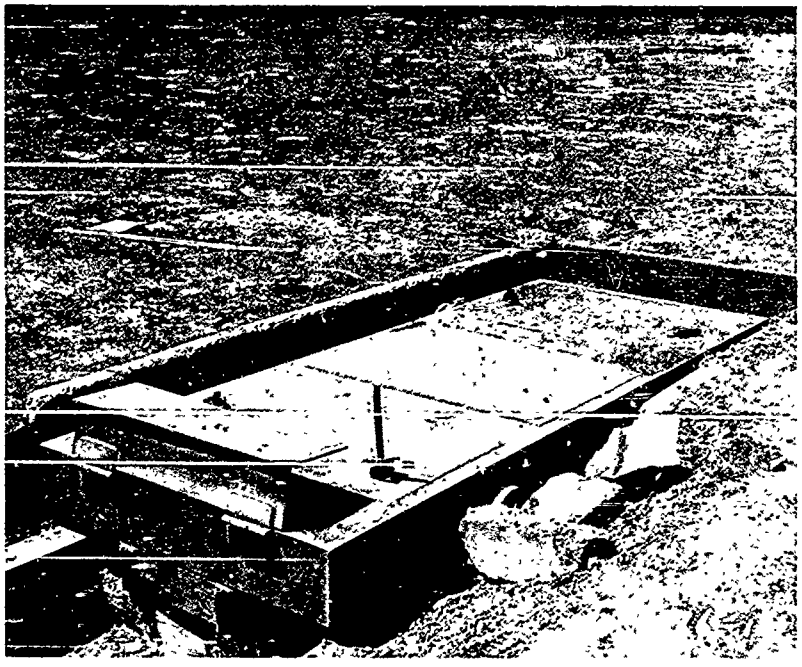

Fig. 5.7—Sliding door slab, Apple II shot; Station 1-34.3 a-2.

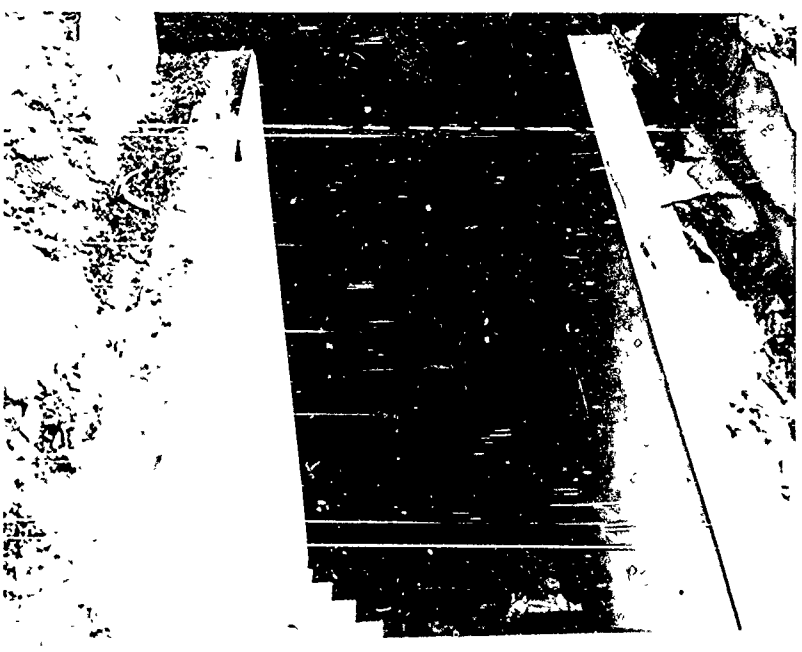

Fig. 5.8—Shelter entrance, post-Apple II shot; Station 1-34.3 a-2.

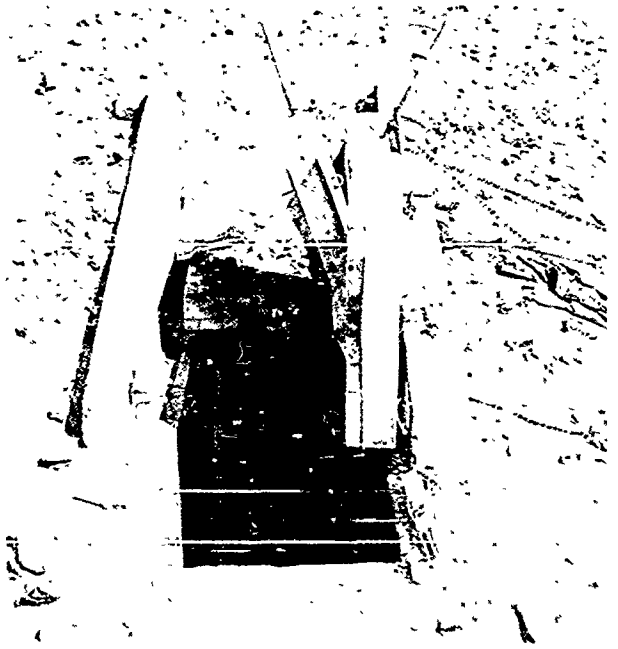

Fig. 5.9—Closed basement exit shelter, post-Apple I shot; Station 4-34.1 b-1.

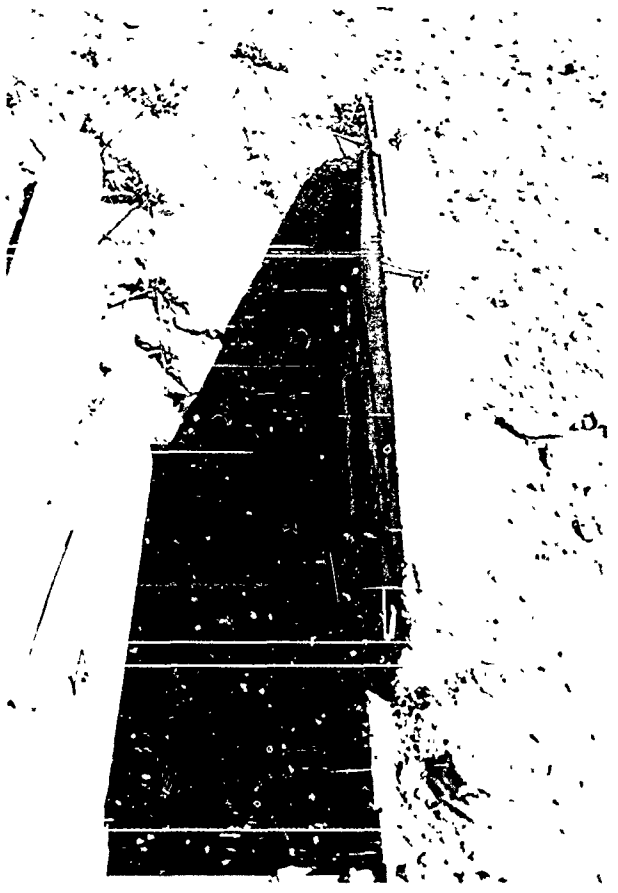

Fig. 5.10—Entrance to partially closed basement exit shelter, post-Apple I shot; Station 4-34.1 b-2.

Fig. 5.12—Interior of closed basement exit shelter, post-Apple I shot; Station 4-34.1 b-1.

Fig. 5.11—Entrance to open basement exit shelter, Apple I shot; Station 4-34.1 b-3.

Fig. 5.13—Damage to wall of partially closed basement exit shelter, Apple I shot; Station 4-34.1 b-2.

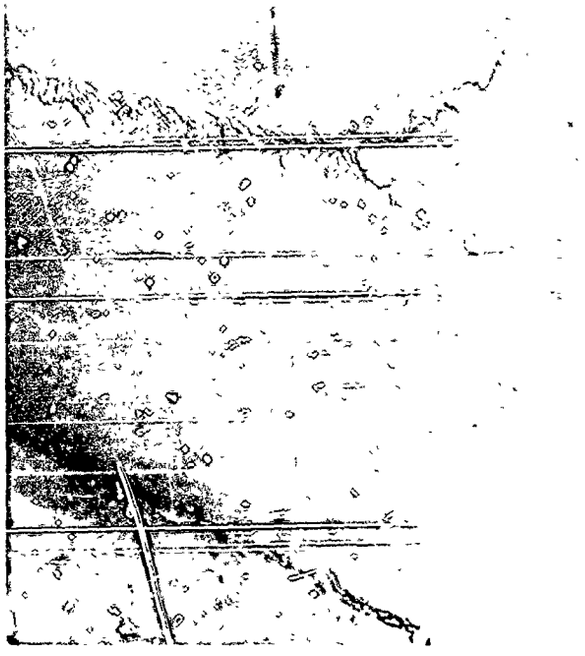

Fig. 5.14—Damage to wall of open basement exit shelter, Apple I shot; Station 4-34.1 ; 2.

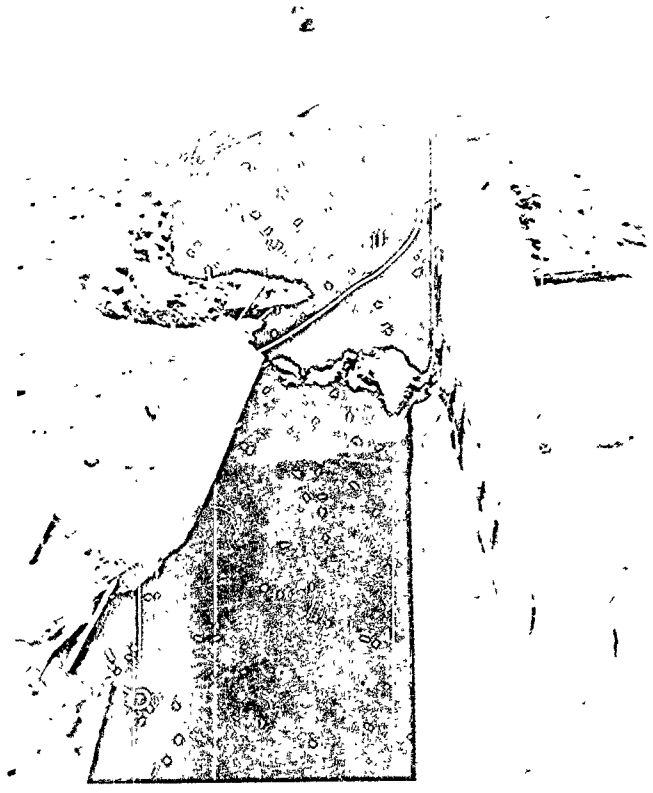

Fig. 5.15—Entrance to closed basement exit shelter, 1270 ft, Apple II shot; Station 1-34.1 c-1.

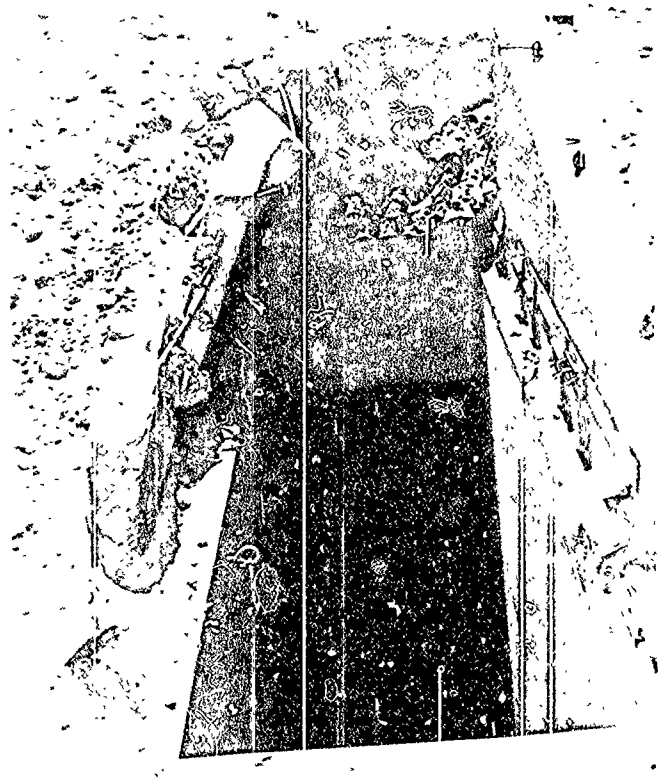

Fig. 5.16—Entrance to closed basement exit shelter, 1470 ft, Apple II shot; Station 1-34.1 d-1.

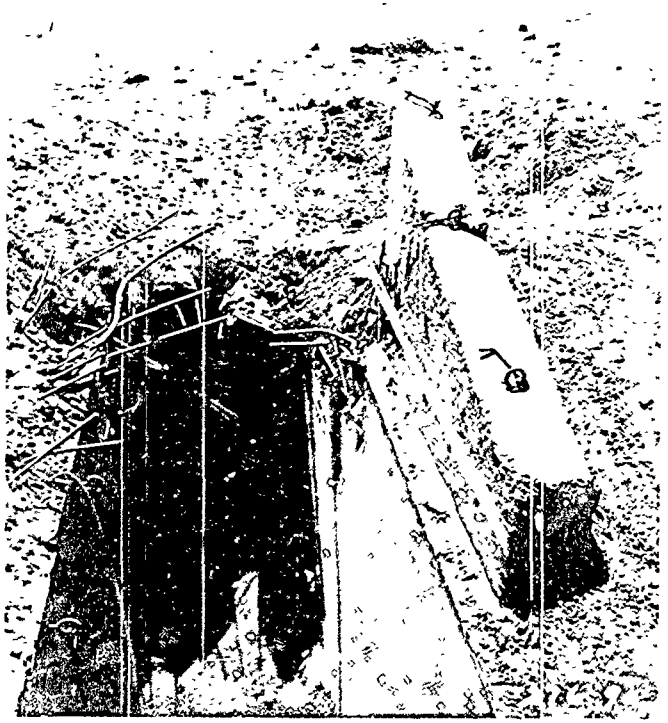

Fig. 5.17—Entrance to open basement exit shelter, 1270 ft, Apple II shot; Station 1-34.1 c-2.

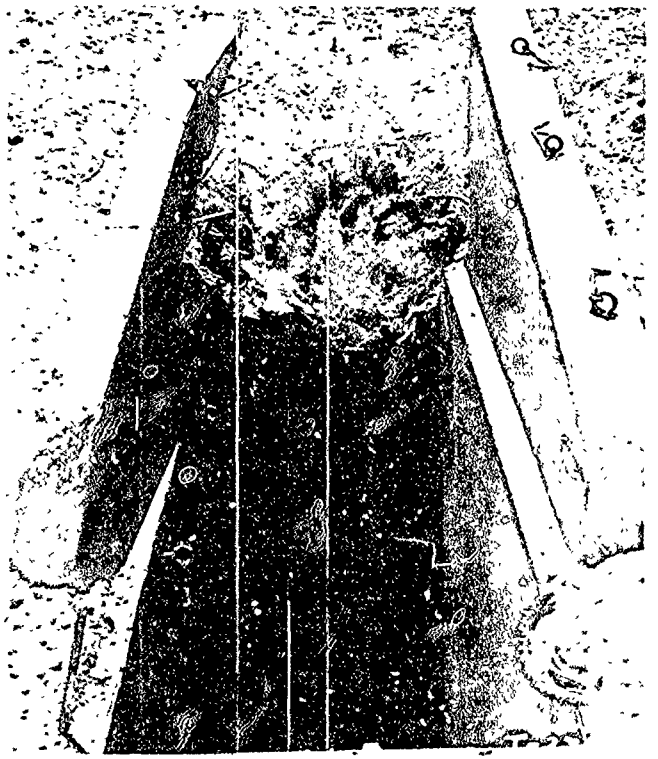

Fig. 5.18—Entrance to open basement exit shelter, 1470 ft, Apple II shot; Station 1-34.1 d-2.

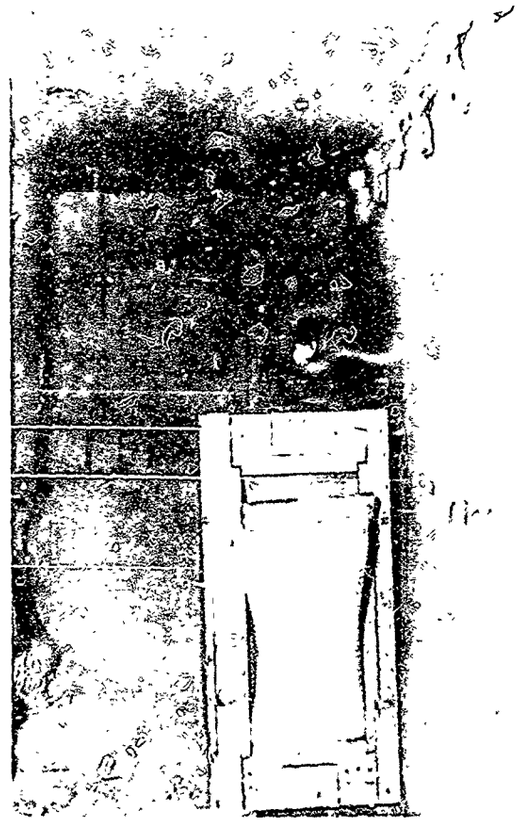

Fig. 5.19—Interior of open basement exit shelter, 1470 ft, Apple II shot; Station 1-34.1 c-2.

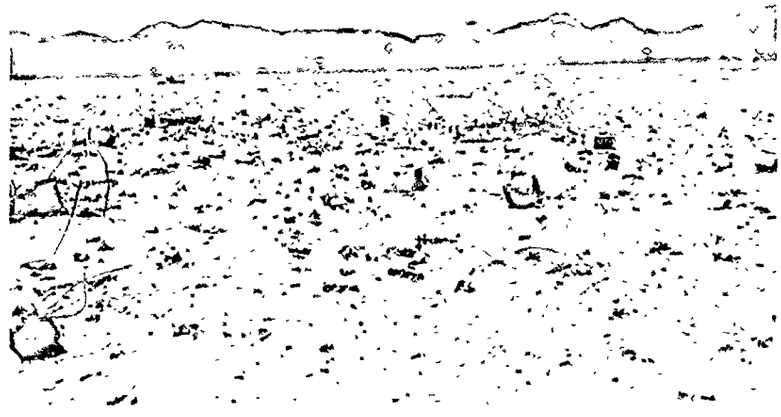

Fig. 5.20—Debris from masonry utility type shelter, 2250 ft, Apple II shot; Station 1-34.1 e.

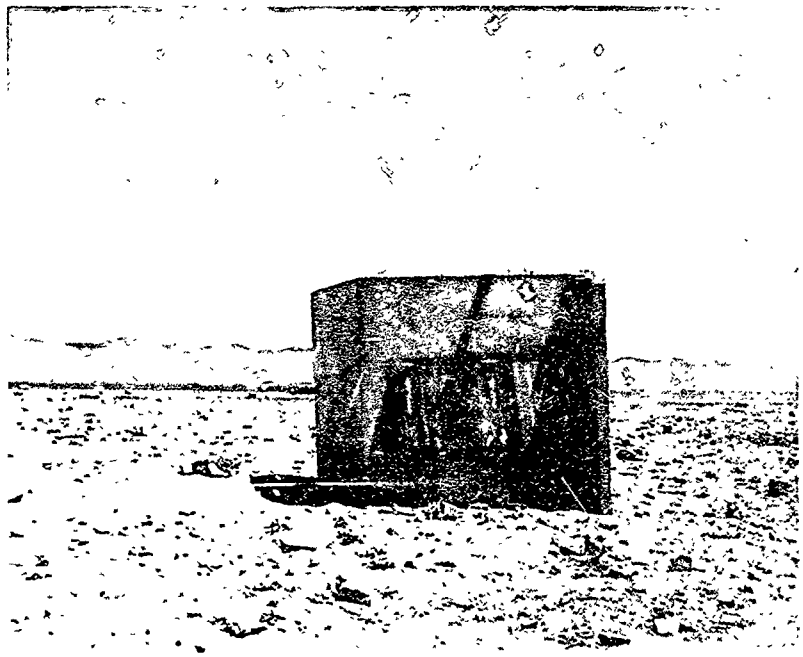

Fig. 5.21—Reinforced-concrete (poured-in-place) utility type shelter, 2250 ft, Apple II shot; Station 1-34.1 f.

Fig. 5.22—Reinforced-concrete (precast) utility type shelter, 2250 ft, Apple II shot; Station 1-34.1 g.

sure, and suffered no discernible damage. This indicates that the structures have the required strength and stability at the design pressure but have little reserve strength against an increase of this pressure.

Outer doors were intact, but there was some evidence that rebound latches yielded. Each interior door was blown off its hinges, and the latch was found lying against the opposite wall. Failure of the interior door connections would not have occurred had the doors been left open as was intended by the designers.

5.3.3 Shot Apple II (Stations 1-34.1 k, l, m), 3750 Ft

The shelters suffered no structural damage. Inner doors, however, also failed at the hinges and latches at this distance. The bolts latching the outer door of Station 1-34.1 m were badly deformed, but on the whole the rebound latches were effective — more effective than the original design which featured latches on the inside of the door.

5.4 INDOOR FAMILY TYPE SHELTERS

Basement lean-to shelters in the brick and wood-frame houses on Apple II (at 4700, 5500, 7800, and 10,500 ft) suffered no damage. Despite the fact that the houses at the closer ranges were virtually destroyed, the first floor framing system did not fail, and there was no debris load in the basement.

Basement corner-room shelters in the same houses as the lean-to shelters were undamaged, as were the reinforced-concrete basement shelters in wood-frame houses at 5500 and 7800 ft.

Fig. 5.23 — Concrete bathroom shelter, 4700 ft, Apple II shot.

Reinforced-concrete bathroom shelters in the one-story rambler houses at 4700 and 10,500 ft suffered no damage (Fig. 5.23), although the house at 4700 ft was totally destroyed and the shelter was subjected to a pressure of 5 psi. On each, the blast door was intact, but on the closest one the blast shutter latch failed. However, neither the glass nor the sash was broken.

CHAPTER 6

SHELTER EVALUATION

6.1 NUCLEAR RADIATION PENETRATION

It is anticipated that occupants of a group shelter would have rescue or other duties which would require their being exposed to radiation outside the shelter in pursuance of these duties. Therefore underground personnel group shelters were designed to reduce radiation inside to not more than 25 r since to design for an irradiation-to-sickness threshold would render occupants useless for emergency activities. It is not unreasonable to extend the 25-r limit criterion to family type shelters because present high-intensity fall-out weapons will subject shelter occupants to large amounts of radiation as the shelters are evacuated.

Gamma radiation measurements inside the shelters can be converted directly into radiation effect on shelter occupants. For neutron radiation effect, however, the process is not so direct. Dr. Payne S. Harris (Project 39.7) has given the conversion factors to roentgen equivalent physical (rep) as 5×10^{-11} rep neutron cm^2 for gold and 3.9×10^{-9} rep/neutron/cm^2 for sulfur.[1] Thermal neutrons contributed not more than 1 to 2 per cent to the total rep, assuming the 2 per cent should give a lower limit on biological effect. It should be expected that the sulfur neutrons would contribute 10 per cent to the total rep from an unshielded weapon. Since Apple I and Apple II shots were shielded, Dr. Harris expected the contribution to be from 1 to 5 per cent. Because the fast-neutron flux on Apple II was only about 10 per cent of that on unshielded Wasp and Hornet shots (neutron yields compared on a 1-kt basis), it is assumed in this report that the contribution from sulfur neutrons is 1 per cent of the total rep. This should give an upper limit on the biological effect.

These values would apply to a biological system at ground level outside a shelter. But what happens to a man inside the shelter? We know from this experiment what happened inside and outside the shelters to the gold and sulfur neutrons only, but we have no information on the neutron energies between. Dr. Harris has found that the percentage of total flux in air contributed by each spectrum band remained essentially constant with distance. Without measurements between gold and sulfur energies, we can only assume that energy distribution within the neutron spectrum did not materially change in passing through earth, concrete, and other materials into the shelter. Thus the only available shelter evaluation consists in assuming that the conversions from gold and sulfur neutrons to rep in air are equally valid inside the shelters. The information in Table 6.1 is based on this assumption. Furthermore, in evaluating the utility type shelters, it is assumed that thermal neutrons inside the shelters are the same as those estimated outside and that the fast neutrons inside are the same proportion of those estimated outside as in the case of the measurement made in the near masonry shelter.

The roentgen equivalent man (rem) equivalent of neutron radiation is based on a relative biological effectiveness (RBE) of 1.6 (reference 2) from a reevaluation of Hiroshima and Nagasaki data by Dr. Harris. To evaluate the total exposure, curves from Hiroshima and Nagasaki

of percentage affected vs exposure in roentgens were obtained from Dr. Harris and are used here (Fig. 6.1).

The closed underground personnel shelter at 1050 ft probably provided satisfactory protection from radiation. The high reading on a sulfur detector from the end of this shelter away from the entrance on Apple II prevents a positive conclusion that the shelter is satisfactory.

None of the basement exit and utility type shelters provided satisfactory radiation protection.

Indoor family type shelters were satisfactory beyond 1 mile. There is some doubt about the three indoor shelters at 4700 ft. It should be borne in mind that the basement lean-to and the basement corner-room shelter were located in the best possible position with respect to the burst point. If they had been located on the opposite side of the basement, it is likely that total exposure would be closer to that of the incident fast-neutron radiation

The amount of shielding provided by the shelters against prompt gamma radiation is significant. Although the energy of prompt gamma radiation is generally higher than that of fall-out radiation and the shielding provided is more effective against fall-out radiation, the shielding against prompt radiation may be used as a lower limit of the shielding which would be provided against fall-out. Table 6.2 gives the ratios of gamma radiation (as measured outside the shelters to that inside). In general, shielding efficiency of a particular design decreases with distance from the source.

With the exception of the reinforced-concrete shelter, basement shelters were not expected to provide significant amounts of radiation protection over that provided by the basement. To evaluate that portion of the protection provided by the basement and that furnished by the shelter, the ratio of the average gamma radiation inside the basement to that inside the shelter is also given in Table 6.2.

6.2 THERMAL CONVECTION

Measured temperatures were all less than had been anticipated. Although it is possible that they were actually less, it is also possible that there was a steep temperature gradient away from the cool concrete walls of the biomedical shelter. The whistle temperature gauge was flush-mounted in the wall and was measuring a small amount of air from near the wall. If it had sampled air a greater distance from the wall, a higher temperature might have been recorded.

There is some literature on the effect of radiant thermal energy of short duration on the skin of humans and animals, but little information exists on the effect of heat transfer by convection to skin from air with short-duration thermal transients. Extrapolating information from Buettner[3] to shorter durations, assuming that pain involves a skin temperature of 42 to 45°C and third-degree burns result from four times the pain dosage and that the effect of heat transferred to the skin by convection is no different than that transferred by radiation, it is possible to estimate thermal convection effects. This would indicate that both measured temperatures and expected higher temperatures were insufficient to burn human skin. Despite this, some experimental animals showed singeing and scorching of fur. A few had minor burns on exposed skin. Both skin burn and singeing were functions of the location and orientation of the animals within the shelter. In the fast-fill room the burning and singeing pointed to a source entering the door and rotating counterclockwise in the room; that is, the animal beside gauge P-7 (Fig. 1.19) was singed as if the heat were coming from the direction of gauge P-6. This indicates convection or dust carried by the air transferred heat to skin and fur. In the slow-fill room where thermal effects were directional, the sources appear to be planar, originating from the wall in which gauge P-10 was located.

The only singed animals located near a temperature gauge were those in the Apple II shelter where peak measured temperatures were also the highest measured (over 300°C). In this respect measured temperatures were consistent with the results on animals. At some of the other locations, animals were subjected to higher temperatures than those measured.

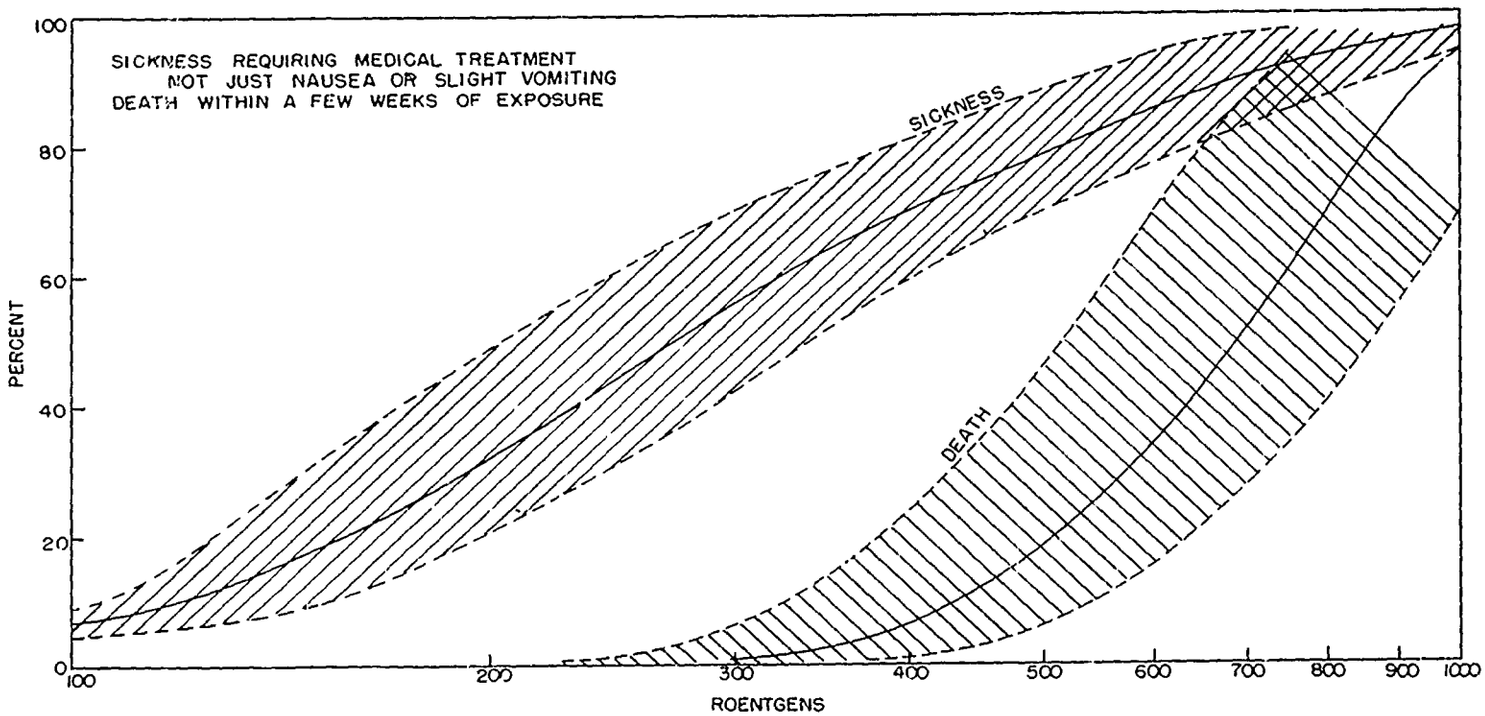

Fig. 6.1—Percentage affected vs exposure.

Table 6.1 RADIATION SUMMARY

Shelter	Ground distance, ft	Neutron flux, Incident, Fast	Incident, Thermal	Exit, Fast	Exit, Thermal	Rep, Upper limit	Rep, Lower limit	Rem, Upper limit	Rem, Lower limit	Average gamma inside, r	Gamma exposure, Upper limit, r	Gamma exposure, Lower limit, r	Sick, Lower	Sick, Upper	Dead, Lower	Dead, Upper
Apple I																
Underground group shelter																
4 [illegible]	1,650	2.87×10^{11}	1.33×10^{9}	1.72×10^{9}		64		109		0.4	109			7	0	0
4 34.3 b-1 (fast-fill)	1,050			7.18×10^{9}		285		456		14	470			75		15
4 34.3 b-1 (slow-fill)	1,050			(entrance)						130	586			85		30
Basement exit shelters																
4 34.1 b-1	1,350	1.39×10^{11}	5.9×10^{12}	5.9×10^{11}	7.3×10^{11}[a]	2,300	1,800	3,680	2,880	84	3,764	2,964	100	100	100	100
4 34.1 b-2	1,350			9×10^{11}	9.7×10^{11}[a]	3,500	2,400	5,600	3,840	194	5,794	4,034	100	100	100	100
4-34.1 b-3	1,350			1.2×10^{12}	1.24×10^{12}[a]	4,700	3,100	7,520	4,960	226	7,746	5,186	100	100	100	100
Apple II																
Underground group shelter																
1-34.3 a-2	1,650	1.53×10^{2}	3×10^{3}	4.01×10^{8}		160		256		1.57	258		0	45		0
				2.94×10^{7}	2.33×10^{8}	12	<1	19	<1		20.5	2	0	0	0	0
				$<2\times10^{5}$	$7.75-8.85\times10^{6}$	<1	2	1	3		2	5	0	0	0	0
1-34.3 b-2 (fast-fill)	1,650			1.62×10^{9}	1.03×10^{11}	650	260	1,040	416	50	1,090	466	75	100	15	100
1-34.3 b-2 (slow-fill)	1,650			5.93×10^{9}	8.56×10^{11}	2,000	2,100	3,200	3,360	460	3,660	3,820	100	100	100	100
Basement exit shelters																
1-34.1 c-1	1,270	7.6×10^{11}	1.6×10^{13}	3.76×10^{10}	2×10^{12}	15,000	4,900	24,000	7,840	377	24,377	8,217	100	100	100	100
1-34.1 c-2	1,270			8.43×10^{10}	3.4×10^{12}[b]	22,000	8,300	35,200	13,300	600	35,800	13,900	100	100	100	100
1-34.1 d-1	1,470	5.2×10^{11}	9.6×10^{12}	1.92×10^{10}	1.13×10^{12}	7,500	2,900	12,000	4,640	229	12,229	4,869	100	100	100	100
1-34.1 d-2	1,470			5.72×10^{10}	2.02×10^{12}	25,000	4,900	40,000	7,840	388	40,388	8,228	100	100	100	100
Utility type shelters																
1-34.1 e (precast)	2,250	6.5×10^{9}	1.5×10^{12}	1.55×10^{10}[c]	1.51×10^{12}[c]	6,000	3,700	9,600	5,920	2,650	12,250	8,570	100	100	100	100
1-34.1 f (poured)	2,250			1.55×10^{10}[c]	1.51×10^{12}[c]	6,000	3,700	9,600	5,920	2,388	11,988	8,308	100	100	100	100
1-34.1 g (masonry)	2,250			1.55×10^{10}	1.51×10^{12}	6,000	3,700	9,600	5,920	7,250[d]	12,020	8,340	100	100	100	100
1-34.1 h (precast)	2,750	3.1×10^{10}	5.1×10^{11}	5.45×10^{9}[c]	5.1×10^{11}[c]	2,300	1,250	3,680	2,000	1,205	4,885	3,205	100	100	100	100
1-34.1 i (poured)	2,750			5.45×10^{9}[c]	5.1×10^{11}[c]	2,300	1,250	3,680	2,000	1,075	4,755	3,075	100	100	100	100
1-34.1 j (masonry)	2,750			5.45×10^{9}[c]	5.1×10^{11}[c]	2,300	1,250	3,680	2,000	1,179	4,859	3,179	100	100	100	100
1-34.1 k (precast)	3,750	4.4×10^{9}	6.9×10^{9}	7.75×10^{8}[c]	6.9×10^{10}[c]	300	175	480	280	277	757	557	85	95	25	50
1-34.1 l (poured)	3,750			7.75×10^{8}[c]	6.9×10^{10}[c]	300	175	480	280	275	755	555	85	95	25	60
1-34.1 m (masonry)	3,750			7.75×10^{8}[c]	6.9×10^{10}[c]	300	175	480	280	226	706	506	80	90	20	50
Reinforced-concrete bathroom	4,700	6.8×10^{8}	1.1×10^{10}			<350	<25[e]	<560	<40	51	<611	<91	<5	85	0	35
	10,500	1.0×10^{8}	5.8×10^{8}			<1	<1[e]	1	<1	0.24	<1	<1	0	0	0	0
Reinforced-concrete basement room	5,500	2.4×10^{8}	2.7×10^{9}			<95	<7[e]	<152	<11	1.77	<154	<13	0	20	0	0
	7,800	6.2×10^{8}	5.2×10^{7}			<2.5	<1[e]	4	<1	0.20	<4	<1	0	0	0	0
Basement corner room	4,700	8.8×10^{8}	1.1×10^{10}			350	<25[e]	560	<40	28	<588	<68	0	85	0	30
	5,500	2.4×10^{8}	2.7×10^{9}			95	7[e]	152	11	21	<173	<32	0	25	0	0
	7,800	6.2×10^{8}	5.2×10^{7}			<2.5	<1[e]	<4	<1	1.22	5	<2	0	0	0	0
	10,500	1.0×10^{8}	5.8×10^{8}			1	<1[e]	<1	<1	0.13	1	<1	0	0	0	0
Basement lean-to shelter	4,700	8.8×10^{8}	1.1×10^{10}			350	<25[e]	<560	<40	6.7	<567	<47	0	85	0	30
	5,500	2.4×10^{8}	2.7×10^{9}			<95	[illegible][e]	152	<11	2.48	<155	<14	0	20	0	0
	7,800	6.2×10^{8}	5.2×10^{7}			<2.5	[illegible][e]	4	<1	0.67	<4	<1	0	0	0	0
	10,500	1.0×10^{8}	5.8×10^{8}			<1	<1[e]	<1	<1	>0.10	<1	<1	0	0	0	0

[a] Estimated as same or intermediate percentage of incident neutron flux as measured in Apple II.
[b] Estimated as same percentage of incident neutron flux as Station 1-34.1 d-2.
[c] Estimated as same percentage of incident neutron flux as measured for Station 1-34.1 g.
[d] Average of only two dosimeters, both of which read high because of relatively long postshot contact with the ground, 2420 r used for calculations in table.
[e] Based on unadjusted values of estimated external radiation, probably overestimates interior neutron effect by two to four times.

Table 6.2—RATIO OF PROMPT GAMMA RADIATION INSIDE SHELTERS TO THAT OUTSIDE

Shelter	Ratio: incident to average inside	Ratio: average in basement to average in shelter
	Apple I	
Underground personnel		
4-34.3 a-1	25,000	
4-34.3 b-1 (fast-fill)	710	
4-34.3 b-1 (slow-fill)	77	
Basement exit		
4-34.1 b-1	140	
4-34.1 b-2	62	
4-34.1 b-3	53	
	Apple II	
Underground personnel		
1-34.3 a-2	11,000	
1-34.3 b-2 (fast-fill)	350	
1-34.3 b-2 (slow-fill)	38	
Basement exit		
1-34.1 c-1	93	
1-34.1 c-2	58	
1-34.1 d-1	103	
1-34.1 d-2	60	
Utility type		
1-34.1 e (precast)	1.5	
1-34.1 f (poured)	1.7	
1-34.1 g (masonry)		
1-34.1 h (precast)	1.8	
1-34.1 i (poured)	2.0	
1-34.1 j (masonry)	1.9	
1-34.1 k (precast)	2.3	
1-34.1 l (poured)	2.3	
1-34.1m (masonry)	2.8	
Reinforced-concrete bathroom		
4,700 ft	3.8	
10,500 ft	1.2	
Reinforced-concrete basement room		
5,500 ft	40	8.7
7,800 ft	26	6.5
Basement corner-room		
4,700 ft	6.8	0.9
5,500 ft	3.4	0.7
7,800 ft	4.2	1.1
10,500 ft	2.3	1.3
Basement lean-to		
4,700 ft	25	1.1
5,500 ft	29	2
7,800 ft	7.7	2
10,500 ft	3.0	2

The temperatures cannot be inferred from the results on animals until experimental work is done which points out the temperature-time parameters required to singe fur or burn skin by convection and/or dust.

6.3 BLAST EFFECTS AND STRUCTURAL DAMAGE

Underground group personnel shelters appear to provide sufficient protection for occupants against blast and missiles for peak incident pressures of 92 psi or less. Antiblast closures operated successfully to prevent entry of damaging overpressures. Doors and escape hatches, if not as originally operable, were capable of being jacked open from the inside. Structurally, the shelters proved the validity of their design. Shelter displacement (1.7 in. downward) was insufficient to cause harm to occupants.

An unbalance between interior and exterior pressure resulting from failure of the doors caused the severe interior structural damage to basement exit shelters. Possibly a revised door design would reduce the pressure inside enough to offer occupants refuge from blast effects.

The fact that the three utility type structures at 2750 ft withstood overpressures of 11.6 psi and those at 2250 ft failed under 11.7 psi indicates that the shelter is capable of withstanding the design overpressure of 10 psi in an ideal shock wave and that it is not capable of withstanding the same overpressure in a precursor. Of the three types (masonry, precast, and poured-in-place), the poured-in-place reinforced-concrete shelter seems to have the most resistance to blast and the reinforced-masonry shelter the least. Strengthening of the interior door and its connections is required. Rebound latches are adequate as tested.

Basement corner-room, lean-to, and reinforced-concrete shelters provide protection from missiles and debris and the effects of a sharp shock, but they do not significantly alter the maximum overpressure within the basement. Since there was no debris loading, the relative effectiveness of these shelters under such loading cannot be evaluated from these tests.

At the distances tested, reinforced bathroom shelters would have provided adequate protection from blast and missiles.

REFERENCES

1. P. S. Harris, Physical Measurement of Neutron and Gamma Radiation Dose from High Neutron Yield Weapons and Correlation of Dose with Biological Effect, Operation Teapot Report, ITR-1167 (to be superseded by WT-1167).
2. P. S. Harris, Biological Effectiveness of Nuclear Radiation from Fission Weapons, Report LA-1987, August 1955.
3. Konrad Buettner, Effects of Extreme Heat on Man. I. Protection of Man Against Conflagration Heat, Report No. 1, USAF School of Aviation Medicine, Randolph Field, Tex., February 1950.

CHAPTER 7

CONCLUSIONS AND RECOMMENDATIONS

7.1 CONCLUSIONS

7.1.1 Radiation Penetration

The closed underground group personnel shelters provided satisfactory protection from radiation. One unexplainably high reading from a fast-neutron detector casts some doubt on this conclusion. These shelters had been designed to reduce radiation to at least 25 r.

Using these same design criteria, the basement shelters and the utility type shelters did not provide satisfactory radiation protection. The reinforced-concrete bathroom shelter at 4700 ft was also unsatisfactory.

The reinforced-concrete bathroom shelter at 10,500 ft and the indoor basement shelters beyond 4700 ft provided satisfactory protection against radiation. At 4700 ft the indoor basement shelters, except the lean-to, had exposures in excess of 25 r. If the lean-to had been built on the opposite side of the basement or extended higher, it might have received a larger amount of radiation.

7.1.2 Thermal Convection

Temperatures inside the open biomedical shelter were less than had been predicted. Although this shelter would not ordinarily be used as an open shelter, it has shown that occupants of an open similarly designed shelter at this distance would sustain some burns.

7.1.3 Blast Effects and Structural Damage

(a) Apple I Shot. The antiblast closure unit in the closed underground personnel shelter operated satisfactorily and prevented damage to the diffusion-board installation inside the shelter. No build-up of pressure existed within the shelter when it was exposed to a peak overpressure of 47 psi. Persons inside the closed underground shelter would have been protected from blast and from the results of structural damage from a weapon of the yield of Apple I shot.

Experimental animals in the closed basement exit shelters at 17.3 psi indicate that occupants of the shelters would not have become fatalities but probably would have been injured or subjected to more than an unobjectionable amount of discomfort. It is doubtful that the closed shelter should be expected to provide protection from overpressures in excess of 10 psi.

(b) Apple II Shot. The reinforced-concrete door of the underground personnel shelter suffered superficial damage which a redesign should correct. The antiblast closure operated satisfactorily and prevented any overpressure within the shelter proper. The shelter, as tested, would provide protection from missiles and overpressure.

The basement exit shelters would not have furnished effective protection against blast of the overpressure levels to which they were subjected.

The indoor family type shelters provided adequate protection from missiles and debris under the conditions tested. The concrete bathroom shelter reduced the overpressure by a significant amount, but in the other types the overpressure inside the shelter was about the same as in the incident wave. Although no measurement was made, it is believed that the basement concrete room shelter would have reduced the overpressure in much the same manner as the concrete bathroom shelter.

7.2 RECOMMENDATIONS

7.2.1 Radiation Penetration

Every opportunity should be taken to measure radiation inside and outside of structures to determine shielding factors. Particular emphasis should be given to measuring the full neutron spectrum inside and outside.

Only the closed group personnel shelters and the indoor family type shelters (other than the bathroom shelter at 4700 ft) should be considered satisfactory as tested.

7.2.2 Thermal Convection

Experiments should be performed which would relate the thermal effects of transient convection to the large amount of information on effects of thermal radiation on the skin.

The reliability of the temperature whistle gauge should be improved.

7.2.3 Blast Effects and Structural Damage

Bolts on the rebound locks on the sliding concrete door of the underground personnel shelter should be increased in diameter. The door should be redesigned so that it seats just at the end of the run and so that it extends over the wheels to provide protection against missiles.[a]

The basement exit shelters require a redesign of the blast door, rebound lock, and retaining walls to withstand incident overpressures in excess of 10 psi. The inner door should be eliminated.

Although with the modifications recommended below they would provide satisfactory protection from blast, no other shelter, as tested, provided less protection from nuclear radiation than the aboveground utility type shelters. Unless redesigned to carry a significant amount of earth cover with a radiation baffle arrangement at the entrance, it is recommended that the concept of an aboveground shelter of this type be dropped. If redesigned, the inner door of the aboveground utility shelters should be eliminated, and heavier rebound latches should be provided with a more positive attachment to the door than screws.

Although the indoor family type shelters provided adequate blast protection under the conditions tested, it is doubtful if the protection would be adequate against high-level fall-out radiation. Therefore it is recommended that attention be given to the development of the simple shelter types which would give protection from fall-out and still provide the same blast protection as those shelters tested on Operation Teapot.

[a]Note in Appendix A that these recommendations have been incorporated in the final design.

APPENDIX A

DESIGN OF AN UNDERGROUND PERSONNEL SHELTER

By

Edward Laing

Ammann & Whitney, Consulting Engineers

ANYTHING ABSTRACTED FROM THE MATERIAL IN APPENDIX A MAY BE TREATED AS UNCLASSIFIED

NOMENCLATURE

R = resistance at support
L = length
$M_{\mathbb{C}}$ = moment of force at center line
M_S = moment of force at end
ULT = ultimate
p = pressure per unit area
f'_{dc} = dynamic ultimate unit stress of concrete
f'_c = static ultimate unit stress of concrete
f_{dy} = dynamic unit stress of steel at yield
f_y = static unit stress of steel at yield
b = breadth or width
d = over-all depth
t = thickness
V = total shear
j = ratio of distance between resultants of compressive and tensile stresses to effective depth
v = unit shear
P = load
e = eccentricity of application of load
A_s = area of steel
a = coefficient used in determining the area of steel
X_{yp_1} = centerline deflection at first yield (see resistance vs deflection curve, Sec. A.7.2)
X_{yp_2} = centerline deflection at second yield point (see Sec. A.7.2)
E = modulus of elasticity
I = moment of inertia
K = kip
k = stiffness
μ = Poisson's ratio for concrete

APPENDIX A

DESIGN OF AN UNDERGROUND PERSONNEL SHELTER

A.1 GENERAL

The underground personnel shelter was designed to provide protection against the blast effects of a nuclear weapon detonated at a distance that would produce a relatively long-duration surface overpressure of 100 psi above the shelter. The earth cover and arrangement of the entrance corridor were chosen to provide reduction of the prompt radiation dosage in the shelter to a safe level. A suitable ventilation system was provided to ensure protection against residual radiation and possible bacteriological or gas contamination.

The shelter area is separated from the entrance corridor by an airtight steel-plate door. A blast door at the surface was necessary because a feasible labyrinth configuration could not be found which would provide a substantial reduction of the reflected pressures at the end of the corridor for all the possible orientations. It was decided that the best type of entrance door was one that would be flush with the ground surface and therefore loaded by side-on pressures rather than the higher intensity reflected pressures to which a conventional vertical type door would be subjected. The horizontal door is mounted on commercial type wheels and rails and may be rolled into position to close off the shelter corridor. A modified commercial jack, which is mounted on the corridor ceiling, provides for opening of the door if it should become damaged or jammed by debris.

An emergency exit which consists of a sand-filled vertical shaft above a steel-plate trap door is located in one corner of the shelter area. The trap door is opened by pulling down on a lever mechanism mounted in the ceiling. The sand drops into the shelter, leaving an open exit to the surface. A vertical steel ladder is built into the wall for ascending through the shaft to the surface.

A.2 DESIGN BLAST LOADING

The roof slab was designed to withstand a constant overpressure of 100 psi with an instantaneous time of rise. The upward blast pressure on the floor slab was taken as 75 psi. The estimated blast pressures on the walls were not critical since the strength of the wall was determined by the requirements of the roof and floor slabs.

A.3 STRENGTH CRITERIA

The entire structure was designed for dynamic behavior using ultimate strength theory.[1]

Concrete was required to have a minimum compressive strength of 4000 psi at 28 days. Reinforcing steel was intermediate grade with deformations conforming to ASTM Designation A305-50T, with a minimum specified yield point of 40,000 psi and a probable average of

50,000 psi. The latter figure was used for design. The structural steel conformed to ASTM Designation A7-50, with a minimum specified yield point of 33,000 psi and a probable average value of approximately 40,000 psi. The figure of 40,000 psi was used for design. The dynamic design tensile and compressive yield stresses for steel and the dynamic ultimate compressive stress for concrete were increased over the static values to account for the rapid strain rates[2] caused by the blast loading.

A.4 DESIGN

Most of the structure was designed for plastic deformation. The sliding door at the entrance and the trap door at the escape hatch were designed elastically to avoid excessive deformation which could result in jamming.

The sliding door is a 9 ft 6 in. by 3 ft 9 in. by 8 in. reinforced-concrete slab in a structural steel channel frame, subdivided into three two-way panels by structural steel wide-flange sections. This arrangement gave a minimum slab thickness and weight. To provide against negative phase pressures, a latching device consisting of four bolts passing through the door and secured to the corridor walls was incorporated in the design.

The 3- by 3-ft steel-plate trap door below the emergency escape hatch is composed of a ½-in. steel plate supported by three structural steel channels.

The roof slab, floor slab, and longitudinal side walls of the shelter proper were designed as one-way panels. The end walls were designed as two-way panels using crack line theory.[3] Typical design computations are shown in Sec. A.7 for the roof slab of the shelter.

A.5 ANALYSES

The analyses of the various members of the structure which are exposed to blast consists in the solution of the equation of motion, $F - R = m_e\ddot{x}$, where F is the applied blast force, R is the internal resistance of the structural member, m_e is the mass of an equivalent one-degree-of-freedom system,[4] and $\ddot{x}$ is the acceleration of the mass.

This equation of motion can be readily solved by any of several numerical-integration[5] methods. The numerical method illustrated in Sec. A.7.2 for the analyses of the roof slab of the shelter is the "trial-and-error-solution" described in reference 2.

A.6 ARCHITECTURAL AND STRUCTURAL DRAWINGS

The architectural and structural drawings for the personnel shelter are shown in Figs. A.1 through A.5. The structure shown on these drawings, except for the architectural, is essentially the same as the as-built structure. Several modifications and additions have been made on these drawings subsequent to the test of the shelter. The most significant of these modifications and additions are:

1. Toilet added.
2. Wooden airtight door between exhaust air chamber and intake air chamber replaced with a steel-plate airtight door.
3. Concrete parapet framing around rolling door strengthened.
4. Angle guards for protection of wheels of rolling door added.
5. Size of rebound bolt assembly in rolling door increased.
6. Change in capacity from 50 to 30 persons.

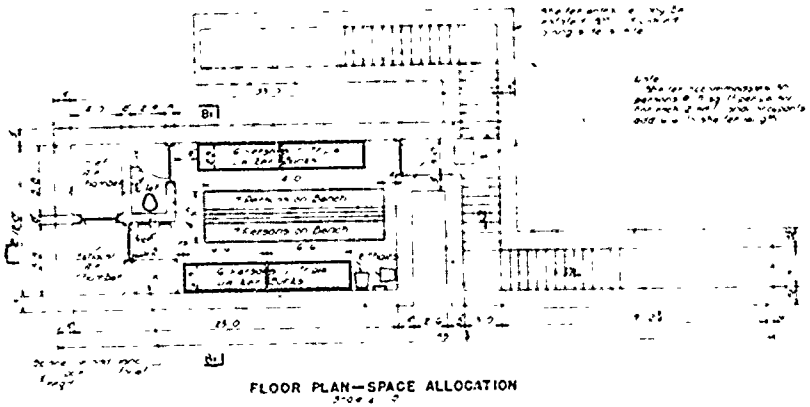

FLOOR PLAN—SPACE ALLOCATION

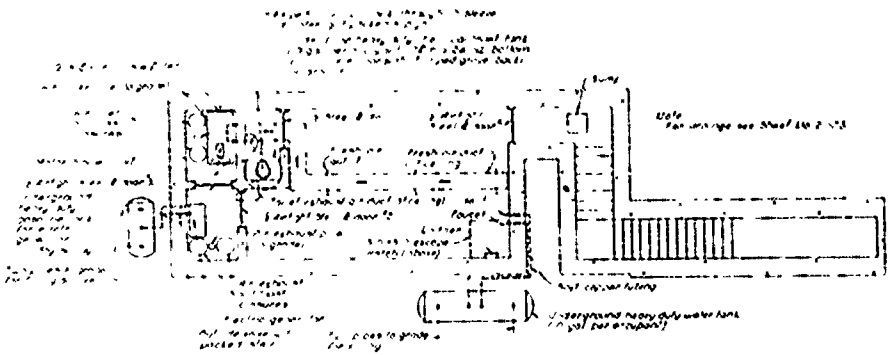

FLOOR PLAN—MECHANICAL EQUIPMENT LAYOUT

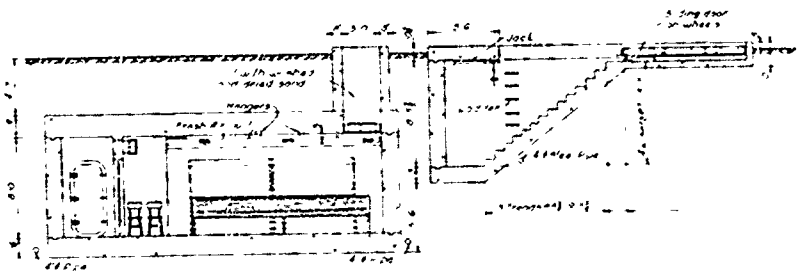

SECTION A1–A1

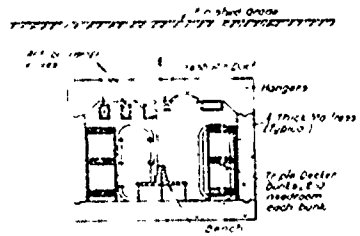

SECTION B1–B1

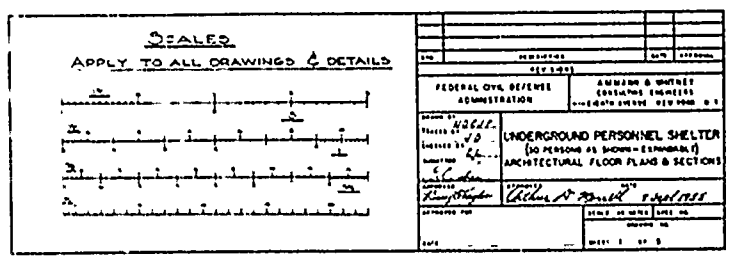

Fig. A.1—Architectural plans and sections, underground personnel shelter.

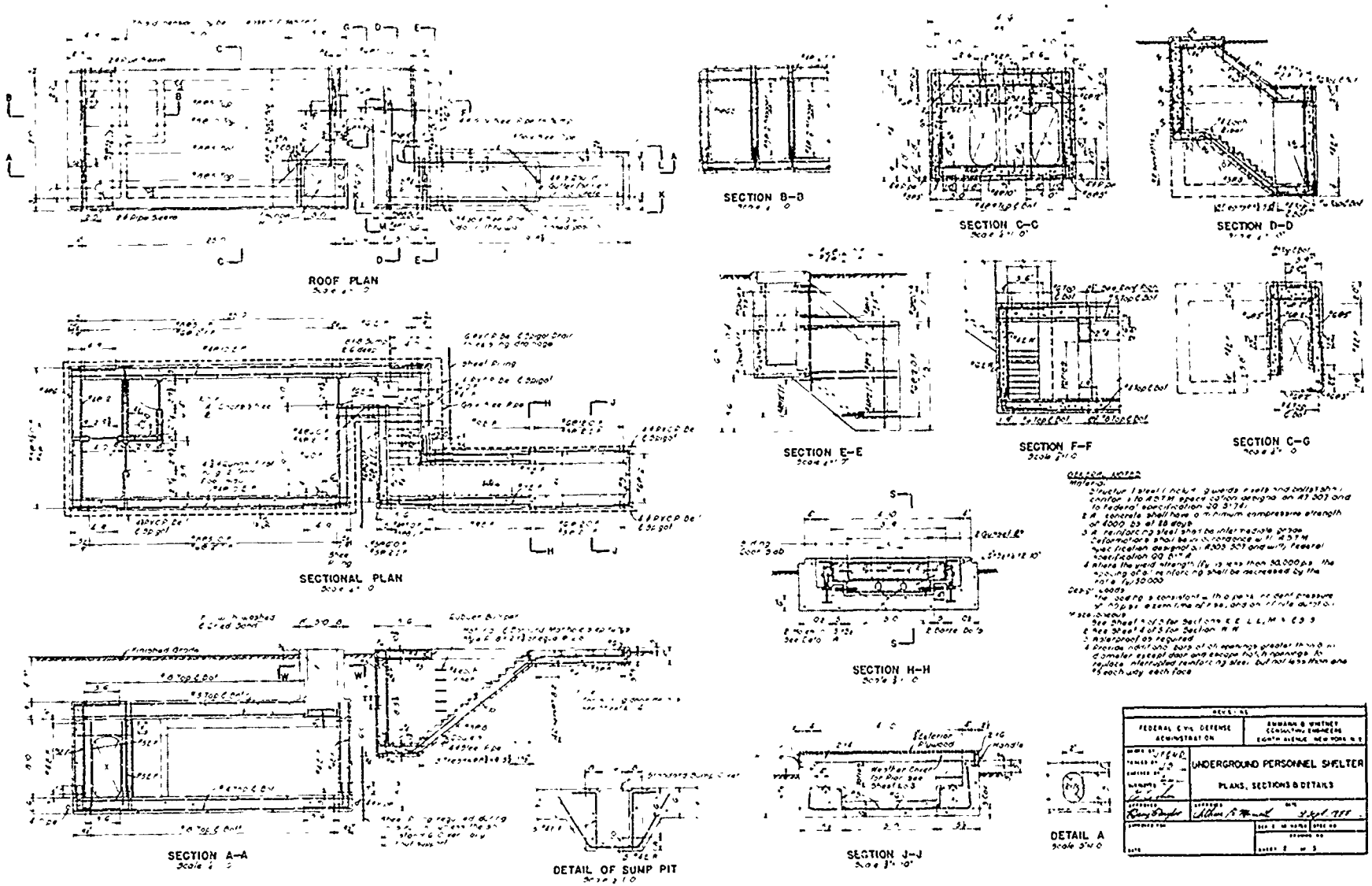

Fig. A.2—Plans, sections, and details, underground personnel shelter.

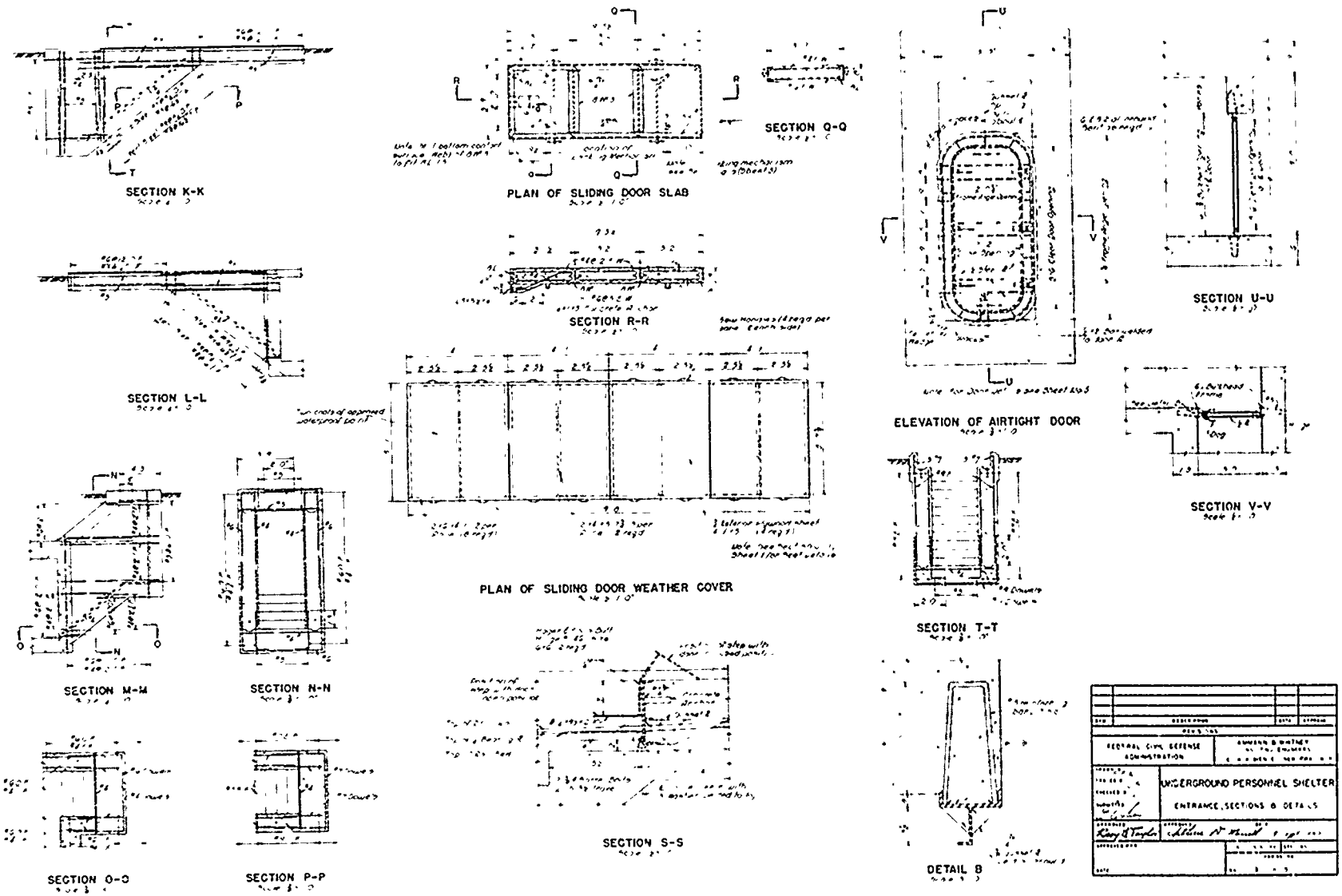

Fig. A.3—Entrance, sections, and details, underground personnel shelter.

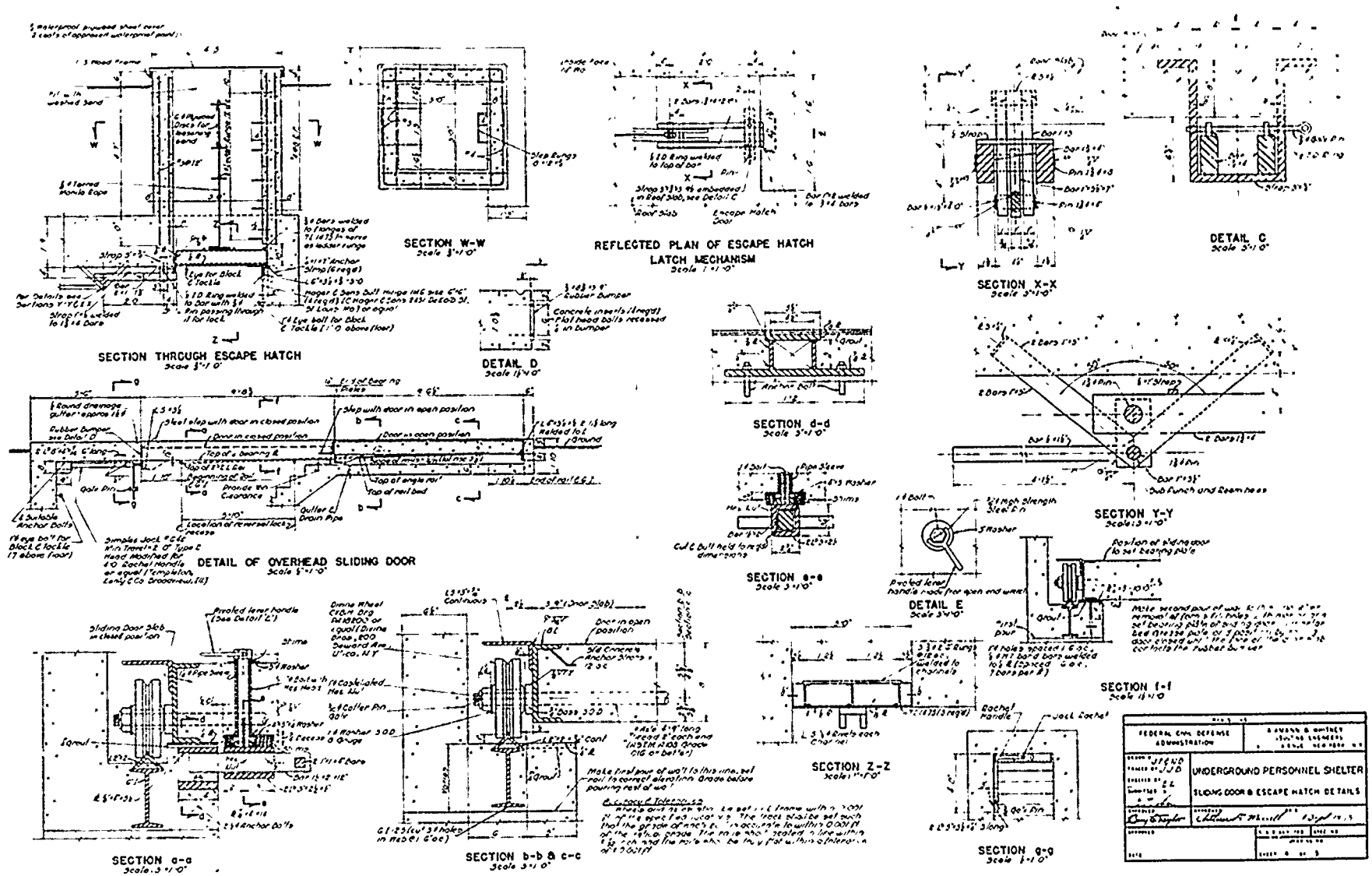

Fig. A.4—Sliding door and escape-hatch details, underground personnel shelter.

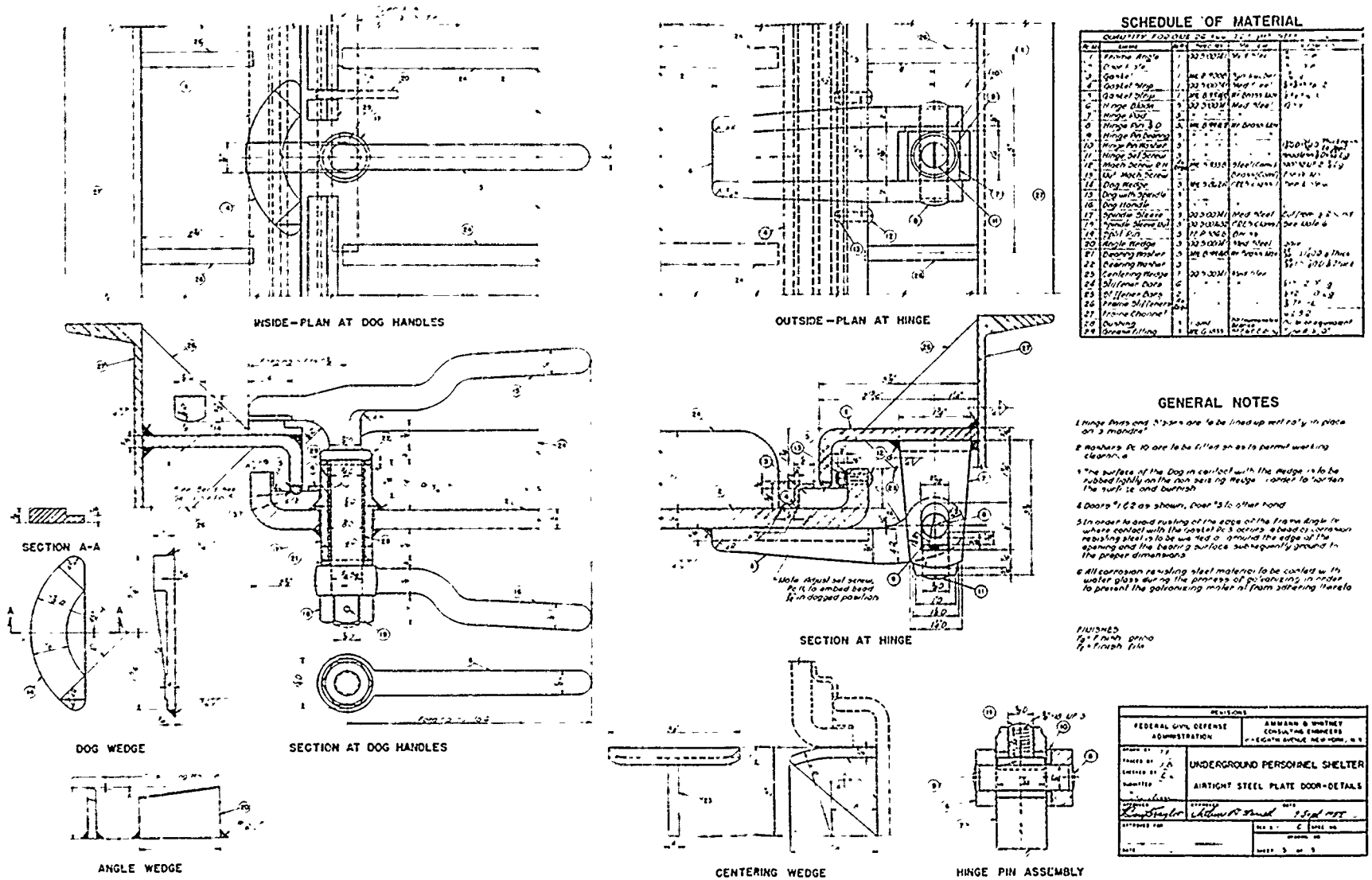

Fig. A.5—Airtight steel-plate door details, underground personnel shelter.

A.7 SAMPLE COMPUTATIONS

A.7.1 Roof Slab Design

Clear span: 12 ft 0 in.
Centerline span: 13 ft 3 in.

Loading:

Blast (assuming 10 per cent increase over static load)	100 psi × 1.10 × 0.144	= 15.85
Soil (4-ft 7-in. cover)	0.100 × 4.58	= 0.46
Concrete (assuming a 1-ft 9-in. thickness)	0.150 × 1.75	= 0.26
		16.57 K/ft^2

Thickness

(1) Moment

$$(M_{\mathbb{Q}} + M_S)_{ULT} \doteq \frac{R_{max} L}{8}$$

$$= \frac{16.57(12.0)^2(12)}{8}$$

$$= 3560 \text{ in. k}$$

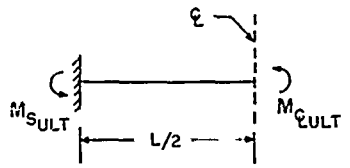

For $M_{℄_{ULT}} = M_{S_{ULT}}$; p = 1.5%; $f'_{dc} = 1.35 f'_c = 5400$ psi; and $f_{dy} = 1.35\ f_y = 67{,}500$ psi

$$\frac{M_{℄_{ULT}}}{bd^2} \doteq 900 \text{ psi K/in.}^2 \text{ (reference 1, page 267)} \qquad \text{(A.1)}$$

$$d = \sqrt{\frac{1780(1000)}{12(900)}} = 12.8 \text{ in.}$$

t(req'd) ≃ 15 in.

(2) Shear

$$d = \frac{V}{bjv} = \frac{16.57(6)(1000)}{12(0.875)(400)} = 23.6 \text{ in.}$$

t(req'd) ≐ 26 in.

From this it is seen that shear governs. Now try 12- by 12-in. haunches to reduce thickness.

$$d = \frac{5}{6}(23.6) = 19.7 \text{ in.}$$

t(req'd) ≐ 21 in.

Therefore try a 21-in. section with 12- by 12-in. haunches.

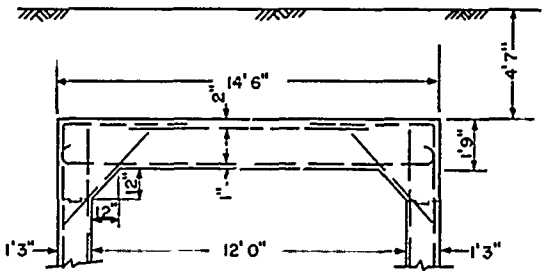

Reinforcement

For the assumed sections the moment capacity of the support is controlled by the wall steel at the construction joint below the haunch.

(1) Capacity at Support

Try #8 at 5 in. outside face; #6 at 12 in. inside face for wall reinforcement.

$$M_{S_{ULT}} = Pe = A'_s f_{dy} d' + 0.85\, f'_{dc} ab(1/2)(d' + t - a) - 0.5\, Pd' \qquad (A.2)$$

$$P \doteq 16.57(13.25)(1/2) = 109.5\ K$$

$$a = \frac{P}{0.85bf'_{dc}} + (A_s - A'_s)\frac{f_{dy}}{0.85bf'_{dc}} \qquad (A.3)$$

$$a = \frac{109.5}{0.85(12)(4 \times 1.25)} + \frac{(1.00 - 0.44)(50 \times 1.25)}{0.85(12)(4 \times 1.25)} = 2.15 + 1.79 = 3.94\ \text{in.}$$

[The dynamic increase factor (1.25) is assumed as the average of recommended maximum values for section in flexure and section in pure compression, i.e., (1/2)(0.35 + 0.15) = 0.25.] Therefore

$$M_{S_{ULT}} = 0.44(62.5)(11.13) + 0.85(5)(3.94)(6)(11.13 + 15.00 - 3.94) - 0.5(109.5)(11.13)$$

$$\underline{M_{S_{ULT}} = 1932\ \text{in. K}}$$

and

$$M_{S_{ULT(1)}} = 0.44(62.5)(11.13) + 0.85(5)(3.04)(6)(26.13 - 3.04) - 0.5(64)(11.13)$$

$$M_{S_{ULT(1)}} = 1741\ \text{in. K}$$

$$R_1 = \frac{1741}{13.25} = \underline{130\ K} \doteq 128\ K$$

(2) Resistance R_{max} at ℄ Yielding

℄ yield moment $M_{℄_{ULT}} = A_s f_{dy}(d - 0.5a)'$

A_s = #8 at 5 in., 1-in. cover

$$a = \frac{A_s f_{dy}}{0.85bf'_{dc}} = \frac{1.90(67.5)}{0.85(12)(5.4)} = 2.33\ \text{in.}$$

$$M_{\mathbb{Q}_{ULT}} = 1.90(67.5)(19.50 - 1.16) = \underline{2360} \text{ in. K}$$

$$M_{S_{ULT}} = 1912 \text{ in. K} \quad \text{(by trial using Eq. A.2)}$$

Therefore

$$R_{max} = \frac{8}{13.25(12)}(2360 + 1912) = \underline{215 \text{ K}}$$

(3) Stiffness

It is sufficiently accurate for stiffness computations in this case to neglect the effect of the haunches. The resistance function for the roof slab is shown in Sec. A.7.2.

$$X_{yp_1} = \frac{R_1 L^3}{384EI} + \frac{kL(1+\mu)R_1}{4AE}$$

$$= 130\left[\frac{13.25^3}{384(432\times10^3)\left(\frac{1}{12}\right)(1.75)^3} + \frac{1.2(13.25)(1.1)}{4(1.75)(432\times10^3)}\right]$$

$$= 130(0.0315 + 0.0057)10^{-3} = \underline{0.00483} \text{ ft} \qquad \text{(A.4)}$$

$$X_{yp_2} = \frac{5(R_{max} - R_1)L^3}{384EI} + \frac{kL(1+\mu)(R_{max} - R_1)}{4A_S E} + X_{yp_1}$$

$$= (215 - 130)(0.1575 + 0.0057)10^{-3} + 0.00483 = \underline{0.01873} \text{ ft}$$

(4) Capacity at $\mathbb{Q}$

$$M_{\mathbb{Q}_{ULT}} = \frac{R_{ULT} \cdot L}{8} - M_{S_{ULT}} = \frac{219(13.25)(12)}{8} - 1932 = \underline{2408} \text{ in. K}$$

$$A_S(\text{req'd}) = \frac{M_{\mathbb{Q}_{ULT}}}{f_{dy}(d - 0.5a)}$$

$$a = \frac{A_S f_{dy}}{0.85 f'_{dc} b} = 1.225\, A_S$$

$$A_S(\text{req'd}) = \frac{2408}{(1.35\times50)(19.50 - 0.612\, A_S)} = 1.95 \text{ sq in.}$$

Therefore <u>try #8 at 5 in.</u>

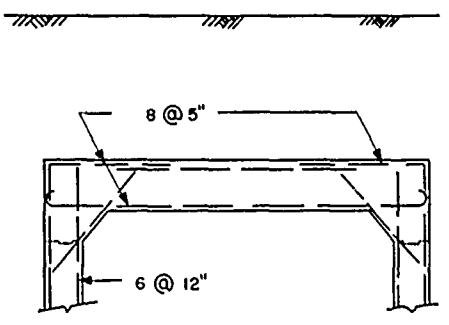

A.7.2 Resistance Function

Resistance R_1 at Support Yielding

$$R_1 = \frac{12M_{S_{ULT(1)}}}{L} = \frac{M_{S_{ULT(1)}}\ (\text{in. K})}{13.25}$$

$M_{S_{ULT(1)}}$ is obtained using Eq. A.2, and, since the value of $(1/2)R_1 = P$ is necessary to solve this equation, the solution is obtained by converging trials. The final trial is shown below.

From preceding trial $R_1 = 128$ K, therefore $P = 64$ K. Using Eq. A.3

$$a = \frac{64}{51} \div 1.79 = 3.04 \text{ in.}$$

Therefore elastic range stiffness

$$k_1 = \frac{R_1}{X_{yp_1}} = \underline{26900} \text{ K/ft}$$

and elasto-plastic range stiffness

$$k_2 = \frac{R_{max} - R_1}{X_{yp_2} - X_{yp_1}} = \underline{6110 \text{ K/ft}}$$

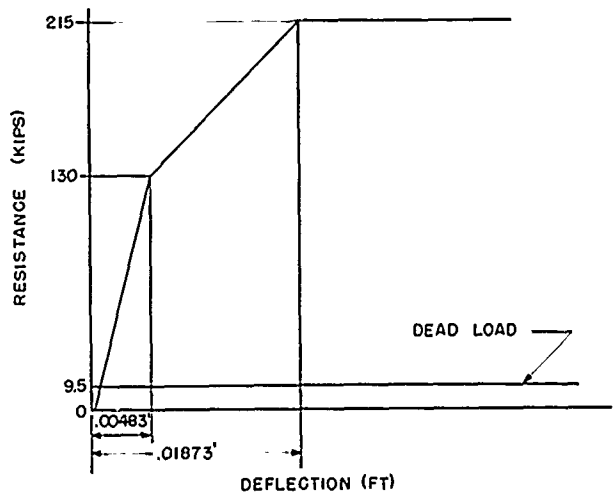

Equivalent Masses for Analysis

$$m = \frac{D.L.}{32.2} = \frac{9.53}{32.2} = 0.296 \text{ kip-sec}^2/\text{ft}$$

Elastic	$m_1 = 0.766(0.296) = 0.227$
Elasto-plastic	$m_2 = 0.790(0.296) = 0.234$
Plastic	$m_3 = 0.667(0.296) = 0.197$

Numerical-integration Solution for Deflection

t, sec	$\bar{F}$, kip	$\bar{R}$, kip	$\bar{F} - \bar{R}$	$\frac{\Delta t}{m_e}$	$\Delta\dot{X}$	$\dot{X}$	$\bar{\dot{X}}$	ΔX	X	R (calc.)	$\bar{R}$ (calc.)
0						0			0	0	
	191	5	186	0.0044	0.82		0.41	0.00041			5.5
0.001						0.82			0.00041	11	
		27	164	0.0044	0.72		1.18	0.00118			27
0.002						1.54			0.00159	43	
		68	123	0.0044	0.54		1.81	0.00181			67
0.003						2.08			0.00340	91	
		110	81	0.0044	0.36		2.26	0.00226			109
0.004						2.44			0.00566	128	
		135	56	0.0043	0.24		2.56	0.00256			136
0.005						2.68			0.00822	144	
		153	38	0.0043	0.17		2.76	0.00276			153
0.006						2.85			0.01098	161	
		170	21	0.0043	0.09		2.90	0.00290			170
0.007						2.94			0.01388	178	
		188	3	0.0043	0.01		2.95	0.00295			187
0.008						2.95			0.01683	196	
		201	−10	0.0043	−0.04		2.93	0.00293			201
0.009						2.91			0.01976	205.5	
		205.5	−14.5	0.0051	−0.07		2.87	0.00287			
0.010						2.84			0.0226		
				0.0508	−0.74		2.47	0.0247			
0.020						2.10			0.0473		
				0.0508	−0.74		1.73	0.0173			
0.030						1.36			0.0646		
				0.0508	−0.74		0.99	0.0099			
0.040						0.62			0.0745		
				0.0508	−0.74		0.25	0.0025			
0.050						−0.12			0.0770		

Max. X = 0.93 in. $\approx \frac{L}{1.72}$

Therefore use assumed section for final.

Note: $\bar{F}$ = force, $\bar{R}$ = resistance, $\Delta\dot{X}$ = acceleration, $\dot{X}$ = velocity, X = displacement.

REFERENCES

1. Charles S. Whitney, Plastic Theory of Reinforced Concrete Design, Trans. Am. Soc. Civil Engrs., 107: 251-282 (1942).
2. C. S. Whitney, B. G. Anderson, and E. Cohen, Design of Blast Resistant Construction for Atomic Explosions, J. Am. Concrete Inst., 26: 679 (March 1955).
3. C. S. Whitney, B. G. Anderson, and E. Cohen, Design of Blast Resistant Construction for Atomic Explosions, J. Am. Concrete Inst., 26: 634 (March 1955).
4. C. S. Whitney, B. G. Anderson, and E. Cohen, Design of Blast Resistant Construction for Atomic Explosions, J. Am. Concrete Inst., 26: 612 (March 1955).
5. C. S. Whitney, B. G. Anderson, and E. Cohen, Design of Blast Resistant Construction for Atomic Explosions, J. Am. Concrete Inst., 26: 615 (March 1955).

APPENDIX B

PROTECTIVE VENTILATION

By

Frank G. Ort

and

Ralph V. Schumacher

U. S. Army Chemical Center

ANYTHING ABSTRACTED FROM THE MATERIAL IN APPENDIX B MAY BE TREATED AS CONFIDENTIAL-RESTRICTED DATA

APPENDIX B

PROTECTIVE VENTILATION

B.1 INTRODUCTION

B.1.1 Objective

The purpose of this work was to provide protection against atomic, bacteriological, and chemical attack for two prototype 50-man FCDA shelters and to determine the ability of the protective installations to withstand an atomic detonation.

B.1.2 Background

For a number of years the Chemical Corps has been active in the development of equipment and methods of operation for protective shelters. There are two general methods by which the occupants of a shelter can be provided with protection against all toxic gases and aerosols other than through the use of individual protective equipment such as the gas mask.

The first method involves the use of a motor blower with filter units to provide a continuous supply of filtered air which maintains a positive pressure of purified air within the structure and acts to preclude the entrance of atmospheric contaminants from without. The E_4 antiblast closure was developed for protection of the filter units and personnel within this type of shelter during the extreme overpressures encountered during an atomic detonation. The development and tests conducted using this equipment on a pressurized type of protective shelter at Operation Greenhouse are described in the Project 6.10 report.[1]

The second method of providing the desired shelter protection is through the use of a new filter medium known as "diffusion board." This board is similar to ordinary wall boards, such as Celotex, except that activated charcoal is added to the wet pulp make-up. This board, when used to form the walls of a protective enclosure, acts as a reactive diffusion barrier. Carbon dioxide and water vapor concentrations which would normally increase continually within an enclosure under conditions of prolonged human occupancy increase only to moderate levels and stabilize due to the process of diffusion through the board. The driving force for the diffusion process is the concentration gradient across the barrier. By the same token, an appreciable concentration of toxic gas outside the enclosure would set up a reverse driving force into the enclosure; however, in passage through the board, the toxic agent is removed by the activated charcoal incorporated directly within the board. The protection afforded by a shelter of this type is dependent upon very good seals at all joints and the elimination of all sources of air leakage from without.

The FCDA requested that the Chemical Corps participate in their shelter program being conducted on Operation Teapot at the Nevada Test Site (NTS) in the spring of 1955. Two 50-man shelters designed by Ammann & Whitney were made available for Chemical Corps instrumentation. Each of the shelters was tested in a different test detonation, although the overpressure anticipated at each test shelter was approximately 100 psi.

Since the first of these shelters was tested in the Apple I shot, it was decided to equip this test shelter as a diffusion-board type of protective shelter. The second shelter was involved in the Apple II shot. This shelter was equipped with a motor blower, filter, and pertinent equipment required for operation as a pressurized type protective shelter. Aerosol tests were conducted before and after the shot on each of these shelters to determine in each case if there was any loss in protective efficiency of the shelter as a result of the test detonation.

B.1.3 Preshot Development Work (Diffusion Shelter)

(a) General. The interior of the shelter proper was a room approximately 25 ft long, 12 ft wide, and 8 ft high (see Chap. 1). The entrance door was a Navy type steel bulkhead door equipped with rubber gaskets and a series of levers and dogs for securing a tight air seal. In the roof in the right rear corner of the structure was the emergency escape hatch, 3 by 3 ft, equipped with a steel door and earth-filled to a depth of 6 ft 6 in. It was felt that this dirt cover would be sufficient to preclude the entrance of contaminants through the escape hatch and that the rubber-gasketed steel bulkhead door should provide an airtight seal when the door was clamped into position.

The diffusion-board installation was made on a wood framing of nominal 2- by 4-in. lumber attached to the masonry walls. A special type of construction was used to set the wood framing away from the walls and ceiling to provide a continuous and interconnected void area between the diffusion board and the masonry walls. The void width around the walls varied in width from $1\frac{5}{8}$ to $3\frac{5}{8}$ in. except at the closets, which will be subsequently described, and at the ceiling, where the thickness of the void area was approximately 1 ft. The construction of the wood framing was arranged with sufficient clearance around both the escape hatch and entrance door to permit ready access to each of these doors.

Mechanical ventilation of the void area was provided since, during normal shelter occupancy without ventilation of the void, the carbon dioxide and water vapor diffusing through the diffusion-board wall would reach an equilibrium with the concentration on the protected side of the barrier, neutralizing the driving force for diffusion.

The air inlet to the void area consisted of a length of standard 6-in. steel pipe equipped at the top with a pipe tee (whose open ends were covered with expanded metal), which was installed about 3 ft above the level of the dirt fill on top of the shelter. The lower end of the pipe was interconnected to an E_4 antiblast closure, thence to the inlet of a Buffalo Forge motor blower, model No. SKH33HD32. An orifice was installed between the pipe flanges, together with upstream and downstream taps for flow measurement. This equipment is shown in Fig. B.1.

The output side of the blower was connected to a flanged sheet-metal box which contained an adjustable plate for varying the blower exhaust opening and which was used as a method of controlling the output rate of air flow. Surmounting this plate were two 10- by 10-in. Dustop type air filters set in series and a cover plate of expanded metal which was held in place by a series of $\frac{1}{4}$-in. machine screws located around the outer perimeter. The air inlet equipment was housed in a closet covered with $\frac{5}{8}$-in. plywood around the air inlet equipment. Approximate floor dimensions of the closet as shown in Fig. B.2 were $2\frac{1}{4}$ by $9\frac{1}{2}$ ft.

The air exhaust equipment, which is shown in Fig. B.3, consisted of a base of channel iron upon which an E_4 antiblast closure was installed. The top of the antiblast closure was connected to a section of 6-in. pipe running about 3 ft above the dirt fill and surmounted by a pipe tee.

The closet for this equipment was covered with plywood and occupied a floor space 2 by 2 ft. This is shown in Fig. B.4. The open ends of the pipe tees at the inlet and exhaust were oriented to a position 90° from GZ. The pipes were further strengthened by the addition of a 2-ft deep 3- by 3-ft concrete block cast around the pipes to provide additional strength where these pipes extend through the roof of the shelter. Further details of construction are shown in Figs. B.5 through B.8.

(b) Pressure Tests of Diffusion Board. Since the diffusion board represents a very recent development, there were no available test data on what pressure the board would withstand without rupture. A series of static pressure tests was arranged, using a wood frame having a

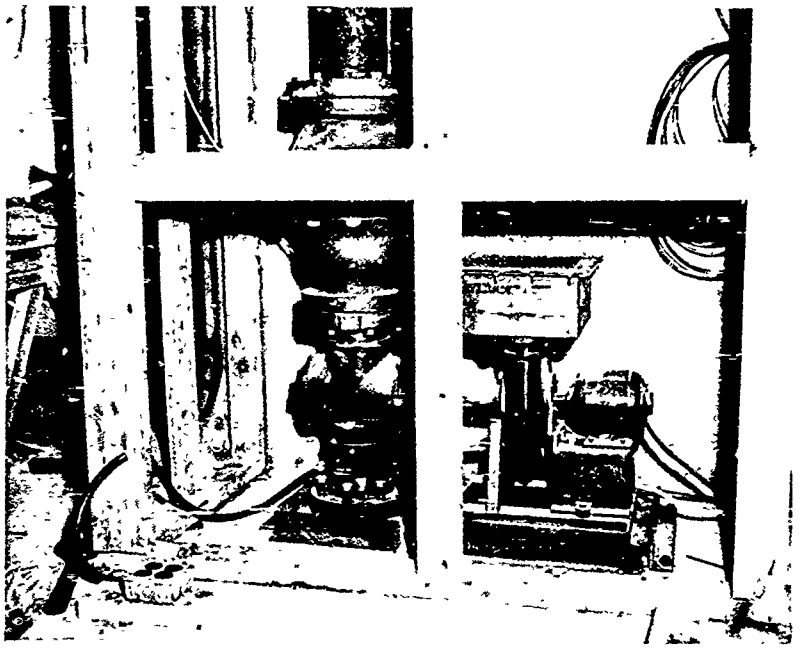

Fig. B.1—Air inlet equipment installation.

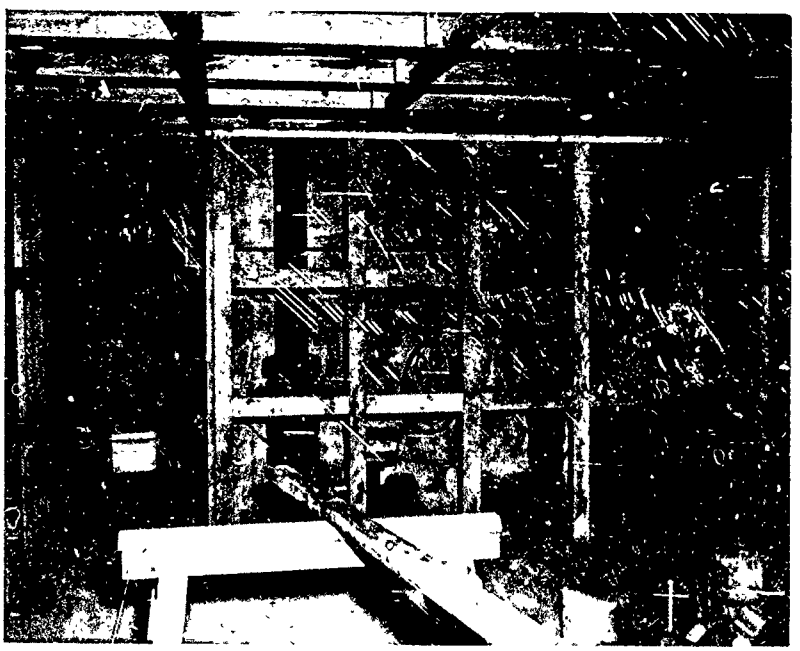

Fig. B.2—Front wall framing construction, showing closet.

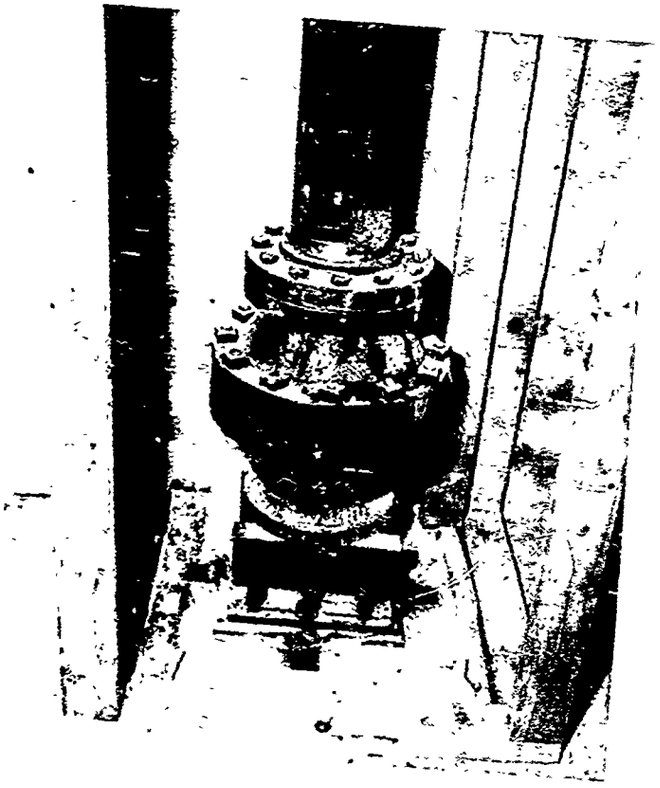

Fig. B.3—Air exhaust antiblast closure installation.

Fig. B.4—Air exhaust equipment and closet.

Fig. B.5—Incomplete construction around escape hatch.

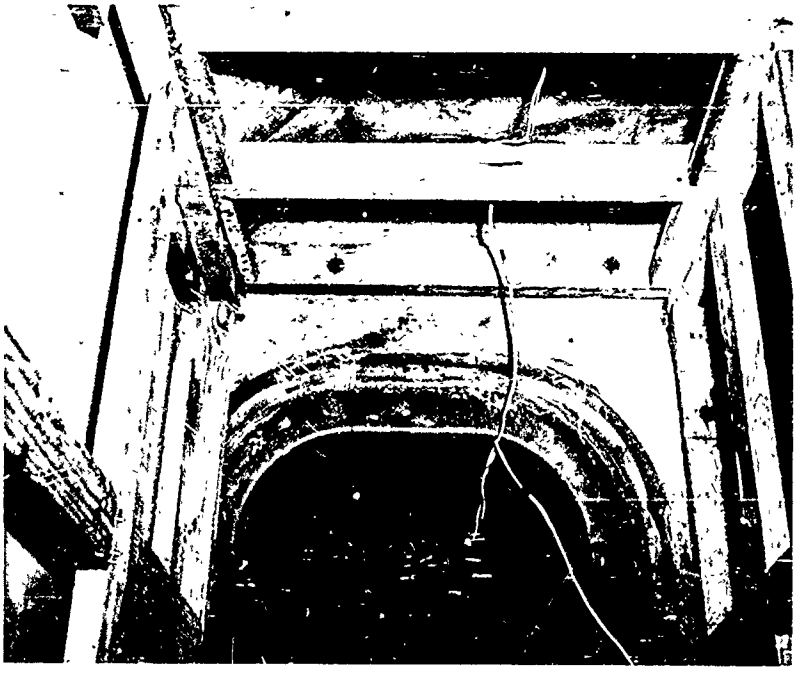

Fig. B.6—Incomplete construction around entrance door.

Fig. B.7—Wall seals around escape hatch.

Fig. B.8—Completed installation around entrance door.

section of diffusion board mounted on the face and a wood back section fitted with two pipe nipples — one for the introduction of compressed air and the second for use as a pressure tap connected to a mercury manometer. By increasing the flow of compressed air into the plenum between the diffusion board and wood sections, the pressure was increased until rupture occurred. A general summary of the test data thus obtained on the diffusion board is given in Table B.1.

Table B.1—STATIC BURSTING PRESSURE OF DIFFUSION BOARD

Test No.	Distance between centers of wood supports		Type of fastening	Bursting pressure, psi
	Width, ft	Length, ft		
1	2	5	Roofing nails at 4-in. intervals	0.39
2	1	5	2- by 2-in. wood stays used along 5-ft length nailed at center of top and bottom of frame	0.49
3	1	5	2- by 4-in. wood strip replaced 2- by 2-in. strip in test 2	0.98
4	2	5	$1\frac{5}{8}$-in.-wide strips used to fasten board at edges along 5-ft length	0.69
5	2	2.5	2- by 2-in. support installed in plenum at center of 5-ft span; $1\frac{5}{8}$-in. wood strips used over all interior wood supports	0.98
6	2	2.5	Same as test 5, except $\frac{3}{4}$-in. wood cover strips were used	0.98

From these tests it was shown that the bursting pressure of the diffusion board varies with the distance between supports. It was also shown that the use of wood cover strips in mounting the diffusion board tends to distribute the pressure along each seam and prevents the board pulling loose at the nail locations.

Further tests showed that with an even shorter span of diffusion board a somewhat higher bursting pressure could be realized, but it was felt that the additional framing required, plus the further loss of effective diffusion-board area (area made unusable because of impermeable wood backing), would make such a design undesirable.

On the basis of the foregoing tests, the diffusion board in the shelter installation was supported throughout on 2-ft centers in each direction, and a wood cover strip was used to hold the diffusion board to each of these supports. All the wood framing on which the diffusion board was mounted was of 2- by 2-in. and 2- by 4-in. common softwood lumber. The 2- by 4-in. framing which formed a room within the shelter was attached to the concrete walls by gun-driven nail type anchors. Special care was taken in the mounting of the diffusion board. At each seam a bead of caulking material (Rhino Brand, Pecora Paint Co., Inc., Philadelphia, Pa.) was applied to each diffusion board, and a second bead was applied on top of the joint prior to installation of the cover strip. Similar care was taken where the void area was terminated, with caulking seals between the wood framing and the cement walls of the shelter. Approximately 23 quarts of caulking compounds was used to make all seams and joints impermeable.

(c) Area of Diffusion Board Available. It had been determined by previous human occupancy tests conducted at the Army Chemical Center that an area of diffusion board equivalent

to 10 sq ft per man would provide satisfactory protection and environmental conditions to sustain life. In the FCDA shelter, Station 4-34.3 a-1, the available area of diffusion board was about 431 sq ft. The available areas in different sections of the shelter are indicated in Table B.2. This area of diffusion board would be sufficient for 43 occupants, reducing the design occupancy from 50.

Table B.2—AVAILABLE AREAS OF DIFFUSION BOARD

Location	Diffusion board available, sq ft
Ceiling	198.0
Front wall	19.8
Left wall	102.3
Right wall	75.8
Rear wall	28.7
Escape-hatch perimeter wall	6.6
Total area	431.2

(d) Available Void Area. The void area is important as a means of removing the carbon dioxide and water vapor passing through the diffusion board, and it acts as an expansion chamber to dissipate the pressure which passes through each of the two antiblast closures during the overpressure-initiated closing action of the closure units. In the 50-man FCDA shelter containing the diffusion-board installation, the total void area was approximately 506 cu ft. A more detailed breakdown is shown in Table B.3.

Table B.3—VOID-AREA LOCATIONS

Location	Volume of void, cu ft
Ceiling	249.4
Front wall (including closet)	146.3
Right wall	26.4
Rear wall (including closet)	37.9
Left wall	45.1
Total	505.1

(e) Antiblast Closure Settings. The E_4 antiblast closure is a blast-initiated device designed to protect ventilation systems against the extreme overpressures of an atomic detonation. The unit has flanges for interconnection with standard 6-in. pipe fittings at the inlet and with standard 5-in. pipe fittings on the protected side. At a flow of 300 cfm the air resistance of the unit is about 1 in. of water. A $\frac{1}{8}$-in.-thick $10\frac{5}{8}$-in.-diameter aluminum plate is maintained at a height of about 1 in. above a gasketed perforated steel bedplate by a spring operating on a plunger attached to the plate at its center. In normal position the air moves around the aluminum plate and passes through the perforated bedplate. A sharp rise in overpressure forces the floating aluminum plate down on the gasketed bedplate, sealing off the unit to further air flow. This situation is relieved by the passage of the positive-pressure phase, and the unit reopens in the negative-pressure phase.

Since at Station 4-34.3 a-1 an overpressure of 100 psi was anticipated, a reflected pressure on the aluminum plate would be of the order of 480 psi. Assuming an instantaneous pressure rise of this magnitude, it can be shown by calculation that the closing time would be considerably less than 1 msec. However, even with such a finite closing time some of the air bypasses the valve during its closing operation.

At Aberdeen Proving Ground, shock-tube tests were conducted with a 13-cu ft free volume on the protected side of the closure and shock waves of various magnitudes. These data, when extrapolated to a shock wave pressure of 100 psi, showed a protected side pressure of 8.75 psi in the 13-ft free volume. On the assumption of an adiabatic expansion without change in temperature, a formula was worked out whereby the volume of air passing through the closure for any magnitude of overpressure could be determined if the pressure on the protected side and volume were known. (This derivation is shown in the Operation Greenhouse Project 6.10 report.)[1] The formula is indicated below.

$$Q = V\left(\frac{P_2}{P_1} - 1\right)$$

where Q = the volumetric air flow in cubic feet per minute to create P_2
V = free volume on protected side of closure (cubic feet)
P_2 = pressure in pounds per square inch created by an input of Q cfm
P_1 = pressure of free volume at rest (14.7 psi)

Using the 8.75 psi free volume pressure for a 100 psi shock wave in a 13-cu ft volume

$$Q = 13\left(\frac{23.45}{14.7} - 1\right)$$

$$Q = 7.73 \text{ cfm}$$

As indicated in Sec. B.1.3d, the available free void volume on the protected side of the two closures is 505 cu ft, or 252.5 cu ft per closure. Now resubstituting, using the 7.76 cfm passing the closure in the new free volume of 252.5 cu ft,

$$Q = V\left(\frac{P_2}{P_1} - 1\right)$$

$$7.73 = 252.5\left(\frac{P_2}{14.7} - 1\right)$$

$$P_2 = 15.15 - 14.7 = 0.45 \text{ psi}$$

From the above it can be seen that the calculated pressure build-up in the void will be of the order of ½ lb/sq in., assuming an immediate distribution and equalization of the pressure in all sections of the void area. These pressure calculations were based on operation of the plate at a height of 1 in. above the perforated backplate. In the case of this shelter a flow of about 50 cfm through the void area is deemed adequate. On this basis the inlet and exhaust closure plates were adjusted to a height of ¼ in. about the perforated backplate. The closing time for the closure can be calculated from the formula

$$S = \tfrac{1}{2}at^2 \text{ or } t = \sqrt{\frac{2S}{a}}$$

Therefore, by reducing the plate height from 1 to 0.25 in., the closing time would be reduced by about 50 per cent, further reducing the pressure built up in the void. In addition, the closets housing the intake and exhaust antiblast closures were covered with ⅝-in. plywood to take care of any surge pressures which might momentarily develop prior to equalization of the pressure throughout the void space.

(f) Adjustment of Air Flow Through the Void. By use of the orifice installed between the pipe flanges upstream of the blower and the flow control valve located in the sheet-metal housing containing the Dustop filters, the flow through the blower was measured at 54 cfm. The flow control valve plate, which is held in position by springs, acts as a shock absorber for the high momentary flow which it is anticipated will pass the closure during its operation.

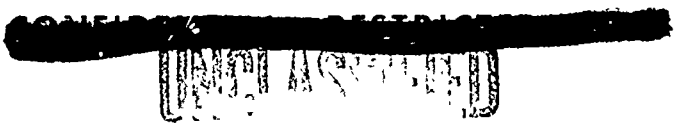

(g) Shelter Aerosol Test. To allow preshot and postshot evaluation of the functional efficiency of the diffusion type shelter, a test aerosol method was devised using fluorescein as the aerosol test agent. The fluorescein was dissolved in a solution of methyl alcohol and sprayed through a number of Spraco (model 125, Spray Engineering Co., Somerville, Mass.) nozzles set up in parallel for dispersal of the aerosol. A series of standards containing known amounts of fluorescein were dissolved in 0.1N sodium hydroxide and were prepared and analyzed, using a Klett fluorimeter to determine the relative intensity of fluorescence. In this manner a calibration curve of Klett scale readings for a range of known fluorescein contents was established. These data are shown in Fig. B.9.

Table B.4—PRESHOT AEROSOL TEST DATA

Sample holder No.	Location[a]	Critical orifice flow, liters/min	Klett reading	Net Klett reading[b]	Concentration,[c] μg/ml	Total weight collected, μg	Av. conc.,[d] μg/liter
1	1U	1.005	160.0	135.0	0.455	11.4	0.763
2	1L	0.965	126.5	101.5	0.350	8.75	0.605
3	2U	0.964	127.0	102.0	0.350	8.75	0.605
4	2L	1.005	129.5	104.5	0.355	8.87	0.587
5	3U	0.952	122.0	97.0	0.335	8.38	0.586
6	3L	1.012	121.0	96.0	0.335	8.38	0.551
7	4U	0.988	123.0	98.0	0.335	8.38	0.565
8	4L	1.040	131.5	106.5	0.365	9.12	0.585
9	5U	1.000	122.0	97.0	0.335	8.38	0.558
10	5L	1.005	127.0	102.0	0.350	8.75	0.579
11	6U	1.018	126.0	101.0	0.350	8.75	0.573
12	6L	1.058	127.5	102.5	0.350	8.75	0.552
13	7U	0.958	123.0	98.0	0.335	8.38	0.582
14	7L	1.0	122.5	97.5	0.335	8.38	0.558
Void	L	1.01	149.0	124.0	0.43	1290	85.10
Void	U	1.042	134.0	109.0	0.38	1140	72.75
Blank				25			

[a]U, sample taken at 6-ft height; L, sample taken at 1-ft height.
[b]Gross Klett reading less blank.
[c]From calibration curve of scale reading vs μg/ml of fluorescein.
[d][Total weight collected (μg)]/[critical orifice flow (liter/min) × time of sample (min)] = av. concentration (μg/liter).

In the preshot aerosol test of the shelter, the fluorescein solution was sprayed through the six nozzles within the void section closet near the air inlet for a period of 15 min. The inlet and exhaust pipe tees were taped closed so that the compressed air from the nozzles would create a slight positive pressure in the void area, thus simulating normal operating conditions. Air samples within the void and in the shelter proper were drawn through, and the solid aerosol collected on two pieces of Chemical Corps type 6 filter material mounted in series in a plastic holder. The flow rate for each of the samples was about 1 liter/min, which was metered through critical orifices and drawn through the filter material by a number of vacuum pumps. The locations of the sampling stations used are shown in Fig. B.10. At each of these locations a sample was drawn at both the 1- and 6-ft levels for a period of 15 min. The aerosol samples thus collected were subsequently extracted in a 0.1 NaOH solution and analyzed on the Klett fluorimeter. The physical data are shown in Table B.4. An average was taken of the fluorescein concentrations per liter determined at the various sampling stations within the shelter proper. The average value was 0.589 μg/liter. The void samples were similarly averaged and deter-

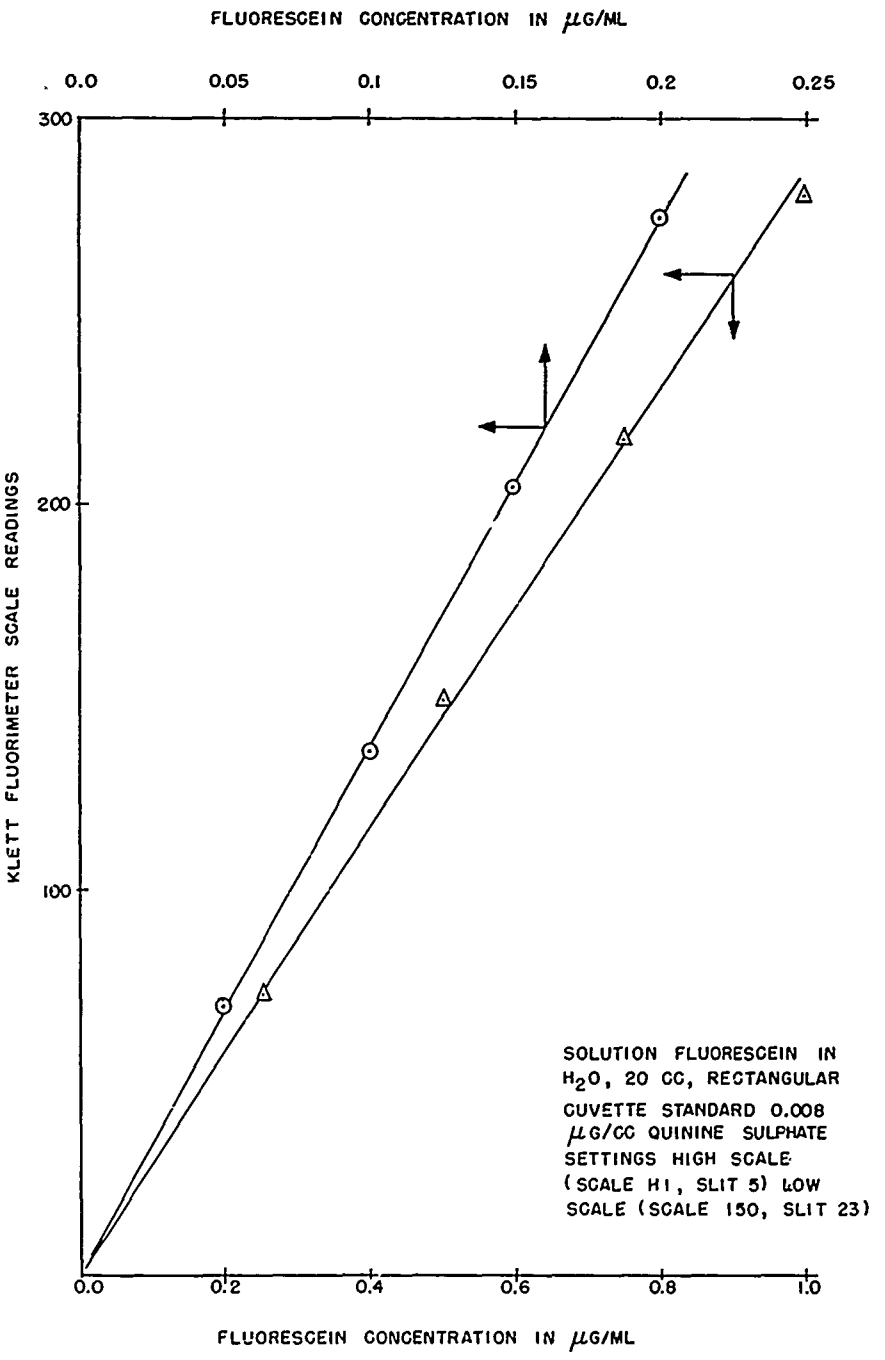

Fig. B.9—Fluorimeter calibration curve.

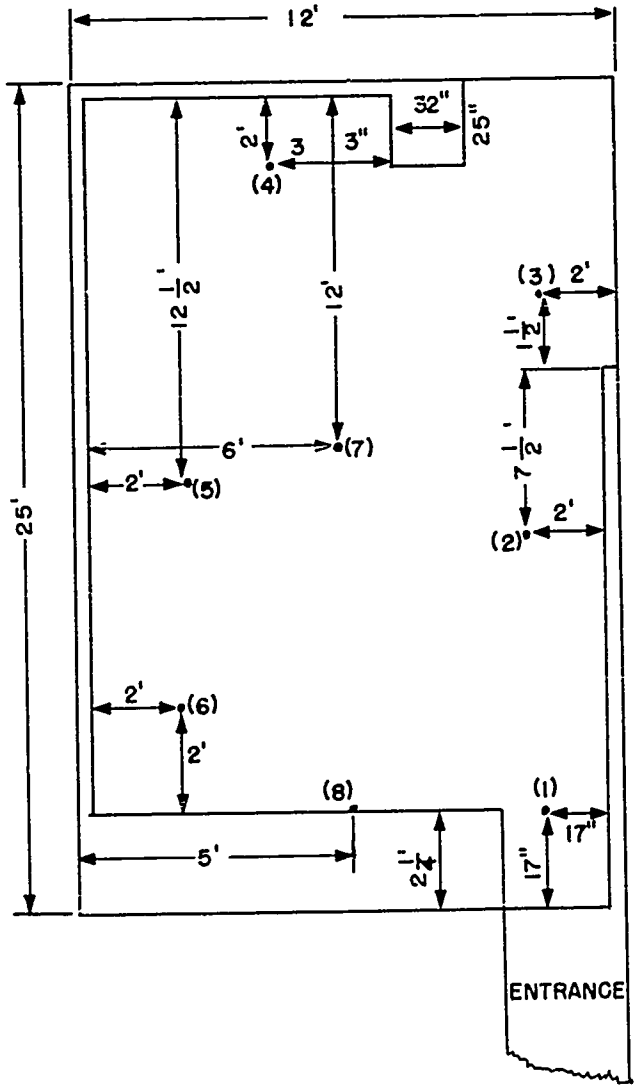

Fig. B.10—Sampling stations for aerosol test.

mined to be 78.98 μg/liter. The percentage of penetration into the shelter can be readily determined from these values as follows:

$$\frac{0.589\ \mu g/\text{liter}}{78.98\ \mu g\ \text{liter}} \times 100 = 0.746 \text{ per cent infiltration}$$

Since the penetration samples as determined at the various locations within the shelter were generally in the same order of magnitude, there were apparently no specific sources of high leakage. Owing to the limitations of equipment available at the test site, no further effort was made to ascertain the cause of the slight leakage as shown by the aerosol test. In addition, it was felt that the principal objective of this test was the assessment of any change in protective efficiency of the shelter due to the test detonation, and for this purpose the test data obtained could be satisfactorily correlated with the postshot aerosol test data to provide the desired information.

(h) Pressure Instrumentation. Pressure instrumentation stations were used at three locations in the shelter. The first was located outside the Navy type bulkhead door; the second was located in the void area between the masonry wall and the diffusion-board installation in the closet housing the motor blower unit; and the third pressure gauge was located in the shelter proper underneath the escape hatch. Calibration of the gauge and pressure measurements were conducted by the Sandia Corporation.

B.1.4 Preshot Development Work (Pressurized Type of Shelter)

(a) General. The 50-man shelter tested in the Apple II shot was similar to that used for the diffusion type shelter. However, in this installation the escape hatch was located in the ceiling where the left wall (wall nearest GZ) intersected the front wall of the shelter. An exterior view of the shelter showing the blast door, escape hatch, and inlet and exhaust pipe tees is shown in Fig. B.11. In addition, an 8-in. reinforced-concrete wall was installed 4 ft from the rear shelter wall. The room thus formed was further subdivided into two rooms of equal size by an additional concrete wall of similar thickness. The room on the right (when facing the installation from the shelter entrance door) contained the antiblast closures, inlet piping, and the motor blower and filter installation, as well as ducting through the wall to supply filtered air to the shelter proper. The left equipment room or air exhaust chamber contained the exhaust antiblast closures and piping, and two E_1R_6 anti-back draft valves set in the forward wall for shelter pressure regulation (Fig. B.12). In addition, this room contained a 110-volt a-c 3-kw Onan, gasoline-powered electric generator to provide a continuous power supply in the event of a power failure from the normal source, which was an Onan 5-kw generator installed outside the shelter. This equipment is shown in Fig. B.13. A Navy type steel bulkhead door was used as the entrance to the left equipment room. This door is shown in Fig. B.14. Entrance to the right equipment room could be made only by entering the left equipment room and removing a wood panel (Fig. B.15) in the partition between the two rooms. The equipment in the inlet air chamber and a general layout of the pressurized shelter are shown in Figs. B.16 and B.17, respectively.

(b) Basis of Design. The design was advantageous in that the concrete wall would provide good shielding for the occupants from any accumulation of radioactive particulate matter in the filter equipment located in the right equipment room. In addition, each of these rooms contained a gross volume of 182 cu ft which would be available for alleviation of the pressure due to the air bypassing the antiblast closures during the passage of the positive pressure wave of the detonation.

Since all the filtered air leaving the shelter would be through the left equipment room, this room was a good location for the emergency power supply. This location would provide adequate blast protection for the generator, and the hazard of a carbon monoxide build-up from exhaust would be minimized by the mixing action with the filtered air supply and the immediate exhaust of the mixture from the room through the air exhaust piping. Although not planned as

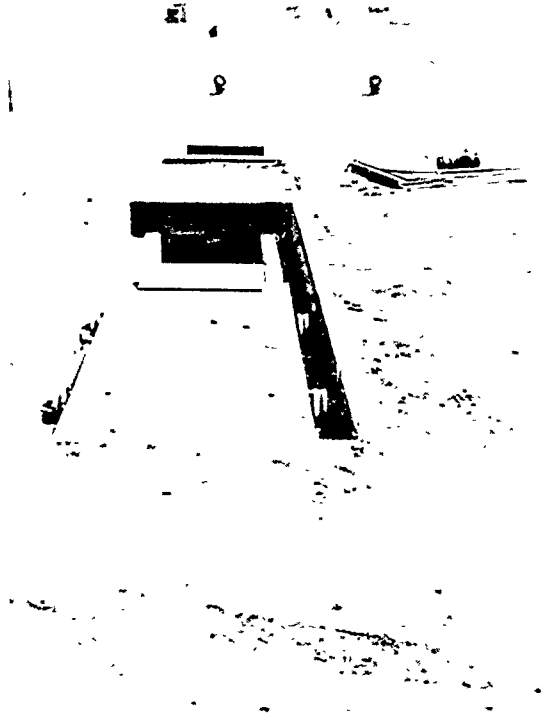

Fig. B.11 — Exterior view of underground personnel shelter.

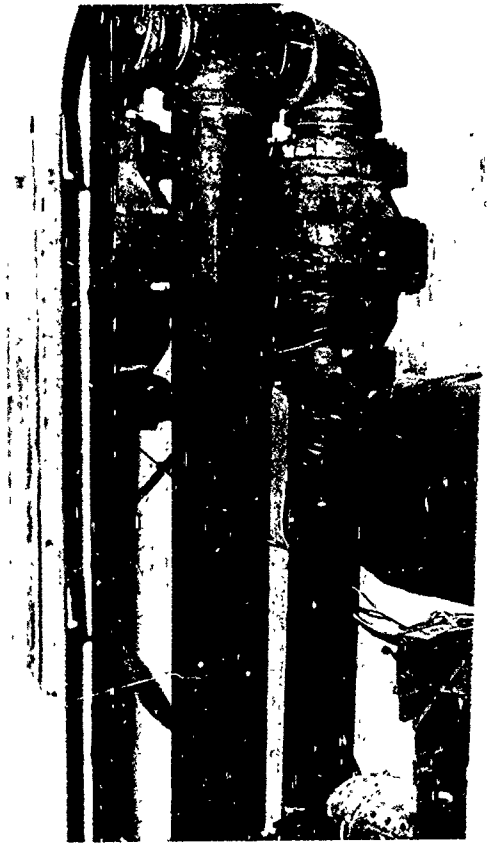

Fig. B.12 — Air exhaust chamber.

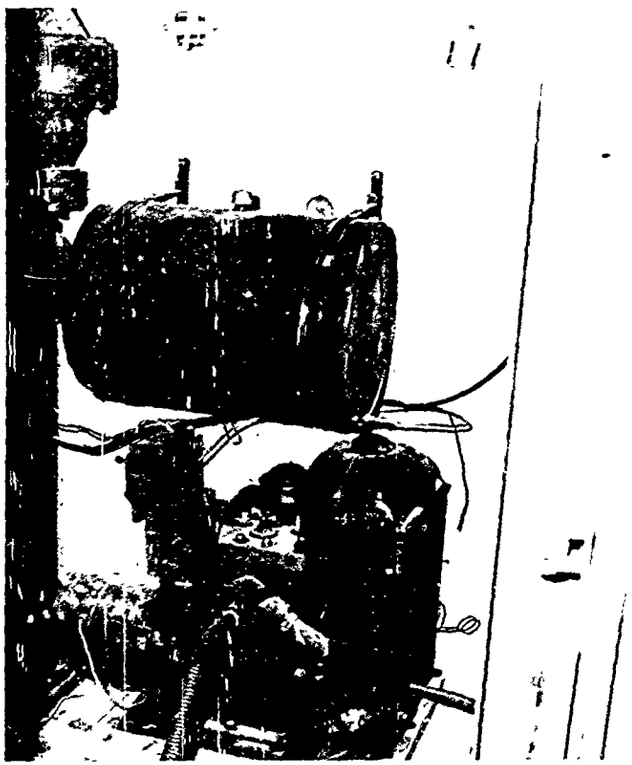

Fig. B.13—Motor generator in air exhaust chamber.

Fig. B.14—Entrance door to air exhaust chamber.

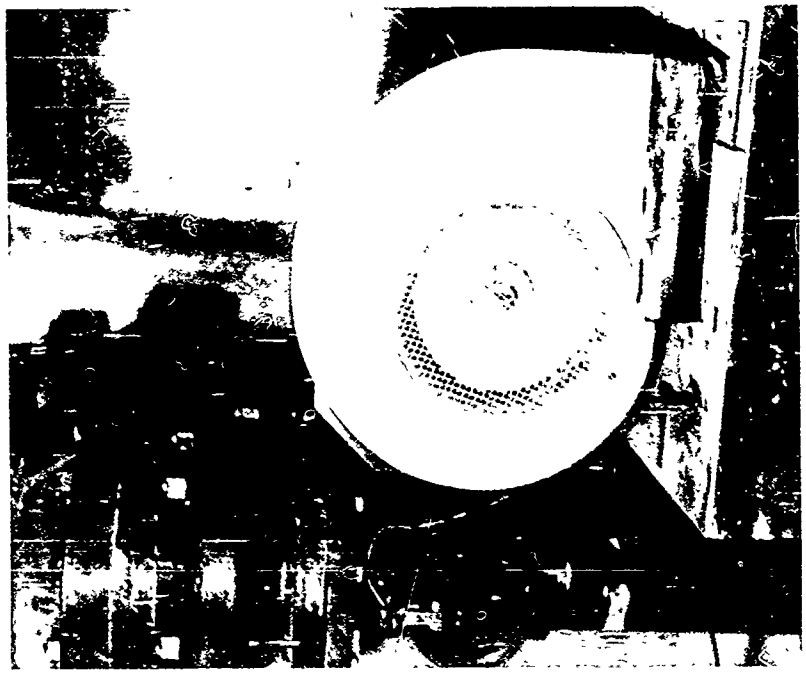

Fig. B.16—Equipment in inlet air chamber.

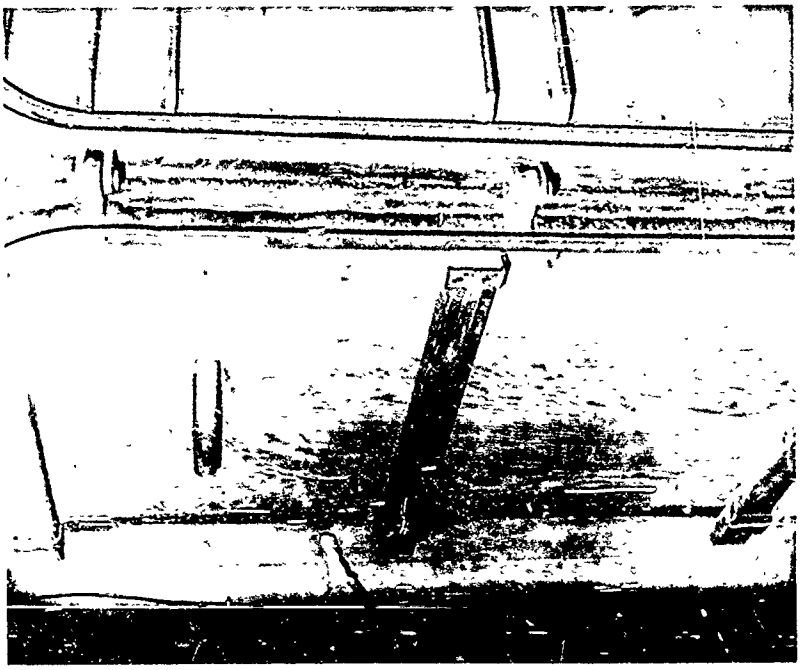

Fig. B.15—Wood panel between inlet and exhaust air chamber.

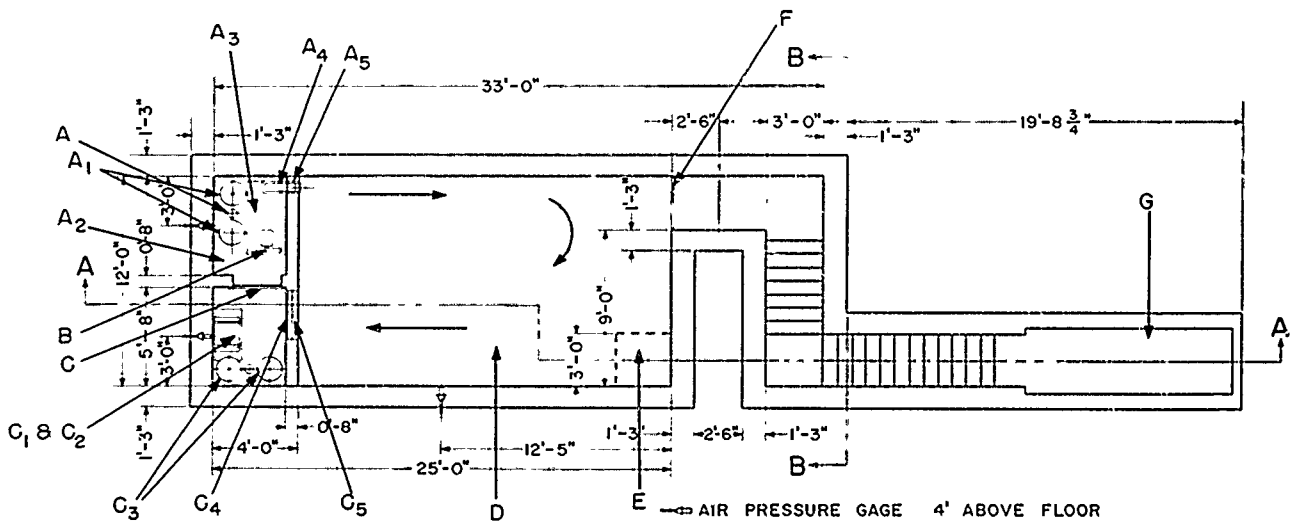

LEGEND:

- A INLET AIR CHAMBER
- A_1 E_4 ANTIBLAST CLOSURES
- A_2 MOTOR BLOWER UNIT
- A_3 E_{25} GAS AND PARTICULATE FILTER
- A_4 ELBOW
- A_5 FILTERED AIR DISCHARGE REGISTER
- B WOODEN DOOR BETWEEN CHAMBERS
- C EXHAUST AIR CHAMBER
- C_1 & C_2 EMERGENCY POWER GENERATOR
- C_3 E_4 ANTIBLAST CLOSURES
- C_4 E_1 R_6 ANTI-BACKDRAFT VALVES
- C_5 NAVY-TYPE STEEL DOOR
- D SHELTER PROPER
- E ESCAPE HATCH
- F NAVY-TYPE STEEL DOOR
- G CONCRETE SLAB BLAST DOOR

Fig. B.17—Layout of pressurized shelter.

a part of this test installation, it was felt that this room would be a good location for the installation of a chemical type toilet for the use of the shelter occupants.

The Chemical Corps filter used was the E_{25} gas and particulate filter, 600 cfm, and at this rated flow it provides protection equivalent to that of the standard military gas mask canister. This air flow by standard ventilation practices would provide satisfactory ventilation for 60 persons. The filter unit was equipped with plywood plenums at both inlet and exhaust ends. The inlet plenum was further equipped with a replaceable Dustop type prefilter to prolong the life of the main filter unit. This plenum arrangement permitted the installation of the motor blower unit and exhaust elbow on top of the filter unit, minimizing the floor space requirement for the filter installation. Two E_4 antiblast closures were installed in parallel in both the inlet and exhaust piping systems to accommodate the full rated air flow of the filter unit.

(c) Inlet and Exhaust Piping Systems. Both the inlet and exhaust piping installations were identical. In each, at the top was a standard threaded 6-in. pipe tee extending about $1\frac{1}{2}$ ft above the dirt fill. The 6-in. pipe running down through the roof of the shelter contained a pipe coupling surrounded by a concrete pier 2 by 3 by 3 ft for anchorage and support. Near the ceiling in each installation, a set of 6-in. threaded flanges was used to permit the uncoupling of the entire piping system within the structure if necessary.

A short distance beneath the flange installation a pipe tee was installed, the bottom connection of which was connected to a section of pipe extending down to the concrete floor with a flange at the base providing anchorage and support for the whole assembly. The two side connections of the pipe tee were connected by right-angle ells and pipe nipples to an antiblast closure located on each side of the central support pipe.

Standard 5-in. pipe tees were installed beneath each antiblast closure with the 90° connection used to permit air flow and for ready access to the base of the antiblast closure spindle for a periodic inspection of the free operation of the spindle and plate assembly. Flanges whose height above the floor was adjustable were attached at the base of the pipe section connected to the tees to facilitate removal of the antiblast closures. This arrangement was common in both inlet and exhaust piping installations. The aluminum plates of all antiblast closures were set at a level of 1 in. above the gasketed bedplate.

(d) Motor Blower for E_{25} Filter Unit. A blower capable of producing an air flow of 600 cfm at an operating head of $5\frac{1}{2}$ in. of water was procured from Revcor, Chicago, Ill. The unit had a $9\frac{1}{8}$-in.-diameter impeller and would meet the flow and operating requirements; however, the 115-volt a-c 1-hp 3450-rpm electric motor used was definitely overloaded in producing this air flow at the specified operating head.

A test was conducted with the blower producing a flow of about 540 cfm at a head of 5.8 in. of water continuously for a period of 6 hr. In this test the rise in motor temperature stabilized at about 25°C, which was considerably less than the 40°C rise allowed by the manufacturer of this motor. From this test it appeared that the motor could run continuously under these conditions without undue overheating.

This flow output would be more than sufficient for a shelter of this type since with reduction in floor space due to the equipment rooms the shelter proper has 243 sq ft of floor space and could accommodate only 40 persons on the basis of 6 sq ft per person. According to ASHVE Ventilation Standards, 10 cu ft per person is an acceptable minimum ventilation rate.

(e) Predetonation Aerosol Tests of Filter. The major potential source of blast damage to the E_{25} gas and particulate filter in the pressurized structure lay in the possibility of rupture of the filter material. As indicated in the Operation Greenhouse Project 6.10 report,[1] rupture of similar types of filters using type 6 filter material occurred at about a 5-psi pressure differential across the filter material.

To assess any change in protective efficiency of the filter unit, "before" and "after" test detonation aerosol tests were run on the filter unit. The test aerosol used was a 0.3-μ dioctyl phthalate liquid aerosol, which is a standard type of Chemical Corps acceptance test for this type of particulate filter. With the upstream concentration set at 100 per cent on the smoke penetration meter scale, a six-point penetration traverse was made of the $2\frac{1}{2}$- by 6-in. opening

in the plenum on the effluent side of the filter. The penetration values thus determined are indicated in Table B.5.

An additional aerosol test was conducted on the installed filter with fluorescein as a test agent and the general test method previously described in Sec. B.1.3g. In this test the chamber air near the filter air inlet was preheated with an 1800-watt heater to increase the rate of volatilization of the methyl alcohol in forming the fluorescein aerosol. This heater was turned off prior to the active aerosol generation, which was conducted for a period of 15 min using 40 psi air pressure at the nozzles.

Table B.5—PRESHOT PENETRATION DATA FOR FILTER

Location	Measured penetration, %
1	0.011
2	0.011
3	0.015
4	0.020
5	0.012
6	0.014

Sampling stations were located near the filter air inlet and exhaust, critical orifices were used for flow measurement, and the aerosol samples were collected on two plies of Chemical Corps type 6 filter material arranged in series in each sample holder. The motor blower unit and sampling air flows were initiated immediately following the period of aerosol generation and were allowed to run for a period of 15 min.

The samples thus obtained were analyzed on the Klett fluorimeter, and the penetration of the filter was found to be 0.078 per cent. This penetration measurement was considerably higher than that previously determined using the 0.3-μ dioctyl phthalate aerosol. The higher penetration found in the fluorescein aerosol test could have been due to the possible action of the fluorescein soaking through the filter material while still in the methyl alcohol solution, drying, and forming an aerosol on the protected side of the particulate filter. This conjecture was further substantiated by the amount of liquid (alcohol and fluorescein) noted on the outside surfaces of the filter equipment and walls immediately following the test.

An average of the values of Table B.5 gives an average penetration of 0.0139 per cent.

(f) Power Supply Circuit. Electrical power was supplied to the shelter from an externally installed gasoline-operated electric generator whose power supply could not be guaranteed after time zero. The emergency electrical power supply (a 115-volt a-c 3-kw, gasoline-operated electric generator) was provided to sustain the power supply after the detonation. This generator would operate continuously and, upon failure of the external power supply, would assume the electrical load.

To provide an automatic switchover to this power source upon failure of the external power supply, a Struthers Dunn 30-amp double-pole double-throw relay was used. This relay was wired so that as long as the solenoid was activated from the external power supply the power from this circuit would be maintained. Failure of the external power supply would deactivate the solenoid, breaking this circuit, and the spring action of the relay would close the emergency power supply circuit.

An Esterline-Angus recorder whose paper feed is powered by a 115-volt a-c synchronous electric motor was used to obtain a permanent record of how long power remained available from the outside power source and from the emergency generator. The paper feed rate was set at 6 in./hr The pen circuits of the recorder were wired with single-pole single-throw relays so that failure of each power source would change the pen setting and the time of failure could be established from the chart. The wiring diagram is shown in Fig. B.18.

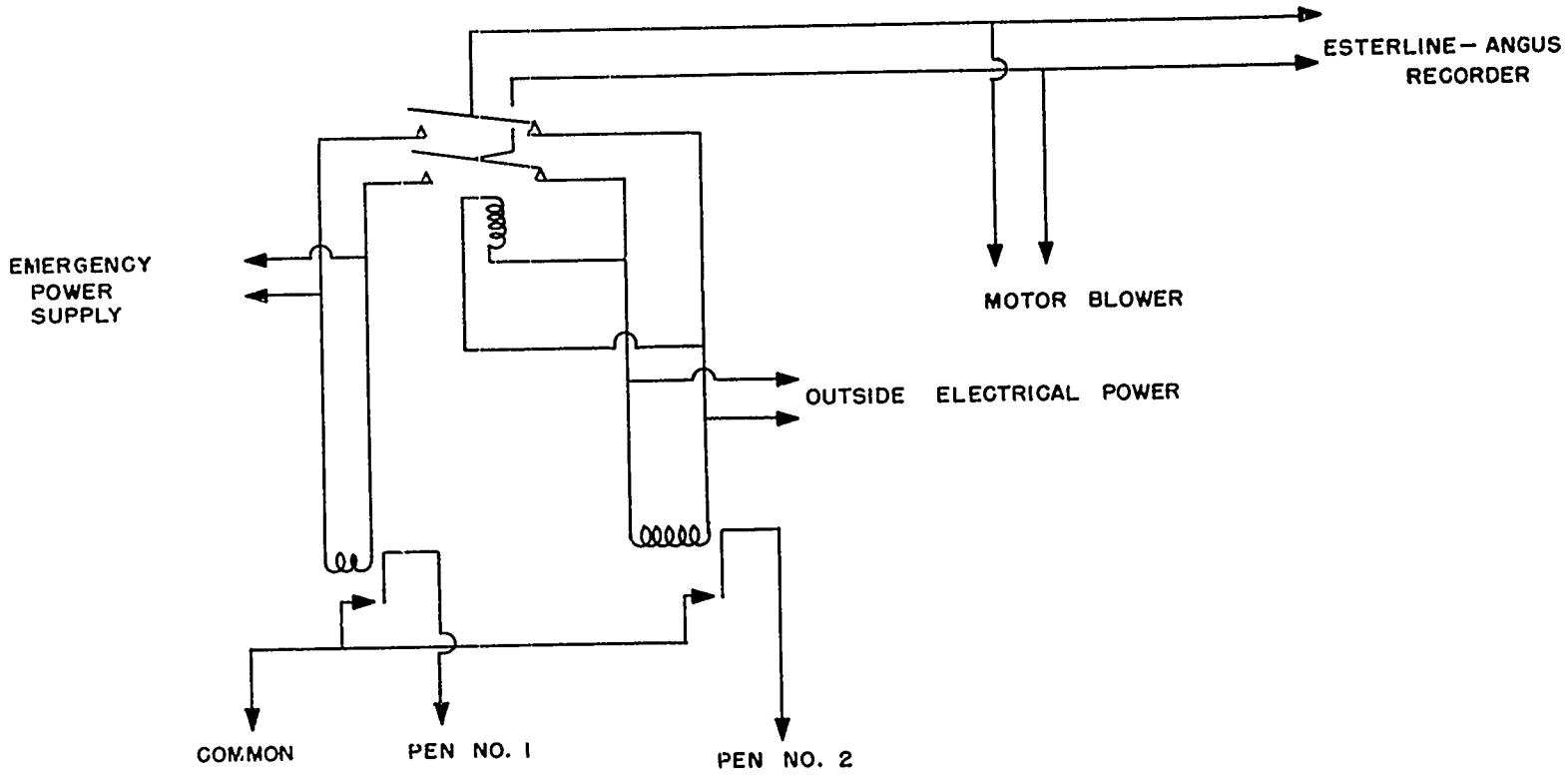

Fig. B.18 — Wiring diagram for Shelter 1-34.2 a-2 (115-volt alternating current).

(g) Predicted Pressure Build-up in Inlet and Exhaust Air Chambers. The calculated free volume in the inlet air chamber was determined to be 160.35 cu ft and that of the exhaust chamber, 161.18 cu ft. As in the Apple I shot, the anticipated peak overpressure was 100 psi. However, two E_4 antiblast closure units were located in each of these chambers; thus for the foregoing calculation it was assumed that each closure would have a free volume of about 80 cu ft. It was felt that subsequent reexpansion into the 1930 cu ft free volume of the shelter proper would reduce the pressure in this space to a negligible level. Using a free volume of 80 cu ft and resubstituting in the following equation:

$$Q = V\left(\frac{P_2}{P_1} - 1\right)$$

where Q = the volumetric air flow in cubic feet per minute to create P_2
V = free volume on protected side of closure (cubic feet)
P_2 = pressure in pounds per square inch created by an input of Q cfm
P_1 = pressure of free volume at rest (14.7 psi)

$$7.73 = 80\left(\frac{P_2}{14.7} - 1\right)$$

$$P_2 = 16.1 - 14.7 = 1.4 \text{ psi}$$

From this calculation and based on shock-tube data, an overpressure of 100 psi would produce a pressure of about 1.4 psi in both the inlet and exhaust air chambers. This pressure is far below the 5 psi estimated to cause filter rupture. With subsequent reexpansion of this pressure into the shelter proper, free volume of about 1930 cu ft would reduce the pressure in the shelter proper to a negligible level. The antiblast closure plate settings on all valves were at 1 in. above the gasketed bedplate as originally used in the shock-tube tests.

(h) First Operational Tests on Shelter. The wooden door was installed between the inlet and exhaust chambers, and the crack around the edges of the door was taped with masking tape. All shelter doors were closed, including the escape hatch which was sealed with masking tape in lieu of the dirt fill normally used. Using the pressure taps at the influent and effluent ends of the filter to obtain the pressure drop across the filter, an air flow could be ascertained from previous air flow vs pressure drop taken on this filter at the Army Chemical Center.

The shelter pressure was measured by means of a draft gauge, the high pressure side of which was open in the shelter, with the low pressure side referenced to atmospheric air. In this manner the level of shelter pressure for a known input air flow could be established. The two E_1R_6 anti-back draft valves through which the shelter air is conducted into the exhaust chamber act to stabilize the shelter pressure; and, through the use of known counterweight settings and fixed flap openings, the volumetric air flow could be determined from predetermined calibration data.

The first series of data taken of shelter pressures at various rates of input air flow was subsequently found to be erroneous because of the leakage of air around the wooden door installed between the inlet and exhaust air chambers. Since the recirculated air would not contribute to the shelter pressurization level and only a total flow measurement through the filter was obtained, the relative amounts of fresh and recirculated air could not readily be established.

The leakage was discovered during subsequent tests in which the gasoline-powered electric generator was operated in the exhaust chamber, with the filtered air supply on and all doors closed. In these tests, after 20 min of operation, the carbon monoxide content of the shelter was found to be 0.04 per cent, using a Mine Safety Appliance Co. carbon monoxide detector. It was felt at the time that this carbon monoxide level could have resulted from initial leakage in setting up this test, and under these conditions the continuous input of fresh air would act to dilute and reduce the carbon monoxide content in the shelter. However, at the end of 1 hr the carbon monoxide content in the filtered air supply to the shelter proper was measured and determined to be 0.04 per cent, firmly establishing that there was leakage between the exhaust and inlet air chambers.

It was also noted that the temperature in the exhaust chamber where the gasoline-powered electric generator was operated rose only to 80°F during the test, which indicated that the air supply through the exhaust chamber was adequate for ventilation of the gasoline-powered electric generator.

(i) Final Operational Tests on Shelter. To eliminate leakage around the wooden door separating the inlet and exhaust air chambers, a commercial caulking compound was used to seal the crack around the perimeter of the door; the caulked area was covered with masking tape; and the three wooden bars holding the door in place were tightened with wooden wedges to further improve the seal. With the improved door seal, the operational test of the shelter was reinitiated with the gasoline-operated generator with the filtered air supply on and with all shelter doors closed.

At the end of 15 min, the carbon monoxide in the filtered air which was discharged into the shelter was measured and was found to be zero. The content in the shelter after 17 min of operation was similarly found to be zero. At a time level of 25 min, the carbon monoxide content in the exhaust chamber where the generator was located was found to be 0.06 per cent. After 1 hr of operation the carbon monoxide content in the filtered air discharged to the shelter and within the shelter was again determined to be zero. At this time the level in the exhaust chamber was 0.08 per cent.

During this test the shelter pressurization level was maintained at about 0.75 in. of water as referred to atmosphere. The counterweight settings on the two E_1R_6 anti-back draft valves located in the wall between the shelter proper and the exhaust chamber were $2\frac{5}{8}$ in. on valve 1 and $2\frac{1}{8}$ in. on valve 2. The combined flow through the valves was about 250 cfm. For the last 10 min of this test, the main electrical power source was cut off and the system reverted to operation on the emergency electrical power generator. This power source assumed the electrical load without difficulty and operated adequately for the 10-min period. It was noted that the shelter pressure during operation on the emergency power source was about 0.1 in. of water lower than with the system operating from the outside current supply. This condition was presumably due to a lower voltage output from the emergency generator and was not deemed serious.

(j) Final Pressurization Tests of Shelter. With the wooden door between inlet and exhaust chambers caulked and sealed, access to the filter for pressure drop–air flow measurements was no longer possible without breaking the sealing on this door. This condition precluded the measurement of air flow by the pressure drop method, and, since direct flow measurement equipment was not available, an indirect method of ascertaining the air flow through the electrical power input to the motor blower unit was used in these tests.

The electrical power input to the motor blower was measured with a wattmeter (model 432, Weston Electrical Instrument Corp., Newark, N. J.). The laboratory data of flow vs power input, as shown in Fig. B.19, were used to obtain the flow measurement for measured power values at the test site. The data thus obtained, together with the flow through the anti-back draft valves and shelter leakage, are shown in Table B.6 and in Fig. B.20. During these tests all doors were closed, and the escape hatch was taped in lieu of the dirt fill normally utilized. Although the method used did not utilize a direct method of flow measurement, the data are believed to be substantially correct. As indicated in Table B.6, the flow setting to be used during the detonation was about 378 cfm with a protective level of pressurization of 0.71 in. of water.

B.2 TEST RESULTS

B.2.1 Test Results on the Diffusion Shelter

(a) General. The 50-man shelter equipped with diffusion board was tested on Apple I shot. Since the yield of the weapon was below that anticipated, the peak shock wave pressure at the shelter location was approximately 47 psi. There was no discernible structural damage.

Table B.6—SHELTER PRESSURIZATION DATA

Power to motor blower		Air flow,[a]	Shelter pressure,	Scale readings		Air flow,[b] cfm		Total air flow through valves,	Shelter leakage,[c]	
Kw	Hp	cfm	in. H_2O	Valve 1	Valve 2	Valve 1	Valve 2	cfm	cfm	Remarks
1.03	1.38	399	0.75	0.35	0.40	130	142	272	127	
0.82	1.10	277	0.54	0.32	0.35	122	125	247	30	
0.75	1.05	250	0.48	0.30	0.20	115	71	186	64	
0.63	0.83	120	0.34	0.15	0.18	55	65	120	0	Questionable data
1.01	1.35	397	0.765	0.38	0.40	148	142	290	107	
1.10	1.475	430	0.81	0.30	0.55	115	197	312	118	
1.06	1.42	415	0.82	0.38	0.4	148	142	290	125	
1.09	1.46	428	0.838	0.38	0.4	148	142	290	138	
0.99	1.33	378	0.71	0.35	0.38	130	135	265	113	Final setting of air flow

[a] Air flow was controlled by the adjustable louvres in air discharge register.

[b] Obtained from E_1R_6 anti-back draft valve calibration data not included in this report.

[c] Air flow not passing through E_1R_6 anti-back draft valves, including the leakage of the entrance door, escape hatch, bulkhead door between shelter and exhaust air chamber, and that of the walls, floor, and ceiling of the shelter at the indicated pressure level.

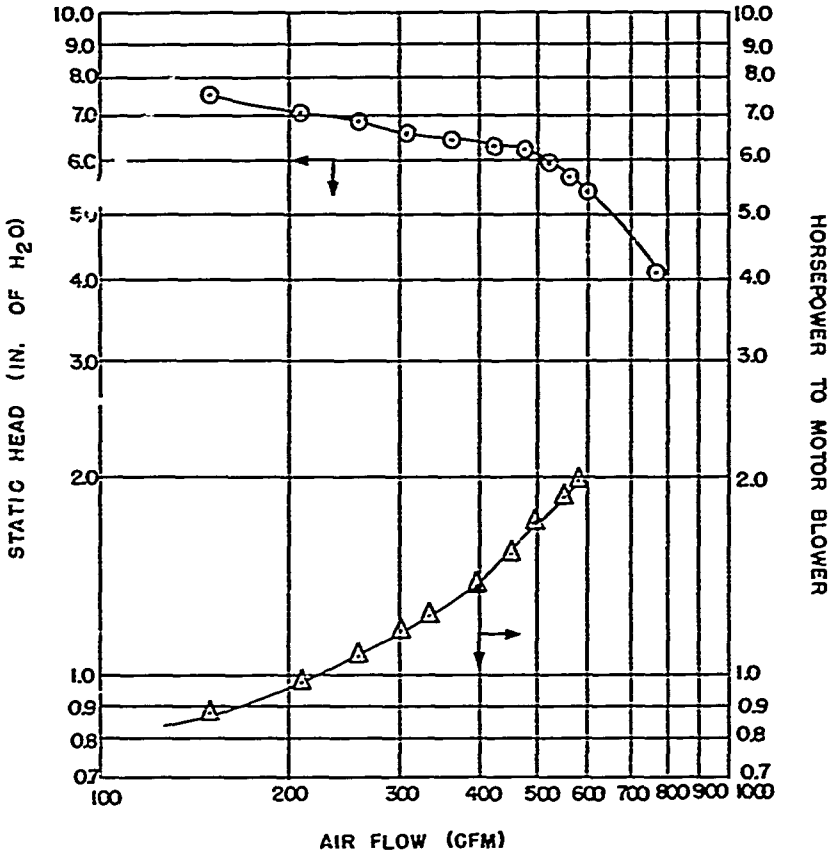

Fig. B.19—Laboratory data of flow vs power input.

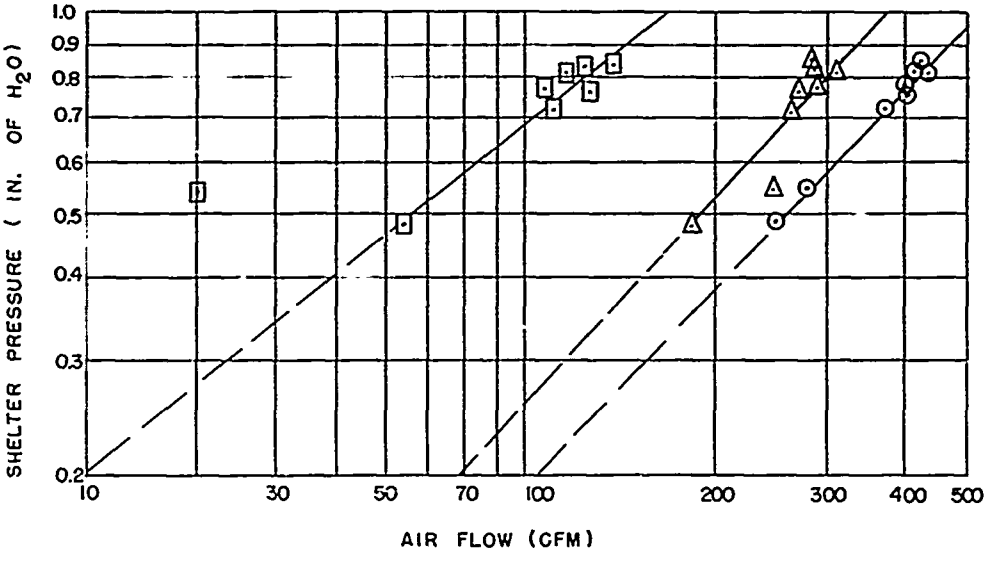

Fig. B.20—Flow measurements for measured power values compared with flow through anti-back draft valves and shelter leakage. O, total filtered air input. Δ, flow of air leaving shelter through valves. □, shelter leakage.

Table B.7—POSTSHOT AEROSOL TEST DATA[a]

Sample holder No.	Location[b]	Critical orifice flow, liters/min	Klett reading	Net Klett[c] reading	Concentration,[d] μg/liter	Total weight collected	Av. conc.,[e] μg/liter
1	1U	0.988	54.0	32.0	0.11	2.75	0.186
2	1L	1.042	56.0	34.0	0.12	3.00	0.192
3	2U	0.958	54.5	32.5	0.11	2.75	0.191
4	2L	1.000	56.0	34.0	0.12	3.00	0.200
5	3U	1.005	53.0	31.0	0.10	2.50	0.166
6	3L	0.965	60.0	38.0	0.13	3.25	0.222
7	4U	0.964	50.0	28.0	0.10	2.50	0.175
8	4L	1.005	63.0	41.0	0.14	3.50	0.232
9	5U	1.018	52.5	30.5	0.10	2.50	0.164
10	5L	1.058	54.0	32.0	0.11	2.75	0.173
11	6U	0.970	53.5	31.5	0.11	2.75	0.189
12	6L	0.957	51.0	29.0	0.10	2.50	0.174
13	7U	1.005	47.0	25.0	0.09	2.25	0.149
14	7L	1.010	51.0	29.0	0.10	2.50	0.165
Void	8U	1.012	132.0	110	0.38	760.00	50.0
Void	8L	1.000	131.0	109	0.38	760.00	50.7
Blank				20			

[a]Active period of generation 15 min; sampling time 15 min.
[b]U, sample taken at 6-ft height; L, sample taken at 1-ft height.
[c]Gross Klett reading less blank.
[d]From calibration curve of scale readings vs μg/ml of fluorescein.
[e][Total weight collected (μg)]/[critical orifice flow (liter/min) × time of sample (min)] - av. concentration (μg/liter).

(b) Inlet and Exhaust Pipes. The inlet and exhaust pipes whose tees were about 3 ft above the ground were bent to an angle of 60° from the perpendicular, but it appeared that these pipes could still have provided the requisite ventilation for the void area between the diffusion board and the structural walls of the shelter.

(c) Diffusion-board Installation. A visual inspection of the diffusion-board installation was made, and it revealed no signs of rupture or visible damage.

(d) Pressure Within Shelter. Pressure instrumentation by the Sandia Corporation of the void area behind the diffusion-board walls and within the shelter proper indicated a zero pressure reading at each location.

(e) Electrical Power from Gasoline-powered Generator. The chart record from the Esterline-Angus recorder indicated that power was available to the motor blower unit (used for ventilation of the void area) for a period of about $2\frac{1}{2}$ hr following the test detonation. This evidence is important since it shows that a gasoline-operated electric generator of this type with both air inlet and exhaust open to blast pressures of this magnitude can provide an uninterrupted power supply throughout the detonation.

(f) Motor Blower Unit. The motor blow unit with filters used for ventilation of the void area was not visually damaged.

(g) Postshot Aerosol Test of Shelter. Three days after the shot an aerosol test was conducted on the shelter to determine if the protective efficiency of the diffusion-board installation had been impaired by the detonation. The procedure followed was similar to that previously described in Sec. B.1.3g. The data are shown in tabular form in Table B.7. Sampling locations were as indicated in Fig. B.10.

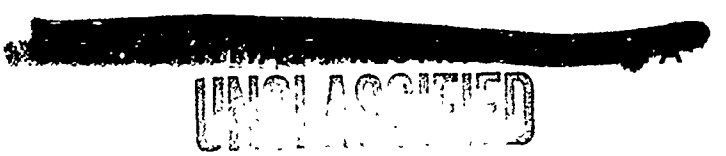

From the data it can be seen again that the concentration of aerosol in the shelter proper is fairly uniform. An average was taken of the fluorescein concentrations per liter at the various sampling stations within the shelter. The average value thus obtained was 0.184 μg/liter. The void samples were similarly averaged, and a value of 50.35 μg/liter was obtained. The percentage of penetration of the shelter can be readily obtained from these values as follows:

$$\frac{0.184\ \mu g/liter}{50.35\ \mu g/liter} \times 100 = 0.366 \text{ per cent infiltration}$$

B.2.2 Test Results on Pressurized Shelter

(a) General. The 50-man shelter equipped as a pressurized shelter was tested in the Apple II shot. The peak overpressure at the shelter was 92 psi, which is considered very close to the 100 psi predicted. The structure was for all practical purposes undamaged by the blast.

(b) Air Inlet and Exhaust Pipe Tees. The threaded pipe tees whose open ends were oriented to 90° from GZ and whose height above the ground was about 18 in. were torn off by the blast and blown approximately ¼ mile from the shelter location. The 6-in. air exhaust pipe was bent about 20°, and the air inlet pipe was bent about 5° from the perpendicular.

(c) Pressure Instrumentation in Shelter. As previously indicated, pressure instrumentation by the Sandia Corporation was at three locations in the shelter: the inlet air chamber, the exhaust air chamber, and within the shelter proper. Two of these pressure records were not usable because of malfunction. The third pressure record, which was of the inlet air chamber, showed a negligible pressure during the positive pressure wave and clearly showed the changeover to the negative or vacuum phase of the shock front. A preliminary review of this record indicated that the peak of the negative phase would be of the order of about 2 psi, which is a reasonable value for a shock wave of this magnitude. It is believed that the shelter proper was subjected to even less pressure owing to the large free volume available for alleviation of the pressure.

(d) Functioning of E_4 Antiblast Closure Units. The E_4 antiblast closure units functioned very well in reducing the 92 psi overpressure to a negligible level within the shelter. The valves were checked on D + 1 day, and each appeared to function satisfactorily; however, the valves were not disassembled at this time.

(e) Preliminary Visual Inspection of Equipment. In the D + 1 entry a visual inspection of the gasoline generator, tank, anti-back draft valves, motor blower, and filter equipment was made. This inspection did not disclose any visual damage to any of the equipment indicated above from the effects of the blast nor were there any discernible thermal effects such as scorching of the wooden door between the inlet and exhaust air chambers. An aerosol test was used to determine whether the Chemical Corps filter was damaged or not.

(f) Power Supply. The Esterline-Angus recorder provided a permanent record of how long the power supply was available from the outside and inside gasoline-operated electric generator units. This chart indicated that the outside power source failed at 0448 and the inside generator power failed at 0452. The time of the detonation was 0510.

(g) Postdetonation Aerosol Tests of Filter. A postdetonation fluorescein aerosol penetration test was conducted on the filter unit using the same general procedure described in Sec. B.1.4e. Three sampling points were utilized in the influent air supply to the filter and a like number in the filter effluent. The indicated percentage of penetration determined in this test was 0.132 per cent, as against the 0.078 per cent penetration measured prior to the detonation. The indicated change in penetration was not deemed significant.

The dioctyl phthalate aerosol test was repeated at the Army Chemical Center under laboratory conditions following Operation Teapot. The procedure used was the same that had previously indicated a penetration of 0.0139 per cent for this filter unit (see Sec. B.1.4e). The penetration data obtained in the postdetonation aerosol test are given in Table B.8.

Table B.8—POSTSHOT DOP PENETRATION DATA FOR FILTER

Location	Measured penetration, %
1	0.015
2	0.008
3	0.012
4	0.008
5	0.009
6	0.010
Av.	0.014

The average of the values shown in Table B.8 indicates that the penetration for the filter in this test was 0.014 per cent, which was less than that obtained in the predetonation aerosol test.

B.3 DISCUSSION

B.3.1 Diffusion Shelter

(a) Aerosol Tests of Diffusion Type Shelter. The results of the preshot aerosol test of this shelter using the fluroescein aerosol test agent indicated an infiltration value of 0.746 per cent. The postshot aerosol infiltration value was 0.366 per cent. This increase in filtration is attributable to the plugging action which takes place in any mechanical filter used in aerosol filtration. In this process the resistance of the mechanical filter for a given air flow will increase, but at the same time the aerosol filtration will similarly increase.

On this basis it appears reasonable to assume that due to the additional aerosol loading during this test and through use following the initial aerosol test the filtration property of the diffusion-board installation would increase. However, the principal information gained from the aerosol tests was that the filtration property of the diffusion-board installation was not imparied by the effects of the blast.

(b) Antiblast Closure Operation. The E_4 antiblast closures performed well in the protection of the diffusion-board installation. Static pressure tests indicated that a pressure of 1 psi would produce rupture of the board. With a peak overpressure of 47 psi, the diffusion-board installation was not visually damaged, and aerosol tests confirmed that the filtration property of the installation was not imparied by the blast. Pressure gauges both in the void and in the shelter proper showed zero pressure readings.

(c) Diffusion-board Installation. The principal objective of this test work was to determine whether a diffusion-board installation of this type could be adequately protected from the effects of blast. From the test results this condition was met. However, even with the extreme care utilized in the construction of the diffusion-board installation, there was some leakage of the installation as indicated by the aerosol tests. This condition points up the requirement for additional development work on sealing methods and for improved test methods for locating any minor sources of leakage in an installation of this type.

(d) Ventilation of the Void Area. Details of the film dosimeter data are presented in Chap. 2, Tables 2.2 through 2.17.

In an underground shelter of this type, ventilation of the void area between the diffusion board and the structural walls is necessary to provide optimum conditions for the diffusion of carbon dioxide and water vapor through the diffusion board. In this shelter two Dustop filters arranged in series were used for dust filtration of the air supply in the void.

Although the film dosimeters located at the filters registered only 1.2 r as compared to a range of 0.6 to 1.0 r in the various film dosimeters in the shelter proper, in an area of heavy

fall-out the activity rate would increase considerably, and radiation shielding of the air inlet and air exhaust equipment should be incorporated in subsequent designs of shelters of this type. Similarly, consideration should be given to the use of standard Army Chemical Corps types of particulate filters for a more absolute filtration of dust and radioactive materials of various types since contamination of the void area with radioactive materials would pose a distinct radiation hazard for the occupants of the shelter.

B.3.2 Pressurized Shelter

(a) Inlet and Exhaust Pipes. The inlet and exhaust pipe tees, because of their orientation 90° from GZ, were subjected to the maximum bending and shear forces at the 1050-ft station. Although the pipe tees were torn off by the force of the blast and the pipes bent, the damage incurred would not have affected the operation of the ventilation system within the structure. The lowering of the height of the inlet tees from 36 in. in the Apple I shot to 18 in. in the Apple II shot reduced the bend in the pipes from 60 to 20° despite the fact that the peak overpressure on Apple II shot was approximately twice that measured on Apple I shot. It is suggested in future pipe inlet configurations that these tees be welded to the pipe rather than be dependent upon the thread strength alone.

(b) Aerosol Tests and Ventilation Equipment. The slightly lower penetration measured in the postdetonation test of the filter at the Army Chemical Center was probably due to the plugging effect caused by the prior aerosol tests and the subsequent removal of particulate matter by a mechanical filter of this type in normal operation. Under these circumstances the accumulation of particulate matter tends to increase both the aerosol filtration of the filter and its pressure drop for a given air flow. It is felt that the aerosol tests of this filter show conclusively that there was no adverse effect on filtration due to the test detonation.

Based on a surveillance of the ventilation equipment, it was concluded that the E_4 antiblast closure had functioned well in preventing damage to the motor blower, the E_{25} filter, the elbow and air register, and the anti-back draft valves.

(c) Power Supply. As previously indicated, the Esterline-Angus chart indicated failure of the outside power generator at 0448 and failure of the generator located in the exhaust air chamber at 0452. From this data it would appear that both power sources failed prior to zero. However, the chart was driven by a 115-volt 60-cycle synchronous motor, and, owing to the relatively heavy loading on the generator circuit in supplying power for this shelter and at Station 1-34.3 a-2, it is possible that reduced voltage and frequency lowered the chart speed, making the power supply available through time zero. The possibility of a lowered frequency was brought about by the perceptible flicker in the light bulbs during previous dry runs. In three of these dry runs, the generator ran a number of hours after the anticipated shot time. The electrical load of the shelter equipment was only about one-half of the rated capacity of the emergency power generator. In a number of prior tests this generator had assumed this load without malfunction. With the protection of the antiblast closures, the generator was exposed to only a negligible overpressure, and, from the Apple I shot results, the outside generator continued operation despite a 47-psi overpressure.

The assumptions that the emergency power generator operated through the blast and that failure was due to lack of oxygen on the premise the antiblast closures failed to reopen are invalid since this generator had been run for periods of about 10 min in previous tests without ventilation and did not malfunction. To date, no valid reason has been found for the failure of the inside generator. The amount of debris and dirt deposited in the outside generator could have caused its failure if the generator was operating at time zero.

(d) Design Changes in Emergency Power Generator Installation. Since there were no personnel in the shelter during the test detonation, in order to protect the gasoline-operated power generator in so far as possible from the effects of overpressure, the engine exhaust was allowed to discharge directly into the air in the exhaust chamber. As was shown in the operational tests of the shelter, leakage around the wood panel between the inlet and exhaust air

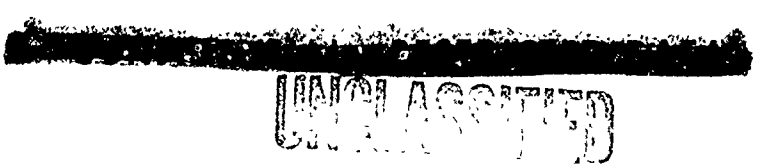

chambers was a potential hazard because of the carbon monoxide in the generator exhaust. This leakage was subsequently eliminated by caulking and taping around the edges of the panel.

In shelters designed for actual use rather than test, the exhaust from the gasoline generator should not be discharged directly into the air in the exhaust chamber. An improved design for the engine exhaust would utilize an exhaust system constructed of standard pipe and pipe fittings. This line would run directly from the exhaust manifold of the engine to the outside atmosphere and would be equipped with a gate valve which would normally be closed as long as commercial power is available. This would prevent possible blast damage to the generator. When the commercial power supply failed because of blast, the valve could be opened and the generator started by one of the shelter occupants. The exhaust line above ground level would utilize a standard tee fitting at the discharge end of the line. In this way the generator would be protected from blast, and the hazard of carbon monoxide within the exhaust air chamber or the shelter proper would be minimized.

(e) Open Shelters Vs Closed Shelters. The effectiveness of the closed shelter can be evaluated by considering that the pressure inside would have been as high as 75 psi had the shelter been left open, against no pressure in the shelter as tested. The residual radiation would have been 14 r as against 10 mr in the closed shelter. Heat within 3 ft of the entrance of the shelter would have been sufficient to cause serious burns had the shelter been left open. These comparisons are possible by the open shelter design used by Project 33.1 (reference 2).

(f) Design Changes in Chemical Corps Filter Assembly. As previously indicated in Sec. B.1.4d, the 1-hp motor coupled to the motor blower on the E_{25} gas and particulate filter was overloaded in producing an air flow of 600 cfm at a static pressure of $5\frac{1}{2}$ in. of water. Within the time limitations imposed by the Teapot test program, there was insufficient time to procure a more suitable electric motor. Although no operating difficulties were encountered due to overloading of the 1-hp motor during this test, it is felt that a more powerful motor should be provided for the motor blower installation if the present Revcor blower is retained in subsequent filter designs of this type.

The E_{25} gas and particulate filter with plenums and skid had a height of about $30\frac{3}{4}$ in., a width of 27 in., and a length of $53\frac{1}{2}$ in. The steel bulkhead door between the shelter proper and exhaust chamber has a net clearance in the width dimension of 26 in. through which the filter unit had to be moved for final installation in the inlet air chamber. In the Teapot operation the E_{25} filter width was reduced from 27 to $25\frac{1}{2}$ in. by removing the $\frac{3}{4}$-in. plywood cover strips on each side of the filter. These strips were subsequently replaced prior to final positioning of the filter unit. If the present steel bulkhead door is retained in future shelter designs, the $\frac{3}{4}$-in. plywood cover strips on each side of the filter should be replaced with thin sheet-metal strips which will provide the necessary air seal and permit movement of the filter through the 26-in. door width without disassembly of the cover strips.

B.4 CONCLUSIONS AND RECOMMENDATIONS

B.4.1 Conclusions

(a) Diffusion Shelter. Under the 47-psi shock wave loading at the shelter location, the protective characteristics of the shelter and its air filtration system were not imparied by the test detonation.

(b) Pressurized Shelter. The 92-psi peak overpressure encountered during the test detonation did not adversely affect the efficiency of the protective ventilation of the pressurized shelter.

B.4.2 Recommendations

(a) Air Ducting, Diffusion, and Pressurized Shelters. Weld type pipe fittings and heavy-duty pipe should be employed in the exposed duct sections above the shelter in future designs to provide increased resistance to damage by blast.

(b) Wood Panel Between Inlet and Exhaust Chambers. Future designs should utilize gasketing together with a positive type of mechanical clamping device for the panel installation to eliminate air leakage between the inlet and exhaust chambers.

(c) Exhaust from Gasoline-powered Electric Generator, Pressurized Shelter. The exhaust from the gasoline-powered electric generator in future shelter designs should not be discharged directly into the air in the exhaust chamber but should be handled as described in Sec. B.3.2d.

(d) Design Changes in Chemical Corps Filter Assembly. (1) Motor Blower. An electrical motor of increased power should be utilized if the present Revcor blower is retained for use with the E_{25} gas and particulate filter.

(2) Plywood Cover Strips on E_{25} Gas and Particulate Filter. The $\frac{3}{4}$-in. plywood cover strips on the sides of the E_{25} filter should be replaced with thin sheet-metal strips to permit passage through the steel bulkhead door between the shelter proper and air exhaust chamber without disassembly as explained in Sec. B.3.2f.

(e) Draft Gauge Installation, Pressurized Shelter. In future shelter designs the shelter should be equipped with a permanently installed draft gauge so that the level of the protective pressure within the structure can be readily determined at any time by the shelter occupants.

REFERENCES

1. Frank G. Ort and Merton D. Mears, Evaluation of Collective Protection Equipment, Operation Greenhouse Report, WT-42.
2. C. S. White et al., Effect of Overpressures on Biological Systems, Operation Teapot Report, ITR-1179 (to be superseded by WT-1179).

APPENDIX C

PREDICTION OF BLAST LOADING INSIDE CAVITIES

By

Craig C. Hudson

Sandia Corporation

ANYTHING ABSTRACTED FROM THE MATERIAL IN APPENDIX C MAY BE TREATED AS CONFIDENTIAL-RESTRICTED DATA

NOMENCLATURE

P = absolute pressure
p = overpressure
u = fluid speed
a = sound speed
U = shock speed
T = absolute temperature
t = time
y = pressure ratio P/P_x, where P_x is some reference pressure like P_0 or P_r
γ = ratio of specific heats C_p/C_V
ρ = density
α = ratio of aerodynamic area to the geometric area (choking factor)

Special Notation

P_0, a_0 = pressure or sound speed at ambient conditions
t_+ = duration of positive phase
p^*_m = maximum overpressure; asterisk indicates association with incident wave
$\lambda = Ut_+$
$\sigma = Vt/\lambda$, where V is an appropriate speed, often approximated by U
K = proportionality factor in rate of change of pressure equation
T_t, P_t, etc. = temperature, pressure, etc., at throat
T_r, P_r, etc. = reservoir temperature, pressure, etc.

APPENDIX C

PREDICTION OF BLAST LOADING INSIDE CAVITIES

C.1 INTRODUCTION

To estimate set ranges for pressure gauges used inside shelters at Operation Teapot, shock-tube tests were undertaken by the Ballistics Research Laboratory (BRL) which yielded typical interior pressures on a $\frac{1}{24}$ scale model. These values served the purpose for which they were intended. However, for the benefit of the blast biology program, the tests were extended to attempt to describe how fill time and rate of pressure rise in the chamber might be affected by the size of the model opening. These experiments will be described in more detail in the body of this appendix.

After the results of the full-scale experiment and the model experiment were compared, assuming a certain scaling law, a considerable discrepancy was found in the measured pressures in the two cases. Incident pressure pulses were not similar, and it became apparent that something more than shock-tube experimentation would be necessary to predict the rise of pressure within a chamber subjected to a nonideal blast wave. This study is a preliminary examination of this problem; other studies relating to filling are given in references 1 through 4.

C.2 FUNDAMENTAL IDEAS

C.2.1 Scaling

It has been shown (see reference 1, Appendix A) that the appropriate model law is

$$\frac{P_2}{P_0} = f\left(\frac{P_1}{P_0}, \frac{P_0 t_1^2}{\rho_0 A_1}, \frac{A_1^3}{V_1^2}\right) \tag{C.1}$$

where P_2 and P_1 are pressures in the prototype and the model, A and V are the opening area and chamber volume, and t_1 is the time scale of the model. It is obvious that A^3/V^2 is constant when the model is made. Also t_1^2/A is proportional to t_1^2/L^2, where L is the dimension of the entrance. For similarity then

$$\frac{L_1}{t_1} = \frac{L_2}{t_2} \tag{C.2}$$

Let us now define a characteristic length $\lambda = Ut_+$, where U is the shock speed and t_+ is the positive-phase duration

$$\frac{L_1}{\lambda_1} U_1 = \frac{L_2}{\lambda_2} U_2 \tag{C.3}$$

If we choose the strengths of the incident waves equal and call $L/\lambda = \eta$, then

$$U_1 = U_2$$

and

$$\eta_1 = \eta_2$$

In short, similarity is achieved when the ratio of entrance diameter to pulse size is the same in both cases. It is also consistent with the foregoing to write

$$\frac{V}{A\lambda} = \frac{b^3 L}{\lambda} = b^3 \eta \tag{C.4}$$

where this length, L, is the dimension of the entrance and b is the ratio of volume to entrance dimensions. Now b is the same for both model and prototype and cancels out when the η's are compared. Thus b will be dropped in what follows.

We shall take it as self-evident that, for a transient phenomenon associated either with the model or the prototype, at a given scaled time, t, t_+, the event is the same in both cases provided the model and the prototype are in fact properly related. Then if the phenomenon can be represented by a function without dimension, f,

$$f\left(\frac{t'}{t'}\right) = f\left(\frac{t}{t_+}\right) \tag{C.5}$$

where the functions are identical because we presume that the phenomena are similar. To obtain this relation, the functions must be normalized, and it is appropriate to write

$$\frac{p(t/t_+)}{p_m^*} = \frac{p'(t'/t'_+)}{p_m^{*\prime}} \tag{C.6}$$

where p and p_m^* are the overpressure at any time and the overpressure at a given reference time, respectively. If $p_m^* = p_m^{*\prime}$, the scaling law for time is

$$\frac{t'}{t'_+} = \frac{t}{t_+} \tag{C.7}$$

In summary, if $\eta' = \eta$, $p_m^{*\prime}/P_0' = p_m^*/P_0$, and if the model and prototype are in exact proportion, then the overpressure ratio, p/p_m^*, at a given time, t/t_+, in the model is identical to $p'/p_m^{*\prime}$ in the prototype at time t'/t'_+.

To compare shock-tube data with full-scale data, the coordinates (p,t) of each point on each curve must be divided by p_m^* and t_+ or $p_m^{*\prime}$ and t'_+, respectively. These points having identical values, t/t_+ and t'/t'_+, are to be compared. Their values, p/p_m^* and $p'/p_m^{*\prime}$, may or may not coincide, depending upon the actual similarity of the phenomena.

C.2.2 Exact Analogue Solution

Briefly and qualitatively, the effect we are going to examine and some important parameters are contained in the following simple analogue. Although this solution is less accurate than one which will be given later, it lacks no essential property.

Let the chamber volume be V and the entrance effective area be αA.[a] The incident blast wave[b] may be represented by an overpressure-time function

$$\frac{p^*}{p_m^*} = 1 - \frac{t}{t_+} \exp\left(\frac{-Ct}{t_+}\right) \tag{C.8}$$

where p^* is the overpressure at any time, p_m^* is the maximum overpressure, t is the independent variable, and t_+ is the positive-phase duration.

The blast wave passes across the mouth of the entrance, and after a short time the diffraction effects decay. In the quasi-steady flow which follows, the blast pressure pulse acts as a reservoir from which air is forced through the open entranceway.

The rate of mass transport into the chamber is

$$\frac{dm}{dt} = \alpha A \rho_t(t)\, u_t(t) \tag{C.9}$$

where the quantities ρ_t and u_t are measured in the throat. The rate of increase in density in the chamber is

$$\frac{d\rho}{dt} = \frac{\alpha A}{V} \rho_t u_t \tag{C.10}$$

As the chamber fills, the temperature inside becomes that of the reservoir. Let us assume that it is a slowly varying time function, $dT_r\ dt \sim 0$. Then by the ideal gas equation

$$\frac{dP}{dt} = \frac{\alpha A}{V} R T_r \rho_t u_t \tag{C.11}$$

The influx of material, ρu, depends upon some function of the difference of pressure between outside and inside. Let us choose an arbitrarily simple one

$$\rho_t u_t = \frac{p^*(t) - p(t)}{a_r} \tag{C.12}$$

where the asterisk indicates the incident pulse and a_r is the reservoir sound speed.

The problem is believed to have similarity properties like diffraction such that a basic length related to the positive-phase duration of the pulse serves as a length scale. This suggests the transformation $t \rightarrow Ut$, $\lambda = \sigma$, where U is an appropriate velocity (say the shock velocity). Then

$$\frac{dP}{dt} = \frac{dp}{dt} = \frac{dp}{d\sigma} \cdot \frac{d\sigma}{dt} = \frac{U}{\lambda} \frac{dp}{d\sigma} \tag{C.13}$$

becoming in similarity form

$$\frac{dp}{d\sigma} = \frac{RT_0}{a_r U} \cdot \frac{\alpha A \lambda}{V} (p^* - p) \frac{T_r}{T_0} = \frac{\alpha K}{\eta} (p^* - p) \frac{T_r}{T_0} \tag{C.14}$$

---

[a] If A is the physical area of the channel and A′ the aerodynamic area, then α A′/A.

[b] Incident blast pulse pressure or overpressure or its maximum or characteristic value will henceforth be designated with an asterisk.

where p^* and p are the same functions of σ that they were of t, $RT_0/a_r U = K$, and $V/A\lambda = \eta$; in other words, $\eta \sim L/\lambda$, where L is an appropriate dimension of the shelter and λ is the dimension of the blast wave.[a]

Notice that this simple differential equation contains an important parameter, $A\lambda/V$, which describes how the initial condition (geometry of the chamber and size of the wave) affects the filling. The integral is

$$p(\sigma) = \exp\left[-\left(\frac{\alpha K}{\eta}\right)\sigma\right]\left\{\frac{\alpha K}{\eta}\int \exp\left[\left(\frac{\alpha K}{\eta}\right)\sigma\right] p^*(\sigma)\, d\sigma + \text{const.}\right\} \tag{C.15}$$

When the blast pulse in Eq. C.8 is substituted for p^*, and letting $B = \alpha K/\eta$, we find

$$\frac{p}{p_m^*} = \frac{B}{(B-C)^2}\left\{[(B-C)(1-\sigma)+1]\, e^{-C\sigma} - [(B-C)+1]\, e^{-B\sigma}\right\} \tag{C.16}$$

A typical blast wave pulse is obtained when $C = 1$. Then for values of $\alpha K/\eta = 2$, 10, and 100 and with $T_r/T_0 = 1$ the overpressure in the chamber, p, has been calculated (Fig. C.1). Although actual magnitudes are not quite right, these curves correctly show one important feature of the problem — the way in which filling depends on the parameter η.

C.2.3 Important Physical Concepts

The analysis of the filling problem will proceed from the following basic hydrodynamic equations of one dimensional flow:[5]

Momentum: $$\frac{\partial u}{\partial t} + u\frac{\partial u}{\partial x} + \frac{1}{\rho}\frac{\partial P}{\partial x} = 0 \tag{C.17}$$

Continuity: $$\rho u A = \text{constant} = dm/dt \tag{C.18}$$

Energy: $$u^2/2 + C_p T = C_p T_r \tag{C.19}$$

The equation of state is

$$P = \rho R T \tag{C.20}$$

When this relation is substituted into the energy equation, with $\gamma = C_p/C_V$ and the first law of thermodynamics $C_p = R + C_V$, it becomes

$$\frac{u^2}{2} + \frac{\gamma}{\gamma-1}\frac{P}{\rho} = \frac{\gamma}{\gamma-1}\frac{P_r}{r} \tag{C.21}$$

If the pressure that causes the flow, u, to be set up is a function of time while the flow itself is essentially steady, it is called quasi-steady flow. Under the condition of quasi-steady flow, the time rate of change is independent of the geometry, and we neglect $\partial u/\partial t$ in the momentum equation, writing

$$u(x,t)\frac{\partial V(x,t)}{\partial x} = -\rho^{-1}(x,t)\frac{\partial P(x,t)}{\partial x} \tag{C.22}$$

where time dependence is indicated functionally here for completeness but will henceforth be omitted.

---

[a] This definition of η, seemingly arbitrary, comes from an analogous formulation for blast diffraction. There the significant variable is $\sigma - \eta$; this variable would also be appropriate here if the interaction were considered primarily one of diffraction.

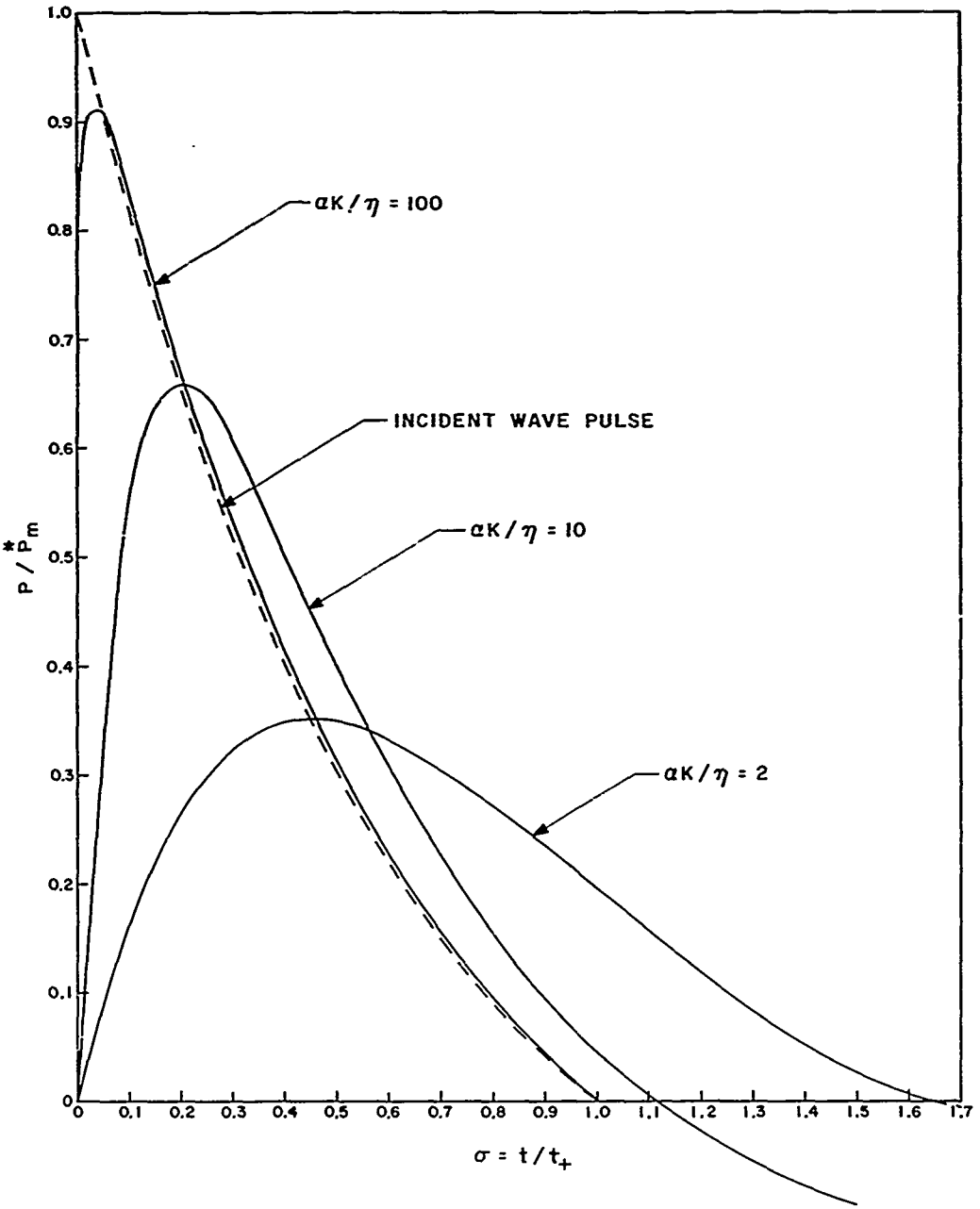

Fig. C.1 —Variation in chamber pressure, analogue theory.

The entropy of a gas with the aid of the ideal equation of state may be written as

$$S = C_P \log \left(\frac{T}{P}\right)^{(\gamma-1)/\gamma} + S_0 \tag{C.23}$$

and, if there is no change in entropy between positions x_1 and x_2, then

$$S(x_2) - S(x_1) = 0$$

and

$$\frac{T_2}{T_1} = \left(\frac{P_2}{P_1}\right)^{(\gamma-1)/\gamma} \tag{C.24}$$

Thus the two points lie on a constant entropy line, and thermodynamic properties between the two are related iso-entropically (isentropically). When this condition exists, the pseudo-steady momentum equation integrates to

$$u_2^2 + \frac{2\gamma}{\gamma-1}\frac{P_1}{\rho_1}\left(\frac{P_2}{P_1}\right)^{(\gamma-1)/\gamma} = u_1^2 + \frac{2\gamma}{\gamma-1}\frac{P_1}{\rho_1} \tag{C.25}$$

If the fluid at x_1 is at rest, this region serves as a reservoir. The equation for reservoir flow is

$$u^2 + \frac{2\gamma}{\gamma-1}\left(\frac{P_r}{\rho_r}\right)\left[\left(\frac{P}{P_r}\right)^{(\gamma-1)/\gamma} - 1\right] = 0 \tag{C.26}$$

Conversely, if a flow at velocity u, and pressure P, is in principle brought to rest isentropically, its pressure and density will be P_r and ρ_r. If no heat transfer takes place, then, even though the flow is not isentropic, the temperatures T_r and T_r' of the originating reservoir and the hypothetical test reservoir will be the same; i.e., the flow will be adiabatic but irreversible.

However, for the filling of a chamber by a blast wave, where the hot air of the blast pulse is the reservoir, there is a transfer of heat from the incoming air to the air already present in the chamber. If the initial difference in temperature is small or if the mass of air moved in at high temperature is large compared with the air already present, then the adiabatic assumption is satisfactory. But, in general, the mixing of inflowing air at reservoir temperature T_r with the air in the chamber at T_0, where $T_r \gg T_0$, is neither adiabatic nor reversible. By making certain intuitive guesses, the necessity of delving into such complex flow problems is postponed for the time being.

C.3 TEAPOT AND SHOCK-TUBE EXPERIMENTS

C.3.1 Incident Wave

Only a partial similarity could be obtained between the two incident waves by letting the more or less ideal shock-tube pulse coincide in time with the major peak of the blast pulse found in the field. When both pulses have been normalized to permit this comparison, the result is as shown in Fig. C.2.

Two important features distinguish the curves: (1) the flat precursor pressure region and (2) the slow rise, both characteristic of the Apple II incident wave. These differences must of course affect the chamber filling.

Nor is this the whole story. The temperature associated with the incident pressure pulse in the field was very high and probably did not decay during the positive-phase duration. For the shock-tube pulse the temperature probably did decay, following the pressure. In neither

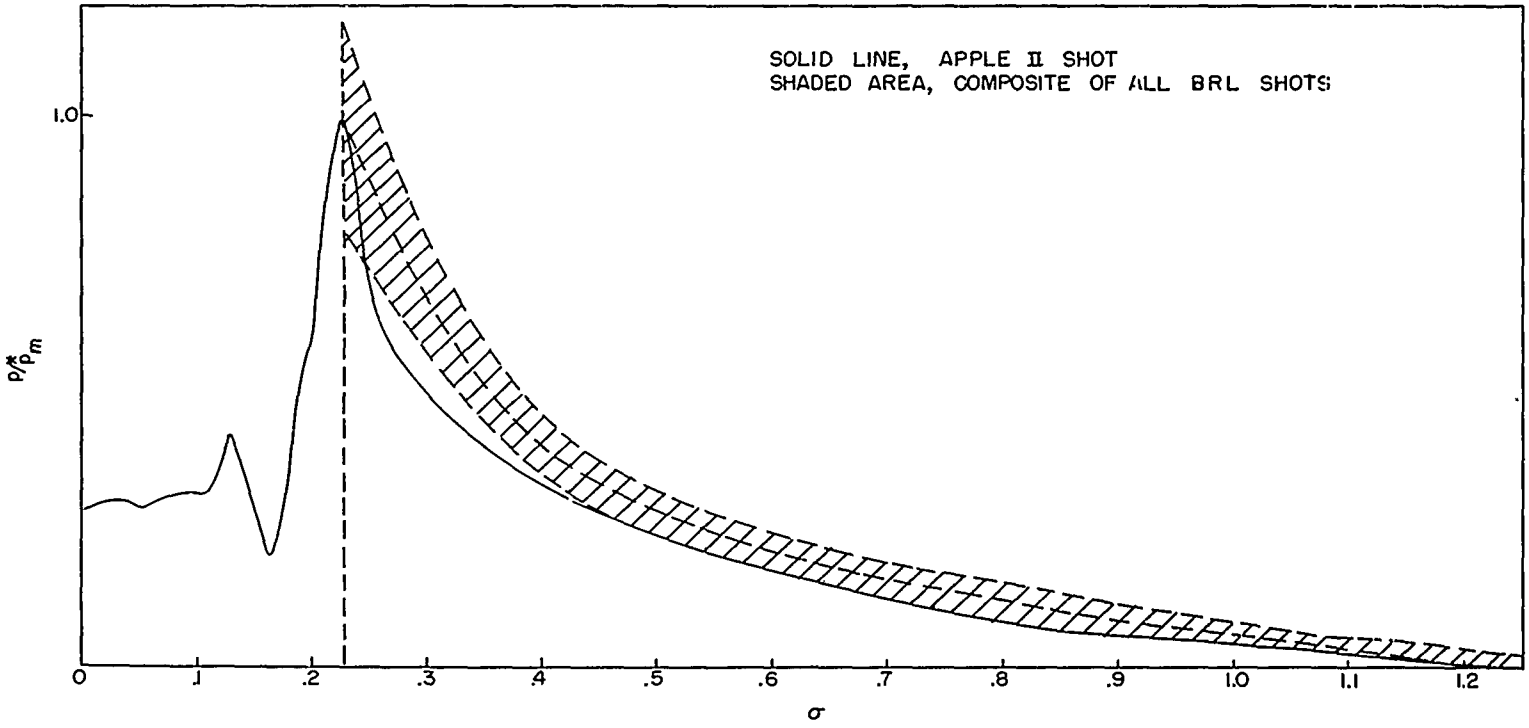

Fig. C.2—Incident wave pressure pulses.

case was the temperature actually measured, but there is evidence that such was the case.[6] Therefore the following assumptions about the temperatures associated with the incident pressure pulses are made:

1. Precursor pulse
   (a) The temperature in the flat precursor pressure region is constant and is given adiabatically from the temperature ahead of the wave (say, 1800°F).
   (b) The temperature behind the main pulse remains constant for the positive phase (from IBM Problem M calculations for a free air burst).[a] Maximum temperature at the peak of the main pulse is given adiabatically from the temperature in the precursor region.
2. Ideal pulse
   (a) The temperature decays after the shock front with the same decay factor as the pressure pulse.
   (b) Maximum temperature is obtained by the shock relation from ambient temperature (say, 70°F).

With these assumptions, the effective reservoir temperatures in the two cases can be estimated.

C.3.2 Scaling Procedures and Comparison of Field and Shock-tube Experiments

According to the scaling discussion above, the following relation will be used:

$$\frac{t}{t_+} = \frac{t'}{t'_+}$$

and

$$\frac{p(t/t_+)}{p^*_m} = \frac{p(t'/t'_+)}{p^{*\prime}_m}$$

Thus p^*_m and t_+ will refer to the peak overpressure and duration of the shock-tube pulses and $p^{*\prime}_m$ and t'_+ will be the corresponding values for the main pulse of the precursor.

The appropriate scaling numbers for the fast-fill side, for instance, are

Shock tube	Full scale
$t_+ = 40$ msec	$t'_+ = 263$ msec
$p^*_+ = 95$ psi	$p^{*\prime}_+ = 91.5$ psi

When the experimental data[b] are smoothed and plotted in normalized form, the curves of Fig. C.3 result. The pressure goes higher and remains positive longer for the prototype than for the shock-tube model. There are three likely explanations of this effect:

1. The scaling is not appropriate.
2. Existence of the precursor modifies the expected flow.
3. The different temperature dependence in the two cases modifies the expected flow.

The last reason appears to be the governing one.

---

[a] IBM Problem M (performed at Los Alamos Scientific Laboratory), original data calculations.

[b] The slow-fill curves from full-scale and shock-tube tests are quite comparable; time has not permitted their complete reduction (see Sec. C.10).

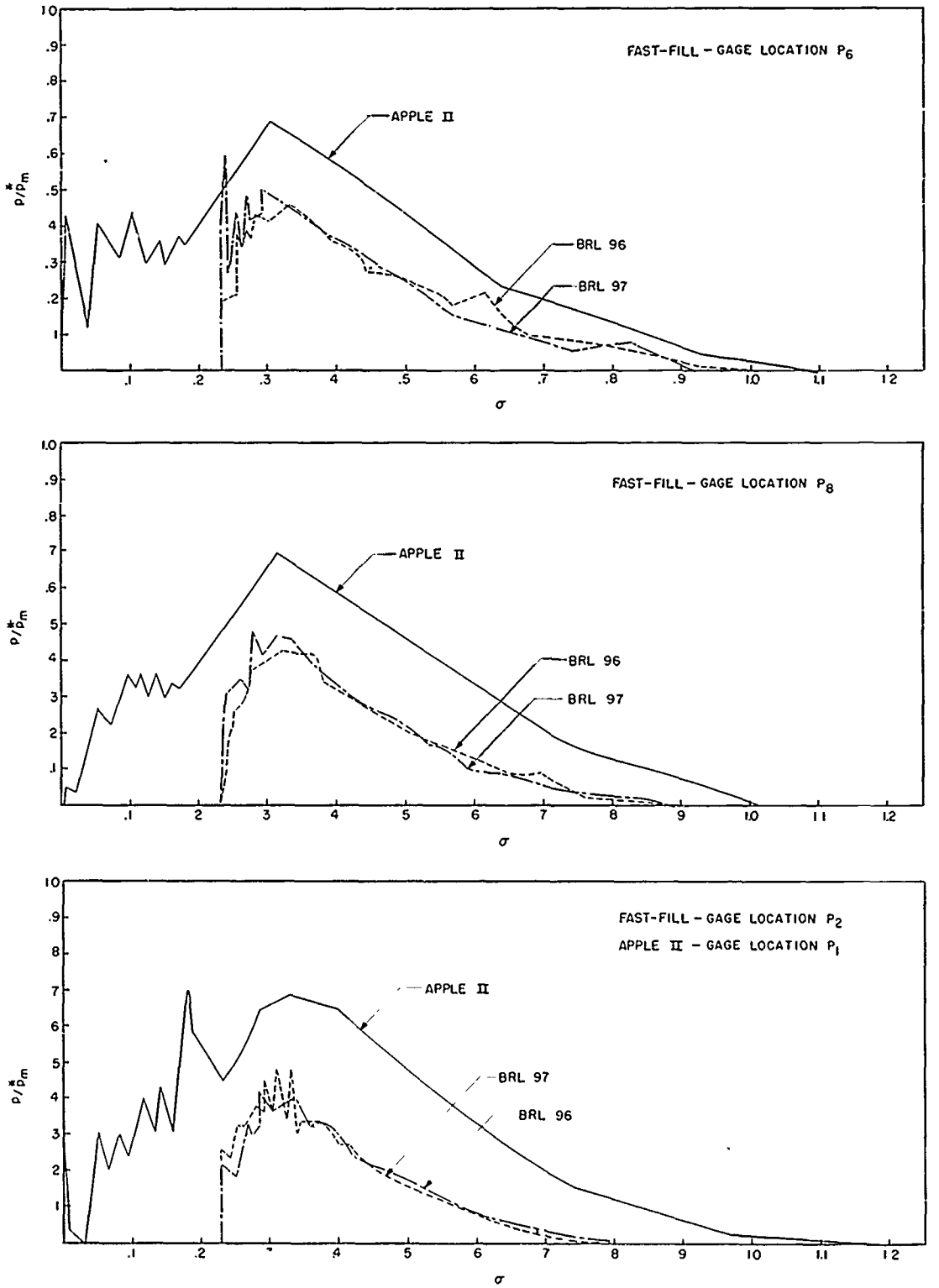

Fig. C.3—Scaled field and shock-tube overpressure-time records for fast-fill chamber.

C.4 EMPIRICAL DATA FOR OPENINGS OF VARIOUS SIZES (BRL STUDY)

At the BRL, in the spring of 1955, two models were tested: the slow fill (SF) and the fast fill (FF). For each the entrance opening was varied by factors of $\frac{1}{4}$. That is, the scale model of the Nevada shelter has a full opening $\frac{1}{1}$; then it is varied to $\frac{3}{4}$, $\frac{1}{2}$, $\frac{1}{4}$, and in one case to $\frac{1}{12}$. These fractions are called the "relative opening ratios," or "ROR." Table C.1 gives pertinent information about the series.

Changes in ROR mean changes in the characteristic parameter, η. The length λ is about 110 ft,[a] whereas the ratio V/A for the slow-fill side (full open) is about 6.8 ft. The value of η_{SF} is thus 0.062, and for the partially closed shelters $\eta = \eta_{SF/ROR}$. On the fast-fill side one

Table C.1—BRL SHOCK-TUBE DATA

Shot	p_m	t_+	ROR	Model
83	112	44	$\frac{1}{4}$	FF
84	75	41	$\frac{1}{4}$	FF
96	85	39	$\frac{1}{1}$	FF
97	80	41	$\frac{1}{1}$	FF
103	95	39	$\frac{1}{4}$	SF
104	100	40	$\frac{1}{4}$	SF
107	100	40	$\frac{1}{1}$	SF
108	95	40	$\frac{1}{1}$	SF
88	90	42	$\frac{1}{2}$	FF
89	90	48	$\frac{1}{2}$	FF
90	80	45	$\frac{3}{4}$	FF
91	75	40	$\frac{3}{4}$	FF
105	110	40	$\frac{1}{2}$	SF
106	105	42	$\frac{1}{2}$	SF
68	70	$17\frac{1}{2}$	$\frac{1}{12}$	SF
109	95	39	$\frac{3}{4}$	SF

opening in the channel remained fixed at about 12 sq ft, whereas the other one varied to a maximum of about 25 sq ft. The plane of this opening, however, was not normal to the air flow in the throat but was at an angle of about 40° to it. However, we shall call η_{FF} that corresponding to the largest channel opening, and it has a value of 1.9/110, or 0.017. It must not be supposed that at large openings this will be the controlling factor in the rate of fill. No correction is made for the angle between the opening and the flow.

The average initial change of pressure with time, called AI, and the average change of pressure to the maximum or to the fill time, called average fill time slope and designated AFT, were measured from the data.

More exactly, the average initial rise on all the records corresponding to gauges in the chamber was obtained. Often the rise of pressure appeared to have been instantaneous, giving an infinite slope. The averaging, therefore, was obtained by taking reciprocals, i.e.,

$$\overline{\frac{\Delta p}{\Delta t}} = \left[\frac{1}{N}\sum_{N}\left(\frac{\Delta t}{\Delta p}\right)_N\right]^{-1} \tag{C.27}$$

Such an averaging procedure has inherent in it certain risks. However, these data are presented just as they were found. To obtain a common value for comparison, the average initial

[a] This is calculated as follows: $\lambda = (U, a_0)\, a_0 t_+ = 2.4 \times 1120 \times 0.040 = 110$ ft. So far, no procedures have been set up for obtaining λ, and intuition plays a large part in choosing appropriate values.

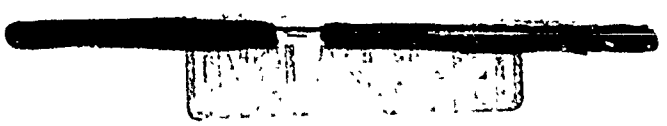

change was normalized, called NAI, so that

$$\text{NAI} = \frac{t_+}{p_m^*}\left(\frac{\Delta p}{\Delta t}\right) \tag{C.28}$$

The average fill time slope was easier to handle because it was always finite. The maximum point on the pressure-time curves was determined and designated by coordinates (p_f, t_f). Then, the averages of the ratio p_f/t_f were obtained straightforwardly and normalized as above so that

$$\text{NAFT} = \frac{t_+}{p_m^*} = \frac{\overline{p_f}}{t_f} \tag{C.29}$$

The tabulation of all these data is shown in Table C.2.

Table C.2—REDUCED BRL SHOCK-TUBE DATA

ROR	η	NAI	NAFT
SF 1/12	0.730	0.094	0.022
SF 1/4	0.240	0.710	0.166
SF 1/2	0.120	3.60	0.22
SF 3/4	0.081	2.60	0.24
SF 1/1	0.061	10.14	0.36
FF 1/4	0.070	2.52	0.49
FF 1/2	0.035	7.37	0.68
FF 3/4	0.023	31.7	1.12
FF 1/1	0.0175	47.1	0.95

The results of this experiment are plotted in Fig. C.4.

We adduce a word of caution concerning these data. It is very difficult to get such information, very tiresome to reduce it, and the results are discouragingly erratic. Thus, although the BRL study is considered to be good experimental work, it is the only work existing in this field and is not extensive enough to permit one to have confidence in the data, statistically speaking. However, it is clear that the data describe qualitatively a single phenomenon. Roughly, at least, this is borne out by the plot of Fig. C.4.

There is no reason yet to believe that the NAFT varies in the same way. However, when the points are plotted (Fig. C.4), most of them fall in lines showing similar relations with different slopes.

C.5 QUALITATIVE DESCRIPTION OF FILLING

C.5.1 Idealized Shelter

Let the chamber (Fig. C.5) be an arbitrary shape having volume V and connected to the outer air by a straight channel of uniform cross section A. It is assumed that this channel is not long relative to its cross-sectional dimension. The edges where the channel intersects the surface and the chamber are sharp, as is usually found in concrete construction.

C.5.2 Diffraction at the Entrance

Two categories are distinguished: (1) where the outside flow is subsonic and (2) where it is supersonic. To discuss these cases clearly, some general ideas of such phenomena should be understood.

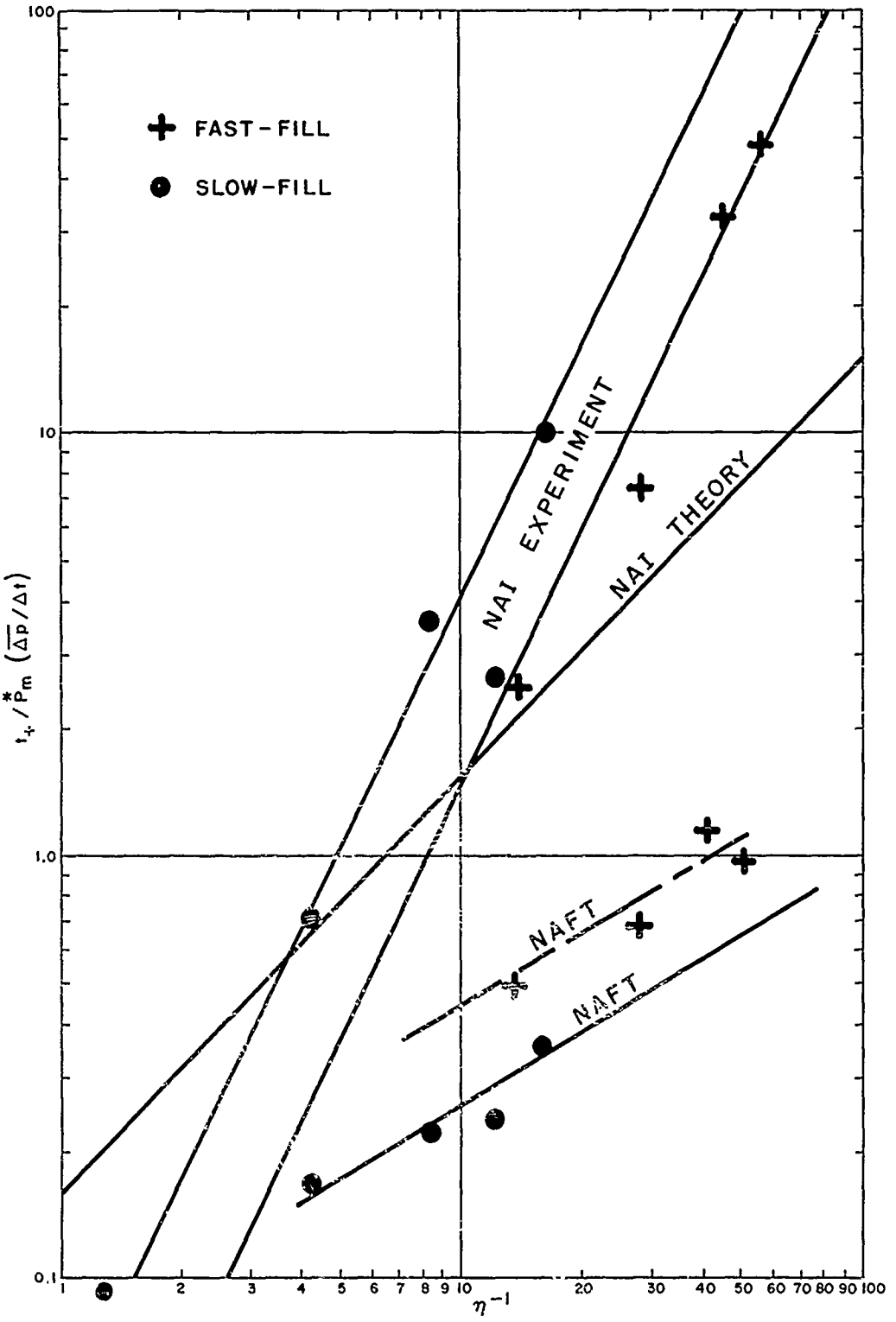

Fig. C.4 — Plot of the BRL shock-tube experiment data vs $1/\eta$.

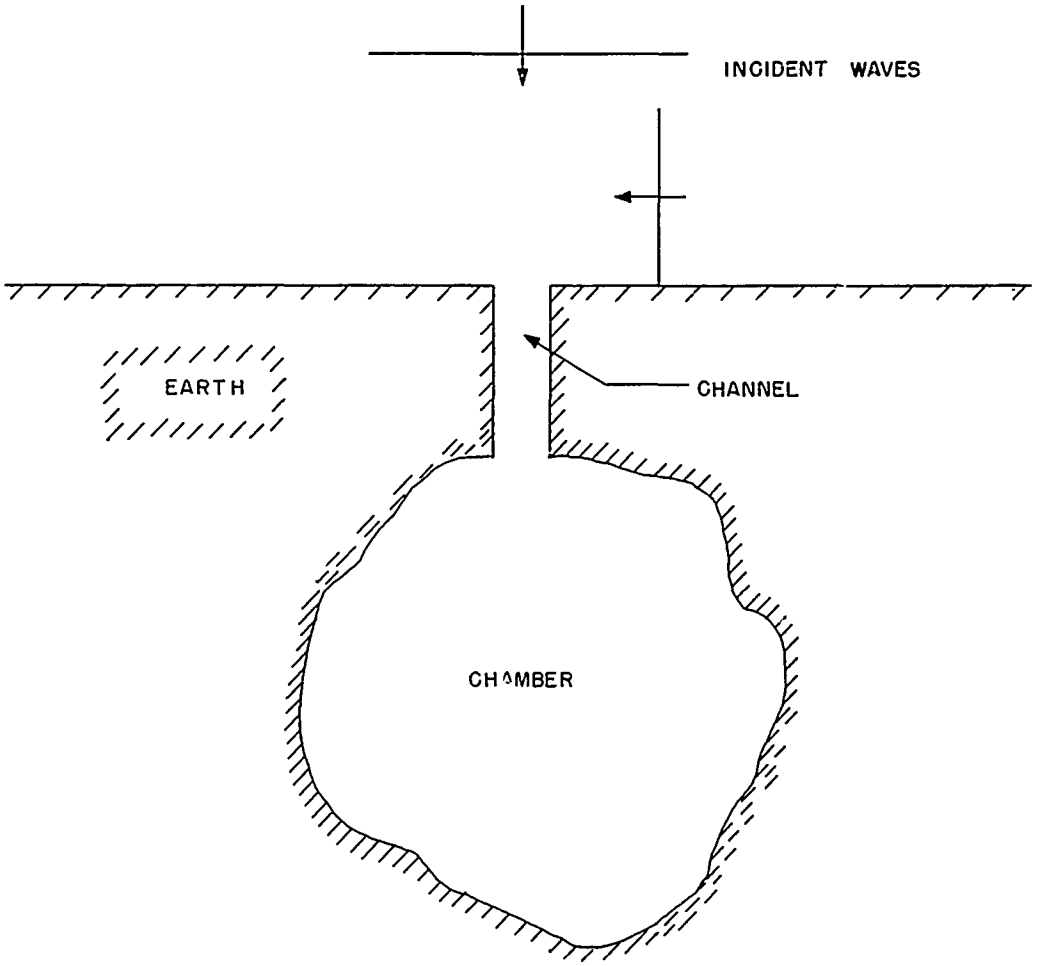

Fig. C.5—Idealized shelter design.

1. It is approximately true that flow associated with a plane shock of $y > 5$ is supersonic.

2. Consider a shock wave moving along one surface of a wedge toward the edge. The wave front is perpendicular to the wedge surface. When diffraction takes place at the edge, an extension of the wave moves down the back or lee side of the wedge. The strength of this wave (y_d) is always less than that of the incident wave (y_i). If we write $(y-1)$ as the overpressure strength of the wave, then empirically $(y_d-1)/(y_i-1) \sim y^{-k}$ with k approximately 1.5. The stronger the incident wave the weaker the diffracted wave is, relative to the incident. For a 90° wedge at $y = 1$, this ratio is $\frac{2}{3}$ (see reference 7).

3. When a shock wave passes a wedge, a discontinuity of flow, called a vortex, is formed in the lee of the edge. This discontinuity is perpetuated in the form of a sheet which connects the edge with the vortex and separates the flow. So long as a high-speed flow moves around the wedge, this separation will exist. The region enclosed by the surface of discontinuity and the wedge is roughly quiescent, and the vortex sheet forms a new boundary for high-speed flow.

4. When a shock wave impinges upon a rigid surface, the flow associated with the shock is changed in direction or brought to rest, and the pressure is increased. This increase of pressure is greater than the overpressure of the incident wave. If the reflected overpressure at the shock front can be represented by

$$p_r = R\, p_i$$

where R is a reflection factor, then it is usually a good approximation to write

$$p_r(t) = R\, p_I(t)$$

so long as no other interactions take place.

5. The diffraction of waves behind which the flow is supersonic has not yet been thoroughly investigated. Figure C.6 shows that the separation is present. It also shows the presence of two new discontinuity surfaces not observed in the diffraction of weaker waves, which seem to

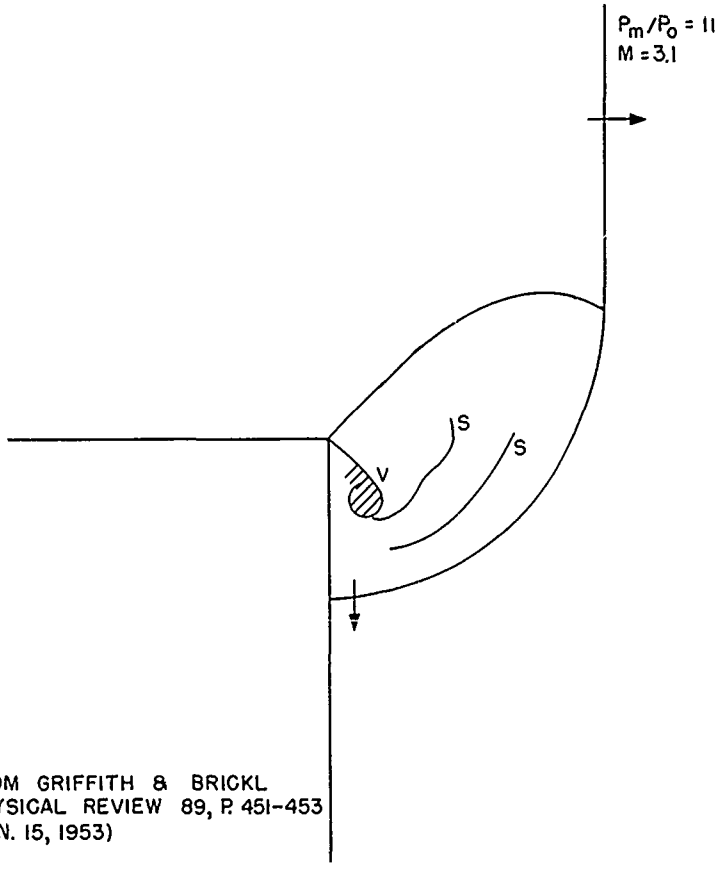

Fig. C.6—Diffraction of a shock with supersonic flow.

be shocks moving upstream by the following argument. The flow on top of the wedge is supersonic. Whenever a supersonic flow turns an angle of greater than 180°, its speed is increased; but the flow associated with the diffracted wave front is unquestionably less than that in the incident wave. These two conditions are therefore connected by a shock, or in this case two shocks, facing upstream.

6. Diffraction of a long blast wave about a two-dimensional rectangular dam (Fig. C.7) has been studied extensively. Part 1 shows the shock just passing the front corner. Parts 2, 3, 4, and 5 show the formation of the separated flow regions and their growth into a single continuous sheath (part 6) which characterizes the steady state. Little change in pressures around the dam takes place after the state of part 4 has been reached. The air speed over the top is greater than free stream speed. There has never been any reason to believe that physical processes behind the shock front and outside the separation surface are anything but isentropic. The supersonic flow case does not differ materially from the subsonic case when separation takes place, as it does in the configuration considered here. We use this device to enable us to use the same equations for both cases.

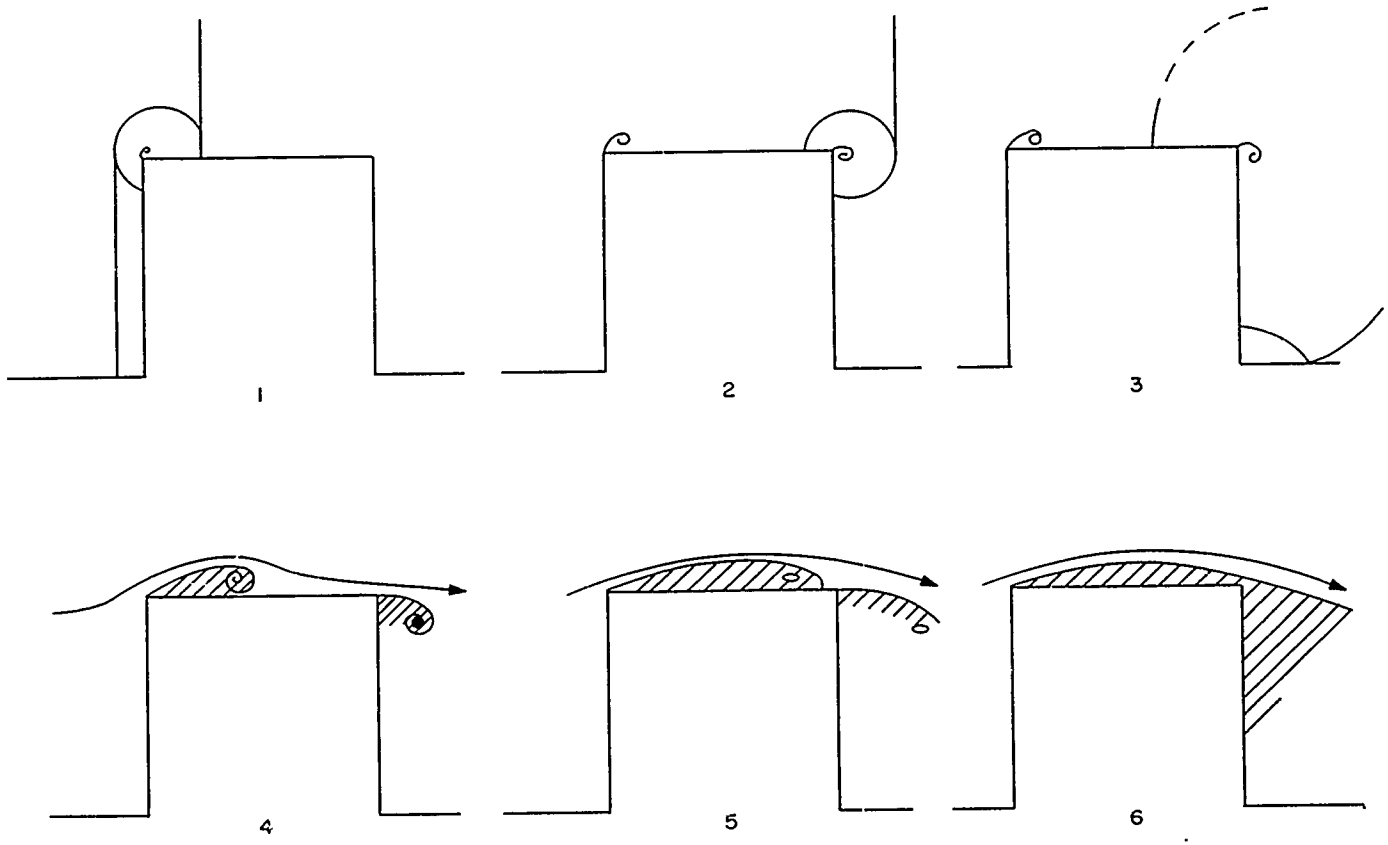

Fig. C.7—Diffraction of a shock by a two-dimensional dam of square cross section.

C.5.3 Shocks Less Than 5 Atm

Let us place two of the dams shown in Fig. C.7 top to top separated by a certain distance (Fig. C.8). Assuming that the bases of the two dams extend so that they no longer affect the flow, the movement of the shock into this short channel (which simulates the configuration of a shelter entrance) will set up a flow on each side similar to that at the top of the single dam. In effect a new boundary will be set up having a throat or constriction through which air moves at a speed perhaps greater than free stream but in any event determined merely by the pressure within the chamber and that outside. At some shock ratio, y_c, but less than 5, the air speed in this particular throat becomes sonic. No further increase in throat speed can take place under these conditions.

C.5.4 Shocks Greater Than 5 Atm

When the free stream flow is supersonic, the initial flow into the channel is also supersonic, and an attached shock (or system of shocks) is formed (Fig. C.9). It is believed, however, that the separation is still present and that eventually a throat forms which becomes small enough to limit flow at that point to sonic. The attached shocks stabilize, and the air speed through the channel becomes sonic and similar to the choked flow for shocks less than 5 atm.

C.5.5 Brief Description of Flow in a Throat

Let the initial conditions be the following: (1) The shock impinges upon the entrance causing diffraction. If the angle of incidence is 90°, then the reservoir pressure will be high; if 0°, the reservoir pressure will be low. (2) The system of wavelets set up by the diffraction passes down the channel. (3) The separation regions develop and the throat forms. What may have been either supersonic or subsonic flow is eventually restrained by the formation of the throat to a specific nozzle flow similar in all cases, provided the reservoir pressure pulse lasts long enough and the chamber does not fill too rapidly. (4) The flow in the throat depends upon the ratio of inside to outside pressures, P/P_r, and can be positive only when $P/P_r < 1$. When the inside pressure exceeds that outside, the roles of P and P_r are interchanged, and the mass flow venting the chamber is positive from $P_r/P < 1$.

For an ideal wave the qualitative properties of flow through a simple nozzle into a chamber are described in Fig. C.10.

C.5.6 Surges in the Chamber

The first knowledge in the chamber of the jet to follow comes in the form of a series of shock waves. These are the diffracted wavelets originating at the entrance which propagated with multiple reflections down the channel and into the room. At the channel exit the overpressure jump across the first of these waves would be: for 0° incidence, less than $\frac{2}{3} p_m$; for 90° incidence, a little greater than p_m. Farther into the chamber the shocks diverge and weaken. The pressure behind the wave rises probably in a series of jumps and steadies at some value about equal to p_m. As the throat forms, the pressure drops through the throat and increases again in a second series of shocks due to the jet type flow.

At some time in this process the first wave must reflect at the far walls and return. If the divergence has been great, only a compression wave returns; but if the cross-sectional area of the chamber in the principal direction of wave motion is of the order of magnitude of that of the entrance, a shock will return. Thus a system of reverberations will be set up. Reverberations will be strongest and last longest when one dimension of the chamber is long compared to the other two. Very little energy leaks out the entrance when the reflected wave returns except in special cases. Usually, therefore, the shelter acts as a trap for the blast wave front, and the blast wave energy must be dissipated through internal mechanisms.

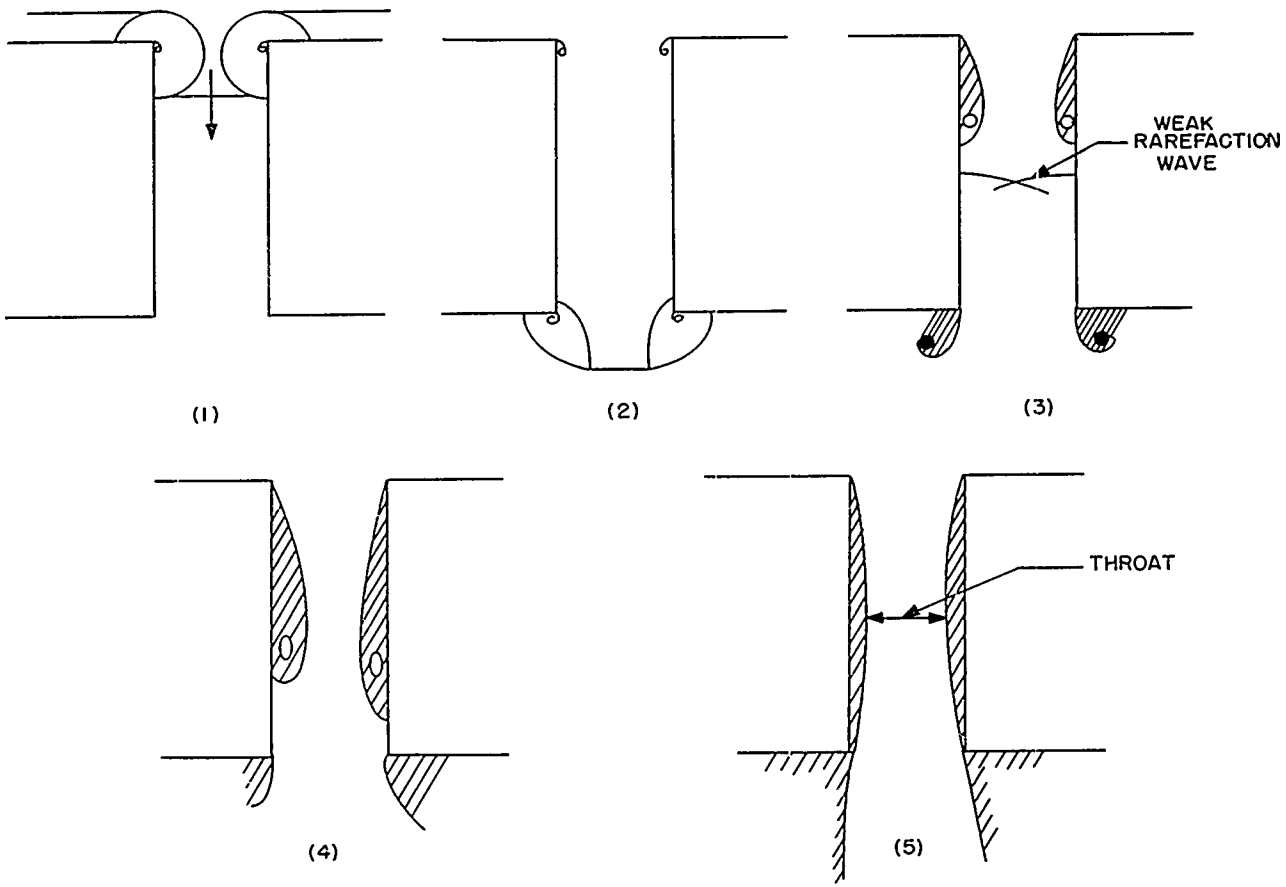

Fig. C.8—Model of an entrance channel for shocks less than 5 atm.

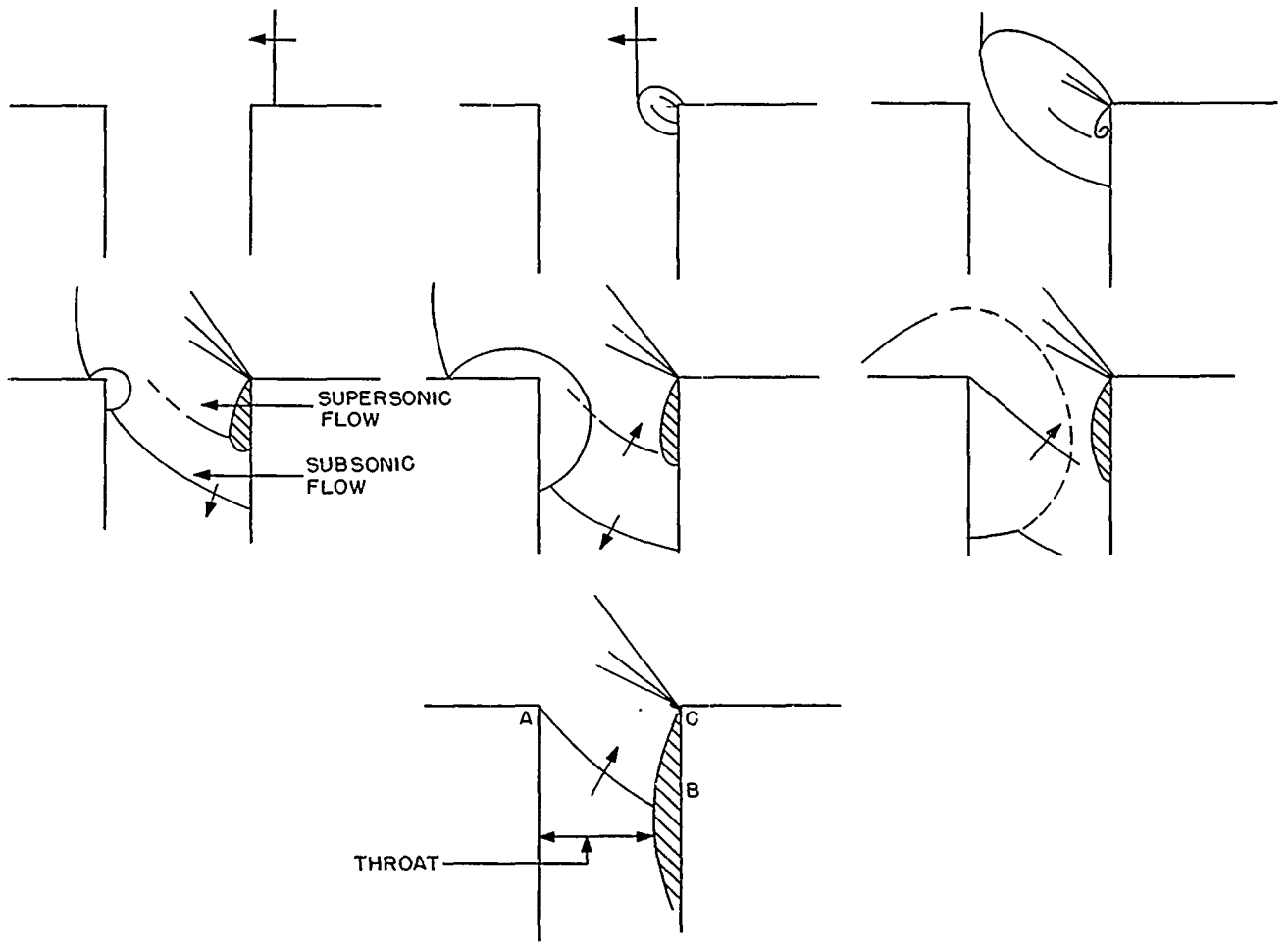

Fig. C.9—Model of channel for shocks greater than 5 atm.

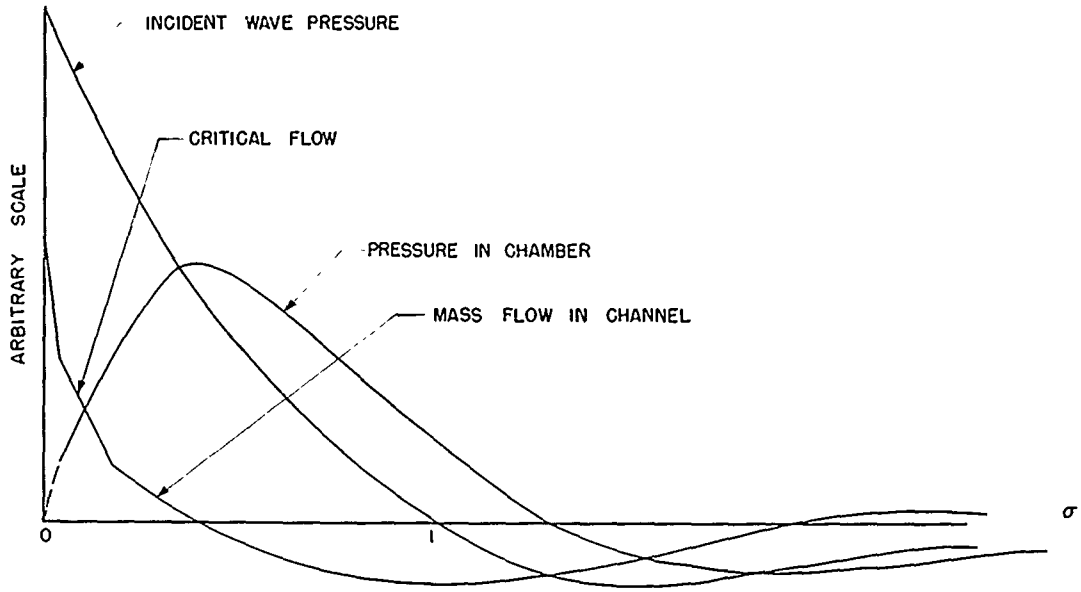

Fig. C.10—Qualitative description of nozzle flow and chamber pressure.

C.6 ANALYSIS OF THE PROBLEM

C.6.1 Subcritical and Critical Mass Flow

Figures C.8 and C.9 show the diffraction phase, with vortex kernels formed, for subsonic and supersonic flow outside. The weak rarefaction wave (part 3, Fig. C.8) makes its way slowly upstream and may come to rest between the two vortex regions forming the throat. As the vortex regions move downstream, a steady flow is set up. Probably the quasi-steady state is set up quicker for subsonic than for supersonic flow.

In effect, the channel develops a sleeve within it, consisting of a free boundary. No pressure differential exists across the boundary. Between the boundary and the channel wall the gas is at rest or in turbulent motion. In the core air moves at high speed.

If the critical point is never reached, the flow remains subsonic, and the mass flow is

$$dm/dt = \alpha A(\rho u)_t \tag{C.30}$$

where the subscript t indicates conditions at the throat. If the critical point is reached, the mass flow becomes fixed at[a]

$$(dm/dt)^\dagger = \alpha A(\rho u)_t^\dagger \tag{C.30a}$$

Bernoulli's equation for compressible flow (Eq. C.26) is

$$u^2 + \frac{2\gamma}{\gamma - 1}\frac{P_r}{\rho_r}\left[\left(\frac{P}{P_r}\right)^{(\gamma-1)/\gamma} - 1\right] = 0$$

[a] Critical flow parameters will be indicated hereafter by the dagger, as $P^\dagger$. Notice also that in compressible flow the overpressure p is not often used.

and from the energy equation (Eq. C.21) and assuming isentropic processes

$$(u/a)^2 = \frac{2}{\gamma - 1}\left[\left(\frac{P_r}{P}\right)^{(\gamma-1)/\gamma} - 1\right] \tag{C.31}$$

When $(u/a)_t = 1$, the critical condition for the throat, then we find

$$\frac{P_r^\dagger}{P_t} = \left(\frac{\gamma + 1}{2}\right)^{(\gamma-1)/\gamma} \tag{C.32}$$

and on the same isentropic assumption

$$\frac{\rho_r^\dagger}{\rho_t} = \left(\frac{\gamma + 1}{2}\right)^{1/(\gamma-1)} \qquad \left(\frac{T_r}{T_t}\right)^\dagger = \frac{\gamma + 1}{2} \tag{C.33}$$

With these equations we can write out the mass flow for each case in terms of the pressure at the throat

$$\frac{dm}{dt} = \alpha A \sqrt{\frac{2\gamma}{\gamma - 1} P_r \rho_r \left(\frac{P_t}{P_r}\right)^{2/\gamma}\left[1 - \left(\frac{P_t}{P_r}\right)^{(\gamma-1)/\gamma}\right]}$$

$$\frac{dm^\dagger}{dt} = \alpha A \sqrt{\frac{2\gamma}{\gamma - 1}\left(\frac{2}{\gamma + 1}\right)^{2/(\gamma-1)} \frac{\gamma - 1}{\gamma + 1} P_r \rho_r} \quad \text{critical} \tag{C.34}$$

Downstream from the throat the effective channel widens, and the subcritical flow decreases. In the critical case, however, as was demonstrated by the rarefaction wave becoming attached in the throat, the speed continues to increase, producing a supersonic flow. Usually such a flow can be brought to rest only by a change in entropy, such as by the formation of a system of shocks. We shall consider that only a single shock is formed.

To calculate in detail any of the quantities downstream of the throat, the boundary shape must be known. We do not know the shape and must resort to other means of finding the pressure in the chamber.

C.6.2 Calculation of Pressure in the Chamber

The density within the chamber increases at a rate given by

$$\frac{d\rho}{dt} = \frac{\alpha A}{V}(\rho u)_t \tag{C.35}$$

where $(\rho u)_t$ is measured at the throat of the entrance channel.

Transforming the left-hand side, consider a thin section of air having mass dm just at the instant it moves through the throat. Its total energy is

$$\left(E_t + \frac{u_t^2}{2} + \frac{P_t}{\rho_t}\right) dm$$

where E is the internal energy per unit mass in excess of the rest energy E_0, $u^2/2$ is its kinetic energy per unit mass, and P/ρ is the work done per unit mass in bringing it to this state. The energy of this element of mass must have been the same in the reservoir since the process accelerating the gas into the throat is isentropic. Thus

$$E_r + \frac{P_r}{\rho_r} = E_t + \frac{u_t^2}{2} + \frac{P_t}{\rho_t} \tag{C.36}$$

and writing the specific enthalpy, E + P/ρ, as H

$$H_r - H_t = \frac{u_t^2}{2}$$

Thus

$$\left(E_t + \frac{u_t^2}{2} + \frac{P_t}{\rho_t}\right) dm = H_r \, dm \tag{C.37}$$

Once in the chamber the energy brought in, $[E_t + (u_t^2/2) + (P_t/\rho_t)]$ dm, is mixed into the fluid already present. Internal dissipation does not change the total particle energy content; it only means a readjustment of the energy among the three agents.

Now the pressure of the air in the chamber of volume V may be written

$$PV = (\gamma - 1)\, mE \tag{C.38}$$

The total energy brought in is converted into internal energy E. The rate of increase of excess internal energy within the chamber is then

$$\frac{d(mE)}{dt} = \left(E_t + \frac{u_t^2}{2} + \frac{P_t}{\rho_t}\right)\frac{dm}{dt} = H_r \frac{dm}{dt} \tag{C.39}$$

The enthalpy H_r of the reservoir is equal to $C_p T_r$; thus

$$\frac{1}{\gamma - 1}\frac{dP}{dt} = C_p T_r \frac{dp}{dt} \tag{C.40}$$

and the desired relation is

$$\frac{dp}{dt} = \frac{1}{(\gamma - 1) C_p T_r}\frac{dP}{dt} \tag{C.41}$$

Let us assume that the diffraction phase is negligible; then for the critical flow case

$$\frac{dP^\dagger}{dt} = (\gamma - 1) C_p T_r \cdot \frac{\alpha A}{V}\sqrt{\frac{2\gamma}{\gamma - 1}\left(\frac{2}{\gamma + 1}\right)^{\gamma/(\gamma-1)}\frac{\gamma - 1}{\gamma + 1} P_r \rho_r} \tag{C.42}$$

Making use of the ideal equation of state and writing y for P/P_0, etc.,

$$\frac{dy^\dagger}{dt} = \frac{\alpha A}{V}\gamma\sqrt{\gamma - 1}\,\frac{C_p T_0}{a_r}\sqrt{\left(\frac{2}{\gamma + 1}\right)^{\gamma/(\gamma-1)}\frac{\gamma - 1}{\gamma + 1}\, y_r \frac{T_r}{T_0}} \tag{C.43}$$

Introducing $\sigma = Ut/\lambda$ and writing η for $V/A\lambda$ and K for $\gamma a_0^2/a_r U\sqrt{\gamma - 1}$, one obtains

$$\frac{dy^\dagger}{d\sigma} = \frac{\alpha K}{\eta}\sqrt{\left(\frac{2}{\gamma + 1}\right)^{2/(\gamma-1)}\frac{\gamma - 1}{\gamma + 1}\, y_r \frac{T_r}{T_0}}$$

and in its final abbreviated form, having evaluated the radical and set $\alpha K/\eta = B$,

$$\frac{dy^\dagger}{d\sigma} = 0.259 B\, y_r(\sigma)\,\frac{T_r(\sigma)}{T_0} \tag{C.44}$$

Under the present assumptions this flow continues until $\sigma = \sigma_c$, at which time subcritical flow begins.

For this flow

$$\frac{dP}{dt} = (\gamma - 1)C_P T_r \frac{\alpha A}{V} \sqrt{\frac{2\gamma}{\gamma - 1} P_r \rho_r \left(\frac{P_t}{P_r}\right)^{2/\gamma} \left[1 - \left(\frac{P_t}{P_r}\right)^{(\gamma-1)/\gamma}\right]} \tag{C.45}$$

where P_t is the pressure in the throat. If the isentropic assumption is made,

$$\frac{P_t}{P_r} = \frac{P_t}{P} \cdot \frac{P}{P_r} = \left(\frac{T_t}{T}\right)^{(\gamma-1)/\gamma} \frac{P}{P_r} \tag{C.46}$$

Although it probably is only a fair approximation, we shall take $(T_t/T)^{\gamma/(\gamma-1)} = 1$ for simplicity.

We observe also that $(P/P_r)^{2/\gamma}$ is a slowly changing function when it is compared with $[1 - (P/P_r)^{\gamma-1/\gamma}]$, and one may make the approximation that $(P/P_r)^{2/\gamma} \approx 1$; then,

$$\frac{dy}{dt} = \gamma\sqrt{\gamma - 1} \frac{C_P T_0}{a_r} \cdot \frac{\alpha A}{V} \sqrt{[1 - (P/P_r)^{\gamma/(\gamma-1)}]} \frac{T_r}{T_0} y_r \tag{C.47}$$

Furthermore, if we let $P/P_0 = y$ and $P_r/P_0 = y_r$ and introduce the σ notation, then the formula in final form is

$$\frac{dy}{d\sigma} = \frac{\alpha K}{\eta} \sqrt{[1 - y^{(\gamma-1)/\gamma} y_r^{-(\gamma-1)/\gamma}]} \frac{T_r(\sigma)}{T_0} y_r(\sigma) \tag{C.48}$$

K is an important quantity given by $2\sqrt{2}\gamma^2/\sqrt{\gamma - 1}[\gamma + 1 + (\gamma - 1)\, y_r]y_r$ and is plotted in Fig. C.11 vs y_m, the pressure ratio across the shock front whose speed is U.

C.6.3 Transition or Critical Point

We have obtained two equations for calculation of the filling:

$$\frac{dy^\dagger}{d\sigma} = 0.259B\, y_r(\sigma) \frac{T_r(\sigma)}{T_0} \qquad 0 < \sigma < \sigma_c \tag{C.49}$$

and

$$\frac{dy}{d\sigma} = B\sqrt{(1 - y^{(\gamma-1)/\gamma}\, y_r^{-(\gamma-1)/\gamma})}\, y_r(\sigma) \frac{T_r(\sigma)}{T_0} \qquad \sigma_c < \sigma < 1 \tag{C.50}$$

The critical point comes on the rising part of the $y(\sigma)$ curve, but the differential equations do not define it. However, we can obtain it approximately by letting the pressure in the throat equal that in the chamber. Actually, of course, the pressure P_t always exceeds P during the filling process; thus σ_c calculated in this way is a little large. Then from the definition of critical flow and using the flat-topped wave $y = y_r$, $T = T_r$

$$\frac{1}{y_r} \int_1^{y_m(2/\gamma+1)^{\gamma/(\gamma-1)}} dy = 0.259B \int_0^{\sigma_c} \frac{T_r}{T_0}\, d\sigma \tag{C.51}$$

which integrates to

$$\left(\frac{2}{\gamma + 1}\right)^{\gamma/(\gamma-1)} - \frac{1}{y_m} = 0.259B\, y_m \left(\frac{6 + y_m}{6y_m + 1}\right)\sigma_c$$

and

$$B\sigma_c = \frac{0.528y_m - 1}{0.259\, y_m^2\, (6 + y_m/6y_m + 1)} \tag{C.52}$$

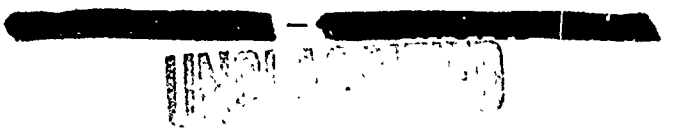

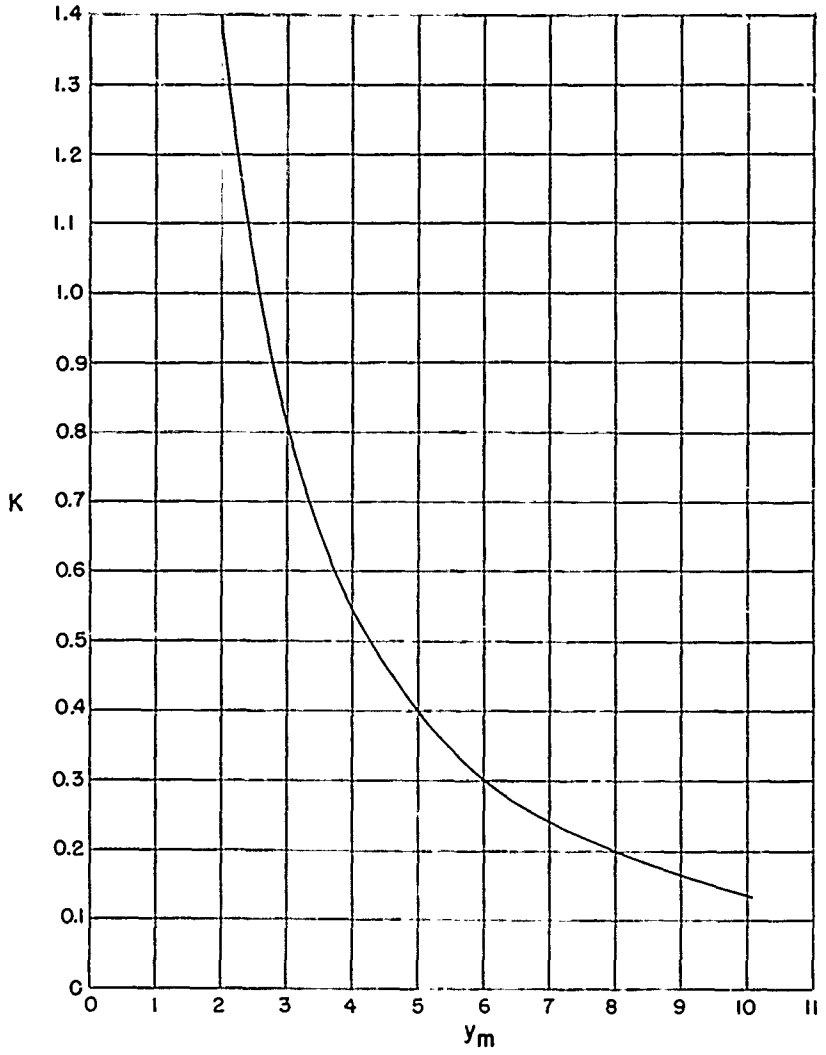

Fig. C.11—Plot of the constant K vs y_m.

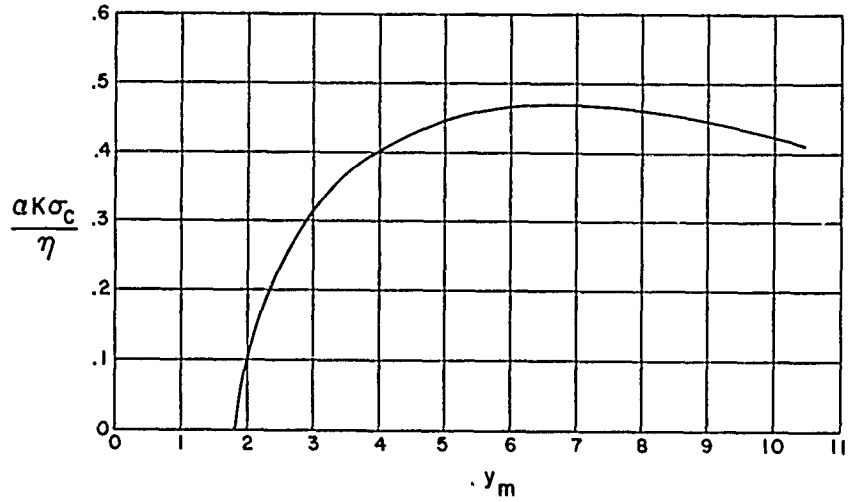

Fig. C.12—Plot of the critical scaled time σ_c vs y_m.

This quantity has been calculated for a range of y_m and is plotted in Fig. C.12. The value of σ_c is always small, and the approximation is believed to be unimportant. For a different reason, that of neglecting the diffraction phase, starting the calculation at (y_c,σ_c) is probably not very exact.

C.7 THEORY VS EXPERIMENT

C.7.1 Initial Rate of Rise

The strong pulse theory gives the initial rate of rise as

$$\frac{dy}{d\sigma} = 0.259 \frac{\alpha K}{\eta} \frac{T_m}{T_0} y_m$$

Experimentally we had obtained an average initial rate of rise for the whole chamber normalized by the incident pulse

$$NAI = \frac{t_+}{p_m^*} \left(\frac{\overline{\Delta p}}{\Delta t}\right)$$

Thus approximately the theory gives

$$NAI \approx 0.259 \frac{\alpha K}{\eta} \frac{T_m}{T_0} \frac{y_m}{y_m - 1} \qquad (C.53)$$

The plot of log NAI vs log $1/\eta$ gives a straight line of slope +1 for theory and +2 for experiment.

The experimental points are rather few and probably statistically are not very well defined; it is not what one would call a set of data in which one would have great confidence. Even so, they appear to be consistent, and we take the difference in slope to be a significant quantity.

If we assume that the throat has not formed in the time during which the initial rise is measured, we set $\alpha = 1$ and, for a $y_m = 6.5$, we calculate from the theory that

$$NAI = 0.259 \times 0.26 \times 1.87 \times \frac{6.5}{5.5} \times \frac{1}{\eta}$$

where the value of K is obtained from Fig. C.12; then

$$NAI = 0.15/\eta$$

Empirically fitting the data, we would find

$$NAI = 0.015/\eta^2$$

It seems to be entirely coincidence that the two curves agree at $1/\eta = 10$ (see Fig. C.4).

C.7.2 Average Fill Time Slope

In this case one might expect a little better agreement between theory and experiment. Again one assumes a smearing out process to reduce the values of the peak pressure to a single quantity.

$$NAFT = \frac{\overline{p_m}}{p_m^*} \cdot \frac{\overline{t_+}}{t_m}$$

where p_m and t_m are the overpressure at maximum and the time (related to zero time at arrival of the pulse) of this maximum, respectively.

The analogue theory gives an explicit expression for the maximum by setting $dp/d\sigma = 0$. Thus we start with

$$\frac{p}{p_m^*} = \frac{B}{(B-C)^2}\{[(B-C)(1-\sigma)+1]\,e^{-C\sigma} - (B-C+1)\,e^{-B\sigma}\}$$

where now $B = (\alpha K/\eta)\cdot(T_m/T_0)$. If $C = 4$, we obtain a good approximation to the real pulse shape. Then

$$\frac{dp}{d\sigma} = \frac{p_m^*\,B}{(B-4)^2}[4(B-4)(\sigma-1)e^{-4\sigma} - Be^{-4\sigma} + B(B-3)e^{-B\sigma}] \qquad (C.55)$$

Now if we set $dp/d\sigma = 0$, we obtain σ_m, as

$$B(B-3) - [4(B-4)(1-\sigma_m) + B]\,e^{(B-4)\sigma_m} = 0 \qquad (C.56)$$

With B as a parameter, a set of σ_m may be obtained which, in turn, gives a corresponding set of p_m. Then $p_m/\sigma_m p_m^*$ gives the desired NAFT.

Upon making these rather laborious calculations, it appears that again the NAFT for both slow- and fast-fill cases would be a straight line in Fig. C.4 having a slope of unity. The experimental data show slopes of about 0.58. Now, however, the absolute magnitude of the theoretical NAFT is considerably greater than that of the experiment. At $1/\eta = 10$, the ratio of NAFT calculated to NAFT experimental is 5.

C.7.3 Conclusions

Two explicit comparisons have been made between experiment and theory. Even though the data are rather sketchy, it is clear that the resemblance between theory and experiment is not close. First, the experimental initial rise (NAI) is probably mostly due to diffraction effects and can hardly be expected to follow from the present theory. Second, the fill time (NAFT) also depends upon diffraction effects, but the comparison suffers from still another fault—the check with theory was made with the analogue because of the difficulty of calculating with the regular theory. Probably the use of the regular theory would give better results here. We conclude that we are "in the ball park," as the saying goes, but that neglect of the diffraction phase has considerable effect on actual magnitudes. It will be shown later (Secs. C.8 and C.9) that even though this simple theory does not seem very useful physically still it does give integrals that may be valuable from the point of view of qualitative reasoning and in making rough estimates in difficult situations.

C.8 NUMERICAL CALCULATIONS

It was pointed out earlier that the pressure in the chamber depended upon both the reservoir temperature and pressure. However, experimentally, only pressure measurements are available. If one has to guess at the value of one of two factors of equal importance, it seems only a little less rigorous to guess at both. Thus we shall represent the measured reservoir pressure by typical equations and postulate corresponding temperature functions. Calculations made in this way are not intended to compare quantitatively with experiment. They are primarily intended to test the reasonableness of the equations. If they also give a good approximation of the real pressure, this is mixed tribute both to the theory and to the assumed pressure and temperature time profiles.

Two types of calculations are performed. The first obtains the general pulse shapes due to varying the parameter $\sigma K/\eta - B$. The second type chooses values of the parameters similar to those of the experimental situations and attempts to show some similarity between the analysis and experiment.

C.8.1 Working Equations

Equations C.49 and C.50 show the rate at which the pressure ratio, y, built up in the chamber as a function of time for both critical and subcritical flow. The critical time σ_c is obtained from Fig. C.12. One recalls that this value was computed for a flat-topped pulse, whereas the actual pulse decays; a certain error is therefore implicit in Fig. C.12, giving critical flows for a somewhat longer time than actually exists. This error is believed to be unimportant in most cases since σ_c is itself so small. Also, K is a function of y_m and is obtained from Fig. C.11. Again there is a small error implicit in this property which depends upon $a_r(\sigma)$, the sound speed associated with the reservoir temperature. It has been assumed to be constant with σ, which is only true for the field experiment. Actually it varies with the square root of the absolute temperature and is a slowly varying function of time; again it is believed that this is an unimportant approximation. The last two parameters α and η must be obtained from independent considerations: η is given by the geometry and by the size of the incident pulse; α must surely be a function of the pressure differential across the entrance and hence a function of time. This relation is not known. For all the calculations it was arbitrarily set equal to $\frac{1}{2}$ throughout the period of interest. This is probably a rather serious oversimplification since intuition suggests that $\frac{1}{2} < \alpha < 1$ as a function of time.

C.8.2 Computations

(a) Ideal Pulse. Here it is assumed that the pressure pulse has the form

$$y_r = y_m \exp(-k\sigma) \qquad 0 < \sigma < 1 \tag{C.57}$$

with the associated temperature

$$T_r = T_m \exp(-k\sigma) \qquad 0 < \sigma < 1 \tag{C.58}$$

where k is the same in both cases. After y_m, T_m, and K are specified, the parameter $B = \alpha K/\eta$ is permitted to vary over an appropriate range. It was given the values 2, 10, and 100 to compare with the analogue theory. The problem is now completely specified, and computations may be carried out.

The value of y_m was taken to be 7, and T_m/T_0 was computed by the shock relation

$$T_m/T_0 = y_m \frac{(6 + y_m)}{(6y_m + 1)} \tag{C.59}$$

The constant, k, was determined by specifying that $y_r = 1$ at $\sigma = 1$, a criterion which causes the exponential pulse to resemble closely the usual blast pulse

$$p = p_m (1 - \sigma) \exp(-\sigma)$$

It does not fit the actual pulse very well; a much better fit is obtained by using

$$y_r = \tfrac{1}{2} y_m (e^{-k_1\sigma} + e^{-k_2\sigma}) \tag{C.60}$$

with k_1 and k_2 determined separately at the head and tail of the pulse. Much ease of calculation was achieved by using the simpler pulse. The effect of using the more exact pulse is discussed in Sec. C.9.2.

Let $y_m = 7$; then the critical flow equation becomes

$$\frac{dy}{d\sigma} = 0.259 \times 14.8 \times B \exp(-3.90\sigma) \qquad 0 < \sigma < \sigma_c \tag{C.61}$$

Upon integrating

$$y_c = 0.983B\,(1 - e^{-1.87/B}) + 1$$

where $\sigma_c = 0.480/B$ from Fig. C.12. By taking B = 2, 10, and 100 as for the analogue theory, three initial values of (y_c, σ_c) are obtained. With these initial values, numerical computation may be started on

$$\frac{dy}{d\sigma} = 14.8B\sqrt{|1 - 0.575\,y^{2/7}\,e^{0.56\sigma}|}\;e^{-3.90\sigma} \qquad \sigma_c < \sigma < 1 \tag{C.62}$$

where the absolute value signs imply a change of sign of y after the right-hand side goes through zero. The step-by-step integration[8] gives

$$y_i = y_{i-1} + \Delta y \tag{C.63}$$

and the significant ratio p/p_m is given by

$$\frac{y_i - 1}{y_m - 1} = \frac{y_{i-1} + \Delta y - 1}{6} \tag{C.64}$$

The curves resulting from these calculations are shown in Fig. C.13.

(b) Precursor Pulse. The precursor shelf has the shape

$$y_r = 2.96 \qquad \frac{T_r}{T_0} = 5.76 \qquad 0 < \sigma < 0.22 \tag{C.65}$$

Then

$$y = 1 + 0.259B\,y_m\,\frac{T_m}{T_0}\,\sigma \qquad 0 < \sigma < \sigma_c \tag{C.66}$$

where the following quantities are used and obtained:

$B = \frac{1}{2} \times 0.89/0.0775 = 0.588$ with $\alpha = \frac{1}{2}$
$\sigma_c = 0.15/B = 0.0256$
$y_c = 1.64$

The temperature ahead of the precursor used to obtain this configuration was 1000°C, chosen more or less arbitrarily.[a] We finally decided to use an isentropic law to calculate the temperatures throughout the precursor; there is not unanimous agreement on this decision. The computing formula is

$$\frac{dy}{d\sigma} = 100\,\sqrt{1 - \frac{y^{2/7}}{1.36}} \qquad 0 < \sigma < 0.026 \tag{C.67}$$

[a]In this regard the author was fortunate in being able to discuss the situation with several Sandia people who had first-hand experience with the field phenomenon: John Banister, Carter Broyles, and Frank Shelton. Banister confirmed our model by showing that the ratio P/ρ remained fairly constant during the precursor shelf in one of his experiments.

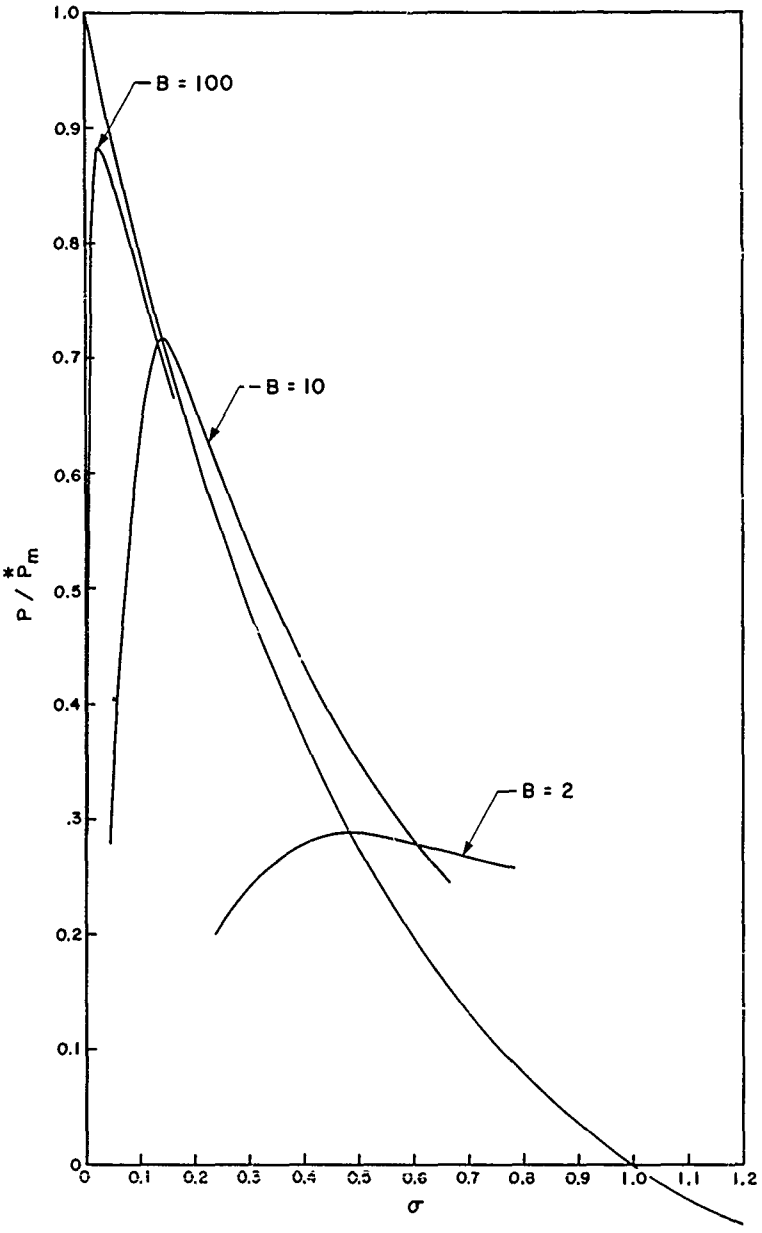

Fig. C.13—Plot of ideal pulse calculations.

The main pulse is given by

$$y_r = 8.08 \exp(-2.09\sigma) \qquad 0 < \sigma < 1 \tag{C.68}$$

where it is understood that the main pulse is continuous with the precursor shelf. It greatly simplifies calculation to consider them separately. If y_0 is the final pressure computed from the precursor shelf, then the starting point for the main pulse is $(y_0,0)$, but it is plotted as if it started at $\sigma = 0.22$. The equation is

$$\frac{dy}{d\sigma} = 362 \sqrt{1 - \frac{y^{2/7} e^{0.97\sigma}}{1.82}}\, e^{-2.09\sigma} \qquad 0 < \sigma < 1 \tag{C.69}$$

The resulting pressure curve is plotted in Fig. C.14.

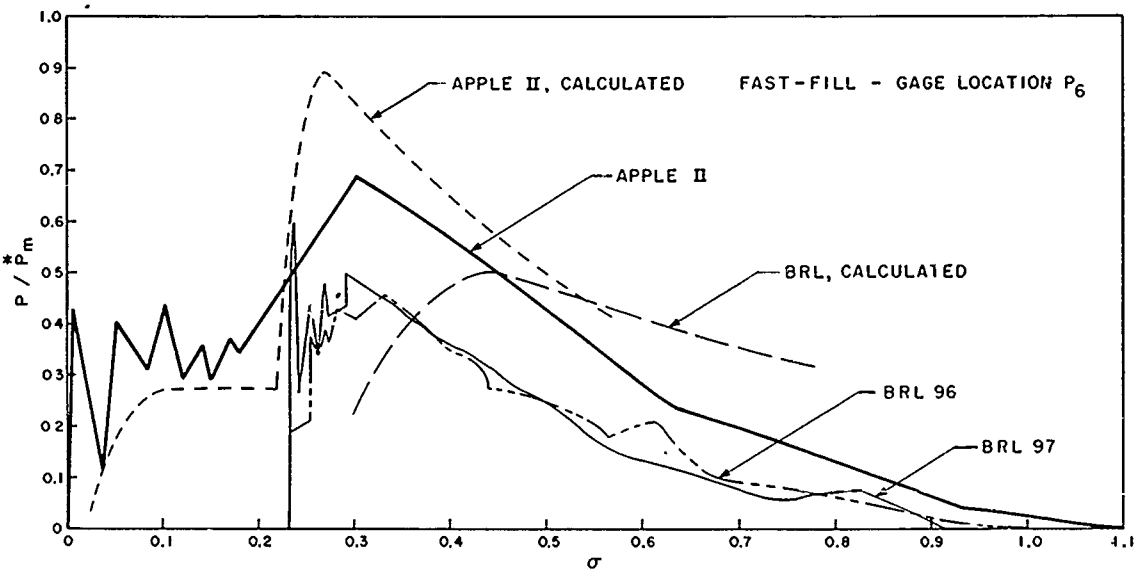

Fig. C.14—Apple II and shock-tube tests compared to calculations.

(c) BRL Calculation. The same calculation was also set up for Shots 96 and 97 of the BRL study. The incident wave was

$$y_r = 7 \exp(-1.95\sigma) \qquad 0 < \sigma < 1 \tag{C.70}$$

B was found to be 6.0, $\sigma_c = 0.080$, and $y_c = 2.57$. The equation for calculation is

$$\frac{dy}{d\sigma} = 88.2 \sqrt{1 - \frac{y^{2/7} e^{0.557\sigma}}{1.75}}\, e^{-3.90\sigma} \qquad 0 < \sigma < 1 \tag{C.71}$$

These latter calculations also are shown in Fig. C.14 against the actual experimental data. Agreement in the precursor case is reasonable and could be expected to improve by adjusting the initial conditions and by using less formalized reservoir functions. The calculated pressure does not agree with the measured shock-tube values, however. The question of agreement will be discussed in Sec. C.9.

C.9 SUGGESTIONS FOR FUTURE STUDY

Filling of a chamber by an atomic blast is well enough understood to enable one to make estimates in many cases and to say how good these estimates are. If the need exists for improving them for making a refined computation, a great deal of information can be obtained by laboratory studies to supplement the present theories without actually going to full-scale field tests.

C.9.1 Experimental Laboratory Work

The shock tube can probably answer a number of questions about transient nozzle flow. In particular:

1. How long after the shock impinges upon the entrance does quasi-steady mass flow occur? This problem might be resolved by an interferometric study much like that performed by Kohane et al.[9] for a gradual change in channel width. However, from such experiments only density information is obtained, and, although compression waves are characterized by density changes, it is not really clear that a quasi-steady state can be distinguished in this way.

Pressure measurements, like those of BRL,[10] might also be used. Presumably the quasi-steady state could be detected on the side not affected by the vortex by the steadying of the pressure.

2. What is the value of α, the choking factor? In the present analysis it was postulated that the formation of a vortex sheet restricted the effective flow through the channel. A value of 0.5 was assumed for this factor, and the calculated result was reasonable.

The BRL study,[10] in which a shock was permitted to turn 90° from the shock tube into a closed channel 32 in. long and 1 or $\frac{1}{4}$ in. wide, showed very little difference between pressures along the channel walls in the two cases. However, this is not proof that the mass flow divided by the area is the same in each case and does not convincingly demonstrate that the mass flow is independent of the vortex. Interferometric studies on open-ended channels seem more likely to yield acceptable information.

C.9.2 Analytical Studies

The most important assumption made in this study was that the flow could be considered originating from a reservoir whose properties changed slowly with time. Thus no accounting was made of the moving air and dust outside the shelter. To account thoroughly for this effect would be inconceivable. Such problems are difficult to solve; they depend upon specific boundary conditions, and each has to be solved individually. However, it may be possible to generalize a little less and arrive at a somewhat more realistic approach to accounting for the effects due to the incident flow.

The second important assumption was the neglect of the diffraction phase. When the fill time is long enough, this is not an important consideration. For shorter fill times the throat does not have time to become steady, and filling is done essentially by diffraction rather than by reservoir flow. This diffraction type filling is important and should be studied.

A third assumption is that of the time dependence of the temperature of the reservoir. This has an effect on the height and shape of the pressure pulse within the shelter.

Consider the analogue theory for the simple pulse $y_r^*(\sigma) = y_m^* \exp(-\sigma \ln y_m^*)$ while the temperature is given by the arbitrary function $T(\sigma)\, T_0$. Then

$$\frac{dy}{d\sigma} = B\,[y_r^*(\sigma) - y(\sigma)]\,\frac{T_r^*(\sigma)}{T_0} \tag{C.72}$$

How does the shape of the pulse $y(\sigma)$ vary with reasonable changes in $T_r^*(\sigma)$?

A simple differential equation is obtained

$$\frac{dy(\sigma)}{d\sigma} + B\,\frac{T_r^*(\sigma)}{T_0}\,y(\sigma) = \frac{B\,T_r^*(\sigma)}{T_0}\,y_r^*(\sigma) \tag{C.73}$$

which can easily be solved once $T_r^*(\sigma)$ is specified. Let us then consider two cases.

I. $$T_r^*(\sigma) = y_m^*\,\frac{(6 + y_m^*)}{(6y_m^* + 1)}\exp(-\sigma \ln y_m^*) \tag{C.74}$$

II. $$T_r^*(\sigma) = y_m^*\,\frac{(6 + y_m^*)}{(6y_m^* + 1)} \tag{C.74a}$$

The first case can be solved by substituting $T_r^*(\sigma)$ into Eq. C.66 and letting $x = \exp(-\sigma \ln y_m)$. Then, if $R = By_m^*(6 + y_m^*)/(6y_m^* + 1) \ln y_m^*$,

$$y_I = \frac{1}{R}\{y_m^*(Rx + 1) - [R(y_m^* - 1) + y_m^*]\,e^{R(x-1)}\} \qquad 0 < x < 1 \tag{C.75}$$

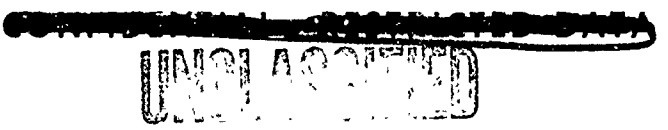

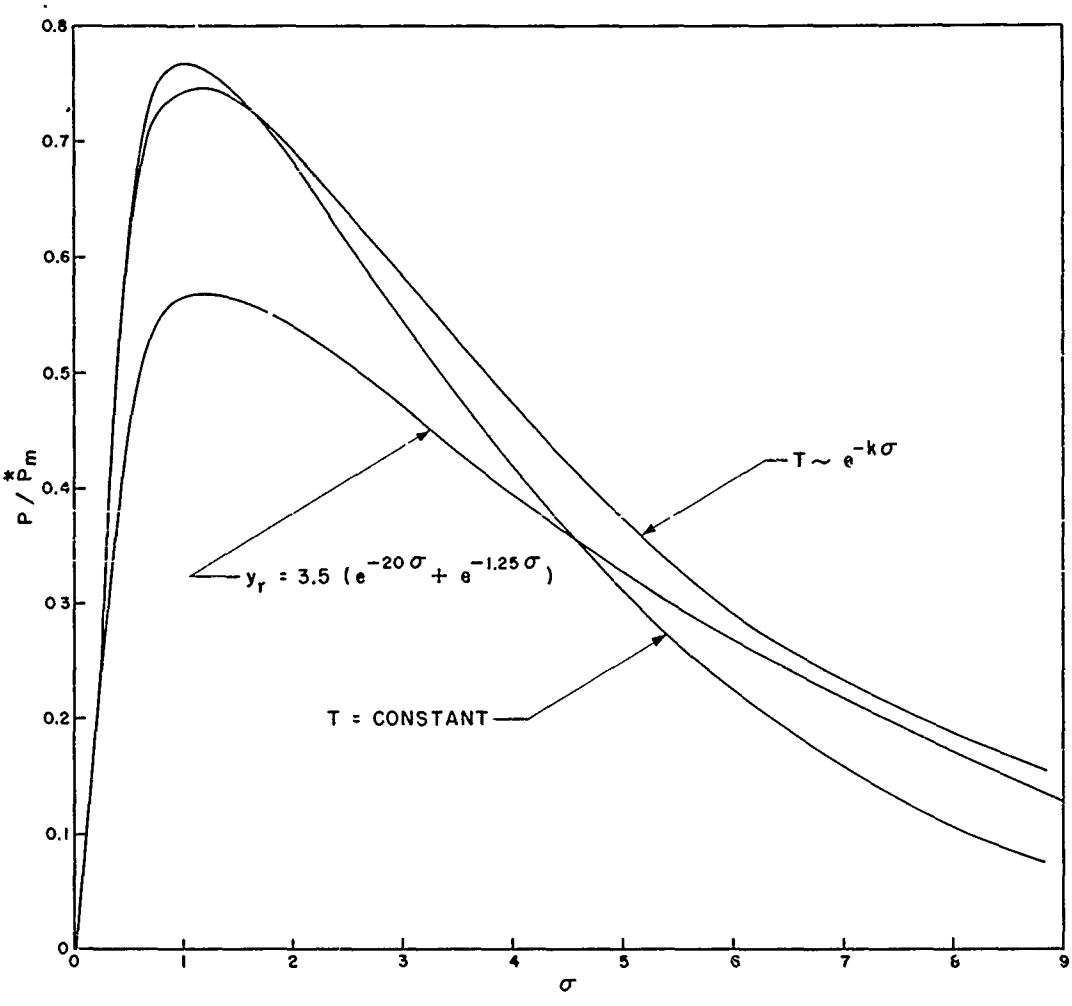

Fig. C.15—Comparison between two cases of filling with different temperature characteristics.

The second case similarly becomes

$$y_{II} = \frac{1}{R-1}\{Ry^*_m x - [R(y^*_m - 1) + 1]x^R\} \qquad 0 < x < 1 \tag{C.76}$$

If we let B = 10 and $y_m = 7$, as is done in some other calculations, then we obtain R = 10.9, and the two curves are plotted in Fig. C.15. It can be seen that the equation giving the pressure within the chamber is singularly unaffected by the shape of the temperature curve.

Now let us examine the analogue theory with a new pulse form which rather closely fits the experimental data

$$y_r = 3.5\,(e^{-20\sigma} + e^{-1.25\sigma}) \qquad 0 < \sigma \tag{C.77}$$

Notice that the impulse associated with this incident wave pulse is less than that of the previously used equation. Inserting this function into Eq. C.72, using the temperature pulse II and evaluating constants as before, gives

$$y = 74.2\left(\frac{e^{-20\sigma}}{13.4} + \frac{e^{-1.25\sigma}}{20.0}\right) - 8.27e^{-21.2\sigma} \qquad 0 < \sigma \tag{C.78}$$

The pressure ratio, y, is plotted as a function of σ in Fig. C.15 and shows a lower peak but a generally similar shape to the other two.

It is probably true that the maximum value is determined by the impulse of the incident pulse. In examining this situation further care should be taken not to normalize the peak pressure of the incident pulse while varying the shape but rather to normalize the impulse [i.e., $\int p(t)\,dt$] while varying the shape.

C.10 CONCLUSIONS

We have focused attention on the problem of fast filling, mostly because the slow-fill problem appears to have been handled rather satisfactorily by the method of Sinnamon et al.[1] The same method could be applied to flow through short tubes, corresponding to our slow-fill problem, and there is every reason to believe now that the pressure calculated in this way would be a good approximation to the real pressure.

The fast-fill problem has been handled here by making several assumptions. It has not been possible to test these assumptions separately, but it appears that the most unacceptable one is that of ignoring the diffraction phase of the interaction. The situation was especially critical in the study of the BRL data, where the equations predicted a much higher and more slowly decaying pressure pulse than was observed. To some extent, the method of integration is responsible for this behavior.

It is certain that better calculations could now be made on the basis of this experience. If some experimental studies, such as those mentioned above, can be performed, one might expect to do a fairly good job of describing the general aspects of blast filling. Problems like reverberations and turbulent diffusion and cases where movements of the boundaries occur will always require special attention.

REFERENCES

1. G. K. Sinnamon et al., Air Blast Effects on Entrances and Air Intakes of Underground Installations, Upshot-Knothole Report, WT-726, 1955.
2. J. H. Bird et al., The Air Pressure Inside a Surface Shelter Produced by an External Blast Wave of Long Duration, Report FWE-48, 1955.
3. Rowe, The Effect of Varying the Incident Shock Pressure II, AWRE Report H, September 1953.
4. H. Vaughn, Experimental and Analytical Methods for Determining the Pressure and Time Lag in Pressure Measuring Systems – Applications to Atomic Weaponry, SC-3244(TR), May 1954.
5. H. W. Liepmann and Puckett, "Introduction to Aerodynamics of a Compressible Fluid," John Wiley & Sons, Inc., New York, 1947.
6. J. R. Banister, J. Beyler, and F. H. Shelton, Special Measurements of Dynamic Pressure Vs Time and Distance, Operation Teapot Report, WT-1110, December 1955.
7. C. C. Hudson, Blast Loading End Effects I, Report AFSWP-461, Aug. 24, 1954.
8. Henry Margenau and G. M. Murphy, "The Mathematics of Physics and Chemistry," D. Van Nostrand Co., Inc., New York, 1943, Chap. 13.
9. A. Kohane et al., A Theoretical and Experimental Study of Finite Amplitude Wave Interaction with Channels of Varying Area, J. Am. Soc., 21: 504-524, 1954.
10. BRL Quarterly Report, BRL-Q-56, Jan. 1, 1956.

DISTRIBUTION

Military Distribution Categories 5-21, 5-30, 5-40, and 5-60

ARMY ACTIVITIES

Asst. Dep. Chief of Staff for Military Operations, D/A, Washington 25, D. C. ATTN: Asst. Executive (R&SW)	1
Chief of Research and Development, D/A, Washington 25, D. C. ATTN: Special Weapons and Air Defense Division	2
Chief of Ordnance, D/A, Washington 25, D. C. ATTN: ORDTX-AR	3
Chief Signal Officer. D/A, P&O Division, Washington 25, D. C. ATTN: SIGOP	4–6
The Surgeon General, D/A, Washington 25, D. C. ATTN: Chief, R&D Division	7
Chief Chemical Officer, D/A, Washington 25, D. C.	8–9
The Quartermaster General, D/A, Washington 25, D. C. ATTN: Research and Development Div.	10
Chief of Engineers, D/A, Washington 25, D. C. ATTN: ENGNB	11–15
Chief of Transportation, Military Planning and Intelligence Div., Washington 25, D. C.	16
Commanding General, Continental Army Command, Ft. Monroe, Va.	17–19
President, Board #1, Headquarters, Continental Army Command, Ft. Sill, Okla.	20
President, Board #2, Headquarters, Continental Army Command, Ft. Knox, Ky.	21
President, Board #3, Headquarters, Continental Army Command, Ft. Benning, Ga.	22
President, Board #4, Headquarters, Continental Army Command, Ft. Bliss, Tex.	23
Commanding General, U. S. Army Caribbean, Ft. Amador, C. Z. ATTN: Cml. Off.	24
Commander-in-Chief, European Command, APO 128, New York, N. Y.	25
Commander-in-Chief, Far East Command, APO 500, San Francisco, Calif. ATTN: ACofS, J-3	26–27
Commanding General, U. S. Army Europe, APO 403, New York, N. Y. ATTN: OPOT Div., Combat Dev. Br.	28–29
Commanding General, U. S. Army Pacific, APO 958, San Francisco, Calif. ATTN: Cml. Off.	30–31
Commandant, Command and General Staff College, Ft. Leavenworth, Kans. ATTN: ALLLS(AS)	32–33
Commandant, The Artillery and Guided Missile School, Ft. Sill, Okla.	34
Secretary, The Antiaircraft Artillery and Guided Missile School, Ft. Bliss, Tex. ATTN: Maj. George D. Breitegan, Dept. of Tactics and Combined Arms	35
Commanding General, Army Medical Service School, Brooke Army Medical Center, Ft. Sam Houston, Tex.	36
Director, Special Weapons Development Office, Headquarters, CONARC, Ft. Bliss, Tex. ATTN: Capt T. E. Skinner	37
Commandant, Walter Reed Army Institute of Research, Walter Reed Army Medical Center, Washington 25, D. C.	38
Superintendent, U. S. Military Academy, West Point, N. Y. ATTN: Prof. of Ordnance	39
Commandant, Chemical Corps School, Chemical Corps Training Command, Ft. McClellan, Ala.	40
Commanding General, Research and Engineering Command, Army Chemical Center, Md. ATTN: Deputy for RW and Non-Toxic Material	41–42
Commanding General, Aberdeen Proving Grounds, Md. (inner envelope). ATTN: RD Control Officer (for Director, Ballistic Research Laboratories)	43–44

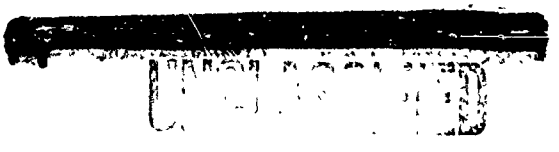

Commanding General, The Engineer Center, Ft. Belvoir, Va. ATTN: Asst. Commandant, Engineer School 45–47
Commanding Officer, Engineer Research and Development Laboratory, Ft. Belvoir, Va. ATTN: Chief, Technical Intelligence Branch 48
Commanding Officer, Picatinny Arsenal, Dover, N. J. ATTN: ORDBB-TK 49
Commanding Officer, Frankford Arsenal, Philadelphia 37, Pa. ATTN: Col Tewes Kundel 50
Commanding Officer, Army Medical Research Laboratory, Ft. Knox, Ky. 51
Commanding Officer, Chemical Corps Chemical and Radiological Laboratory, Army Chemical Center, Md. ATTN: Tech. Library 52–53
Commanding Officer, Transportation R&D Station, Ft. Eustis, Va. 54
Director, Technical Documents Center, Evans Signal Laboratory, Belmar, N. J. 55
Director, Waterways Experiment Station, PO Box 631, Vicksburg, Miss. ATTN: Library 56
Director, Armed Forces Institute of Pathology, Walter Reed Army Medical Center, 6825 16th Street, N.W., Washington 25, D. C. 57
Director, Operations Research Office, Johns Hopkins University, 7100 Connecticut Ave., Chevy Chase, Md., Washington 15, D. C. 58
Commanding General, Quartermaster Research and Development Command, Quartermaster Research and Development Center, Natick, Mass. ATTN: CBR Liaison Officer 59–61
Commandant, The Army Aviation School, Ft. Rucker, Ala. 62
President, Board #6, CONARC, Ft. Rucker, Ala. 63

NAVY ACTIVITIES

Chief of Naval Operations, D/N, Washington 25, D. C. ATTN: OP-36 64–65
Chief of Naval Operations, D/N, Washington 25, D. C. ATTN: OP-03EG 66
Director of Naval Intelligence, D/N, Washington 25, D. C. ATTN: OP-922V 67
Chief, Bureau of Medicine and Surgery, D/N, Washington 25, D. C. ATTN: Special Weapons Defense Div. 68
Chief, Bureau of Ordnance, D/N, Washington 25, D. C. 69
Chief, Bureau of Ships, D/N, Washington 25, D. C. ATTN: Code 348 70–71
Chief, Bureau of Yards and Docks, D/N, Washington 25, D. C. ATTN: D-440 72
Chief, Bureau of Supplies and Accounts, D/N, Washington 25, D. C. 73
Chief, Bureau of Aeronautics, D/N, Washington 25, D. C. 74–75
Chief of Naval Research, Department of the Navy, Washington 25, D. C. ATTN: Code 811 76
Commander-in-Chief, U. S. Pacific Fleet, Fleet Post Office, San Francisco, Calif. 77
Commander-in-Chief, U. S. Atlantic Fleet, U. S. Naval Base, Norfolk 11, Va. 78
Commandant, U. S. Marine Corps, Washington 25, D. C. ATTN: Code A03H 79–82
President, U. S. Naval War College, Newport, R. I. 83
Superintendent, U. S. Naval Postgraduate School, Monterey, Calif. 84
Commanding Officer, U. S. Naval Schools Command, U. S. Naval Station, Treasure Island, San Francisco, Calif. 85
Commanding Officer, U. S. Fleet Training Center, Naval Base, Norfolk 11, Va. ATTN: Special Weapons School 86
Commanding Officer, U. S. Fleet Training Center, Naval Station, San Diego 36, Calif. ATTN: (SPWP School) 87
Commanding Officer, Air Development Squadron 5, VX-5, U. S. Naval Air Station, Moffett Field, Calif. 88
Commanding Officer, U. S. Naval Damage Control Training Center, Naval Base, Philadelphia 12, Pa. ATTN: ABC Defense Course 89
Commanding Officer, U. S. Naval Unit, Chemical Corps School, Army Chemical Training Center, Ft. McClellan, Ala. 90
Commander, U. S. Naval Ordnance Laboratory, Silver Spring 19, Md. ATTN: EE 91
Commander, U. S. Naval Ordnance Laboratory, Silver Spring 19, Md. ATTN: EH 92
Commander, U. S. Naval Ordnance Laboratory, Silver Spring 19, Md. ATTN: R 93
Commander, U. S. Naval Ordnance Test Station, Inyokern, China Lake, Calif. 94
Officer-in-Charge, U. S. Naval Civil Engineering Res. and Evaluation Lab., U. S. Naval Construction Battalion Center, Port Hueneme, Calif. ATTN: Code 753 95
Commanding Officer, U. S. Naval Medical Research Inst., National Naval Medical Center, Bethesda 14, Md. 96

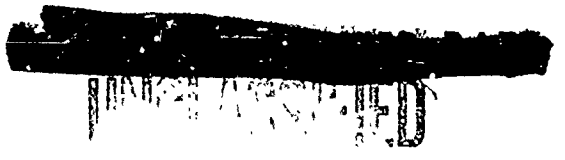

Director, Naval Air Experimental Station, Air Material Center, U. S. Naval Base, Philadelphia, Pa. 97
Director, U. S. Naval Research Laboratory, Washington 25, D. C. ATTN: Mrs. Katherine H. Cass 98
Director, The Material Laboratory, New York Naval Shipyard, Brooklyn, N. Y. 99
Commanding Officer and Director, U. S. Navy Electronics Laboratory, San Diego 52, Calif. 100
Commanding Officer, U. S. Naval Radiological Defense Laboratory, San Francisco 24, Calif. ATTN: Technical Information Division 101–104
Commanding Officer and Director, David W. Taylor Model Basin, Washington 7, D. C. ATTN: Library 105–106
Commander, U. S. Naval Air Development Center, Johnsville, Pa. 107
Commanding Officer, Clothing Supply Office, Code 1D-0, 3rd Avenue and 29th St., Brooklyn, N. Y. 108

AIR FORCE ACTIVITIES

Asst. for Atomic Energy, Headquarters, USAF, Washington 25, D. C. ATTN: DCS/O 109
Director of Operations, Headquarters, USAF, Washington 25, D. C. ATTN: Operations Analysis 110
Director of Plans, Headquarters, USAF, Washington 25, D. C. ATTN: War Plans Div. 111
Director of Research and Development, Headquarters, USAF, Washington 25, D. C. ATTN: Combat Components Div. 112
Director of Intelligence, Headquarters, USAF, Washington 25, D. C. ATTN: AFOIN-IB2 113–114
The Surgeon General, Headquarters, USAF, Washington 25, D. C. ATTN: Bio. Def. Br., Pre. Med. Div. 115
Deputy Chief of Staff, Intelligence, Headquarters, U. S. Air Forces Europe, APO 633, New York, N. Y. ATTN: Directorate of Air Targets 116
Commander, 497th Reconnaissance Technical Squadron (Augmented), APO 633, New York, N. Y. 117
Commander, Far East Air Forces, APO 925, San Francisco, Calif. 118
Commander-in-Chief, Strategic Air Command, Offutt Air Force Base, Omaha, Nebr. ATTN: Special Weapons Branch, Inspector Div., Inspector General 119
Commander, Tactical Air Command, Langley AFB, Va. ATTN: Documents Security Branch 120
Commander, Air Defense Command, Ent AFB, Colo. 121
Research Directorate, Hdqs. Air Force Special Weapons Center, Kirtland Air Force Base, N. Mex. ATTN: Blast Effects Research 122–123
Assistant Chief of Staff, Installations, Headquarters, USAF, Washington 25, D. C. ATTN: AFCIE-E 124
Commander, Air Research and Development Command, PO Box 1395, Baltimore, Md. ATTN: RDDN 125
Commander, Air Proving Ground Command, Eglin AFB, Fla. ATTN: Adj./Tech. Report Branch 126
Director, Air University Library, Maxwell AFB, Ala. 127–128
Commander, Flying Training Air Force, Waco, Tex. ATTN: Director of Observer Training 129–136
Commander, Crew Training Air Force, Randolph Field, Tex. ATTN: 2GTS, DCS/O 137
Commandant, Air Force School of Aviation Medicine, Randolph AFB, Tex. 138–139
Commander, Wright Air Development Center, Wright-Patterson AFB, Dayton, Ohio. ATTN: WCOSI 140–145
Commander, Air Force Cambridge Research Center, LG Hanscom Field, Bedford, Mass. ATTN: CRQST-2 146–147
Commander, Air Force Special Weapons Center, Kirtland AFB, N. Mex. ATTN: Library 148–150
Commander, Lowry AFB, Denver, Colo. ATTN: Department of Armament Training 151
Commander, 1009th Special Weapons Squadron, Headquarters, USAF, Washington 25, D. C. 152
The RAND Corporation, 1700 Main Street, Santa Monica, Calif. ATTN: Nuclear Energy Division 153–154
Commander, Second Air Force, Barksdale AFB, La. ATTN: Operations Analysis Office 155
Commander, Eighth Air Force, Westover AFB, Mass. ATTN: Operations Analysis Office 156
Commander, Fifteenth Air Force, March AFB, Calif. ATTN: Operations Analysis Office 157
Commander, Western Development Div. (ARDC), PO Box 262, Inglewood, Calif. ATTN: WDSIT, Mr. R. G. Weitz 158

OTHER DEPARTMENT OF DEFENSE ACTIVITIES

Asst. Secretary of Defense, Research and Development, D/D, Washington 25, D. C. ATTN: Tech. Library 159
U. S. Documents Officer, Office of the U. S. National Military Representative, SHAPE, APO 55, New York, N. Y. 160
Director, Weapons Systems Evaluation Group, OSD, Rm 2E1006, Pentagon, Washington 25, D. C. 161
Armed Services Explosives Safety Board, D/D, Building T-7, Gravelly Point, Washington 25, D. C. 162
Commandant, Armed Forces Staff College, Norfolk 11, Va. ATTN: Secretary 163

ATOMIC ENERGY COMMISSION ACTIVITIES

ADDITIONAL DISTRIBUTION

AEC, Oak Ridge, Tenn.

END

FILMED

4-86

DTIC